UNIVERSITAT AUTÒNOMA DE BARCELONA

INSTITUT DE CIÈNCIA I TECNOLOGIA AMBIENTALS

Evaluating Submarine Groundwater Discharge to the Mediterranean Sea by using radium isotopes

Valentí Rodellas i Vila

TESI DOCTORAL

2014

Directors:

Dr. Jordi Garcia Orellana

Dr. Pere Masqué Barri

UNIVERSITAT AUTÒNOMA DE BARCELONA

INSTITUT DE CIÈNCIA I TECNOLOGIA AMBIENTALS

Evaluating Submarine Groundwater Discharge to the Mediterranean Sea by using radium isotopes

Valentí Rodellas i Vila Dr. Jordi Garcia Orellana Dr. Pere Masqué Barri

TESI DOCTORAL

Doctorat en Ciència i Tecnologia Ambientals

Setembre de 2014

Aquesta Tesi doctoral ha estat finançada mitjançant una Beca del Programa de Formación de Personal Universitario (FPU) del Ministerio de Ciencia e Innovación (AP2008 – 03044), des de l'any 2010 fins al 2014. El finançament econòmic també ha provingut dels següents projectes d'investigació, així com del grup de recerca consolidat MERS (2014 SGR-1356) de la Generalitat de Catalunya.

- Natural tracers of Submarine Groundwater Discharge to the Mediterranean Sea. Ministerio de Ciencia e Innovación (CGL2011 – 13341 – E).
- Biogeochemical consequences of episodic events in a harbour with restricted exchange (EHRE). Ministerio de Ciencia e Innovación (CTM2009 – 08270).
- Instrumentation for radiological environament monitoring and radon measurement in extreme environmental conditions. Consejo de Seguridad Nuclear (CSN 2686 - SRA)
- Evaluation of groundwater discharge and its effects on the coastal and marine ecosystems (EDASE). Ministerio de Ciencia e Innovación (CGL2008 – 00047/BTE).
- Evaluating Submarine Groundwater Discharge from the Regional Jurassic Aquifer of El Maestrazgo (Castellón) by using radium isotopes (EDASMAR). Ministerio de Ciencia e Innovación (CGL2006 – 09274/HID)

AGRAÏMENTS

Si aquesta Tesi Doctoral és avui una realitat, és gràcies a l'esforç i a la contribució de moltes persones. Cadascuna d'elles, d'una manera o altra, o fins i tots sense saber-ho, han fet que tot això sigui possible.

Dues persones són les que han contribuït decisivament en tots i cadascun dels trams d'aquesta Tesi: els meus directors, el Jordi i el Pere. Res de tot això hauria estat possible sense vosaltres. Gràcies per donar-me l'oportunitat d'iniciar aquest projecte, d'entrar en aquest món desconegut i fer-me'l sentir apassionant. Gràcies per ensenyar-me tot el què he aprés i per encomanar-me les vostres ganes d'aprendre'n encara més. Gràcies per haver confiat en mi i per lluitar cada dia perquè la nostra recerca tiri endavant. Però sobretot, i més enllà de l'àmbit científic, gràcies per haver-me regalat aquesta experiència. Jordi, no cal que et digui res més, ja saps que has estat molt més que un director de Tesi. Moltes gràcies per tots aquests anys!!! Pere, gràcies per ensenyar-me la teva forma d'entendre la ciència i donar-me l'espurna de lucidesa que sovint m'ha fet falta. Per tot això, i molt més, sabeu que us estic infinitament agraït.

Si el meu balanç d'aquesta etapa és tan positiu, és, principalment, gràcies als meus companys i ex-companys del LRA. Gràcies per les estones compartides dins i fora del laboratori, pel suport, pels ànims i, sobretot, per la vostra amistat. Gràcies per fer que cada dia al LRA sigui fantàstic. Un agraïment molt especial al Joan Manuel, que hi ha estat des del primer dia. Gràcies per la quantitat de favors-marrons que, probablement, mai et podré tornar. Pots fer una llista infinita de marrons... i una de propostes d'oci pendents, just al costat de la de cafi-puntos,... I, com no, a l'Ester. Aquesta tesi també és teva! Sense tu, res de tot això hauria començat... Gràcies per tot el que m'has ensenyat i per la paciència dels primers dies... però sobretot, gràcies per ser com ets i per ser-hi sempre! Viena, vam començar junts i ja tenim el final a tocar... gràcies per tots aquests anys! Encara que no t'ho digui mai, saps que m'ha encantat compartir aquesta experiència amb tu! Muntsa, casi ja no recordo quan vas començar... que estrany se'm fa imaginar-me el despatx sense tu. Mil gràcies per fer-ho tot tan fàcil i agradable! Giada, gràcies pels mostrejos i viatges compartits... ens ho hem passat bé, no? Agafes el relleu d'aquesta tesi... disfruta-ho! Maxi, ja era hora que entrés un basc com déu mana en aquest grup! Gràcies per l'energia, pels ànims en forma d'Aupa Ekipo i per fer-nos riure tan sovint! Almuuuu! Que haría yo sin tí? Gracias por la vidilla que has traído al grupo... cuando nos vamos a Huelva??? I també als que ara comenceu aquesta etapa, Ari i Marc, passeu-vos-ho molt bé!!! Ari, tu i jo tenim un partit pendent... prepara't, que penso posar-me en forma! Marc, gràcies per aquest darrer any! M'ha encantat treballar amb tu! i facis el que facis en aquests anys, pensa que sempre hi haurà un tros de Ra en

tu... Y gracias, Teresa, ya te queda poquito... mucha suerte!!! Gràcies també a tots aquells que hi éreu quan jo vaig començar, però que ara esteu a una altra banda: a la Núria, pel teu suport al llarg d'aquests anys... ens seguirem trobant a la plana, a Zurich o a on la vida ens porti! A la Patri, l'Elisabet, el César (ara que estàs en forma, hem de repetir les escapades a la muntanya!), i a la Carolina. Ja saps que, encara que no hi sigui ni respongui mai, sempre estic a l'altra banda! Muntanyes de llibres amb il·lustracions ens esperen per poder-los llegir junts! I també a tots els passavolants que heu deixat empremta al grup: Maria, Oriol, Esther, Marta, Mercè, Dani, Marta, Xènia i Sara... y como no, a Karina!!! Compartir aquellos ocho meses contigo fue fantástico! Gracias por ser como eres... Gentileza gera gentileza... Nos vemos pronto!!!

Vull donar les gràcies també a la resta de companys del Grup de Física de Radiacions i a l'administració de l'ICTA i de Física. Un gràcies molt especial pel Manel, ja saps que a darrere de qualsevol èxit sempre hi ha algun dels teus invents.

Moltes gràcies també als òptics: al Jordi, al Menchi i al Bensi. Gràcies per les estones compartides, per la vostra alegria, pels cafès, dinars, sopars, partits, spinnings... Per cert, tenim una partida de "Valentir la flota" pendent! Mil gràcies!!!

Un agradecimiento muy especial a todo el equipo del IMEDEA (Gotzon, Antonio, Toni, David, Ana, Itzi, Sergio, Joan, José Maria y Cayetana). Gracias por los muestreos inolvidables que hicimos en Mallorca y Menorca! En particular, a Gotzon y a Antonio, por impulsar estos proyectos, por vuestras sugerencias y por el soporte constante. Es un placer trabajar con vosotros. Y, como no, a Ana, la mejor técnico del mundo! Gracias por tu ayuda y por tu sonrisa permanente!... y a David, el único galaico-murciano-balear que conozco… ya sabes que "hay otras formas de vivir, pero son peores".

Muchas gracias también a José Antonio Domínguez, a Bruno Ballesteros y a Miguel Mejías, del IGME por su colaboración indispensable en el proyecto de la Marjal de Peníscola. I parlant de la marjal, moltes gràcies també al Mario Zarroca i al Rogelio Linares, per la seva ajuda constant i disponibilitat, i per descobrir-nos la importància de l'*infierno*…

My acknowledgements to Yishai Weinstein, for his advices, ideas and comments on the manuscript, and to Mor Feldman, for her help in the cruise and in analyzing the samples. I would also like to thank Toste Tanhua for giving me the opportunity to be involved in the Meteor cruise and to all the crew. I will never forget that cruise!!! My acknowledgements to Pieter van Beek, Micha Rijkenberg and Michele Guida for providing me with samples or data along the Mediterranean Sea.

I would also like to sincerely acknowledge Bill Burnett, Kirch Cochran, Henry Bokuniewicz, Billy Moore and Natasha Dimova for hosting me in their institutions, and also Jan Scholten to help me preparing the Ra standards. My honest gratitude for your assistance and the valuable instructions and advices you gave me. Many thanks also to Christina Heilbrun. I'd like to give special thanks to Chiu, for his friendship and help during the days I spent in Tallahasse!

També vull expressar la meva gratitud a totes aquelles persones que han participat activament en la meva recerca en aquests anys de doctorat, encara que la seva col·laboració no estigui directament lligada en els projectes que conformen aquesta Tesi Doctoral; gràcies a l'Elisa Berdalet, la Marta Estrada, la Norma Neszi, la Laia Viure, el Walter Geibert, l'Esther Garcés, l'Albert Reñé, el Joan Bach i, en especial, a l'Albert Folch. Tenim moltes coses pendents!!!

Un gràcies molt especial a tota aquella gent que, fora de la vida universitària, han permès que això tirés endavant. Pels ànims, pel suport i la comprensió però, sobretot, per ajudar-me a gaudir de tot aquest temps! En especial, gràcies als Erolencs (Mui, Anna, Uri, Uri, Elsa i Xevi)... aquesta tesi va començar amb vosaltres!!! Gràcies pels 9 anys que hem passat junts i per la infinitat d'històries surrealistes que hem compartit. No al genocidi, panarolesc! Enc! Livol! Livolenc! Gràcies també als companys d'Ambientals, als que ens veiem sovint i als que en algun moment ens hem deixat de veure. Qui sap si tot això hauria començat sense vosaltres... I un gràcies molt especial als amics de Sant Feliu, els que hi heu estat sempre (Miquel, Meri, Guillem, Mònica, Joan, Lluís, Joan) i els que heu arribat més tard, però espero que per quedar-vos-hi (Jairo, Susanna, Joan Ramón, Pep, Elisenda, Joan, Eli, Quim i Anna).

I per acabar, vull donar les gràcies a tota la meva família. En especial, als meus pares i al Daniel, perquè si he arribat a on sóc és només gràcies a vosaltres. Gràcies per ser al meu costat sempre que us necessito, gràcies per tot! Aquesta tesi també és vostra!!! Encara que no us ho digui mai, us estimo moltíssim!!! Gràcies també a l'Assumpta i l'Albert i, molt especialment, a la Berta.

I ara sí, per acabar, gràcies Laura! Gràcies per tots aquests anys! Gràcies per fer-me costat, per ser-hi sempre. Gràcies per animar-me quan m'ha calgut, gràcies per fer-me riure. Gràcies per compartir amb mi bones i males experiències. Gràcies per les aventures que hem viscut junts, i per les que hem de viure! Gràcies per estimar-me. Gràcies per fer-me feliç!

Table of contents

List of figures

List of tables

PREFACE

The occurrence of fresh groundwater discharge to the sea has been recognized for more than 2000 years, since the time of the Roman Empire (Taniguchi et al. 2002; Burnett et al. 2006). The Roman geographer Strabo (63 B.C. to 21 B.C.) described a submarine spring four kilometers offshore from the Syrian coast (Kohout 1966). Water from this spring was collected from a boat and used as a source of freshwater (Taniguchi et al. 2002). In the 1st century A.D., Pliny the Elder included an extensive list of submarine springs in the Black Sea and in the Mediterranean Sea in his encyclopedia *Natural History* (Moore 2010b). For many years, the investigation on fresh groundwater inputs into the sea was exclusively related to water resource purposes and, scientifically, groundwater discharge to the coastal zone was neglected because of the difficulty in its assessment and the perception that the process was unimportant (Burnett et al. 2006).

However, Submarine Groundwater Discharge (SGD) has received increased attention during the last few decades since it was recognized that it may be both volumetrically and chemically important (Johannes 1980; Moore 1996a). There is now growing consensus and awareness that SGD, that includes both fresh groundwater and recirculated seawater, may represent an important pathway for material transport from land to the ocean, beyond the actual discharge of water, playing a relevant role in coastal ecology and geochemical cycles of several compounds (nutrients, metals, carbon, pollutants…). This growing interest on SGD has lead to a rapid increase in the SGD literature during the last years as well as the publication of several review articles (Burnett et al. 2003, 2006; Slomp and Van Cappellen 2004; Swarzenski 2007; Charette et al. 2008; Moore 2010b; Knee and Paytan 2011; Santos et al. 2012) and five recent journal special issues that focus on this topic (*Biogeochemistry* 66, pp. 1-202, 2003; *Marine Chemistry* 109, pp. 250-408, 2008; *Estuarine Coastal and Shelf Science* 76, pp. 455-552, 2008; *Journal of Environmental Radioactivity* 101, pp. 519-588, 2010; *Marine Chemistry* 156, pp. 1-152, 2013).

SGD-related research conducted within the last years has been mainly focused on the development of new techniques to detect and quantify SGD, measurements of SGD flows at various sites worldwide and the characterization of chemical fluxes associated

to SGD. In this context, radium isotopes (^{223}Ra, ^{224}Ra, ^{226}Ra, ^{228}Ra) have emerged as powerful tools to estimate SGD fluxes (Moore 1996a, 1996b, 2003).

Although relevant improvements on the understanding of the magnitude and significance of SGD have been achieved during the last two decades, several issues related to this process are still insufficiently studied. For instance, more information is required regarding chemical fluxes (e.g. nutrients, metals, carbon) associated to SGD and their impact on coastal ecosystems. Particularly, there is a lack of detailed assessments on the role of SGD as a source of chemical constituents into oligotrophic and semi-arid regions, such as the Mediterranean Sea. In these areas, SGD may be particularly relevant because external nutrient sources are scarce and surface runoff may be insignificant for large periods. Therefore, SGD could be a major and stable pathway for terrestrial compounds to reach the coastal sea. There is also a shortage of large-scale SGD estimates, from both basin and global perspectives. Indeed, one of the major current challenges of the SGD community is estimating the magnitude of the SGD flow at a global scale, as well as its associated inputs of nutrients, metals and other compounds. The quantification of chemical fluxes at the land-ocean interface is part of the overriding goals of the GEOTRACES program (www.geotraces.org), as they are essential to understand the main sources and distribution of these compounds in the ocean.

The present PhD Thesis is overall motivated by the potential relevance of SGD in Mediterranean coastal areas, where limited assessments on SGD-associated chemical fluxes have been carried out, and where we lack of a basin-wide estimate of the magnitude of SGD.

OBJECTIVES

The overall objective of this Thesis is the evaluation of the importance of Submarine Groundwater Discharge (SGD) to the Mediterranean Sea by using Ra isotopes, from both local and basin-wide perspectives, and its role as a source of dissolved chemicals to this basin. This main goal is addressed through three specific aims:

1. The study of contrasting Mediterranean coastal environments to evaluate the magnitude of SGD and testing the appropriateness of Ra isotopes as tracers of SGD in different hydrogeological settings. The selected environments consist of:
    a. A coastal wetland, nourished by various groundwater sources (Peníscola marsh, Castelló)
    b. A semi-enclosed karstic embayment, characterized by the presence of fine sediments that are frequently resuspended (Port of Maó, Minorca, Balearic Islands)
    c. A detrital bay, open to the sea (Palma Bay, Majorca, Balearic Islands).

2. The quantification of fluxes of nutrients and trace metals driven by SGD into a Mediterranean coastal area (Palma Bay (Majorca, Balearic Islands)) and the evaluation of the influence of SGD on the coastal budgets of these compounds.

3. The assessment of the magnitude of SGD and the associated inputs of nutrients into the entire Mediterranean Sea.

THESIS STRUCTURE

This dissertation is organized in seven chapters:

Chapter 1 is a general introduction to the topic of SGD. This chapter is divided in three main sections:

i) A general description of the concept of SGD, including its definition, magnitudes, components and driving forces, its importance and the methodologies commonly used to detect and quantify it.
ii) An introduction to the application of Ra isotopes as tracers of SGD.
iii) A synthetic review of the existing literature on SGD into the Mediterranean Sea.

The analytical techniques used for the determination of Ra isotopes in water samples are described in ***Chapter 2***. The methods include the use of the Radium Delayed Coincidence Counter (RaDeCC) to quantify short-lived radium isotopes (^{223}Ra and ^{224}Ra) and the quantification of long-lived radium isotopes (^{226}Ra and ^{228}Ra) by gamma spectrometry. Specific procedures used in some of the studies carried out in this work to determine the concentrations of radon (^{222}Rn), metals, nutrients and chlorophyll *a* are also briefly described in this chapter.

Chapters 3 to 6 correspond to 4 independent studies, two of them already published. In ***Chapter 3*** we estimate the contribution of distinct groundwater sources to a Mediterranean coastal wetland (Peníscola marsh, Castelló) by using Ra isotopes, ^{222}Rn and salinity measurements. The effectiveness of these tracers of SGD is tested by comparing the obtained results with direct measurements from propeller flow meters. This study was published in the *Journal of Hydrology* in 2012[1].

The influence of sediments on the radium-derived estimations of SGD into a coastal environment is evaluated in ***Chapter 4***. Mass balances for both short- and long-lived radium isotopes are built for the waters of the Port of Maó (Minorca, Balearic Islands), a natural shallow harbor covered by muddy sediments and subject to frequent sediment resuspension events. This study shall be submitted for publication[2].

Chapter 5 is devoted to the study of SGD from a detrital coastal aquifer into the adjacent bay of Palma Beach (Majorca, Balearic Islands). SGD fluxes of nutrients and

trace metals to Palma Beach are also estimated, with the purpose of assessing the role of SGD on the coastal budgets of these compounds and the potential implications in the regulation of nearshore phytoplankton communities. This work was published in *Marine Chemistry* in 2014[3].

The magnitude of SGD into the entire Mediterranean Sea is estimated in ***Chapter 6*** by using a mass balance of ^{228}Ra. The SGD-driven flux of dissolved inorganic nutrients (nitrogen, phosphorous and silica) into the basin is also evaluated in this section. Additional information on the data and calculations conducted to derive the final estimates is provided in the Appendix of this dissertation. This study has been recently submitted for publication[4].

The general and most significant conclusions of this dissertation are delineated in ***Chapter 7***, where a number of future research directions are also explored.

---

[1] Rodellas, V., Garcia-Orellana, J., Garcia-Solsona, E., Masqué, P., Domínguez, J.A., Ballesteros, B.J., Mejías, M., Zarroca, M., 2012. Quantifying groundwater discharge from different sources into a Mediterranean wetland by using ^{222}Rn and Ra isotopes. J. Hydrol. 466-467, 11-22.

[2] Rodellas, V., Garcia-Orellana, J., Masqué, P., Basterretxea, G. Submarine Groundwater Discharge into a coastal embayment: the influence of sediments on radium-derived estimates. In preparation.

[3] Rodellas, V., Garcia-Orellana, J., Tovar-Sanchez, A., Basterretxea, G., Masqué, P., Garcia-Solsona, E., Sánchez-Quiles, D., López, J.M., 2014. Submarine Groundwater Discharge as a source of chemical compounds to a Mediterranean bay (Palma Beach, Balearic Islands). Mar.Chem., 160, 56-66.

[4] Rodellas, V., Garcia-Orellana, J., Masqué, P., Feldman, M., Weinstein, Y. Submarine Groundwater Discharge: a major source of nutrients to the Mediterranean Sea. Submitted.

CHAPTER 1

Introduction

1.1. Submarine Groundwater Discharge

The most general and widely cited definition of groundwater is "water within the saturated zone of geologic material" (e.g. Tolman 1937; Nelson and Nelson 1967; Pfannkuch 1969; Freeze and Cherry 1979; Bates and Jackson 1984; Fetter 1988; Kearey 1996; Jackson et al. 2005). Defining groundwater as "any water in the ground", regardless to its composition (e.g. salinity) or its origin, allows avoiding unnecessary conceptual problems. This is particularly pertinent when examining processes occurring in the coastal zone, where subterranean fluids from terrestrial (fresh) and oceanic (saline) origin grade into each other (Burnett et al. 2003).

Based on the definition of groundwater, Burnett and coauthors (2003) defined Submarine Groundwater Discharge (SGD) as "any and all flow of water on continental margins from the seabed to the coastal ocean, regardless of fluid composition or driving force". When sediments are saturated, water in the pores of submerged sediments (porewater) is therefore synonymous with groundwater (Burnett et al. 2003). Similarly, all saturated permeable material in the coastal zone and on the continental shelf are classified as aquifers (Charette et al. 2008). Thus, advective porewater exchange through coastal sediments is included in this definition of SGD (Moore 2010b). Processes such as deep-sea hydrothermal circulation, fluid expulsion at convergent margins and density-driven cold seeps on continental slopes are excluded from the definition of SGD (Burnett et al. 2003). The broad definition of SGD would technically include small- (cm) and short (minutes) - scale mechanisms of pore water flow, such as bioirrigation or shear flow, that are usually not quantified using the commonly used SGD techniques and models (Santos et al. 2012). Moore (2010a) proposed a new definition of SGD that excludes these small scale processes: "SGD is the flow of water through continental margins from the seabed to the coastal ocean, with scale lengths of meters to kilometers, regardless of fluid composition or driving force" (Fig. 1.1).

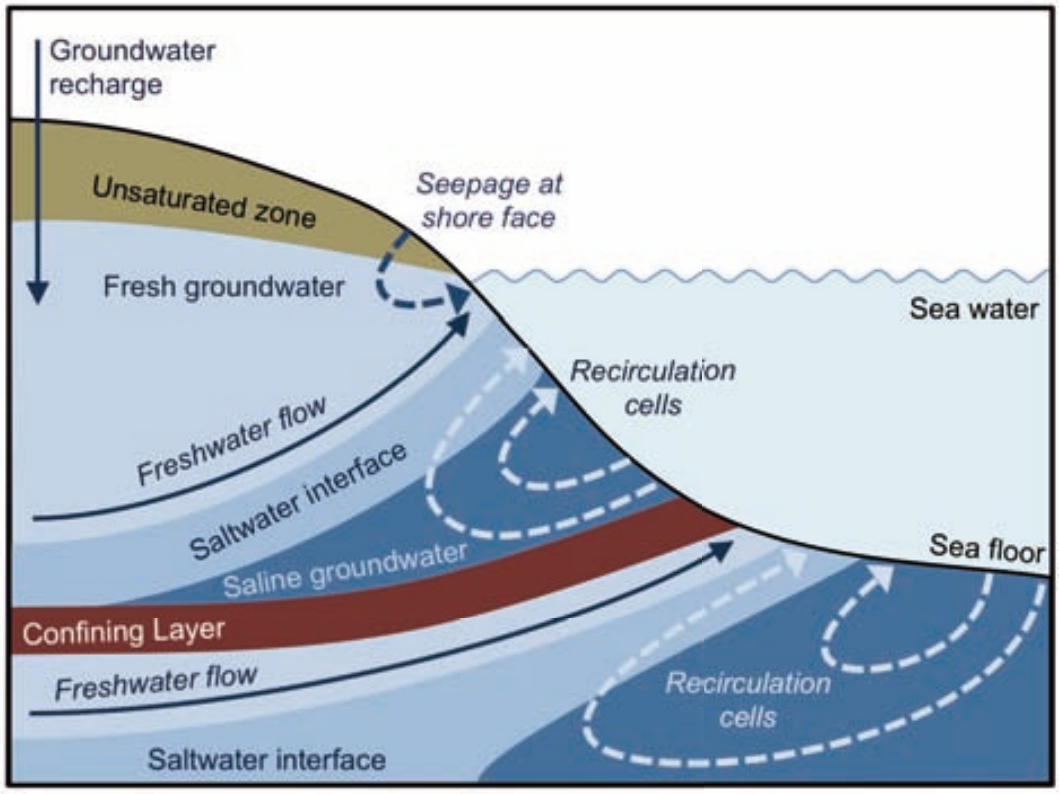

Figure 1.1. Principal pathways for submarine groundwater discharge to the coastal ocean, including fresh groundwater discharge and recirculation of seawater through the coastal aquifer (saline groundwater). Connate waters are excluded from this representation (based on Charette et al., 2008).

1.1.1. Components of SGD

SGD can inflow to the coastal sea as a mixture of three main components (Taniguchi et al. 2002; Burnett et al. 2003): i) meteoric fresh groundwater flow originated from inland recharge; ii) former seawater that circulates through the coastal aquifer (saline groundwater); and iii) connate groundwater, i.e. groundwater whose salinity has been raised by dissolution of salts within the aquifer. The two former fractions are the most common in coastal settings, and hence SGD usually represents a mixture of fresh groundwater and recirculated seawater flows. The cycling of fresh-saline groundwater mixtures trough coastal sediments or aquifers largely depends on a composite of terrestrial and marine forces, as well as the nature of coastal settings, that may consist of complicated assemblages of confined, semi-confined, and unconfined systems (Moore 1999). Moore (1999) introduced the term "subterranean estuary" to describe that part of the coastal aquifer where meteoric fresh groundwater mixes with seawater that has inundated the aquifer through a free connection to the sea (saline groundwater). Such subterranean estuaries are dynamic mixing zones characterized by

biogeochemical reactions that influence the transfer of freshwater, nutrients, metals, carbon and other constituents to the coastal zone in a similar manner to that of surface estuaries (Moore 1999; Charette and Sholkovitz 2002; Talbot et al. 2003; Beck et al. 2010; Gonneea et al. 2014)

1.1.2. Drivers of SGD

The magnitude and location of SGD result from a complex interplay of the characteristics of the coastal settings, with a long list of disparate physical forces (Moore 2010b). Factors influencing SGD related to coastal settings include aquifer characteristics (e.g. porosity, permeability, hydraulic conductivity, homogeneity of the aquifer substrate, the presence of fractures or other preferred flow paths) and geomorphology (e.g. beach morphology or the presence and level of development of stream systems) (Burnett et al. 2003; Knee and Paytan 2011). The major physical forces, either terrestrial or marine, that drive groundwater flow through the coastal aquifer include (Burnett et al. 2006; Santos et al. 2012) (Fig. 1.2):

i) The terrestrial hydraulic gradient, which is the major factor that determines the flux of terrestrially-derived fresh groundwater discharge into the coastal ocean (Alley et al. 2002; Holliday et al. 2007; Stieglitz et al. 2008b). It mainly reflects the terrestrial groundwater recharge rate, which is influenced by precipitation, evapotranspiration and the geological matrix (Burnett et al. 2003).

ii) Seasonal oscillations on the terrestrial water table elevation, which may drive saline water recirculation in coastal aquifers (Michael et al. 2005). The water table oscillations in response to seasonal recharge cycling lead to amplified changes on the fresh-saline groundwater interface depth, which in turn may drive large seasonal flows of seawater in and out of the coastal aquifer.

iii) Tidal pumping (Nielsen 1990; Robinson et al. 2007; Santos et al. 2010; Wilson and Morris 2011), wave setup (Li and Barry 2000; Horn 2006), large storms (Moore and Wilson 2005; Wilson et al. 2011) or sea level fluctuation (Lee et al. 2013). Induced pressure gradients in the nearshore zone shall then drive seawater recirculation through coastal sediments. All these processes basically result in seawater infiltration at the beach face when sea level is high (e.g. flood tide) and porewater discharge when sea level decreases (e.g. ebb tide).

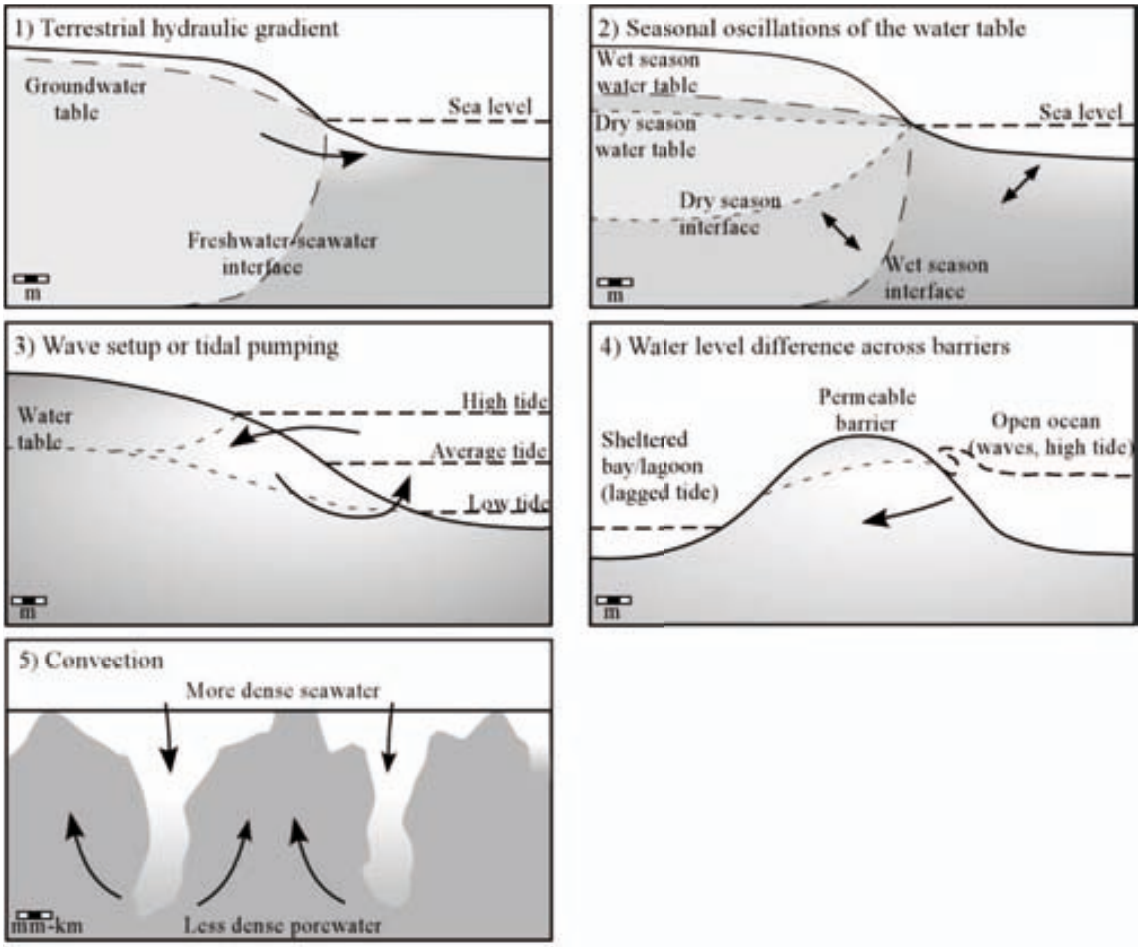

Figure 1.2. Schematic illustration of the major drivers of submarine groundwater discharge through permeable sediments. The terrestrial hydraulic gradient (and, eventually, convection) is the only driving force that results in the input of "new" fresh groundwater to the coastal ocean (Santos et al. 2012).

iv) Water level difference across permeable barriers, which can also induce a subterranean water flow (Bokuniewicz and Pavlik 1999; Reich et al. 2002; Chanton et al. 2003; Rapaglia et al. 2010b). The most common case is the sandy barriers that partially isolate coastal water bodies, such as lagoons, from the ocean. When there is a lag between the ocean and lagoon level oscillations, the hydraulic gradient between both systems induces porewater flows across the barrier.

v) Density-driven convection of porewaters that may develop when the salinity or temperature of the porewaters differs from that of the overlying seawater. Porewater recirculation induced by convection may occur as a consequence of fresh groundwater underlying seawater (Smith 2004), temperature inversions or rapid cooling of the ocean (Moore and Wilson 2005), seasonal salinity

variations in estuaries (Webster et al. 1996), heating of the intertidal sediments during low tide (Rocha 2000) or by large-scale geothermal heating of deep porewaters (Wilson 2005).

1.1.3. Spatial and temporal variability of SGD

Since SGD into the coastal areas results from a composite of spatially and temporally variable physical forces interacting with the geological matrix, the magnitude and the chemical composition of SGD can vary greatly in space and time (Knee and Paytan 2011). SGD in homogeneous aquifers is expected to decrease exponentially with distance from the coast (Bokuniewicz 1980; Fukuo and Kaihotsu 1988; Cable et al. 1997b). However, aquifer heterogeneity can generate preferential flow paths that favor groundwater discharges offshore (Cable et al. 1997a; Burnett et al. 2001c; Taniguchi et al. 2003; Bokuniewicz et al. 2004), such as submarine springs in karst or volcanic systems (Swarzenski et al. 2001; Fleury et al. 2007; Peterson et al. 2009) or leakages of fluids from confining layers (Moore 2010a). Specific site features, such as the presence of natural embayments (Bokuniewicz et al. 2003) or anthropogenic constructions that can cut through confining units (Stieglitz et al. 2007), can also result in highly heterogeneous spatial SGD patterns. In addition, the interaction of different SGD driving forces, acting at different spatial scales, can cause patchy flows even in homogeneous aquifers (Santos et al. 2012) (Fig. 1.3).

The temporal variation in SGD rates has been observed at different timescales (semi-diurnal, diurnal, fortnightly, seasonal or even longer cycles) as a result of changes in the driving forces (Knee and Paytan 2011). Seasonal differences in the water table elevation resulting from variations in precipitation, evapotranspiration or anthropogenic groundwater extraction, may result in seasonal variability of the SGD flows, particularly the fresh component (Oliveira et al. 2006; Charette 2007; Young et al. 2008; Garcia-Solsona et al. 2010b; Heiss and Michael 2014) (Fig 1.4). Greatest SGD flows are thus generally expected during or after (depending on the lag between rainfall recharge and groundwater discharge) the wet season. Seasonal oscillations on the water table elevation can also induce large saline flows in and out of the coastal aquifer (Michael et al. 2005). Changes in the sea-surface height between high and low tide result in variations on the hydraulic gradient between land and sea, which can lead to semi-diurnal or diurnal variations in SGD (Michael 2003; Sholkovitz et al. 2003;

Shellenbarger et al. 2006). Differences between the spring and neap tidal range can also provoke variations on the tidal pumping through the subterranean estuary (Kim and Hwang 2002; Boehm et al. 2004; Rapaglia 2005; Sieyes et al. 2008). And storm surges (Moore and Wilson 2005; Wilson et al. 2011) or global climate variations resulting in sea level change (Lee et al. 2013) can also lead to a short- or long-term, respectively, variations on the SGD flow. Importantly, temporal and spatial changes of SGD do not only affect the quantity of groundwater discharge, but also the chemical flux inflowing to the coastal ocean (Taniguchi et al. 2003; Knee and Paytan 2011).

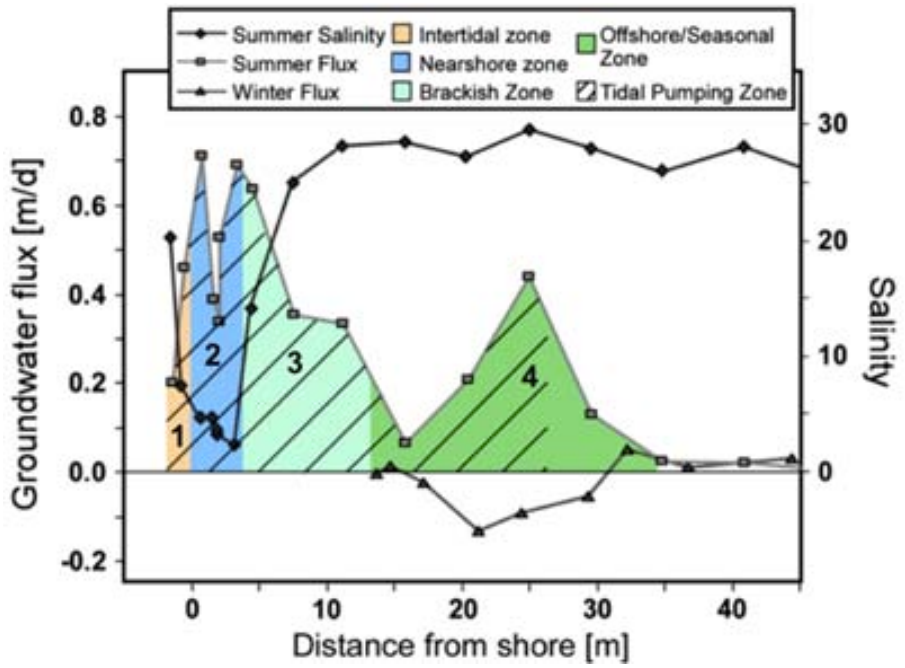

Figure 1.3. Groundwater flux, measured by seepage meters, and salinity along a transect offshore (Waquoit Bay, MA, USA). Colors represent distinct discharge areas, designated based on location and salinity of the flow, and mainly driven by different forcing mechanisms: 1) Intertidal saline circulation driven by tides and wave setup; 2) Fresh groundwater flow driven by terrestrial hydraulic gradient; 3) Offshore saline exchange driven by tides and waves and density driven saline recirculation; 4) Saline exchange driven by movement of the interface on seasonal or other timescales (Michael et al. 2011).

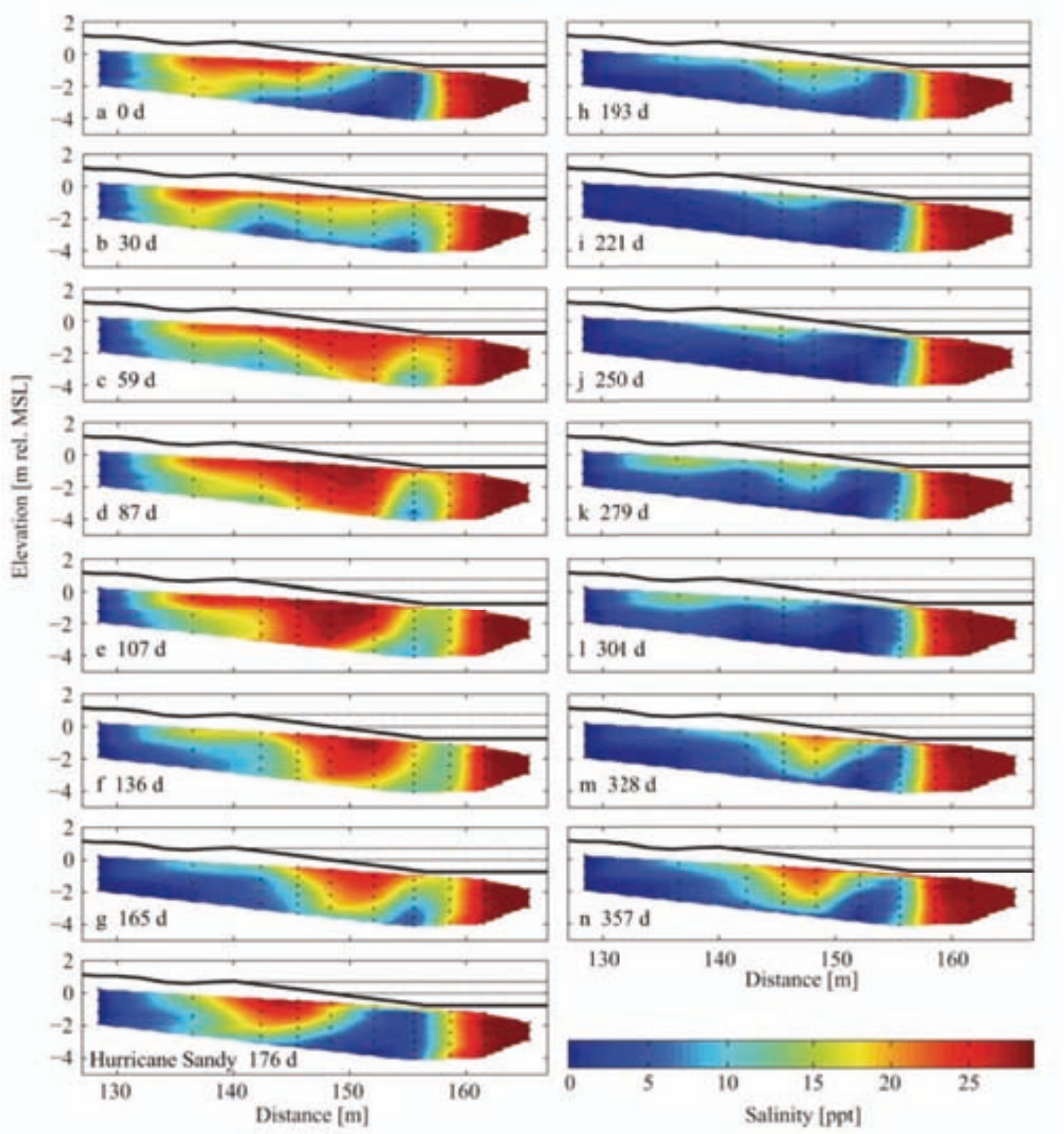

Figure 1.4. Monthly porewater salinity over a 1 year sample period in the intertidal zone of a sandy beach aquifer (Cape Henlopen, DE, USA). Differences on saltwater-freshwater mixing dynamics in the coastal aquifer over tidal, spring-neap and seasonal cycles result in SGD variable in both magnitude and composition over multiple time scales (Heiss and Michael 2014).

1.1.4. Magnitude of SGD

The discharge of fresh groundwater occurs where a coastal aquifer with a positive head relative to sea level is hydraulically connected with the sea through permeable rocks or bottom sediments (Johannes 1980). Moreover, the recirculation of former seawater driven by tides or waves trough the coastal aquifer is also expected to occur at any coastal system. SGD is thus a ubiquitous phenomenon on a global scale (Knee

and Paytan 2011). However, the magnitude of SGD can vary considerably from site to site: SGD ranging from 10^5 to 10^8 $m^3 \cdot km^{-1} \cdot yr^{-1}$ have been reported in local studies (scale lengths of ~1 km) (Charette et al. 2008; Moore 2010b). SGD estimates derived from regional studies (10 – 300 km) are generally larger, ranging from 10^7 to 10^9 $m^3 \cdot km^{-1} \cdot yr^{-1}$; (Charette et al. 2008)). These differences are frequently attributed to the fact that local-scale studies focus on near-shore discharge and may not capture SGD inflowing across the continental shelf (e.g. groundwater springs or seeps, recirculation flows), which may represent a significant fraction of the total SGD (Charette et al. 2008; Moore 2010a). Another study have also evaluated the magnitude of SGD into the entire Atlantic Ocean, estimating a SGD flow of $(2\text{-}5) \cdot 10^8$ $m^3 \cdot km^{-1} \cdot yr^{-1}$ (Moore et al. 2008) .

SGD flows in local studies are typically lower in magnitude than river inputs at locations where large rivers are present (Charette and Buesseler 2004; Ollivier et al. 2008; Liu et al. 2012), but in certain settings, such as karst terrains (Young et al. 2008; Garcia-Solsona et al. 2010b; Mejías et al. 2012), volcanic islands (Street et al. 2008; Knee et al. 2010) or areas with non-permanent stream systems (Shellenbarger et al. 2006; Weinstein et al. 2007), SGD can be the major, or even the only, hydrologic connection between land and sea (Knee and Paytan 2011). In regional or basin-wide studies, that integrate long coastlines of continuous discharge in space, reported SGD was comparable or considerably higher than riverine water inputs: SGD to the South Atlantic Bight (southeastern coast of North America, ~600 km) was 3 times greater than the river flow into this area (Moore 2010a), whereas SGD to the Atlantic Ocean represented 80 -160% of the total river discharge to the Atlantic basin (Moore et al. 2008).

On a global scale, estimates based on hydrological considerations and water balance approaches yielded a terrestrially-derived fresh SGD flow of $(0.1 – 6.5) \cdot 10^{12}$ $m^3 \cdot yr^{-1}$, accounting from 0.2 to 10 % of the total surface water inputs (Taniguchi et al. 2002; Burnett et al. 2003; Zektser et al. 2007). However, the magnitude of the total (including saline groundwater) SGD flow on a global scale is still unknown. Riedl and coauthors (1972) estimated that water pumping alone can recirculate $\sim 100 \cdot 10^{12}$ $m^3 \cdot yr^{-1}$, evidencing the relevance of seawater circulation through coastal marine sediments. A more recent study conducted by Santos et al (2012) roughly quantified the global magnitude of groundwater exchange through permeable sediments, resulting in a flow on the order of $(10–1{,}000) \cdot 10^{12}$ $m^3 \cdot yr^{-1}$.

1.1.5. Importance of SGD

a) Hydrogeological importance

Determining the amount of fresh groundwater discharging to the sea is a major concern for hydrogeologists and coastal managers, as it relates to the freshwater reserve in coastal aquifers and its salinization (Moore 2010b). Since water of proper quality is one of the human primary needs and a crucial resource for societal and economical development, the discharge of fresh groundwater to the coastal sea may be considered as a waste, as the fresh SGD has the potential to be used as freshwater sources (UNESCO 2004). The utilization of coastal (and submarine) groundwater can be a relevant source for drinking water, particularly in those regions where access to suitable freshwater resources is limited or non-existing and thus desalination of seawater has been the most or only realistic solution to meet the increasing water demand (Bakken et al. 2011). Even if the captured water is not entirely fresh, the costs of extracting and desalinating coastal groundwater seem to be economically competitive with traditional desalination of seawater (Bakken et al. 2011). However, overexploitation of coastal water resources can cause problems like groundwater depletion or terrain subsidence, seawater intrusion or aquifer degradation. Therefore, assessing the optimum utilization of coastal water reserves first requires an appropriate knowledge of the aquifer water balance and its associated hydrogeological processes, including an accurate estimation of the fresh SGD (Werner et al. 2011). Coastal aquifer management also demands a comprehensive understanding of the interactions between terrestrial and marine environments, since seawater intrusion is one of the major threats of the coastal freshwater resources (Fisher 2005). Finally, a detailed knowledge of the role played by groundwater discharges to coastal water bodies (particularly coastal lagoons, wetlands or lakes) is also needed to understand the current decline or degradation of coastal water bodies, as well as to substantiate decisions on hydrological policies devoted to its preservation or restoration (Zektser et al. 2007).

b) Biogeochemical importance

In addition to a source of freshwater to the coastal sea, SGD is recognized as an important mechanism for transferring material from the land to the ocean (Moore 1996a, 1999). Concentrations of dissolved compounds (nutrients, metals, carbon,

pollutants…) are typically higher in groundwater than in most terrestrial surface water, and thus SGD often represents a large contribution to the flux of dissolved constituents to the coastal sea (Burnett et al. 2006). The enhanced concentrations of dissolved compounds in SGD may result from natural (e.g. vegetation, soils, rocks, microorganism) or anthropogenic (e.g. sewage, mining waste, agricultural or industrial land uses) enrichment of terrestrial groundwater (Knee and Paytan 2011). In addition, when the terrestrially-derived groundwater mixes with intruded seawater within the coastal aquifer (i.e. the subterranean estuary), biogeochemical reactions between the mixed waters and aquifer solids modify the fluid composition of SGD, resulting in SGD fluids chemically distinct from both the fresh groundwater and seawater endmembers (Moore 1999). The reactions occurring in the subterranean estuary include desorption of ions from adsorbed sites due to increases of ionic strength, dissolution and precipitation of carbonates, remineralization of organic matter leading to carbon, nutrient and metal release, and oxidation-reduction reactions that produce and consume metal oxides, which can release or sequester other ions (Moore 2010b). Therefore, the total SGD (not only fresh groundwater, but also recycled seawater) needs to be considered when estimating material fluxes between land and sea. Indeed, even the tidally-modulated recirculation of seawater through sandy sediments (traditionally thought as geochemical desserts) can result in significant biogeochemical fluxes to the coastal sea (Gibbes et al. 2008; Anschutz et al. 2009; Santos et al. 2012).

Given that diffusive seepage of groundwater and recirculation of seawater trough permeable sediments occur almost everywhere, most of the coastal zones are subject to inputs of dissolved constituents (e.g. nutrients, trace metals or carbon) from SGD (Johannes 1980; Church 1996; Moore 1996a). Inputs of dissolved compounds associated with SGD can have profound ecological implications for coastal ecosystems (e.g. eutrophication of coastal waters or recurrent harmful algal blooms) (Knee and Paytan 2011). Evaluating strategies to prevent or mitigate these outcomes requires identifying the sources of these compounds, as well as quantifying its relative contribution. A detailed knowledge of the SGD-related inputs of dissolved constituents into coastal waters is also a requisite to understand their local, regional and global budgets.

The inputs of different compounds via SGD as well as the impacts these constituents may have in coastal ecosystems are reviewed in the following subsections.

- *Nutrient fluxes*

Studies of nutrient fluxes from SGD usually focus on dissolved inorganic nitrogen species (DIN: nitrate, nitrite and ammonium), dissolved inorganic phosphorous (DIP: phosphate) and dissolved silica (DSi: silicate). Although inorganic fractions of nutrients are most likely forms to imping on coastal water biogeochemical cycles, focusing only on inorganic loading can underestimate inputs of bioavailable nutrients (Santos et al. 2009). Major sources of DIN and DIP to coastal groundwater are natural inputs from organic matter decomposition and mineral dissolution and anthropogenic inputs from fertilizer, manure and wastewater (Slomp and Van Cappellen 2004), whereas the major source of silicates to groundwater is the aquifer substrate (including rocks, sediments and soils) (Knee and Paytan 2011). While DSi is generally conservative in coastal aquifers (Corbett et al. 2002), biogeochemical reactions occurring in the subterranean estuary generally determine the removal, transformation and transport of DIN and DIP (Slomp and Van Cappellen 2004). Thus, aside from the sources of nutrients to groundwater, SGD-derived fluxes of nutrients to the coastal area will largely depend on chemical transformations occurring at the subterranean estuary. Several studies have shown that SGD is a major source of nutrients to coastal sites, particularly in those areas where SGD is the only pathway connecting land and sea, (such as, volcanic islands (Kim et al. 2003; Hwang et al. 2005a; Street et al. 2008), karstic locations (Young et al. 2008; Garcia-Solsona et al. 2010a, 2010b; Tovar-Sanchez et al. 2014) or areas with non-permanent stream systems (Shellenbarger et al. 2006)), but also in areas where rivers are present (Burnett et al. 2007; Liu et al. 2012; Charette et al. 2013) (Fig 1.5).

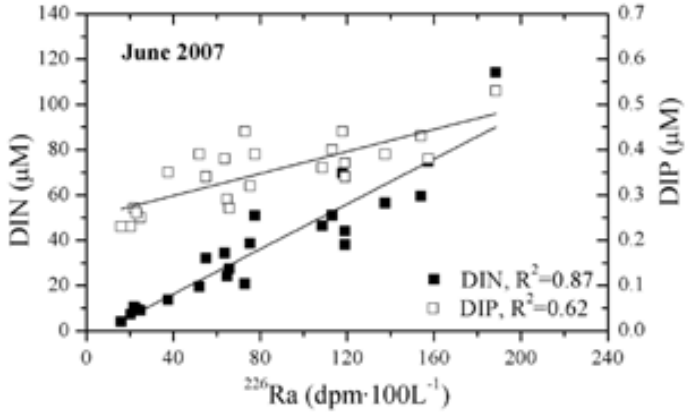

Figure 1.5. Relations between concentrations of dissolved inorganic nutrients (DIN and DIP) and ^{226}Ra activities (proxy for SGD) in coastal waters from a karstic area (Badum, Spain), revealing significant inputs of dissolved inorganic nutrients through SGD (Garcia-Solsona et al. 2010b).

Given that nutrient concentrations in SGD are often considerably higher than receiving water bodies, even small volumetric groundwater inputs can provide significant nutrient subsidies, leading to important ecological effects. SGD-derived inputs of nutrients may sustain the primary production and community composition of phytoplankton in coastal areas (Valiela et al. 1990, 1992; Lapointe 1997; Laroche et al. 1997; Paytan et al. 2006; Garcés et al. 2011) (Fig. 1.6.). However, large inputs of nutrients can impact the nutrient ratio in coastal waters and trigger phytoplankton blooms, promoting eutrophication of coastal waters (Paerl 1997; Hwang et al. 2005b; Tse and Jiao 2008) or supporting recurrent harmful algal blooms (Gobler and Sañudo-Wilhelmy 2001; Hu et al. 2006; Lee and Kim 2007; Lee et al. 2010; Su et al. 2013). SGD-driven nutrients have also been associated with damage to coral reefs and shifts from coral-dominated to macroalgae-dominated reef areas (Knee and Paytan 2011). It has also been suggested that high N:P ratios in SGD (P is more easily removed from groundwater than N) could drive the coastal ocean towards P-limitation, perhaps shifting the present ocean N-limited primary production (Slomp and Van Cappellen 2004).

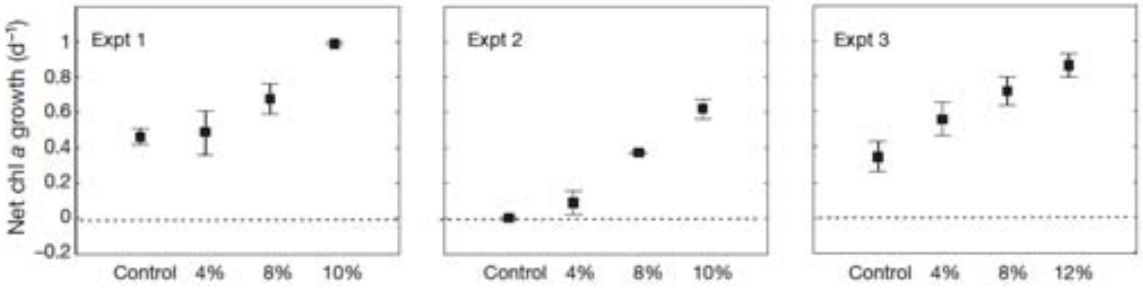

Figure 1.6. Mean (±SD) net growth rates of phytoplankton biomass, measured as Chla, following either the addition of different percentages of groundwater or no addition (control) in 3 experiments. Expt 1 and 3: addition of anthropogenically influenced groundwater extracted from 2 different sites; Expt 2: addition of low-impacted groundwater (Garcés et al. 2011).

- ***Trace metal fluxes***

Trace metals (such as Ag, Cd, Co, Cu, Fe, Hg, Ni, Pb or Zn) can become naturally enriched in groundwater due to its prolonged interaction with the metal-containing aquifer substrate, particularly in areas where the composition and conditions of the subterranean estuary favor the dissolution of significant amounts of metals (Knee and Paytan 2011). Human activities can also enhance the concentrations of trace metals in groundwater, via mining waste leachate, sewage from developed areas or as a

consequence of land reclamation (Martin and Pedersen 2002; Chen and Jiao 2007). Trace metals in groundwater do not behave conservatively along the seaward flow path in most circumstances, and they can be either released or removed from solution due to chemical reactions occurring within the subterranean estuary, usually modulated by pH, oxidation-reduction potential, salinity or the abundance of colloids and humic substances (Charette and Sholkovitz 2006; Beck et al. 2007b, 2010). The precipitation of iron oxides in the subterranean estuary due to the oxidation of ferrous iron-rich groundwater near the saltwater interface, the so called iron curtain, can also act as a geochemical barrier by retaining and accumulaiting other chemical species carried to the coast by groundwater (Charette and Sholkovitz 2002). Chemical cycling within the subterranean estuary, as well as the sources of trace metals to groundwater and the magnitude of SGD, will thus determine the flux of dissolved trace metals to the coastal ocean. Nonetheless, although locally depending on the magnitude of other potential sources, SGD has been recognized to be a major or even dominant source of trace metals to coastal waters in most of the locations where it has been evaluated. In particular, SGD has been shown to be a relevant source of dissolved Fe (Windom et al. 2006; Jeong et al. 2012), Hg (Bone et al. 2007; Black et al. 2009; Lee et al. 2011; Rahman et al. 2013), and other elements, such as Al, Co, Cu, Ni or Zn (Beck et al. 2009; Jeong et al. 2012; Tovar-Sanchez et al. 2014) (Fig. 1.7). For instance, SGD-derived Fe inputs along a 240 km coastline in southern Brazil were estimated to represent 10 % of the atmospheric Fe to the entire South Atlantic Ocean (Windom et al. 2006). On the other side, as a consequence of the nonconservative removal of some species when seawater recirculates through the subterranean estuary, SGD can also act as a sink of some trace metals, such as Mo (Beck et al. 2009) or As (Bone et al. 2006).

Dissolved trace metals supplied by SGD can serve as micronutrients necessary for ecosystem functioning, since they are involved in protein structures, electron transfer reactions and/or enzymatic processes (e.g. Mn, Fe, Co, Ni, Cu, Zn), but also as toxic agents that may interfere with proper functioning of enzymes and associated cofactors (e.g. Pb, Hg) (Morel and Price 2003; Torres et al. 2008; Twining and Baines 2013). Moreover, metals essential to biota may induce detrimental effects if their concentrations exceed threshold levels (Jordi et al. 2012). Thus, inputs of trace metals associated to SGD can support the growth of phytoplankton (Downs et al. 2008; Garcés et al. 2011), but also result in deleterious effects on marine plankton, altering primary production and community structure (Paytan et al. 2009; Jordi et al. 2012) and even

possess a threat to top predators and humans due to bioaccumulation at higher trophic levels (Laurier et al. 2007).

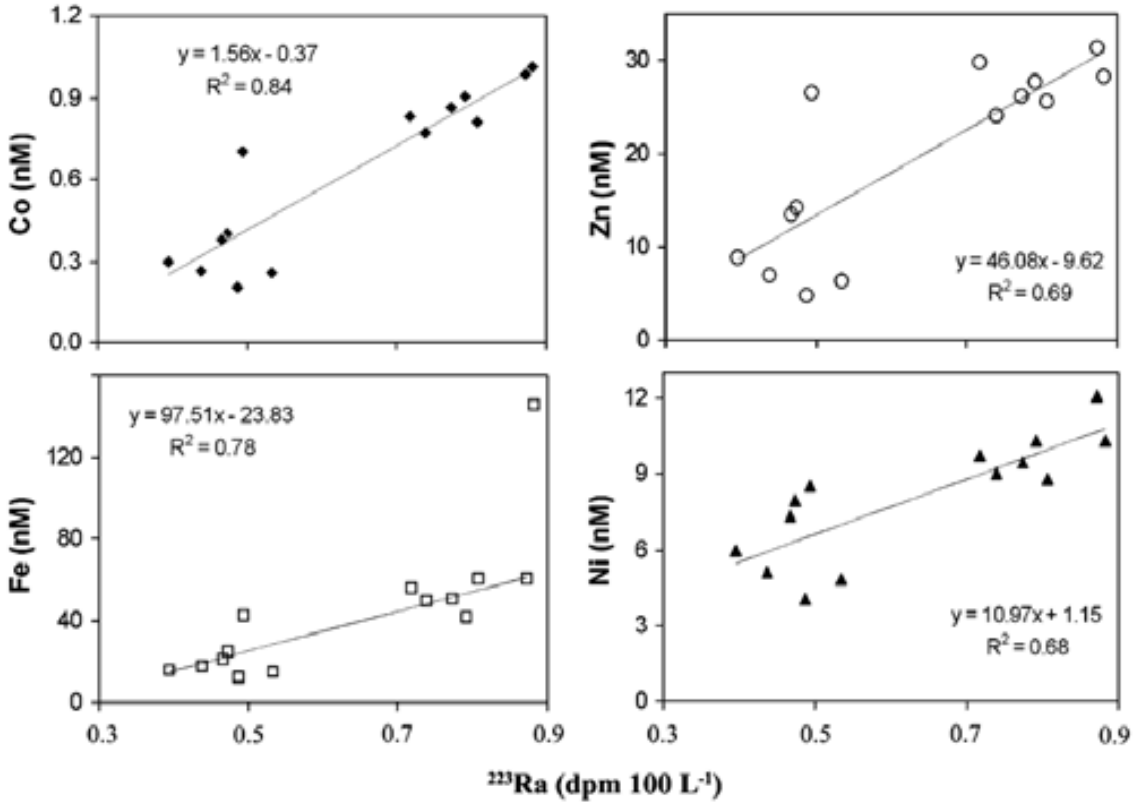

Figure 1.7. Covariation of ^{223}Ra, used as a proxy for SGD, and dissolved metals in bottom waters of Jamaica Bay (NY, USA), suggesting that SGD is an important source of dissolved Co, Zn, Fe and Ni to the Bay (Beck et al. 2009). . inputs of trace metal to the water column of ths binputs from SGD.

- ***Carbon fluxes***

SGD have been shown to be a relevant pathway for the transference of carbon from land to sea, since SGD may supply both dissolved inorganic carbon (DIC) (Cai et al. 2003; Moore et al. 2006; Basterretxea et al. 2010; Cyronak et al. 2014; Porubsky et al. 2014) and dissolved organic carbon (DOC) (Goñi and Gardner 2003; Burnett et al. 2007; Santos et al. 2009) (Fig 1.8). Inputs of DOC to the coastal ocean driven by SGD mainly result from groundwater enrichments related to decomposition of organic matter (Goñi and Gardner 2003). In both the subterranean estuary and the coastal ocean, DOC can fuel the biological activity and affect the behavior of metals (Knee and Paytan 2011). DIC (or CO_2) concentrations in SGD are mainly governed by aquifer characteristics (e.g. $CaCO_3$ dissolution) (Cai et al. 2003). Although only a small fraction of DIC in groundwater is exported to the coastal ocean (~90% is lost to the atmosphere; Cai et al.

2000), DIC fluxes of SGD may be comparable to riverine inputs in a regional scale, requiring its consideration in carbon coastal budgets (Cai et al. 2003; Moore et al. 2006). SGD-derived inputs of CO_2 can also influence the carbonate chemistry of coastal ecosystems, representing a positive feedback to the ocean acidification (i.e. decrease on pH) on a local scale (Cyronak et al. 2014). For instance, high pCO_2 in the water column derived from SGD may result in detrimental effects on coral health through a reduction in calcification rates (Cyronak et al. 2014).

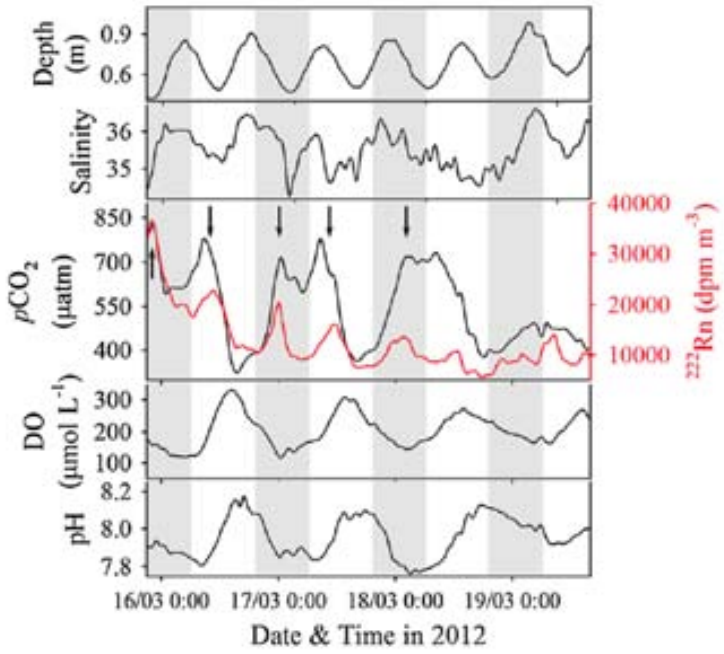

Figure 1.8. The pCO_2, dissolved oxygen (DO), ^{222}Rn (in red, used as a proxy for SGD), salinity and water column depth measured in the water column of a coral reef lagoon at Raratonga (Cook Islands) over 4 days. Gray bars represent nighttime ours and the arrows indicate times when pCO_2 and ^{222}Rn vary concurrently. Significant correlations between pCO_2 and both ^{222}Rn (positive) and salinity (negative) indicate that SGD is an important source of free CO_2 (Cyronak et al. 2014).

- ***Fluxes of other compounds and other impacts***

In addition to those trace metals mentioned above, SGD can also be a relevant source of other metals that are of special interest given their utility as tracers of environmental processes. These include barium (Ba), radium (Ra), strontium (Sr), uranium (U) and neodymium (Nd) and other rear earth elements, among others. Ba, which can be used as a geochemical proxy for ocean paleoproductivity (Dymond et al. 1992), is usually enriched in SGD. SGD-derived Ba inputs have been shown to be larger than riverine inputs (Moore 1997; Shaw et al. 1998) and may represent a major global source for Ba (Santos et al. 2011). Ra is extensively used as a tracer of SGD, mainly because SGD is its

major source to the coastal ocean (Moore 1996b) (see section 1.3). SGD supplies Sr with less radiogenic $^{87}Sr/^{86}Sr$ ratios than seawater, and may constitute a substantial component of the modern oceanic $^{87}Sr/^{86}Sr$ budget (Rahaman and Singh 2012; Beck et al. 2013). The oceanic Sr record can be used as a proxy of continental weathering, hydrothermal circulation and other inputs to the ocean (Capo et al. 1998). Because U can be removed in the subterranean estuary under reducing conditions, SGD can usually acts as a potential sink for U (Charette and Sholkovitz 2006; Moore and Shaw 2008; Beck et al. 2009; Santos et al. 2011). Although not a source, U removal due to recirculation of groundwater should also be considered in global budgets for U, which is used as a proxy of ocean redox state (Tribovillard et al. 2006). SGD-driven fluxes of Nd, used as tracer for water masses mixing and particle-seawater interactions (Lacan and Jeandel 2005; Garcia-Solsona et al. 2014), may also contribute considerably to the global budget of Nd in the ocean (Johannesson and Burdige 2007; Johannesson et al. 2011; Kim and Kim 2011, 2014). For most of these constituents, the impact of SGD on coastal and global inventories has yet to be accurately determined. However, studies conducted so far suggest that deficits in classic sources (e.g. Nd) and sinks (e.g. U) for budgets of these elements could be balanced when considering contributions from SGD (Johannesson and Burdige 2007; Charette et al. 2008; Kim and Kim 2014).

When groundwater is contaminated by sewage, SGD can also represent a pathway for fecal indicator bacteria (FIB) to enter coastal waters (Boehm et al. 2004; Paytan et al. 2004; Yau et al. 2014). FIB are not pathogens themselves, but some epidemiological studies have documented relationships between their concentrations and risk of water-born illness in bathers (Knee and Paytan 2011). SGD can add other constituents to coastal waters, such as caffeine, pharmaceuticals, personal care products or volatile organic compounds (VOCs), all of them commonly enriched in groundwater due to direct and indirect anthropogenic influences (Knee and Paytan 2011).

Inputs of chemicals associated to SGD can also drive other effects in coastal ecosystems. For instance, SGD containing H_2S, NH_4, CH_4, DOC and other reduced metals could contribute to hypoxia (Moore 2010b). SGD inflowing through coastal acid sulfate soils can result in local acidification of coastal waters (de Weys et al. 2011). SGD can also represent a relevant source of natural radioactivity to coastal waters, leading to significant increases of polonium (^{210}Po) and lead (^{210}Pb) in coastal fauna and flora (Garcia-Orellana et al. 2013).

1.1.6. Detection and quantification methods of SGD

Detecting and quantifying SGD can be complicated due to the inherent complexity of the discharge process: SGD can be diffuse and heterogeneous in space and time and occurs below the sea surface, where direct measurements or observations are difficult. Various methodologies have been used to quantify and detect SGD, including (a) thermal imaging, (b) electromagnetic techniques, (c) direct measurements via seepage meters, (d) water balances and hydrogeological modeling, (e) techniques based on natural or artificial tracers and (f) eddy correlation approaches.

a) Thermal imaging

Temperature measurements can be used to detect groundwater discharge wherever there are temperature differences between coastal seawater and discharging groundwater (Johnson et al. 2008) (Fig. 1.9). Although discrete temperature measurements are possible, remote sensing methods of thermal infrared imaging (TIR) are most frequently applied because they allow covering larger areas. TIR technology has been successfully applied to detect SGD at large scales (tens of kilometers), via satellite imagery (Wilson and Rocha 2012), at local scales (meters to few kilometers) via aircraft TIR measurements (Miller and Ullman 2004; Mejías et al. 2012; Kelly et al. 2013), or even at finner scales (few meters) using handheld TIR technologies (Röper et al. 2013). Satellite TIR imagery, which can be inexpensively acquired, provides broad views of SGD but coarse spatial resolution that prevents small localized SGD (Wilson and Rocha 2012). TIR imagery is thus a powerful tool to determine the precise location and extension of SGD inputs, but additional methods have to be used to provide quantitative estimates of SGD.

Figure 1.9. Airborne thermal infrared image (TIR) capturing karstic groundwater springs (Alcossebre and Badum springs) discharging to the Mediterranean Sea from the deep aquifer of El Maestrat (Castelló, Spain) (adapted from Garcia-Solsona et al. 2010b).

b) Resistivity imaging

Variations on the electrical resistivity (inversely proportional to electrical conductivity) of the subsurface, which responds mainly to changes in porewater salinity and porosity (Hoefel and Evans 2001), can be determined by using geoelectrical techniques. Current methods are based on stationary or streaming multielectrode and multichannel systems that allow rapid acquisition of data across relatively long distances (up to some kilometers), either from beaches or coastal terrains (Stieglitz et al. 2008a; Zarroca et al. 2014) or from the seabed (Hoefel and Evans 2001; Manheim et al. 2004). Porewater from areas where fresh SGD occurs are characterized by significant differences on salinity, which can be measured as changes in electrical resistivity of sediments. Resistivity imaging is thus eminently appropriate to identify and map freshwater/seawater interface (Swarzenski et al. 2006; Stieglitz et al. 2008a) as well as to delineate point-sourced groundwater inputs (Zarroca et al. 2014; Fig 1.10), although it does not allow quantifying the SGD flow.

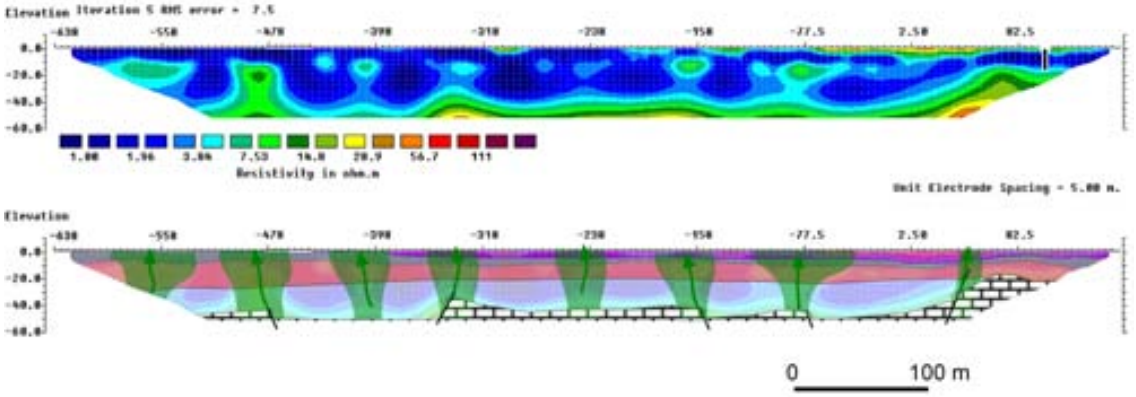

Figure 1.10. Resistivity image (top) collected in a Mediterranean wetland and the hydrological pattern derived from its interpretation (bottom). Resistivity anomalies consisting in high-resistivity vertical lobes reflect ascending groundwater flow paths (in green) (adapted from (Zarroca et al. 2014)).

c) Direct measurements by seepage meters

Seepage meters are devices installed in the seafloor designed to directly measure SGD, as well as to collect SGD samples as it emerges from the bottom sediment for latter chemical analyses. The simplest manual seepage meter consists in a 0.25 m^2 benthic chamber (200-liters drums) with a plastic collection bag attached to a port on the top (Lee 1977; Fig. 1.11). SGD seeping through the sediment will displace water trapped in the chamber forcing it up to the plastic bag. Changes in the volume of water in the bag will thus provide the seepage SGD flow. This device has been improved with more sophisticated, automated artifacts based on heat pulse (Taniguchi and Fukuo 1993), ultrasonic (Paulsen et al. 2001) or dye dilution technologies (Sholkovitz et al. 2003). These new meters can provide high-resolution continuous measurements of SGD seepage rates, allowing monitoring tidal cycles or temporal variations on the seepage flow. Although seepage meters provide a direct measure of the seepage rate at the exact installation site, estimating SGD over large areas (e.g. beaches or bays) requires the installation of numerous meters because of the natural spatial and temporal variability of SGD seepage rates (Taniguchi et al. 2003). In addition, the artifacts themselves can alter the measurements, they have to be deployed in a relatively calm environments and may not work in sites with preferential discharge pathways (e.g. karstic or volcanic areas) (Burnett et al. 2006).

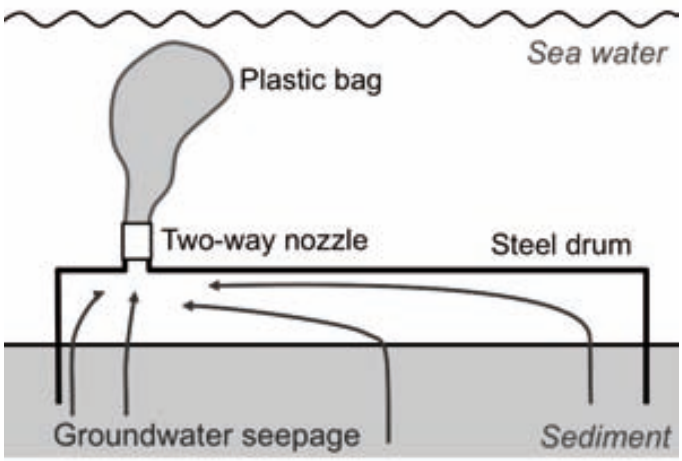

Figure 1.11. Scheme of a standard manual seepage meter (adapted from Lee (1977)).

d) Water balances and hydrogeological models

Water balance approaches rely on quantifying inputs (precipitation) and outputs (evapotranspiration, surface runoff and groundwater discharge) of freshwater into a system (Knee and Paytan 2011). By constraining all the other terms, fresh SGD can be determined by difference as the component needed to balance inputs and outputs. While water balances have been useful in regional studies to estimate the fresh fraction of SGD (Sekulic 1996), these estimates do not include seawater that mixes into the aquifer and often comprises a significant fraction of the total SGD (Burnett et al. 2006). In addition, water balances may not be applicable in local studies or in settings where watershed boundaries do not correspond with groundwater recharge zones (Knee and Paytan 2011). Also, SGD is usually small in comparison with the other terms of the water balance, which often are difficult to constrain (Moore 2010b). Thus, the fresh groundwater discharge estimated by difference may be of the same magnitude as the uncertainties associated with the other terms, resulting in imprecise estimations of the SGD flow (Burnett et al. 2006).

Hydrogeological modeling based on numerical or analytical simulations are also used to estimate the net fresh groundwater discharge to the ocean (Langevin 2003) and to investigate freshwater-seawater interactions in the subterranean estuary (Robinson et al. 2007; Nakada et al. 2011). The main challenge of hydrogeological modeling is obtaining representative values for the input parameters (e.g. hydraulic heads, hydraulic conductivities and boundary conditions) (Knee and Paytan 2011). Since aquifer systems are usually heterogeneous in space and time, it is difficult to obtain

sufficient field data to adequately characterize this heterogeneity (Burnett et al. 2006). Another hydrogeological approach to determine SGD consists in calculating Darcian flows by using multi-level piezometer nests. This approach requires obtaining representative values of the hydraulic conductivity of the aquifer and also characterizing variability in seepage rates due to heterogeneity in the local geology (Burnett et al. 2006).

e) Tracer techniques

Most of the tracer techniques to estimate SGD utilize chemicals that are naturally enriched in coastal groundwater relative to coastal seawater and have low reactivity in the coastal ocean (Moore 2010b). One of the major advantages of these techniques is that the coastal water column presents an integrated signal of the natural tracers entering the system via groundwater pathways, allowing smoothing out small-scale spatial and temporal variability inherent to SGD (Burnett et al. 2001c). To estimate SGD flows, natural tracers are usually incorporated to mass balances, requiring first to evaluate other potential non-SGD sources (e.g. river discharge, sediment inputs, precipitation, in situ production) and sinks (e.g. export offshore, in situ consumption or decay, atmospheric evasion) of the tracer to the system. In addition, the volume of the study site and the residence time of coastal waters must be constrained, as well as a representative concentration of the tracer in discharging groundwater (Burnett et al. 2006). Although accurately assessing all these terms can be a difficult task, tracer techniques provide reliable and integrated SGD flow estimates not possible by other methods. Natural tracers of SGD include radium isotopes (Moore 1996a), radon (Burnett and Dulaiova 2003), helium (Top et al. 2001), silica (Hwang et al. 2005a), barium (Moore 1997) and methane (Cable et al. 1996), among others. Of these, naturally-occurring radionuclides (i.e. radium isotopes and radon) have been the most extensively used (Charette et al., 2008 and references therein).

Ra isotopes (^{223}Ra, ^{224}Ra, ^{226}Ra, ^{228}Ra) are highly enriched in brackish SGD relative to coastal waters (typically 1-2 orders of magnitude) and behave conservatively once released to the coastal ocean. In addition, since their half-lives range from 3.7 days to 1600 years, they can be used to quantify SGD fluxes on a variety of time-scales, to distinguish different groundwater sources and also to estimate residence time of coastal waters (Charette et al. 2008). A major limitation of this tracer is that Ra isotopes

may not be enriched in completely fresh SGD, because Ra is adsorbed to the particles in low-salinity conditions (see section 1.2. for a detailed discussion on the use of Ra isotopes as tracers of SGD).

Radon (^{222}Rn) is largely enriched in SGD over coastal waters (often 1000-fold or greater), both fresh and saline, and it is geochemically unreactive, being an excellent tracer to quantify SGD (Burnett and Dulaiova 2003). Moreover, recent advances in ^{222}Rn detection based on continuous in situ measurements and mapping of concentrations over large areas, allow assessing temporal variations of SGD as well as identifying areas of significant groundwater discharge (Burnett et al. 2001b; Dulaiova et al. 2005). Since it is a gas, aside from other sources and sinks, losses of ^{222}Rn to the atmosphere must be accounted for to estimate SGD flows via ^{222}Rn.

Artificial tracers, including SF_6, ^{131}I, ^{32}P and fluorescent dye, can also be used to estimate SGD (Corbett et al. 2000; Cable and Martin 2008). Experiments are commonly based on an injection of the artificial tracer into the sediment or the coastal aquifer and the subsequent monitoring of the movement of the tracer (Knee and Paytan 2011; Santos et al. 2012).

f) Eddy correlation techniques

The eddy correlation technique is a recent advance in the study of fluxes across the sediment-water interface. This technique relies on measuring continuously and simultaneously the fluctuating vertical velocity just above the sediment-water interface using acoustic Doppler velocimeters (ADCP) and the variations on salinity and/or temperature (Crusius et al. 2008; Ganju 2011). If the SGD salinity or temperature differ from that of the water column, the specific SGD flow at the deployment location can be quantified from either a heat or a salt balance (Crusius et al. 2008). This technique is very promising because it is a non-intrusive method and allows high temporal resolution and long-term records of SGD (Crusius et al. 2008; Santos et al. 2012). Despite the potential of the eddy correlation approach, the method still needs to be tested in different coastal settings, such as sites where SGD flows are small or shallow or open-coastline environments where waves exhibit a major influence on near-bottom currents.

Table 1.1. Comparison between the approaches used to detect and quantify SGD, including information provided by each method and its main advantages and limitations (based on Santos et al. 2012).

Approach	Information provided	Advantages	Limitations
Thermal imaging	Pictures of surface water temperatures	Determines the location/extension of SGD. Covers large areas in a short time.	Needs to be calibrated by other approaches. Expensive. Cannot differentiate between local and advected anomalies. Works only where temperature differences SGD-seawater are present. Cannot provide quantitative estimates of SGD.
Resistivity imaging	Subsurface pictures of resistivity that may be converted into salinity	Identifies freshwater/seawater interface.	Geological features may change resistivity and mislead interpretation. Works only where salinity gradients are present. Cannot provide quantitative estimates of SGD.
Seepage meters	Volume of water released or removed by sediment enclosed by the chamber.	Automatic and continuous measurements are possible. Direct measurements of groundwater inputs.	Cover a small area. Chambers itself can alter groundwater exchange. Require calm environments.
Water balances	Fresh groundwater discharging to the sea	Particularly useful in regional studies to determine fresh SGD. No field work required.	Cannot determine total SGD. Large uncertainties. Work only where aquifer boundaries correspond to the study area.
Hydrogeol. models	Depending on the assumptions	Different scenarios can be tested.	Often overlook sediment heterogenity and oceanic drivers. Need to be validated by observations.
Natural tracers	Tracer inputs from SGD	Particularly useful in heterogeneous systems (integrate all SGD pathways). Allow quantifying total SGD.	Require a complex mass balance, which may introduce uncertainties. Each tracer is restricted to certain time scales.
Artificial tracers	Transport and dispersion rate	Integrate all transport mechanisms.	Difficult to separate the drivers of transport. Affected by degradation and sorption.
Eddy correlation	Vertical fluxes just above the sediment-water interface	Integrate processes occurring over a relatively large area	Restricted to fluxes that can be measured at high temporal resolution. Cannot differentiate advected anomalies. Measurement area may shift with changes in flow direction.

1.2. Using Ra isotopes to estimate SGD

There are four naturally occurring isotopes of Radium (Ra): ^{226}Ra ($T_{1/2}$=1600 years) belonging to the ^{238}U series, ^{224}Ra ($T_{1/2}$=3.66 days) and ^{228}Ra ($T_{1/2}$=5.75 years) in the ^{232}Th series, and ^{223}Ra ($T_{1/2}$=11.4 days) in the ^{235}U series (Fig 1.12). Ra isotopes are widely distributed in nature, existing in soils, rocks, surface waters (including rivers, lakes, seas and oceans) and groundwater, and are continuously generated from the decay of their immediate thorium parents, which are tightly bound to the geological matrix.

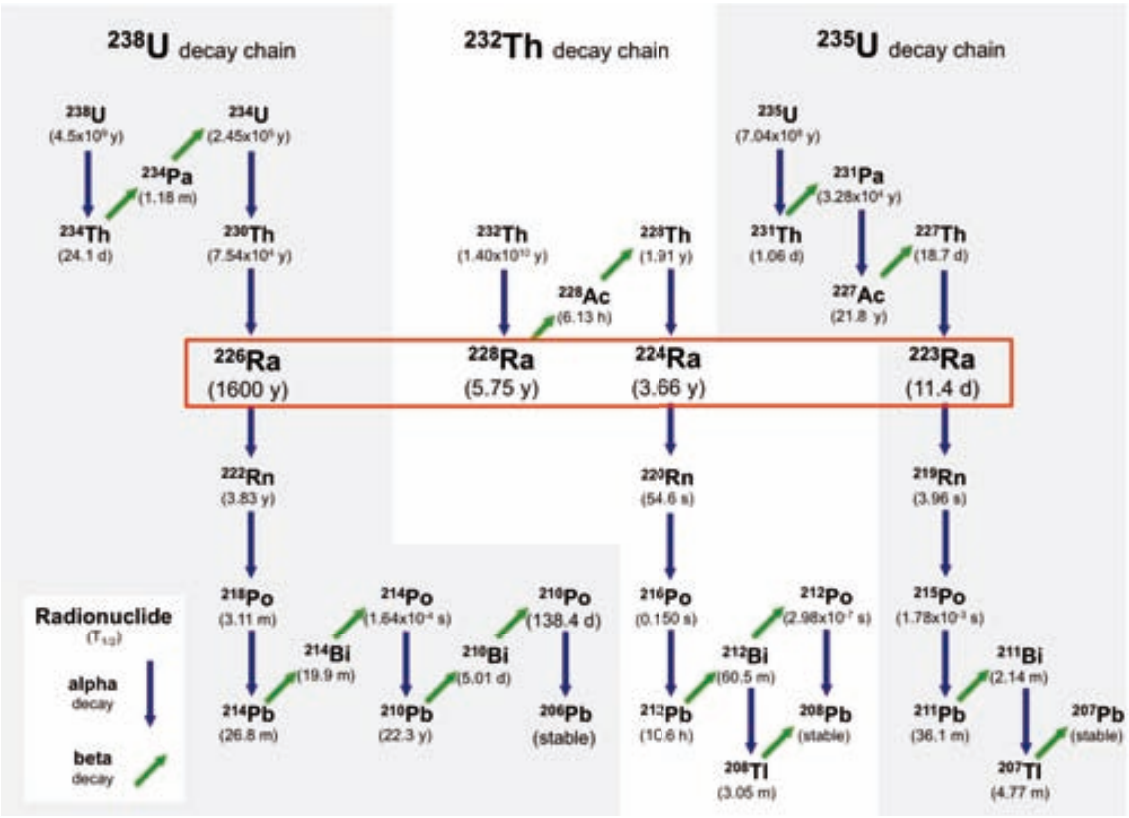

Figure 1.12. Schematic diagram of the natural uranium (^{238}U and ^{235}U) and thorium (^{232}Th) decay series, showing the decay type (alpha or beta) and the half-life of each radionuclide. Ra isotopes are circled in red.

Ra isotopes have proven to be useful tracers of SGD in many environments, including coastal lagoons (e.g. Garcia-Solsona et al. 2008; Young et al. 2008; Rapaglia et al. 2010a; Gattacceca et al. 2011; Su et al. 2013), salt marshes (e.g. Rama and Moore 1996; Krest et al. 2000; Charette et al. 2003; Charette 2007), coves and bays (e.g. Charette et al. 2001; Hwang et al. 2005a; Beck et al. 2007a; Garcia-Orellana et al. 2010; Garcia-Solsona et al. 2010a), estuaries (e.g. Charette et al. 2001, 2013; Yang et al. 2002; Dulaiova et al. 2006; Moore et al. 2006; Santos et al. 2009) or larger coastal areas (Windom et al. 2006; Moore et al. 2008; Ollivier et al. 2008; Moore 2010a). The main attributes that make Ra isotopes ideal tracers of SGD are the fact they are enriched in SGD, up to several orders of

magnitude above seawater, and they behave conservatively once released to the coastal sea (i.e. their activity is a function only of mixing and decay) (Charette et al. 2008). In addition, SGD is commonly the dominant source of Ra isotopes to the site under study (e.g.(Moore 1996a; Beck et al. 2007a; Garcia-Solsona et al. 2008b)), allowing estimating SGD flows even though the other sources (i.e. sediments, streams) are not precisely constrained. The existence of four naturally-occurring Ra isotopes, with distinct half-lives, makes them particularly useful tracers to study SGD and associated water mixing processes at different time-scales and to quantify multiple sources of SGD. SGD inflowing through different matrixes can be differentiated using Ra isotopes mainly due to two distinct mechanisms: i) aquifer with different principal mineral or sediment type can have different relationships among uranium (^{223}Ra and ^{226}Ra) and thorium (^{224}Ra and ^{228}Ra) series isotopes (Fig 1.13); ii) the relative differences in rates of ingrowth from their thorium parents can result in groundwater being enriched in shorter-lived Ra isotopes relative to the longer-lived ones depending on the flushing frequency (Hancock and Murray 1996; Crotwell and Moore 2003; Moore 2003, 2006).

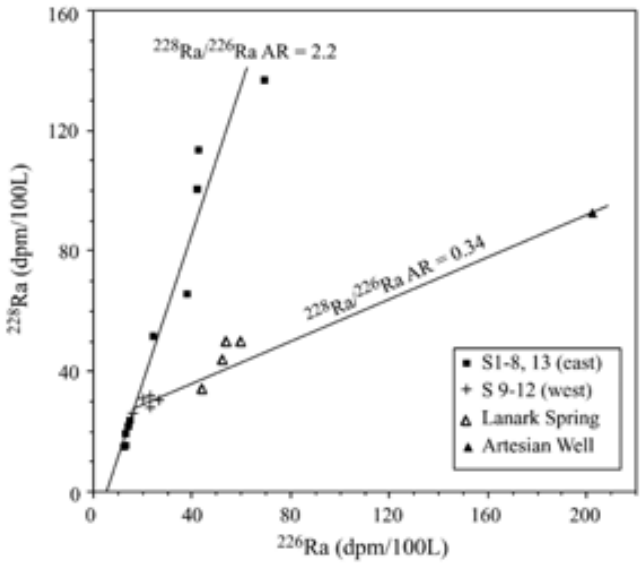

Figure 1.13. The distribution of ^{226}Ra and ^{228}Ra in the northeast Gulf of Mexico reveals two trends, implying there are two Ra sources with different ^{228}Ra/^{226}Ra activity ratios (AR) (Moore 2003).

1.2.1. Ra activities in SGD

The approaches to estimate SGD by means of Ra isotopes rely on capacity to accurately determine the Ra concentrations in SGD (i.e. the endmember of the models). Thus, estimates of SGD would only be resolved to the level that Ra activities in the SGD endmember are well constrained (Charette et al. 2008; Gonneea et al. 2013).

Activities of Ra isotopes in coastal groundwater are controlled by different processes, including ion exchange reactions, the redox cycle of Mn and Fe, weathering of Ra-bearing minerals and ingrowth from decay of their parents, as well as by the aquifer characteristics such as the U/Th content in the substrate and the groundwater transit time (Charette et al. 2008). Adsorption-desorption (ion exchange) reactions onto aquifer solids, which are dependent on the substrate and the chemical composition of groundwater, usually exert a major control on the Ra behavior in the coastal aquifer and largely determine the Ra concentration in SGD (Swarzenski 2007; Gonneea et al. 2008). The ionic strength (salinity) of groundwater has long been recognized as a major influence on the Ra adsorption coefficients, with Ra desorption increasing significantly with salinity (Elsinger and Moore 1980; Webster et al. 1995). This is mainly due to cation competition and displacement, but also due to increases in mineral surface charge, in the stability of inorganic complexes and in the presence of organic complexes (Webster et al. 1995; Porcelli and Swarzenski 2003; Swarzenski 2007). As a consequence, Ra is usually more enriched in brackish to saline groundwater than in completely fresh groundwater. Ra adsorption/desorption also depends on the pH of water (Sanchez and Rodriguez-Alvarez 1999; Beck and Cochran 2013), the temperature (Rama and Moore 1996), the redox potential and the cycling of Fe and Mn oxides (Charette and Sholkovitz 2006; Gonneea et al. 2008; Beck and Cochran 2013), the sediment grain size and porosity (Webster et al. 1995; Hancock et al. 2006) or the fraction of exchangeable Ra (Porcelli and Swarzenski 2003; Gonneea et al. 2008), among others.

The complex processes that control Ra activities in coastal aquifers can lead to Ra activities in SGD varying in a wide range (even one order of magnitude or more), both in space and time. Several recent studies have contributed to the understanding of the geochemical cycling of Ra isotopes in the subterranean estuary (e.g. Charette and Sholkovitz 2006; Gonneea et al. 2008, 2013; Beck and Cochran 2013), helping to refine

the utility of Ra isotopes as tracers of SGD. However, there is not yet a straightforward approach to determine the Ra activity of the SGD endmember, and collecting a large number of samples near the point of discharge is still the best option to obtain a representative value to characterize Ra activities in SGD.

1.2.2. Approaches to estimate SGD using Ra isotopes

The most commonly applied strategies to quantify SGD using Ra isotopes are summarized in this section. All of these approaches depend on estimating the Ra flux to the study site supplied by SGD, which can be converted to a SGD flow by characterizing the Ra activity in discharging groundwater (i.e. the endmember). The selection of the appropriate approach must be based on the characteristics of the area under study and their compatibility with the inherent assumptions associated to each strategy.

a) Mass balance

This approach was first developed by (Moore 1996a) and it has been successfully applied in several studies worldwide (e.g.(Charette et al. 2001; Kim et al. 2005; Beck et al. 2007a; Garcia-Solsona et al. 2008b; Moore et al. 2008; Ollivier et al. 2008; Rapaglia et al. 2012; Garcia-Orellana et al. 2014)). By constraining all the potential Ra sources and sinks to the system under study, the Ra flux supplied by SGD (Ra excess, Ra_{ex}) can be estimated by difference between inputs and outputs (assuming steady state). Potential Ra inputs usually include riverine discharge, release from bottom sediments (diffusion, bioturbation, resuspension…) and SGD, whereas Ra is lost from the system by export offshore and radioactive decay (Fig 1.14). For a given Ra isotope, at steady state, the Ra_{ex} flux supplied by SGD to the study site can be estimated as:

$$Ra_{ex} = \frac{[Ra - Ra_{ocn}]V}{T_w} + [\lambda RaV] - [F_{sed} \cdot A_{sed}] - [Ra_{Riv} \cdot F_{Riv}] \quad (1.1)$$

where Ra is the average activity in the study site, Ra_{ocn} the Ra activity in open seawater, V the volume of the study site, T_w the residence time of coastal waters, λ the decay constant of the Ra isotope considered, F_{sed} the diffusive Ra flux from sediments, A_{sed} the bottom area of the study site, Ra_{Riv} the Ra activity in the river and F_{Riv} the river flow. The magnitude of all these terms can vary widely depending on the study site

characteristics (sediment type, river flow…) and also on the Ra isotope used. For instance, while radioactive decay and inputs from sediments may be very relevant terms on the mass balance for short-lived Ra isotopes (^{223}Ra and ^{224}Ra), they can be negligible for the long-lived ones (^{226}Ra and ^{228}Ra) due to their low decay in the water column and their longer regeneration time in bottom sediments (Beck et al. 2007a). Notice also that riverine inputs of Ra isotopes not only include the dissolved phase, but also the Ra adsorbed to suspended particles, which may be desorbed when ionic strength increases (mixing with seawater) and often constitutes the major riverine source (Li et al. 1977; Webster et al. 1995; Moore and Shaw 2008).

Once the Ra flux supplied by SGD (Ra_{ex}) is determined, it can be converted to an SGD flow by dividing it by the Ra activity in the SGD endmember.

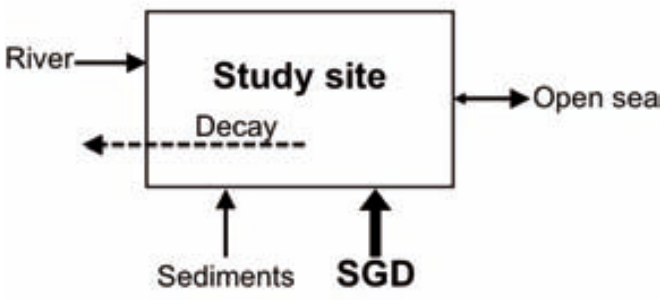

Figure 1.14. Generalized box model to estimate SGD into a coastal area by using Ra isotopes, including the major Ra inputs and outputs to the study site (based on (Moore 1999).

b) Flux offshore from eddy diffusive mixing

In systems controlled by eddy diffusive mixing, where net advection offshore can be neglected, the SGD flow can be calculated using a principle developed by Moore (2000) and successfully applied in several sites (e.g. Moore 2003; Boehm et al. 2006; Dulaiova et al. 2006b; Windom et al. 2006). In such a system, the distribution of the short-lived Ra isotopes with distance offshore will only depend on eddy diffusive mixing and radioactive decay. Since the Ra decay rates are known an assuming that all the Ra inputs occurs at the shoreline, the horizontal eddy diffusion coefficient (K_h) can be estimated from the slope of the natural logarithm of activity as a function of distance (Fig 1.15). Recently, Li and Cai (2011) proposed an improved model using pairs of Ra isotopes to refine the calculation of eddy diffusivity coefficients, showing that the previous approach (Moore 2000b) could be very sensitive to even small advection rates.

The estimated K_h values can be used in conjunction with the cross shelf long-lived Ra activity gradient ($\partial A/\partial x$) to estimate the flux offshore of the long-lived Ra isotope used ($F_{Ra\text{-}off}$):

$$F_{Ra-off} = \left[K_h \left(\frac{\partial A}{\partial x}\right)\right] \cdot z \cdot L \qquad (1.2)$$

where z is the surface layer depth over which Ra is transported and L is the shoreline length. Assuming that all the Ra flux exported offshore is balanced by Ra inputs from SGD, the SGD flow can be obtained by knowing the Ra activity in SGD.

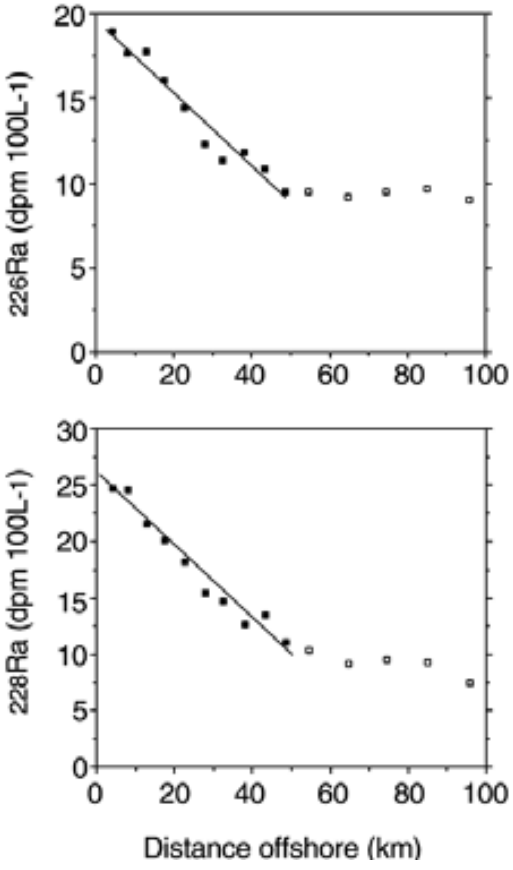

Figure 1.15. Natural logarithm of ^{223}Ra and ^{224}Ra activities for samples collected in South Atlantic Bight (USA) as a function of distance offshore. The horizontal eddy diffusion coefficient (K_h) can be estimated from the slope of the best fit within the study site (within 50 km offshore; solid symbols) (Moore 2000b).

c) Endmember mixing model

Moore (2003) developed a three endmember mixing model to assess the relative contributions of groundwater from different sources, based on the distinct Ra signals of different Ra sources (Fig 1.16). The resulting three equations can be solved to determine the fraction of the three different endmembers (two types of SGD, *SGD1* and *SGD2*, and the coastal ocean, *ocn*) in the waters of the study site:

$$f_{ocn} + f_{SGD1} + f_{SGD2} = 1 \quad (1.3)$$

$$^{226}Ra_{ocn} \cdot f_{ocn} + {}^{226}Ra_{SGD1} \cdot f_{SGD1} + {}^{226}Ra_{SGD2} \cdot f_{SGD2} = {}^{226}Ra_{std} \quad (1.4)$$

$$^{228}Ra_{ocn} \cdot f_{ocn} + {}^{228}Ra_{SGD1} \cdot f_{SGD1} + {}^{228}Ra_{SGD2} \cdot f_{SGD2} = {}^{228}Ra_{std} \quad (1.5)$$

where *f* is the fraction of the three endmembers (*SGD1*, *SGD2* and *ocn*) in the study site, and ^{226}Ra and ^{228}Ra are the ^{226}Ra and ^{228}Ra activities, respectively in the endmembers and the study site (*std*). Short-lived Ra isotopes can also be used in the equations by incorporating the respective decay term. Upon the determination of the endmember fractions, the flow from each SGD endmember (SGD_{SGDx}) can be estimated by:

$$SGD_{SGDx} = \frac{f_{SGDx} \cdot V}{T_w} \quad (1.6)$$

where V is the volume of the study site and T_w the water residence time.

This approach have been applied in marsh systems to differentiate tidally-modulated porewater inputs from aquifer discharge (Charette and Buesseler 2004; Charette 2007) and also in coastal areas with two distinct SGD sources (Moore 2003, 2006; Young et al. 2008; Su et al. 2013). By incorporating or subtracting new equations with other Ra isotopes or other tracers (e.g. salinity, ^{222}Rn), the endmember mixing model can also be used to estimate SGD inputs from one to several SGD sources (Garcia-Solsona et al. 2010a, 2010b; Charette et al. 2013). The application of this approach is constrained to systems where other Ra sources can be neglected, since it assumes that there are no other Ra sources than the endmembers considered.

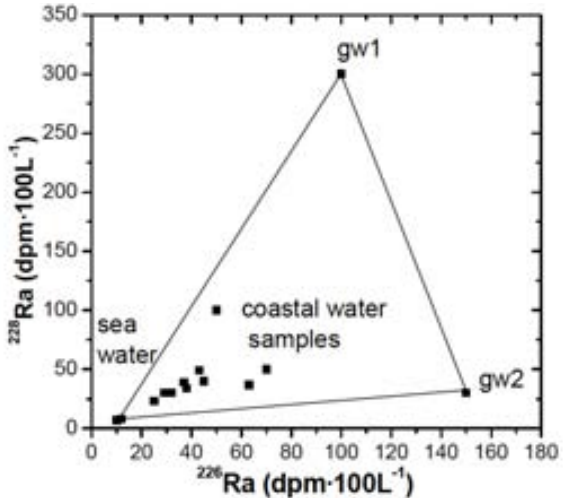

Figure 1.16. Theoretical example of a three endmember mixing model, where Ra activities in coastal water samples are explained by a mixing of seawater and two different groundwater sources (gw1 and gw2) (Garcia-Solsona 2009).

1.2.3. Ra-derived water ages

Some of the Ra-based approaches used to quantify SGD, such as the mass balance or the endmember mixing models, rely on the previous estimation of the water residence time (T_w). Estimates of the water residence time are also required to evaluate the fate of dissolved compounds delivered to the coastal ocean (Moore 2000a). Pairs of Ra isotopes can then be used to estimate the water apparent age, defined as the time a water parcel has spent since entering the study site through one of his boundaries (Moore 2000a; Monsen et al. 2002; Moore et al. 2006). The water age is a different way of quantifying mixing/transport timescales than residence time, being this latter commonly defined as the time it takes for any water parcel to leave a given water body through its outlet to the sea (Monsen et al. 2002). Indeed, both concepts are complementary and may not lead to the same results (Monsen et al. 2002; Moore et al. 2006). However, when using averages for the entire study site, these two measures of time often yield similar results and, as a consequence, both water residence time and water apparent ages are commonly used indistinctively in SGD literature.

Ra-based approaches to estimate water ages are based on the variation of Ra activity ratios due to the time elapsed since Ra isotopes became disconnected from its source (i.e. SGD). The use of activity ratios allows correcting for changes in Ra activities resulting from processes others than radioactive decay (e.g. mixing) (Charette et al. 2008). Two different approaches can be used to estimate water apparent ages, depending on whether Ra is only added to the water near the shoreline (Eq. 1.7; Moore 2000a) or Ra inputs occur continuously over a wider area, such as it would be the case in a marsh, estuary or bay with multiple springs (Eq 1.8; Moore et al. 2006):

$$T_w = \frac{\ln (AR_{ocn}) - \ln (AR_{SGD})}{\lambda_S - \lambda_L} \quad (1.7)$$

$$T_w = \frac{AR_{SGD} - AR_{ocn}}{AR_{ocn} \cdot \lambda_S} \quad (1.8)$$

where AR_{ocn} and AR_{SGD} are the activity ratios of the shorter-lived Ra isotope to the longer-lived Ra isotope in the coastal ocean and SGD, respectively, and λ_S and λ_L are the decay constants of the shorter- and longer-lived isotopes, respectively. Any pair of Ra isotopes can be used, depending on the expected water age of the study site. Both approaches assume that i) Ra activities and ARs are highest in the Ra source; ii) the Ra

source and the receiving water parcel have uniform ARs; and iii) the activities and AR are elevated in coastal waters from the study site as a result of the Ra inputs from the source (SGD) (Moore 2000a; Moore et al. 2006; Knee et al. 2011). Similarly to Ra-based estimates of SGD, the greatest uncertainty of Ra-based water ages is usually the inherent variability in the SGD endmember (Charette et al. 2008).

1.2.4. SGD-derived fluxes of nutrients and metals

The most simple and straight-forward approach to determine SGD-derived fluxes of nutrients and trace metals (as well as other compounds) to the coastal sea is by multiplying the nutrient/metal concentration in the SGD endmember by the Ra-derived SGD flow (Charette et al. 2008; Santos et al. 2008). However, it is often difficult to determine the most appropriate concentration in the SGD endmember, since most chemicals can display non-conservative behavior over short spatial scales due to biogeochemical transformations occurring in the subterranean estuary (Slomp and Van Cappellen 2004; Beck et al. 2007b; Santos et al. 2008; Knee and Paytan 2011; Erler et al. 2014; Gonneea et al. 2014) (see section 1.1.5.).

In order to constrain the nutrient/metal concentration in SGD inflowing to the coastal site under study, a general approach is collecting a relatively large number of samples along the entire length of the mixing zone, including points just before discharge and in the freshwater area, so as to attain reasonable upper and lower limit estimates. In addition, the distribution of concentrations along the mixing zone may provide with some insights on the biogeochemical transformations occurring in the subterranean estuary, which can in turn be used to better constraining the nutrient/metal concentration in the SGD endmember. For instance, in systems where the total SGD is dominated by fresh groundwater and chemical compounds show a conservative behavior (although this is not the usual case), the best estimate of the SGD endmember concentration may be the averaged nutrient/metal concentration in fresh groundwater samples. On the other side, and when investigating constituents displaying non-conservative additions or removals in the subterranean estuary, a pertinent approach may be to focus on groundwater samples collected at the discharge location after all biogeochemical processes have occurred (e.g. samples from seepage meters, shoreline piezometers…) (Beck et al. 2007b; Santos et al. 2008).

1.3. SGD studies in the Mediterranean Sea

SGD studies may be particularly relevant in the Mediterranean Sea for several reasons:

i) Water resources are often scarce in most of the regions of the Mediterranean and the discharge of fresh groundwater to the sea has the potential to be used as freshwater sources (UNEP/MAP 2012).

ii) The Mediterranean basin is rich in coastal wetlands of great ecological, economical and social value, most of them maintained by fresh/brackish groundwater inputs (Pearce and Crivelli 1994).

iii) Since the Mediterranean Sea is an oligotrophic environment, inputs of dissolved compounds from external sources, such as SGD, may play a relevant role on the regulation of the coastal primary productivity (Ludwig et al. 2009; Tovar-Sanchez et al. 2014). In addition, surface runoff may be insignificant for large periods in several Mediterranean coastal areas, making SGD a major and stable pathway for freshwater and dissolved compounds to enter into the coastal sea (Shellenbarger et al. 2006).

Most of the studies conducted to evaluate the discharge of groundwater in the Mediterranean Sea, commonly based on hydrogeological approaches, have only focused on the fresh fraction of SGD (Mijatović 2006; Fleury et al. 2007, and references therein). Particularly relevant for fresh groundwater inputs are karstic regions, which are estimated to contribute up to 75% of the fresh groundwater inputs to the Mediterranean basin (UNESCO 2004). Karstified carbonate aquifers can exhibit rapid responses to rainfall due to their underground structures of fractures and conduits that can rapidly transfer the infiltrated water into the sea, yielding greater flow than runoff in numerous systems (Polemio et al. 2009; Garcia-Solsona et al. 2010b; Tovar-Sanchez et al. 2014). Some studies have also evaluated the fresh groundwater discharge into the entire Mediterranean Sea, which has been estimated to be on the order of $70 \cdot 10^9$ $m^3 \cdot yr^{-1}$, accounting for 20-25 % of the total freshwater inputs to the basin (PNUE/PAM/Plan Blue 2004; Zektser et al. 2007).

Some recent studies have also estimated the total SGD flow into coastal Mediterranean sites, integrating both terrestrial groundwater and recirculated seawater. These works have been conducted in karstic areas (Garcia-Solsona et al. 2010b; Mejías et al. 2012;

Pavlidou et al. 2014), islands (Burnett and Dulaiova 2006; Moore 2006; Garcia-Solsona et al. 2010a; Tovar-Sanchez et al. 2014), coastal wetlands or lagoons (Garcia-Solsona et al. 2008b; Rapaglia et al. 2010a, 2012; Gattacceca et al. 2011; El-Gamal et al. 2012; Stieglitz et al. 2013), detrital beaches (Swarzenski et al. 2006; Weinstein et al. 2007) and entire gulfs (Ollivier et al. 2008). Reported estimates of SGD from local studies conducted in the Mediterranean Sea are compiled in Table 1.2, with shoreline normalized SGD flows ranging from 10^5 to $2{\cdot}10^8$ $m^3{\cdot}km^{-1}{\cdot}yr^{-1}$. Most of these studies have been conducted in the North-Western Mediterranean Sea (mainly Spain and Italy), and only few studies have reported quantitative total SGD estimates from the North-Eastern Mediterranean Sea (Pavlidou et al. 2014), the African (El-Gamal et al. 2012) and the Asian Mediterranean coasts (Swarzenski et al. 2006; Weinstein et al. 2007) (Fig 1.17). There is also a lack of basin-wide estimates of the magnitude of SGD in the Mediterranean Sea.

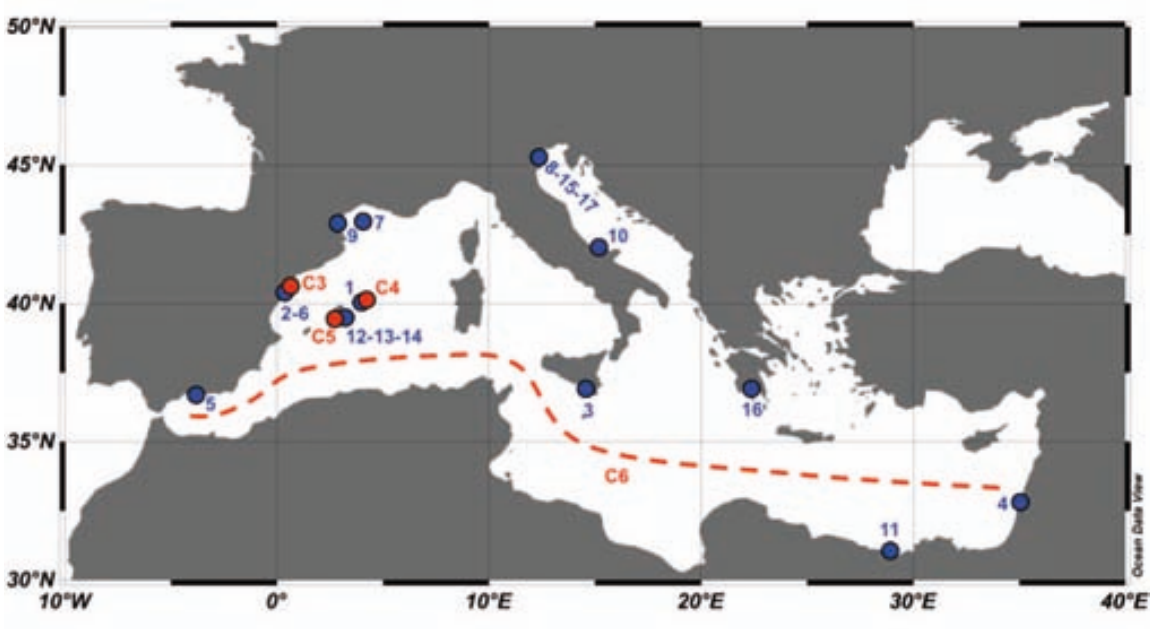

Figure 1.17. Map of sites in the Mediterranean Sea where SGD has been estimated. Details on all the studies (numbers 1-17) can be found in Table 1.2. Studies in red correspond to works belonging to this thesis (Chapters 3 to 6; C3: Peníscola marsh; C4: Port of Maó; C5: Palma Beach; C6: entire Mediterranean Sea).

SGD-derived chemical fluxes have been suggested to play a relevant role in coastal productivity and biogeochemical cycling of the Mediterranean Sea (Basterretxea et al. 2010; Garcia-Solsona et al. 2010a, 2010b; Garcés et al. 2011; Stieglitz et al. 2013). Despite its importance, the literature on the SGD-associated chemical inputs to the

Mediterranean Sea is still scarce. Whereas some local studies have reported fluxes of dissolved nutrients to coastal Mediterranean sites (Garcia-Solsona et al. 2010a, 2010b; Rapaglia et al. 2010a; El-Gamal et al. 2012; Pavlidou et al. 2014; Tovar-Sanchez et al. 2014), there are limited studies focusing on trace metal fluxes associated to SGD (Tovar-Sanchez et al. 2014). Detailed assessments on the relevance of SGD as a source of chemical constituents into the entire Mediterranean basin have yet to be conducted.

Table 1.2. SGD estimates for different sites of the Mediterranean Sea (numbers refer to Fig. 1.18). The average SGD flows was divided by shore length or bay mouth width to determine the shore-normalized SGD flows.

Study site		Type	Shore length km	SGD ($\cdot 10^6$) $m^3 \cdot yr^{-1}$	SGD ($\cdot 10^6$) $m^3 \cdot km^{-1} \cdot yr^{-1}$	Ref.
Alcalfar, Spain	1	Karstic cove	0.4	0.15	0.4	Garcia-Solsona et al. 2010a
Badum, Spain	2	Karstic spring	2.5	26 - 68	19	Garcia-Solsona et al. 2010b
Donnalucatta, Italy	3	Boat basin	0.2	n.r.	365	Moore 2006
Donnalucatta, Italy	3	Boat Basin	0.04	0.44 - 2.70	39	Burnett and Dulaiova 2006
Donnalucatta, Italy	3	Boat Basin	0.04	0.11 - 0.38	6.4	Taniguchi et al. 2006
Dor Beach, Israel	4	Sand beach	0.1	n.r.	2.6	Swarzenski et al. 2006
Dor Beach, Israel	4	Sand beach	0.1	n.r.	1.8	Weinstein et al. 2007
El Gorguel, Spain	5	Detrital bay	0.7	35	48	Trezzi et al, in prep
El Maestrat, Spain	6	Karstic springs	45	250 - 500	8.3	Mejías et al. 2012
Gulf of Lyon, France	7	Entire Gulf	300	876 - 16425	29	Ollivier et al. 2008
Isola la Cura, Italy	8	Coast Lagoon	n.a.	365 - 2190	n.c.	Garcia-Solsona et al. 2008
La Palme Lag., France	9	Coast Lagoon	6	47	7.9	Stieglitz et al. 2013
Lesina Lag., Italy	10	Coast Lagoon	25	328 - 385	13	Rapaglia et al. 2012
Marina Lag., Egypt	11	Coast Lagoon	11	30 - 88	8.0	El-Gamal et al. 2012
Romàntica, Spain	12	Detrital cove	0.15	0.07	0.4	Tovar-Sanchez et al. 2014
Sa Nau, Spain	13	Karstic cove	0.1	2	21	Tovar-Sanchez et al. 2014
Santanyí, Spain	14	Detrital cove	0.1	0.09	1.4	Tovar-Sanchez et al. 2014
S. Venice Lag., Italy	15	Coast Lagoon	15	281 - 913	40	Gattacceca et al. 2011b
Stoupa, Greece	16	Karstic spring	2	6 - 39	11	Pavlidou et al. 2014
Venice Lag., Italy	17	Coast Lagoon	80	10950 - 14965	160	Rapaglia et al 2010a

CHAPTER 2

Analytical methods

This section is devoted to describe the analytical methods used to determine the activities of Ra isotopes and ^{222}Rn and the concentrations of nutrients, metals and chlorophyll *a* in water (groundwater and seawater) samples, as well as the activities of Ra isotopes in solid samples. The description of the different study sites (Peníscola Marsh, Port of Maó, Palma Bay and the entire Mediterranean Sea), as well as the experiments conducted and the set of samples collected in each area, are included in the corresponding chapters where the results are presented and discussed (Chapters 3, 4, 5 and 6, respectively).

2.1. Radium isotopes in water samples

Ra isotopes are typically at such low levels in natural waters, particularly in seawater, that their measurement requires pre-concentration from very large samples (Dulaiova and Burnett 2004). The Ra pre-concentration can be accomplished by using MnO_2-impreganted acrylic fiber (hereinafter, Mn-fiber), which have been shown to quantitatively adsorb Ra isotopes from water (Moore and Reid 1973; Moore 1976). This procedure is the most widely applied pre-concentration method to determine Ra activities in marine studies, mainly because it is a relatively simple, cheap sampling technique and the wide variety of options for measurement of the Ra emissions afterwards (Dimova et al. 2008). Although these Mn-fibers can be prepared at the laboratory, we used Mn-fibers supplied by *Scientific Computer Instruments*.

The separation of the Ra isotopes in the Mn-fiber was accomplished by filtering large volume water samples (5 - 60 L for groundwaters and 50 – 350 L for seawater) through cylindrical PVC cartridges loaded with 25 g (dry weight) of Mn-fiber, previously fluffed to maximize the active MnO_2 surface area (Charette et al. 2012) (Fig 2.1.). Some row fiber was also placed at the top of the cartridge to act as a pre-filter for particles suspended in the water sample (Moore 2008). Samples containing large amounts of suspended solids were previously filtered using a cartridge packed exclusively with raw fiber. Water samples were filtered through the Mn-fiber at a flow rate <1 $L \cdot min^{-1}$ to quantitatively extract Ra isotopes, either by gravitational pressure or by using water pumps (Moore 2008). In some instances, a second cartridge loaded with Mn-fiber was attached in series with the first to test the extraction efficiency of the Mn-fiber. A quantitative Ra uptake in the first cartridge was always obtained (>95 %).

Figure 2.1. Extraction of Ra isotopes from the water sample by gravity filtration trough a cartridge loaded with Mn-fiber.

After filtration, the Mn-fibers containing Ra isotopes extracted from the water sample were rinsed with Ra-free deionized water to wash out any particles and sea salt that could interfere during the measurements (Sun and Torgersen 1998). The Mn-fibers were then partially dried via compressed air or drying paper, adjusting the water content of the fiber to 50-100 % of the Mn-fiber dry weight to reach the optimal efficiency for the determination of short-lived Ra isotopes (^{223}Ra and ^{224}Ra) by using the RaDeCC system (Sun and Torgersen 1998).

2.1.1. ^{223}Ra and ^{224}Ra: Radium Delayed Coincidence Counter (RaDeCC)

Activities of short-lived radium isotopes (^{223}Ra and ^{224}Ra) in Mn-fibers were determined by using the Radium Delayed Coincidence Counter (RaDeCC), pioneered by Griffin (Giffin et al. 1963) and adapted for Ra measurements by Moore and Arnold (Moore and Arnold 1996). It essentially consists of (1) a ZnS coated 1.1 L scintillation cell, connected to a photomultiplier to detect radioactive decay events; (2) a pump, which continuously circulates helium through the Mn-fiber sample (previously placed in a PVC cartridge and connected to the system) and subsequently to the scintillation chamber; and (3) an electronic gateway system, which registers counts and splits the registered events into three different channels ("Total ", "^{219}Rn" and "^{220}Rn"), depending on the time elapsed between two subsequent decay events (Fig. 2.2.). The

Rn atoms produced by the decay of Ra atoms adsorbed onto the Mn-fiber are transported to the scintillation cell. Alpha decays of Rn isotopes are recorded in the "Total" channel, producing an electronic signal that opens the gate to a delayed coincidence circuit. This electronic gate remains open for 5.6 ms for the "^{219}Rn" circuit and for 600 ms for the "^{220}Rn" circuit. If a second decay takes place within this time intervals, the signal will be counted in its respective channel. Interferences between channels, as well as random counts due to background and the decay of ^{222}Rn produced by ^{226}Ra in the Mn-fiber, may occur and need to be corrected for. For a more detailed description on the measurement technique and corrections see (Moore and Arnold 1996; Garcia-Solsona et al. 2008a; Moore 2008).

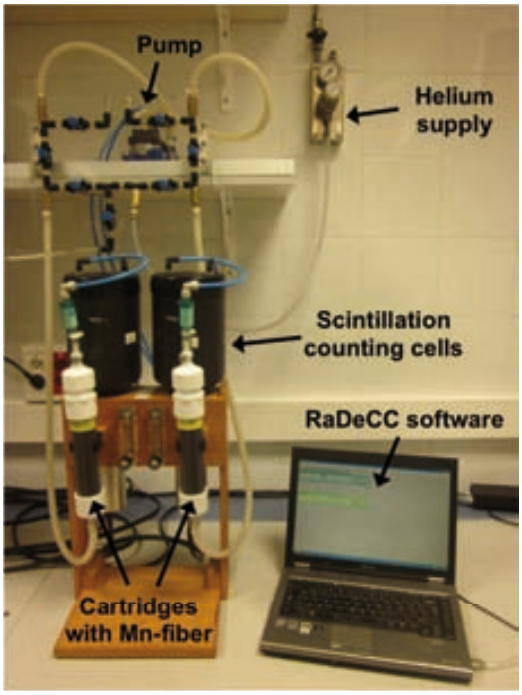

Figure 2.2. Two RaDeCC systems loaded with cartridges containing the sample (Mn-fiber). The main components of this equipment are identified in the figure.

Commonly, each sample was counted three times:

1) A first measurement (1-4 hours counting time) to determine ^{224}Ra activities, conducted shortly after the sampling collection (1-3 days) to minimize its decay.

2) A second measurement (8 - 16 hours counting time) to determine ^{223}Ra, conducted 7-10 days after collection. After this period, ^{224}Ra has decreased considerably (~75 %), but ^{223}Ra has only decreased by only ~35%, minimizing the interference of ^{224}Ra in the ^{223}Ra channel, which is appropriately corrected.

3) A third measurement (~8 hours counting time) conducted at least 1 month after sample collection, when the initial ^{224}Ra has completely (>99%) decayed and the ^{224}Ra measured is essentially ^{224}Ra supported by its ^{228}Th parent. This allows determining ^{228}Th and correcting for supported ^{224}Ra (typical ^{228}Th activities in the coastal ocean are <2 dpm·100L$^{-1,}$ while ^{224}Ra ranges from 1 to 50 dpm·100L^{-1}) (e.g. (Moore and Arnold 1996; Garcia-Solsona et al. 2008a). No corrections for supported ^{223}Ra were applied, since ^{227}Ac (^{223}Ra parent) activities can be neglected compared with ^{223}Ra (<0.05 dpm·100L^{-1} for ^{227}Ac compared with 0.5-10 dpm·100L^{-1} for ^{223}Ra in the coastal ocean) (Moore and Arnold 1996; Moore and Krest 2004; Garcia-Solsona et al. 2008a).

The system was purged for more than 30 minutes both before and after each measurement using an air pump (purging time dependent on the Ra activities measured), in order to maintain low backgrounds. Background measurements were always carried out before counting each sample, and the results were corrected accordingly. All the Ra measurements were also decay corrected to the time of collection.

Counting rates recorded in the "^{219}Rn" and "^{220}Rn" channels need to be converted to ^{223}Ra and ^{224}Ra activities in the Mn-fiber, respectively, and thus the efficiencies of the RaDeCC system need to be determined. To this aim, two single standards of Mn-fiber impregnated with known ^{223}Ra and ^{224}Ra activities were prepared on February 2010 at the IAEA- Marine Environmental Laboratories (Monaco), following the procedures described in Scholten et al. (2010). The ^{223}Ra standard was spiked with 8.86 ± 0.50 dpm of ^{227}Ac in radioactive equilibrium with ^{223}Ra, and the ^{224}Ra standard with 13.41 ± 0.42 dpm of ^{232}Th in equilibrium with ^{224}Ra. Standards were measured in each RaDeCC detector in the same way samples are measured. Standards prepared with ^{227}Ac for ^{223}Ra measurements significantly decrease with time after their preparation in the amount of ^{219}Rn they release from the Mn-fiber to the helium stream, likely due to changes in the surface structure of Mn-fibers, hampering the long-term use of these standards for efficiency calibration (Scholten et al. 2010; Moore and Cai 2013). For this reason, the detection efficiency for ^{223}Ra was determined by measuring the ^{223}Ra standard just after (few weeks) its preparation (Scholten et al. 2010). Contrarily, since ^{224}Ra (^{232}Th) standards have been proven to be extremely reliable over time (Scholten et al. 2010; Moore and Cai 2013), the ^{224}Ra standard was measured periodically, allowing

to determine and control the detection efficiencies. Since the ^{224}Ra detection efficiency remained constant along the years of measurement, it was not necessary to reassess the ^{223}Ra detection efficiencies (any change in the detector system would affect both ^{223}Ra and ^{224}Ra efficiencies) (Scholten et al. 2010). Detection efficiencies ranged from 32 to 40 % for the "^{219}Rn" channel (^{223}Ra), 49 to 54% for the "^{220}Rn" channel (^{224}Ra) and 116 to 129% for the "Total" channel (it can also be used to estimate ^{224}Ra), depending on the RaDeCC system used (6 systems) (Table 2.1.).

Table 2.1. Detection efficiencies (Mean ± SD) of the different RaDeCC systems used.

System	Efficiency (%)		
	^{219}Rn Channel	^{220}Rn Channel	Total Channel
A	32 ± 2	49 ± 2	116 ± 3
B	36 ± 2	54 ± 2	126 ± 6
C	39.9 ± 1.2	54 ± 2	121 ± 5
D	39.7 ± 0.7	53 ± 2	121 ± 2
1	38.0 ± 1.4	55 ± 2	128 ± 3
3	33 ± 2	54 ± 2	129 ± 4

2.1.2. ^{226}Ra and ^{228}Ra: Gamma spectrometry

Activities of ^{226}Ra and ^{228}Ra were determined by gamma spectrometry, which relies on the detection of photon emissions and the unique energy signature of each radionuclide. This is the most conventional method for the determination of long-lived ^{226}Ra and ^{228}Ra in water samples, mainly because other analytical techniques such as alpha spectrometry (Hancock and Martin 1991) or mass spectrometry (Hsieh and Henderson 2011) require time-extensive laboratory work and/or the availability of costly instrumentation. Long-lived Ra isotopes can also be measured using the RaDeCC system. ^{226}Ra can be determined via the ^{222}Rn ingrowth from ^{226}Ra, which is recorded in the "Total" channel (Waska et al. 2008; Geibert et al. 2013), and ^{228}Ra by measuring the Mn-fiber after enough time has elapsed (> 6 months) to produce distinguishable ^{228}Th (in equilibrium with ^{224}Ra) from the ^{228}Ra decay (Moore 2008). This method allows quantifying ^{226}Ra and ^{228}Ra at low cost and without requiring a different equipment than the one used for short-lived Ra isotopes, but it requires independent measurements for the two Ra isotopes, long waiting times (for ^{228}Ra) and it has larger uncertainties than the gamma spectrometry technique (Moore 2008; Geibert et al. 2013).

Measuring ^{226}Ra and ^{228}Ra on Mn-fibers by gamma spectrometry requires either chemical leaching of the fibers with strong acids, followed by $BaSO_4$ coprecipitation (Moore 1984), or ashing the fiber and packing it into a vial for gamma counting (Charette et al. 2001). This latter procedure is the method adopted in this work. Once short-lived Ra measurements were completed, each Mn-fiber was placed in a porcelain crucible (250 mL) and ashed at 820 ºC for 16 hours to reduce the sample volume. The ash was then carefully ground, homogenized, and transferred into cylindrical counting vials of 5.6 cm^3 capacity. Counting vials were then sealed to prevent ^{222}Rn escape from the sample, and stored for a minimum of three weeks before counting to ensure the equilibrium between ^{226}Ra and its daughter radionuclides.

Samples were placed in a well-type (1.45 cm diameter, 40 mm length), low-background, high-resolution, high-purity germanium detector (HPGe) from CANBERRA and counted for 1-4 days (depending on the counting rate of the selected radionuclides) (Fig 2.3). The detector consists on a high-purity germanium crystal in a cryostat (temperature is normally reduced to -196ºC by using nitrogen liquid) placed in an iron, copper and lead shielding. The pulse generated by photon emissions is electronically stored to the multichannel analyzer (MCA), which consists of 8192 channels set to allow the determination of emission lines ranging from 40 to 3000 keV. The analyses of the spectra were conducted by using the Genie 2000 Gamma Analysis Software, which includes a set of algorithms to calculate net peak areas (the background of the detectors was measured periodically). The activity of ^{228}Ra was determined through the photopeak of its daughter ^{228}Ac ($T_{1/2}$ = 6.1 h; Q = 27.7%) at 911.6 keV, whereas ^{226}Ra emissions were measured through the ^{214}Pb peak at E_γ = 351.9 keV (Q = 37.2%). The ^{214}Pb photopeak was used instead of the direct photopeak of ^{226}Ra (E_γ = 185.7 keV; Q = 3.6%) because it has lower backgrounds and significantly higher quantum yields (Q), both of which result in improved sensitivities and lower measurement errors (Dulaiova and Burnett 2004; Scholten et al. 2013). Quantifying ^{226}Ra via the activity of ^{214}Pb requires radioactive equilibrium between both radionuclides, and thus aging the vials for a minimum of three weeks before counting and sealing them to prevent ^{222}Rn escape.

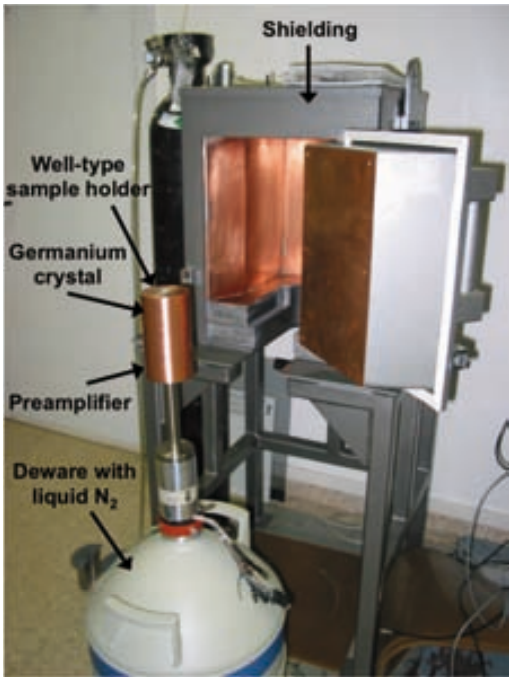

Figure 2.3. Main components of the well-type HPGe detector used to quantify long-lived Ra isotopes. Electronic associated components (amplifier, analog-to-digital converter (ADC) and multichannel analyzer (MCA)) are not shown in this figure.

The detection efficiencies for ^{226}Ra and ^{228}Ra were determined for different counting geometries (different ash volumes) using the standard solution MCR2009-018 supplied by CIEMAT. Efficiencies ranged from 20 to 29% for ^{226}Ra and from 6.5 to 9.0% for ^{228}Ra, depending on the detector used (2 detectors) (Table 2.2.). ^{226}Ra activities obtained from gamma measurements were compared with results obtained from the RaDeCC system to assess the quality of the data (Geibert et al. 2013). Results obtained from independent analysis of the same Mn-fibers were in good agreement (Fig 2.4) (Geibert et al. 2013).

Table 2.2. Detection efficiencies of the gamma spectrometers used for the determination of the ^{226}Ra and ^{228}Ra activities for different sample geometries.

Detector	Radionuclide	Emission line (keV)	Efficiency (%)			
			V4 (3.5 cm^3)	V5 (2.8 cm^3)	V6 (2.1 cm^3)	V7 (1.4 cm^3)
GM3	^{226}Ra*	351.9	19.8 ± 0.2	23.0 ± 0.2	24.8 ± 0.2	26.0 ± 0.2
	^{228}Ra**	911.6	6.50 ± 0.04	6.96 ± 0.05	7.63 ± 0.05	7.69 ± 0.05
GM4	^{226}Ra*	351.9	22.9 ± 0.3	26.0 ± 0.2	27.0 ± 0.2	29.3 ± 0.3
	^{228}Ra**	911.6	7.62 ± 0.06	8.40 ± 0.07	8.88 ± 0.06	9.01 ± 0.07

* Quantified via ^{214}Pb emissions
** Quantified via ^{228}Ac emissions

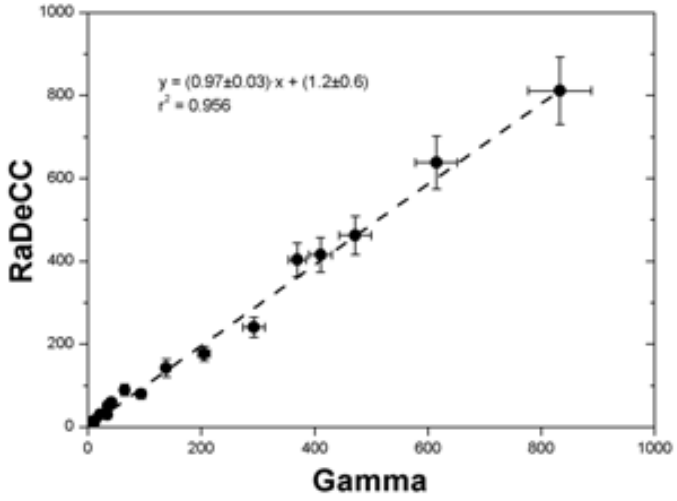

Figure 2.4. ^{226}Ra activities (dpm·fiber^{-1}) on Mn-fibers measured with two independent analyses: a RaDeCC system and by gamma spectrometry. The solid line represents the best linear fit to the data.

2.2. ^{226}Ra and ^{228}Ra in sediments

To determine the concentrations of ^{226}Ra and ^{228}Ra in sediments, samples were dried in an oven at 60 ºC for 24-48 hours. Then, sediments were milled, homogenized, placed into plastic vials (100 cm^3), sealed and stored for a minimum of three weeks to be analyzed by gamma spectrometry. Unlike the Mn-fibers, which require ashing the samples, the gamma analysis of sediments is a non-destructive technique. Samples were measured during 1-2 days by using a coaxial HPGe detector, as detailed above. Detectors were calibrated for efficiency by using a standard solution (MCR2009-018 supplied by CIEMAT).

2.3. ^{222}Rn in water samples: RAD7

The RAD7 (Durridge Inc.) is a radon-in-air monitor that is portable, durable, very sensitive and can operate in a continuous mode (Burnett et al. 2001a). The RAD7 uses a high electric field with a silicon semiconductor detector at ground potential to attract the positively charged polonium daughters of ^{222}Rn, ^{218}Po$^+$ ($T_{1/2}$ = 3.1 min; E_α = 6.00 MeV) and ^{214}Po$^+$ ($T_{1/2}$ = 164 μs; E_α = 7.67 MeV), which are counted as a measure of the ^{222}Rn concentration in air (Burnett et al. 2001a). The system uses an internal air pump to circulate the air to be analyzed through the detector. To adapt this radon-in-air detector to water measurements, the RAD-H_20 accessory (Durridge Inc.) was used. It

consists on a collection vial (250 mL) containing the sample and a closed air loop with an aerator (Fig 2.5). The system uses the internal pump of the RAD7 to sparge ^{222}Rn from the sample and circulate it to the detection chamber for measurement. A drying column is included in the air loop to ensure low moisture content (<10%) of the recirculating air. After 10 minutes of aeration and equilibration, most (>95%) of the ^{222}Rn is extracted from the water to the air loop and ^{222}Rn in water can be directly derived from the measurement of ^{218}Po (in equilibrium with ^{222}Rn). For a more detailed description on the measurement technique see (Burnett et al. 2001a; Dulaiova et al. 2005) and www.durridge.com.

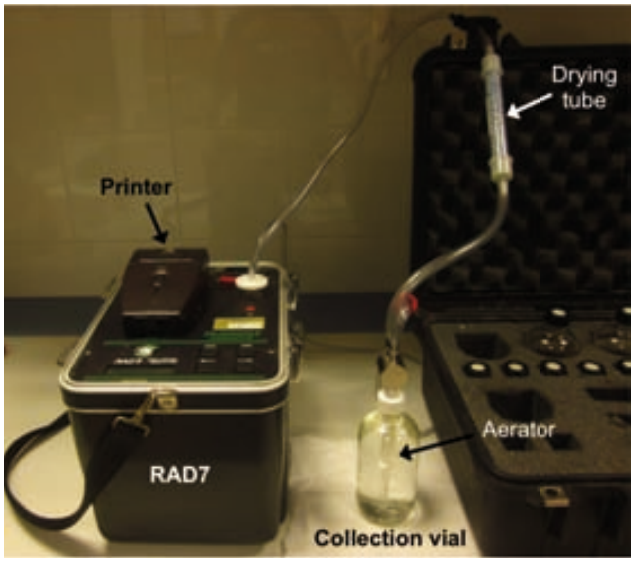

Figure 2.5. Measurement of ^{222}Rn from a water sample (250 mL) by using the RAD7 monitor and the RAD-H_2O accessory (Durridge Inc.). The main components of these systems are identified in the figure.

2.4. Nutrients, metals and Chl*a* in water samples

Analysis of nutrients, metals and chlorophyll *a* (Chl*a*) in water samples were conducted at the Mediterranean Institute for Advanced Studies (IMEDEA) (Balearic Islands, Spain).

Concentrations of dissolved NO_3^- and NO_2^- (DIN) and PO_4^{3-} (DIP) were determined with an autoanalyzer (Alliance Futura) using colorimetric techniques (Grasshoff et al. 1983). The accuracy of the analysis was established using Coastal Seawater Reference

Material for Nutrients (MOOS-1, NRC-CNRC; recoveries were 107 ± 11 %, 107 ± 6 % and 100 ± 6 % for PO_4^{3-}, NO_3^- and NO_2^-, respectively).

Trace-metal samples were acidified to pH<2 with ultrapure grade HCl (Merck) in a class-100 HEPA laminar flow hood and stored for at least 1 month before extraction. Dissolved (<0.22 μm) metals (Fe, Ni, Cu, Zn, Mo, Pb) were preconcentrated by the APDC/DDDC organic extraction method and analyzed by ICP-MS (PerkinElmer ELAN DRC-e) (Tovar-Sánchez 2012). The accuracy of the analysis was established using Coastal Seawater Reference Material for trace metals (CASS-4 and NASS-5, NRC-CNRC; recoveries were 113%, 105%, 106%, 96%, 112% and 103% for Fe, Ni, Cu, Zn, Mo and Pb, respectively).

The concentration of Chl*a* in water samples was determined by fluorometric analysis (Parsons et al. 1984). The filters were extracted in 90% acetone overnight and fluorescence was measured on a Turner Designs fluorometer calibrated with pure Chla (Sigma Co.).

CHAPTER 3

Quantifying groundwater discharge from different sources into a Mediterranean wetland by using ^{222}Rn and Ra isotopes

This chapter is based on:

Rodellas, V., Garcia-Orellana, J., Garcia-Solsona, E., Masqué, P., Domínguez, J.A., Ballesteros, B.J., Mejías, M., Zarroca, M., 2012. Quantifying groundwater discharge from different sources into a Mediterranean wetland by using ^{222}Rn and Ra isotopes. J. Hydrol. 466-467, 11-22.

3.1. Objective

The main objective of this study is to estimate the relative contribution of groundwater from four distinct sources into a Mediterranean coastal wetland by using Ra isotopes (^{223}Ra, ^{224}Ra, ^{226}Ra and ^{228}Ra) and ^{222}Rn, coupled with salinity and temperature measurements. In addition, we also aim to test the effectiveness of these radionuclides by comparing the results obtained with direct measurements of marsh water flows, and to evaluate the temporal variability of groundwater discharges in an interannual basis.

3.2. Methods

3.2.1. Study site: Peníscola marsh

The Peníscola marsh is a relatively small (105 ha), shallow (<1 m), brackish-water wetland, located in the Spanish Mediterranean coast (Fig. 3.1). Although this wetland is separated from the sea by a coastal sandy barrier, the Peníscola wetland was artificially channelized to the sea by three main channels that converge into a single one before flowing into the Mediterranean Sea through a narrow outlet (Fig. 3.1).

Since there is no surface water inflow, the only water sources to the Peníscola marsh are rainfall (average annual precipitation of 450 L·m-2; AEMET) and groundwater. Several groundwater sources converge into the wetland from four different pathways (Fig. 3.1): (i) a shallow and horizontal flow path of fresh groundwater from the detrital aquifer of the Vinaròs-Peníscola coastal plain and the Irta Range, (ii) an intermediate (mid-depth) flow of groundwater from the Vinaròs-Peníscola aquifer and the Irta Range that inflows to the wetland seeping through marsh sediments, (iii) a deep groundwater flow from the regional carbonate Jurassic aquifer of El Maestrat, also inflowing through marsh sediments, and (iv) intruded seawater that mixes with inflowing groundwaters either in the sediments or in the coastal aquifer. Although the Irta Range belongs to the hydrogeological unit of El Maestrat, here we differentiate this system because it refers to local shallow karstic flows of groundwater with its own hydrochemical signal. The regional carbonate Jurassic aquifer of El Maestrat is the most important groundwater reservoir in the area (recharge rates from $0.37 \cdot 10^9$ to

$0.42 \cdot 10^9$ $m^3 \cdot y^{-1}$; (Ballesteros et al. 2007)) and is strongly karstified, mostly draining to the sea through coastal springs in Peníscola, Alcossebre and Badum (Mejías et al. 2007, 2012; Garcia-Solsona et al. 2010b). A portion of this groundwater is advected to the Peníscola marsh ultimately passing through marsh sediments, where it converges with saline intrusion and groundwater from the mid-depth shallow systems and seeps into the Peníscola marsh as brackish groundwater. The upward-seeping of brackish groundwater through marsh sediments is mainly located in the central part of the wetland, developing several spring pools (locally named ullals) in topographical depressed areas.

Water outflows from the Peníscola marsh essentially occur through the surficial outlet to the Mediterranean Sea (evaporation can be neglected due to the short residence time of marsh waters). The micro-tidal conditions of the Mediterranean Sea (10-20 cm) preclude observing any tidal modulation in the Peníscola marsh.

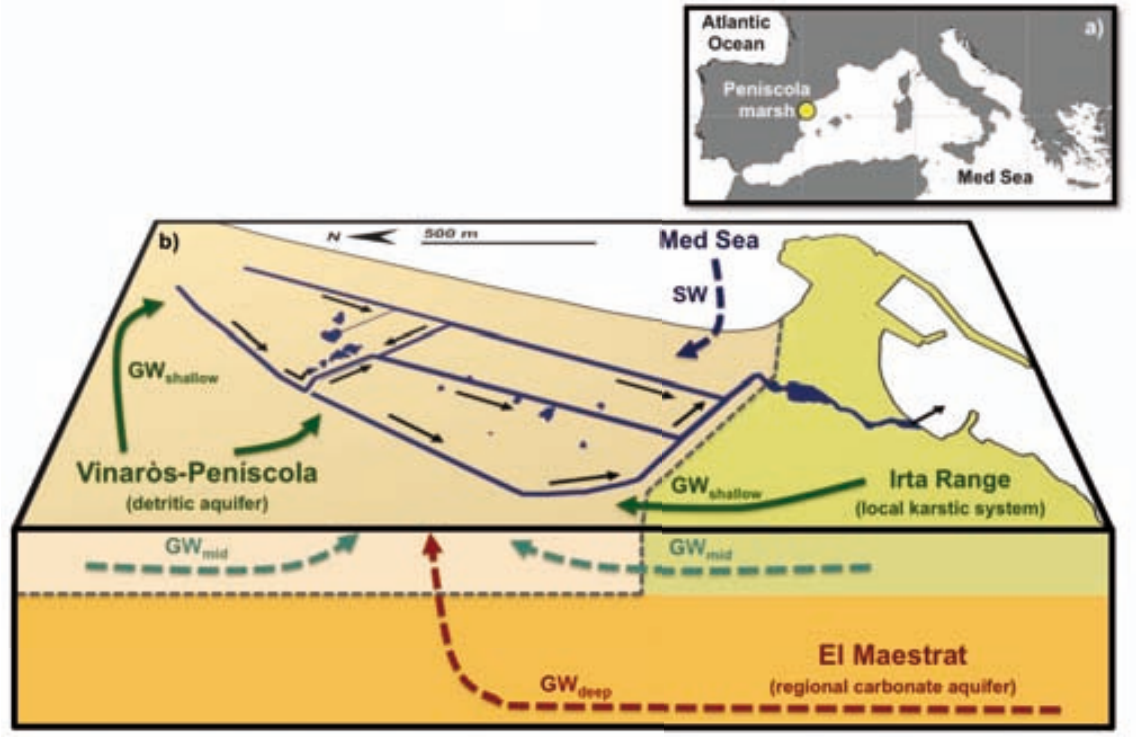

Figure 3.1. (a) Location of the Peníscola marsh in the Mediterranean Sea. (b) Schematic map of the Peníscola marsh area displaying the wetland channels and the spring pools. The flow direction of channelized waters is also indicated. The different systems (El Maestrat, Vinaròs-Peníscola and Irta Range) are represented together with the groundwater flow paths inflowing into the wetland. The solid arrows represent shallow horizontal flows, whereas the dashed ones illustrate upflowing groundwater discharging through marsh sediments.

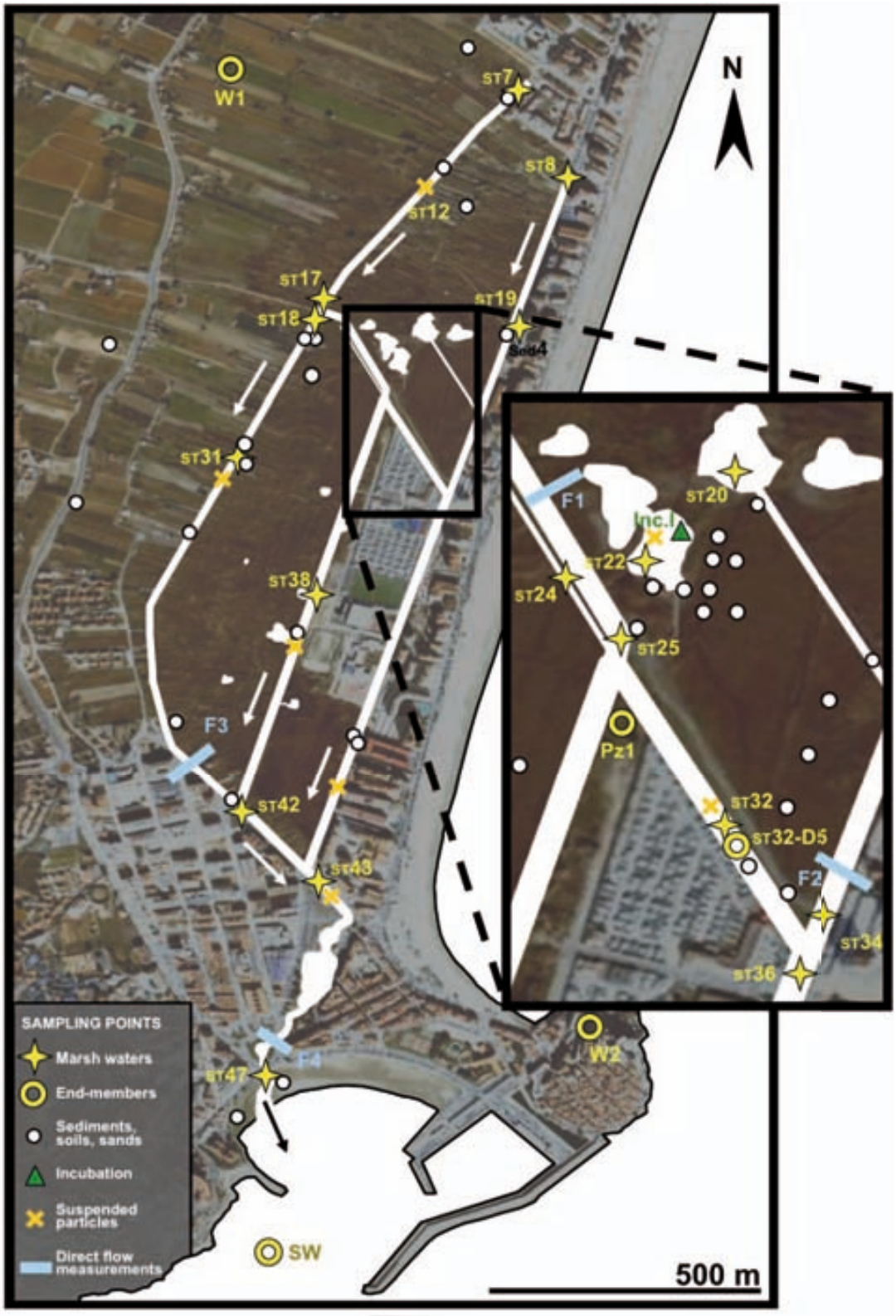

Figure 3.2. Sampling stations in the studied area: marsh water samples (yellow stars) and endmembers (yellow circles), sediment, soil and sand samples (white circles), the incubation experiment (green triangles), samples for suspended particles (orange crosses) and direct flow measurements (blue lines). The channels are emphasized with white lines. All the stations were sampled in August 2007. Stations ST7, ST32-D5 and ST47 were also sampled in February 2011 and station ST47 was sampled monthly from April 2007 to February 2008.

3.2.2. Sampling

Water sampling was conducted in the Peníscola marsh in August 2007, in February 2011 and between April 2007 and February 2008 in a monthly basis. During the first campaign, 16 surface water samples from wetland channels were collected for Ra isotopes and ^{222}Rn analysis (Fig. 3.2). The samples were pumped from 30-50 cm below the water surface, taken as representative of the water column. Direct flow measurements were conducted in the marsh outlet using a propeller flow meter (A.OTT Kempten, Z-30). The section of the outlet was accurately determined in order to calculate the volumetric flow. Endmember sampling for salinity, Ra isotopes and ^{222}Rn consisted in water collection from two wells (W1, W2) representative of shallow groundwater flows from the Vinaròs-Peníscola aquifer and the Irta Range, respectively, as well as a seawater sample from the Peníscola coastal area (SW). A submerged spring (ST32-D5) detected in marsh waters via temperature (>28ºC) and salinity (>10) measurements was also sampled by pumping water from the deepest part of the water column. A 60-m deep standpipe piezometer was installed at the central part of the wetland (Pz1) in February 2012. This piezometer had a slotted section at the bottom of the pipe to characterize deep groundwater from the Maestrat aquifer. Temperature and salinity were measured in all water samples using an YSI-556 handheld probe.

For Ra analyses, large volumes of water (10 to 50 L) were passed through columns loaded with MnO_2-impregnated acrylic fiber (hereafter Mn-fibers) at a flow rate <1 $L \cdot min^{-1}$ to quantitatively extract Ra isotopes (Moore and Reid 1973). ^{222}Rn samples were collected into 250 mL bottles to be analyzed with a RAD-H_2O system (Durridge Inc.). Although the RAD-H_2O system is unsuitable for determining ^{222}Rn concentrations in most surface waters, the high ^{222}Rn activities measured here allowed us to use this equipment. To minimize the contact of the ^{222}Rn samples with air, water was pumped directly through a tube ending at the bottom of the bottle and leaving the water overflow the bottle for several seconds.

On February 2011 a survey was carried out to compare groundwater discharge estimations with the flows obtained through direct measurements of marsh waters. The stations ST7, ST32-D5 (the submerged spring) and ST47 were re-sampled concurrently with direct marsh water flow measurements (four marsh sections; Fig. 3.2). Ra isotopes, ^{222}Rn, temperature and salinity were measured in all samples. A

propeller flow meter was used in section F4, while in sections F1, F2 and F3 the low flow and the amount of vegetation only allowed to measure the surficial flow by means of the float method. In order to evaluate the temporal variability of groundwater discharges, from April 2007 to February 2008 a monthly measurement of ^{222}Rn and ^{226}Ra concentrations and salinity in outflowing marsh waters (ST47) was carried out, coupled with direct flow measurements.

A total of 38 soil, sediment and sand samples were collected to obtain the distribution of long-lived Ra isotopes throughout the Peníscola marsh. Diffusive fluxes of Ra and ^{222}Rn from sediments were estimated from one shallow (15-20 cm), large (25 cm in diameter) sediment core. The core was collected in August 2009 at the station Inc_I (Fig. 3.2), where high ^{226}Ra concentrations in sediments had been previously measured. To determine the amount of suspended particles in marsh waters a volume of 3 L of water from seven stations (Fig. 3.2) was passed through pre-dried-weighed filters of 1 μm. The filters were dried and weighed again after sampling to calculate a net concentration of suspended particulate matter.

All the samples collected to determine ^{222}Rn activities in marsh waters and activities of Ra isotopes in both waters and sediments were analyzed as described in Chapter 2 (Analytical methods).

3.2.3. Ra and ^{222}Rn diffusive flux experiments

The sediment core collected for the incubation experiment (Inc_I) was placed in a bin filled with water to prevent artificially impressed flow along the core. The overlying water was extracted, and the tube was refilled with Ra-free water (2-3 L) from the same marsh location. Overlying waters were constantly aerated to prevent changes in redox conditions (Beck et al. 2007a).

To estimate the diffusive flux of Ra, a closed water loop was created (two tubes were connected to the core) and interconnected to a column containing Mn-fiber (Fig. 3.3a). We used a peristaltic pump (constant rate of 0.2 L·min^{-1}) to recirculate the overlying waters through the Mn-fiber to quantitatively extract the Ra isotopes and bring the filtered water (free of Ra) back to the incubation chamber. Without interrupting the

water flow, the Mn-fiber was replaced by a new one after progressively longer time periods (12, 24, 36, 48, 72 hours). The Ra diffusive fluxes were estimated from the slope of the best fit of the Ra activity per core surface area (dpm·m^{-2}) plotted against incubation time (h).

A similar experiment was conducted to determine the ^{222}Rn diffusive flux (Fig. 3.3b). After the Ra experiment, the incubation chamber was sealed to avoid ^{222}Rn losses to the atmosphere. A water flow from the free-air core was circulated to the RAD-Aqua commercial equilibrator (Durridge Inc.) at a rate of 0.5 L·min^{-1} (0.03 m^3·h^{-1}), where water was sprayed in a cylinder allowing the ^{222}Rn exhalation. The extracted ^{222}Rn was pumped through a closed air loop interconnected to the RAD7 alpha-detector (Durridge Inc.), what allows the ^{222}Rn quantification after correcting for temperature (continuously monitored) (Burnett et al. 2001a). After the water sample had been sprayed, it was derived to a carboy where it was permanently aerated to eliminate the remaining ^{222}Rn before being introduced again to the incubation chamber. Considering the high ^{226}Ra activities of marsh sediments, the time that recirculated water remains in contact with sediments is large enough to allow the quantification of the ^{222}Rn concentrations in outflowing waters using the RAD7 + RAD-Aqua system if measurements are integrated for 1 hour. We estimated the ^{222}Rn diffusive flux from the hourly-averaged concentrations over 48 hours (dpm·m^{-3}), multiplied by the water circulation rate (m^3·h^{-1}) and divided by the core surface area (m^2).

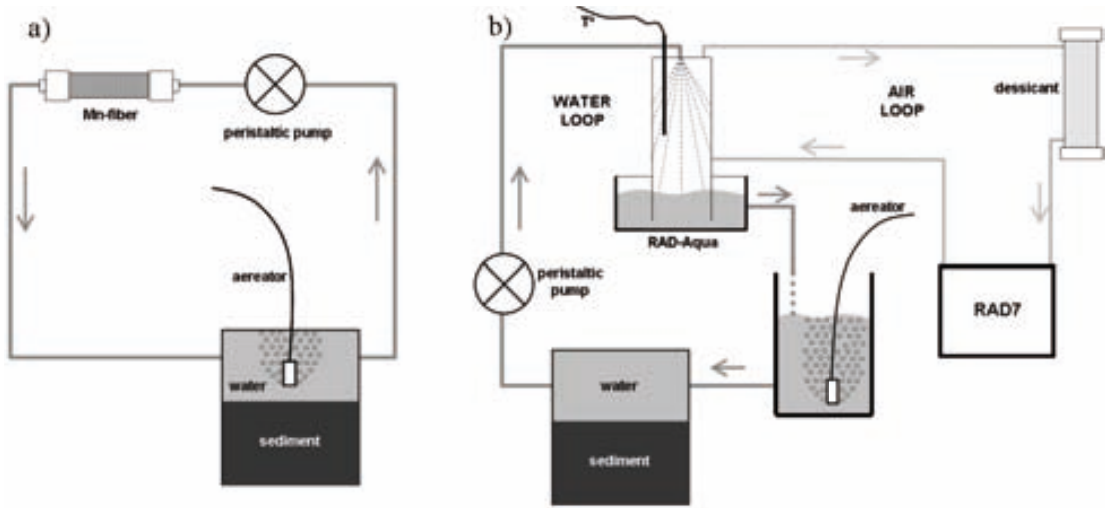

Figure 3.3. Schematic representation of Ra (a) and ^{222}Rn (b) diffusive flux experiments.

3.2.4. Desorbable Ra flux experiments

To determine the surface-bound desorbable Ra from suspended particles in marsh waters, about 10 g of sediments collected from seven different stations were added to 10 L of filtered, Ra-free brackish marsh water (salinity ~ 6.7, the highest measured in marsh waters). The sediments were collected in stations where the load of suspended particles was quantified (Fig. 3.2). Each sample was stirred several times during 24 hours and decanted to another container. The decanted water was filtered through a column containing clean acrylic fiber and Mn-fiber to remove the remaining suspended particles and extract all the Ra that had been desorbed, respectively. The content of Ra isotopes in the Mn-fiber was determined as described above. The desorbable Ra flux was determined from the load of suspended particles ($g \cdot L^{-1}$) and the experimental Ra desorption ($dpm \cdot g^{-1}$).

3.3. Results

The concentrations of ^{222}Rn and Ra isotopes in water samples collected in August 2007 are presented in Table 3.1, together with their activity ratios (AR) and data of salinity and temperature at the time of collection. Data on potential endmembers, including wells (W1 and W2), seawater (SW), the piezometer (Pz1) and the submerged spring (ST32-D5), are also included in Table 3.1.

A salinity gradient was measured along the marsh waters, with lower salinities (S<1) in the northern area, and higher salinities towards the marsh outlet (S~5.7). The marsh water samples with higher salinities (~ 6-7) were located in stations near or within surficial spring pools (ST22, ST24 and ST38). The sample collected directly from the submerged spring (ST32-D5) presented the highest salinity (13.7) of marsh waters. Temperature measurements showed similar distributions, with the highest temperatures (up to 28ºC) associated with spring pools or focused groundwater discharges. The temperature results might be only used as a qualitative parameter, as temperature measurements were conducted along the day, and thus, they are clearly influenced by diurnal temperature fluctuations.

A significant enrichment in Ra isotopes and ^{222}Rn along the marsh was also observed (by a factor of 16, 21, 180, 15 and 410 for ^{223}Ra, ^{224}Ra, ^{226}Ra, ^{228}Ra and ^{222}Rn, respectively),

with lower activities in the northern part and increasing concentrations towards the wetland outlet. The activities of all Ra isotopes and ^{222}Rn were significantly higher at stations ST24 and ST38, and for the long-lived Ra isotopes at ST22, all of them located close or within spring pools. These activities, particularly for ^{226}Ra and ^{222}Rn, are among the highest activities previously measured in wetlands, coastal lagoons or similar environments (e.g. (Charette et al. 2003; Cook et al. 2008; Garcia-Solsona et al. 2008b; Schmidt et al. 2010)). Activities of both short- and long-lived Ra isotopes, showed a strong positive correlation with salinity (Fig. 3.4). The ^{226}Ra activities were 1-3 orders of magnitude higher than the other isotopes, with ^{228}Ra/^{226}Ra activity ratios (AR) ranging from 0.03 to 0.06 in the central part of the marsh. Most of the marsh water samples presented a ^{224}Ra/^{228}Ra AR ranging from 1 to 1.9. Enrichment of ^{224}Ra relative to ^{228}Ra have been reported for many estuaries and salt marshes, and is attributed to the continuous leaching of Ra from sediments and the faster regeneration of ^{224}Ra (e.g. (Hancock and Murray 1996; Rama and Moore 1996; Charette et al. 2003)). The sample from the submerged spring (ST32-D5) presented the highest activities measured in marsh waters for all Ra isotopes and ^{222}Rn (Table 3.1).

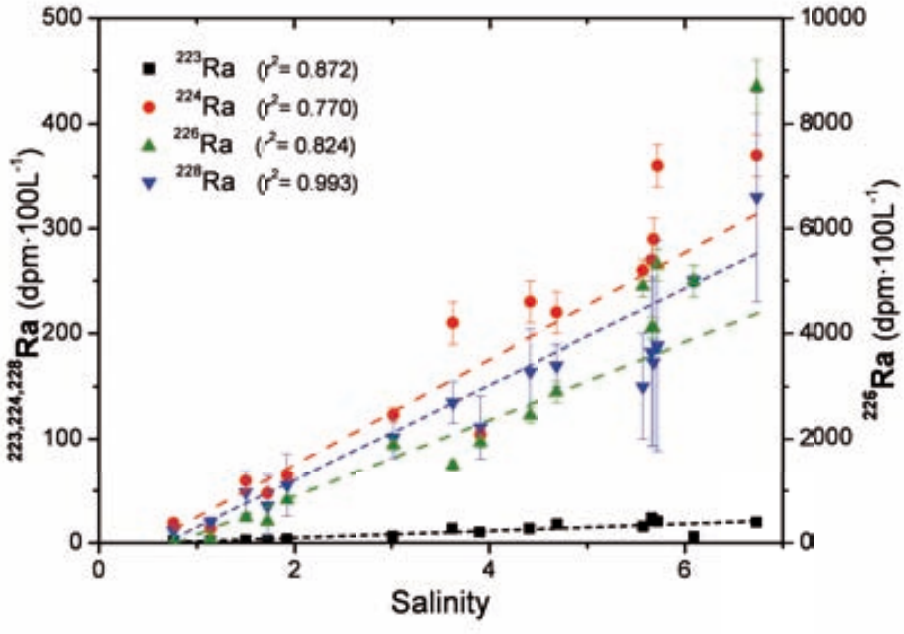

Figure 3.4. Ra isotopes vs salinity for samples from the Peníscola marsh. Positive linear correlations are observed for all Ra isotopes.

Regarding the direct groundwater measurements, samples measured in shallow wells from the Vinaròs-Peníscola aquifer (W1) and the Irta Range (W2) had low salinities (<1) and the concentrations of Ra isotopes and ^{222}Rn were between 1 and 3 orders of magnitude lower than those measured in waters of the marsh channels. Water collected at 60 m in the deep piezometer (Pz1) presented higher temperatures (up to 45 ^{o}C), higher salinities (up to 20) and higher Ra activities (e.g. $2.7 \cdot 10^{4}$ dpm·100L^{-1} for ^{226}Ra) than all the samples measured in marsh waters, but lower ^{222}Rn activities ($7.4 \cdot 10^{5}$ dpm·100L^{-1}).

The data corresponding to the samples collected in February 2011 survey are also included in Table 3.1. The highest Ra and ^{222}Rn activities, as well as temperature and salinity, were measured at the submerged spring (F-ST32-D5). The ^{222}Rn activities measured at this station were comparable to those determined in August 2007 and February 2011, whereas the salinity and Ra activities were considerably lower in the latter survey.

The ^{226}Ra activities in marsh sediments ranged from 13 to 47 dpm·g^{-1}, and found to be high relative to world average concentrations (2.1 dpm·g^{-1}: (UNSCEAR 2000)) and soils collected in the Western Mediterranean (0.5 – 3 dpm·g^{-1}: (Garcia-Orellana et al. 2006)). Concentrations of ^{228}Ra ranged from 0.6 to 3.3 dpm·g^{-1}, comparable to the world average concentration (1.8 dpm·g^{-1}; (UNSCEAR 2000)). The highest ^{226}Ra concentrations were observed in the central-western part of the marsh, resulting in ^{228}Ra/^{226}Ra AR ranging from 0.03 to 0.06.

The diffusive Ra fluxes from the sediments obtained from the incubation of marsh sediments were 3.2 ± 0.7, 122 ± 10, 1850 ± 140 and 71 ± 10 dpm·m^{-2}·d^{-1} for ^{223}Ra, ^{224}Ra, ^{226}Ra and ^{228}Ra, respectively. The ^{228}Ra/^{226}Ra flux ratio (0.038 ± 0.006) is comparable with the ^{228}Ra/^{226}Ra AR of sediment from the marsh central part (0.03 – 0.006), revealing that the flux differences among Ra isotopes derive from the different Ra concentrations in sediments. The ^{222}Rn flux obtained with this experiment was 1,200±300 dpm·m^{-2}·h^{-1}. It should be taken into account that Ra and ^{222}Rn diffusive fluxes are both upper limit estimates, not only because we incubated a marsh sediment with one of the highest ^{226}Ra activities, but also because replacing continuously the overlying enriched waters by water free of these radionuclides maximizes the gradient between pore water and overlying waters, thus increasing the diffusion flux.

Table 3.1. Salinity, temperature, Ra and ^{222}Rn activities and activity ratios (AR) of the marsh waters and endmembers sampled in August 2007 and February 2011.

Sample	Salinity	Temperature	^{223}Ra	^{224}Ra	^{226}Ra	^{228}Ra	^{222}Rn	^{224}Ra/^{228}Ra
		ºC			(dpm·100L^{-1})		(·10^{3} dpm·100L^{-1})	
August 2007								
Marsh samples								
ST7*	0.76	18.70	1.5 ±0.2	19 ± 1	12.8 ± 0.6	11.5 ± 0.9	46 ± 9	1.63 ± 0.15
ST8	1.14	24.58	1.7 ±0.2	14 ± 1	74 ± 4	19 ± 3	21 ± 5	0.70 ± 0.11
ST17	1.50	21.15	2.5 ±0.5	60 ± 3	480 ± 30	48 ± 9	250 ± 20	1.2 ± 0.2
ST18	1.92	21.95	4.0 ±0.6	65 ± 3	820 ± 40	56 ± 4	550 ± 30	1.17 ± 0.11
ST19	3.62	24.34	13.6 ±1.2	210 ± 20	1490 ± 90	135 ± 9	460 ± 20	1.52 ± 0.15
ST20	3.90	23.62	10.0 ±1.5	104 ± 7	1940 ± 110	111 ± 11	270 ± 30	0.94 ± 0.11
ST22	6.09	23.47	6.1 ±1.3	130 ± 8	5000 ± 300	250 ± 30	44 ± 6	0.52 ± 0.06
ST24	5.72	25.85	20 ±2	360 ± 20	5300 ± 300	189 ± 13	3510 ± 100	1.9 ± 0.2
ST25	3.01	23.72	6.1 ±0.9	123 ± 7	1890 ± 110	101 ± 8	630 ± 20	1.21 ± 0.12
ST31	1.72	22.34	2.8 ±0.2	47 ± 3	410 ± 20	35 ± 3	980 ± 30	1.34 ± 0.14
ST32-D1	4.69	17.20	18 ±2	220 ± 20	2900 ± 200	170 ± 20	560 ± 20	1.3 ± 0.2
ST36	4.41	25.05	14 ±2	230 ± 20	2460 ± 150	164 ± 10	450 ± 40	1.41 ± 0.13
ST38	6.73	28.62	20 ±3	370 ± 20	8700 ± 500	330 ± 20	2970 ± 100	1.12 ± 0.09
ST42	5.57	25.24	16 ±2	260 ± 10	4900 ± 200	150 ± 9	1800 ± 50	1.74 ± 0.13
ST43	5.68	25.78	21 ±2	290 ± 20	4100 ± 200	173 ± 11	1680 ± 80	1.7 ± 0.2
ST47	5.66	26.15	24 ±2	270 ± 20	4100 ± 200	183 ± 10	1770 ± 90	1.5 ± 0.1
Endmembers								
W1	0.83	19.52	1.5 ±0.2	12.6 ± 1.0	22.8 ± 1.4	12 ± 1	4 ± 2	1.02 ± 0.10
W2	0.30	n.a.	n.a.	n.a.	12.7 ± 0.4	n.a.	4.9 ±1.1	-
ST32-D5*	13.73	28.31	83 ±6	1040 ± 60	17100 ± 1100	580 ± 40	3700 ±200	1.8 ±0.2
Pz1*	19.47	42.11	n.a.	3430 ± 110	27100 ± 600	2500 ± 100	740 ± 20	2.1 ± 0.2
SW*	38.05	n.a.	3.4 ±0.4	44 ± 3	46.2 ± 0.8	17 ± 1	4.6 ± 0.9	2.5 ± 0.2
February 2011								
F-ST7*	0.77	15.90	0.7 ±0.2	16.2 ± 1.4	n.a.	n.a.	50 ± 20	-
F-ST32-D5*	11.79	33.55	41 ±5	630 ± 50	7200 ± 400	420 ± 20	3990 ± 130	1.5 ± 0.2
F-ST47	4.70	18.88	8.0 ±1.2	194 ± 15	1690 ± 60	150 ± 9	1900 ± 70	1.30 ± 0.13

n.a. not analyzed

* samples used as endmembers in the mixing models

The desorption experiment conducted in seven marsh sediment samples resulted in desorbable Ra activities of about 0.010 ± 0.003 dpm·g^{-1} for ^{223}Ra, 0.25 ± 0.04 dpm·g^{-1} for ^{224}Ra, 4.5 ± 0.5 dpm·g^{-1} for ^{226}Ra and 0.31 ± 0.21 dpm·g^{-1} for ^{228}Ra. These estimates are an upper limit because we used Ra-free water with the highest salinity observed in marsh waters (6.7), which increased Ra desorption. Concentrations of suspended particles in the seven water samples analyzed range from 0.3 to 2.1 g·100L^{-1}, with an area-weighed average of 0.68 ± 0.07 g·100L^{-1}.

3.4. Discussion

The distribution of salinity and Ra and ^{222}Rn concentrations measured in marsh waters suggests the presence of two distinct groundwater types discharging to the Peníscola marsh: (i) the discharge of fresh groundwater in the northeastern and eastern parts of the wetland characterized by low salinities (<1) and low activities of Ra isotopes and ^{222}Rn; and (ii) brackish groundwater discharging via springs or seeps distributed throughout the marsh, characterized by higher salinities, temperatures and Ra and ^{222}Rn concentrations. Considering the observed pattern and the hydrogeological functioning of the Peníscola marsh (Fig. 3.1), we assume that: i) groundwater inflowing into the northeastern and eastern parts of the wetland accounts mainly for the shallow flow of fresh groundwater from the Vinaròs-Peníscola and the Irta Range systems ($GW_{shallow}$); ii) Groundwater seeping through the marsh sediments (GW_{seep}) is dominated by the deep flow of groundwater from the carbonate Jurassic aquifer of El Maestrat (GW_{deep}), which actually mixes with seawater intrusion (SW) and an intermediate flow of groundwater from the mentioned two local shallow systems (GW_{mid}) before discharging to the wetland (Fig. 3.1).

3.4.1. Evaluation of potential sources of Ra isotopes and ^{222}Rn

In order to estimate the contribution of each groundwater source by using Ra isotopes and ^{222}Rn, the other potential inputs of these radionuclides must first be evaluated. Aside from groundwater inputs, the other potential Ra and ^{222}Rn sources that we identified are desorption of surface-bound Ra from resuspended particles, diffusive fluxes of ^{222}Rn and Ra from bottom sediments and ingrowth of ^{222}Rn by decay of dissolved ^{226}Ra.

To evaluate the importance of each possible source term we need to estimate the average concentration of Ra isotopes and ^{222}Rn in marsh waters. Since (i) sampling stations were not homogenously distributed throughout the marsh and (ii) each channel had its own water flow, the integrated inventories should be calculated weighting both considerations. However, since all marsh water outputs occur through the marsh outlet (station ST47), the concentrations of Ra isotopes, ^{222}Rn and salinities measured in marsh outflowing waters (appropriately corrected for losses for radioactive decay and ^{222}Rn evasion to the atmosphere) can be considered the best representation of integrated marsh waters. In the following subsections, each source term will be discussed in order to evaluate its relative contribution to the Ra and ^{222}Rn inventories in marsh waters.

a) Diffusive fluxes from sediments

Considering an average marsh waters depth of 1.5 m and the marsh water apparent age calculated in section 4.2.1.2. (T_R= 1.2 d), the maximum experimental diffusive fluxes from underlying sediments would represent 1.1, 3.8, 3.7, 0.1, 0.1 % of the total ^{223}Ra, ^{224}Ra, ^{226}Ra, ^{228}Ra and ^{222}Rn concentrations, respectively (Table 3.2). Thus, even if the fluxes obtained in our experiment are maxima, the diffusion from sediments represents a negligible input of Ra and ^{222}Rn into the marsh channels.

b) Desorption from resuspended particles

Since there are no surface water inputs carrying particles in suspension, the suspended particles comprise the major source of desorbable Ra. The maximum desorption that could occur in marsh waters was on the order of 0.07 ± 0.02, 1.7 ± 0.2, 30.5 ± 0.3 and 2.4 ± 1.4 dpm·100L^{-1} for ^{223}Ra, ^{224}Ra, ^{226}Ra and ^{228}Ra, respectively (Table 3.2). These concentrations are also maxima estimates, as it is implicitly considered that new sediments (with regenerated Ra) are resuspended at each time interval (marsh waters age, T_R) (Beck *et al.*, 2007). Even so, the maximum desorption would only contribute with less than 1% of the total Ra concentrations measured in outflowing waters (ST47).

c) Production of ^{222}Rn from dissolved ^{226}Ra decay

^{222}Rn activities measured in marsh waters were 2-3 orders of magnitude higher than ^{226}Ra activities dissolved in marsh waters (Table 3.1). Thereby, ^{222}Rn activities produced by decay of dissolved ^{226}Ra contribute to a very little fraction (~ 0.2%) of the total amount of ^{222}Rn (Table 3.2).

d) Groundwater inputs

Since the contribution of diffusion, desorption and production of Ra isotopes and ^{222}Rn account for less than 5% of the activities of these radionuclides in marsh waters (Table 3.2), the remaining source (groundwater discharges) should account for the most part of Ra isotopes and ^{222}Rn inputs to the Península marsh. It should be noted that the contributions estimated in the previous subsections correspond to upper limits, as the ST47 does not account for the losses for radioactive decay and ^{222}Rn evasion to the atmosphere which had occurred all along the water pathway. Hence the contribution of groundwater discharges (>95%) represents a minimum estimate.

Table 3.2. Supply (dpm·100L^{-1}) and relative importance (%) of each Ra isotope and ^{222}Rn source to average marsh waters concentrations (ST47). Sources considered (aside from groundwater) are: diffusion from sediments, desorption from suspended particles and production for decay.

	^{223}Ra	%	^{224}Ra	%	^{226}Ra	%	^{228}Ra	%	^{222}Rn (·10^3)	%
^{22X}Ra-^{222}Rn diffusion sediments	**0.26 ± 0.06**	**1.1**	**10.1 ± 0.8**	**3.8**	**153 ± 12**	**3.7**	**0.24 ± 0.03**	**0.1**	**2.4 ± 0.6**	**0.1**
$M_{dif.}$ modeled diff. (dpm·m^{-2}·d^{-1})	3.2 ± 0.7		122 ± 10		1850 ± 140		71 ± 10		29 ± 7	
$T_{R.}$ water age (d)	1.2		1.2		1.2		1.2		1.2	
$h_{av.}$ average water depth (m)	1.5		1.5		1.5		1.5		1.5	
^{22X}Ra desorption susp. particles	**0.07 ± 0.02**	**0.3**	**1.69 ± 0.20**	**0.6**	**30.5 ± 0.3**	**0.7**	**2.1 ± 1.4**	**1.2**	**-**	
$M_{des.}$ modeled des. (dpm·g^{-1})	0.010 ± 0.003		0.25 ± 0.04		4.5 ± 0.5		0.31 ± 0.21			
P_{sus}: susp. particles (g·100L^{-1})	0.68 ± 0.08		0.68 ± 0.08		0.68 ± 0.08		0.68 ± 0.08			
^{222}Rn production ^{226}Ra decay	**-**		**-**		**-**		**-**		**4.2 ± 0.2**	**0.2**
TOTAL		**1.4**		**4.4**		**4.5**		**1.3**		**0.4**
Total ^{22X}Ra-^{222}Rn (ST47)	**24 ± 2**		**270 ± 20**		**4200 ± 300**		**166 ± 11**		**1770 ± 90**	

3.4.2. Groundwater contribution from each source

3.4.2.1. Mixing model

Since more than 95% of the total amount of Ra and ^{222}Rn entering the wetland can be attributed to groundwater discharges, activities of these radionuclides in marsh waters should be explained by a mixing of the shallow flow of fresh groundwater from the Vinaròs-Peníscola and the Irta Range systems ($GW_{shallow}$) and groundwater seeping through marsh sediments (GW_{seep}). The mixing of these two groundwater types should also explain the salinity of marsh waters, as no other sources were identified and salinity behaves conservatively. However, as evidenced from the relationship between ^{222}Rn and salinity (Fig. 3.5), several marsh water samples do not fall on the mixing line between the low ^{222}Rn - low salinity waters ($GW_{shallow}$) and the high ^{222}Rn – high salinity waters (GW_{seep}), requiring the development of a more appropriate mixing model for the Peníscola marsh system.

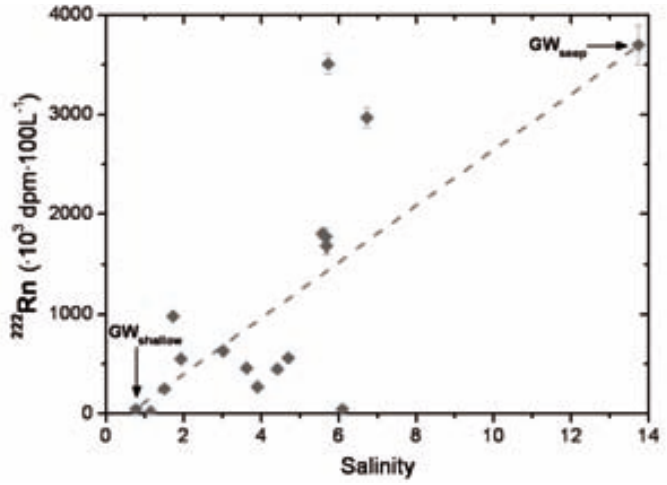

Figure 3.5. ^{222}Rn vs salinity for samples from the Peníscola marsh waters. The dashed line represents the mixing line between the low ^{222}Rn - low salinity waters ($GW_{shallow}$) and the high ^{222}Rn – high salinity waters (GW_{seep}).

The high Ra activities measured in the 60-m piezometer ($2.7 \cdot 10^4$ dpm·100L^{-1} for ^{226}Ra at Pz1) suggest that groundwater from the deep Jurassic aquifer of El Maestrat (GW_{deep}) could be the main source of Ra isotopes to the Peníscola marsh waters. However, ^{222}Rn activities measured in the piezometer ($700 \cdot 10^3$ dpm·100L^{-1}) were 5-6 times lower than the ^{222}Rn activities measured in the submerged spring ($4 \cdot 10^6$ dpm·100L^{-1} at ST32-D5; Table 3.1). In addition, the maximum ^{222}Rn groundwater activities measured directly from the local shallow aquifers, either from wells close to the Peníscola marsh ($4 \cdot 10^3$

and $5 \cdot 10^3$ dpm·100L^{-1} at station W1 and W2, respectively; Table 3.1) or coastal springs (Badun: 10^3 - 10^4 dpm·100L^{-1}, unpublished data), are 2-3 orders of magnitude lower than the ^{222}Rn activities measured in the marsh submerged spring. The lack of any endmember with ^{222}Rn activities high enough to support the activities measured in marsh waters and the high ^{226}Ra activities measured in the Peníscola marsh sediments (up to 47 dpm·g^{-1}), suggest that groundwater discharging via seeps or springs (GW_{seep}) becomes enriched in ^{222}Rn during its advection through marsh sediments.

Considering that the primary source of Ra isotopes is the deep groundwater flow (GW_{deep}), the mixing of the GW_{deep} with seawater intrusion (SW) and intermediate groundwater flows from the local shallow systems (GW_{mid}) prior to discharge to the wetland results in inflowing groundwaters (GW_{seep}) having Ra activities and salinities depending on this three endmember mixing. Unlike Ra, as marsh sediments are the main source of ^{222}Rn, the ^{222}Rn activity of the GW_{seep} should be constant and independent of this mixing. These processes are summarized in a schematic plot (Fig. 3.6), where water fluxes are drawn together with the salinities and ^{226}Ra and ^{222}Rn activities measured at stations ST32-D5 and ST24. Both samples were collected where seeping of the GW_{seep} seemed to be the only source of water: salinity (13.73) and temperature (28.3ºC) at station ST32-D5 indicated a point-source groundwater discharge, whereas station ST24 was located in a shallow (0.4 m depth) and narrow (0.5-1 m) channel without inputs other than seeping groundwater. The ^{222}Rn activities measured in both stations agree well ($(3.7 \pm 0.2) \cdot 10^6$ and $(3.5 \pm 0.1) \cdot 10^6$ dpm·100L^{-1}), whereas salinities (13.7 and 5.7 for ST32-D5 and ST24, respectively) and Ra activities (e.g. $(17.1 \pm 1.1) \cdot 10^3$ and $(5.3 \pm 3) \cdot 10^3$ dpm·100L^{-1} of ^{226}Ra for ST32-D5 and ST24, respectively) present significant differences.

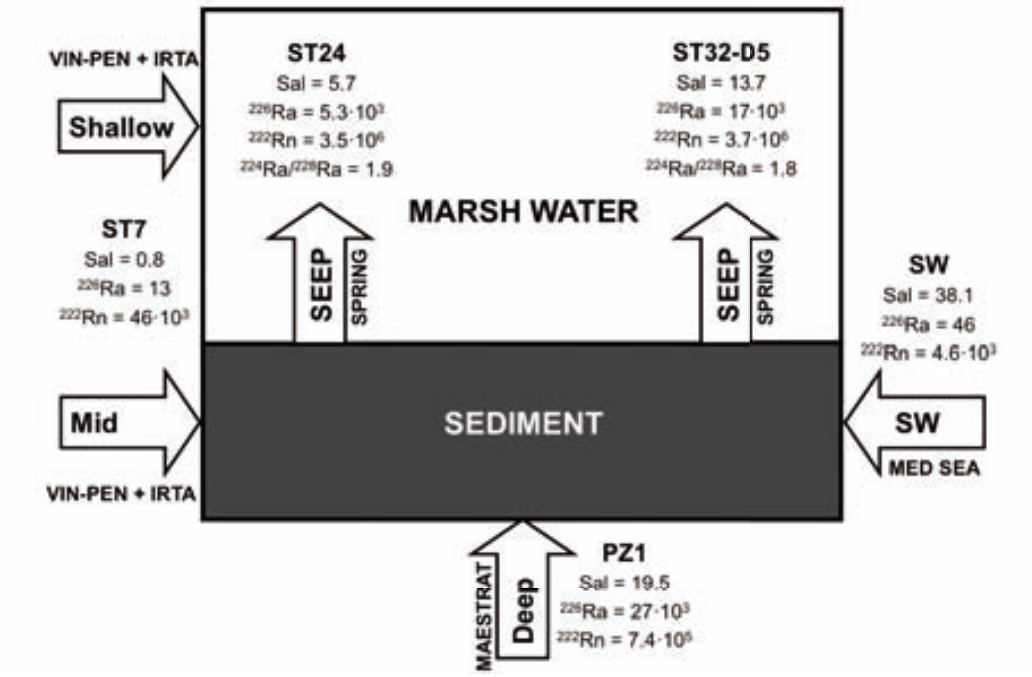

Figure 3.6. Schematic representation of fluxes of waters to the Peníscola marsh; salinity, ^{226}Ra and ^{222}Rn concentrations (dpm·100L^{-1}) are also indicated. Data of stations ST24 and ST32-D5 are also shown to emphasize the variations in salinity, ^{226}Ra, ^{222}Rn and ^{224}Ra/^{228}Ra of GW_{seep} in different submerged springs.

In summary, the Peníscola marsh system is described by a binary mixing between the shallow flow of fresh groundwater ($GW_{shallow}$) and groundwater inflowing through marsh sediments (GW_{seep}). This latter fraction represents the mixing of the flows of deep groundwater (GW_{deep}), mid-depth groundwater (GW_{mid}) and seawater intrusion (SW) prior to inflow into the wetland waters. Considering the different enrichment processes for Ra isotopes and ^{222}Rn, the appropriate mixing model to describe the relative contributions of distinct water types to the Peníscola marsh can be written as follows:

$$f_{GWshal} + f_{GWdeep} + f_{GWmid} + f_{SW} = 1 \quad (3.1)$$

$$^{222}Rn_{GWshal} \cdot f_{GWshal} + {}^{222}Rn_{GWseep} (f_{GWdeep} + f_{GWmid} + f_{SW}) = {}^{222}Rn_{STxx} \cdot e^{(\lambda \cdot T + K \cdot T/h)} \quad (3.2)$$

$$^{226}Ra_{GWshal} \cdot f_{GWshal} + {}^{226}Ra_{GWdeep}\, f_{GWdeep} + {}^{226}Ra_{GWmid}\, f_{GWmid} + {}^{226}Ra_{SW}\, f_{SW} = {}^{226}Ra_{STxx} \quad (3.3)$$

$$Sal_{GWshal} \cdot f_{GWshal} + Sal_{GWdeep}\, f_{GWdeep} + Sal_{GWmid}\, f_{GWmid} + Sal_{SW}\, f_{SW} = Sal_{STxx} \quad (3.4)$$

where f_i, $^{222}Rn_i$, $^{226}Ra_i$ and Sal_i are the relative fractions, the ^{222}Rn the ^{226}Ra activities and the salinity, respectively, of each water source: $GW_{shallow}$, GW_{deep}, GW_{seep}, SW and GW_{seep}. The terms $^{222}Rn_{STxx}$, $^{226}Ra_{STxx}$ and Sal_{STxx} represent the ^{222}Rn, the ^{226}Ra activities and the salinity measured in a given sample; λ is the decay constant of ^{222}Rn (0.181 d^{-1}), K is the ^{222}Rn gas exchange velocity, h is the area-weighed average of marsh water

depth (1.5 m), and T is the time elapsed since the water mass entered the system (marsh water age). The term $e^{(\lambda \cdot T + K \cdot T/h)}$ accounts for the ^{222}Rn losses related to decay and evasion to the atmosphere along the water pathway before the water reached the sampling station. Although other Ra isotopes could be used, here we favored ^{226}Ra because it is the most enriched isotope in marsh waters and its radioactive decay can be neglected. The use of this model requires the characterization of all endmembers ($GW_{shallow}$, GW_{deep}, GW_{mid}, SW and GW_{seep}) and the estimation of the ^{222}Rn gas exchange velocity and the apparent marsh water age, all of them established in the next subsections.

a) Selection of endmembers

Since the shallow flow of groundwater from the Vinaròs-Peníscola aquifer has the same characteristics as the shallow flow from the karstic Irta Range system (low Ra, ^{222}Rn and salinities), we cannot distinguish both flows using these tracers. Either the sample from the north part of the eastern channel (ST7) or the samples from the wells nourished by groundwater from the Vinaròs-Peníscola littoral plain (W1) or the Irta Range (W2) may be used to characterize the fresh groundwater endmember from the local shallow aquifers ($GW_{shallow}$). Salinities and Ra concentrations are similar at these stations, whereas ^{222}Rn activities are one order of magnitude lower in both wells. These differences can be explained by the shallowness of the wells (20-40 cm), which could enhance the ^{222}Rn evasion to the atmosphere. For this reason, station ST7 is taken as the best representation of the $GW_{shallow}$ endmember. This station is also used to characterize the GW_{mid}, as this endmember refers to the deeper flow of groundwater from the same local shallow systems that discharge to the wetland via seeps through marsh sediments.

The sample collected from the 60-m deep piezometer (Pz1) was used to characterize the deep groundwater from the regional carbonate Jurassic aquifer of El Maestrat (GW_{deep}). The high temperature (>40ºC) measured in Pz1 reveals its hydrothermal origin, a feature of the deep Maestrat aquifer already documented (Sánchez Navarro et al. 2004). The station SW collected at the Peníscola coastal sea is used to characterize the seawater endmember (SW).

Since the GW_{seep} discharge to the marsh channels occurs through submerged springs or seeps, the best approach to obtain a representative endmember for ^{222}Rn associated to

the GW_{seep} may be the direct collection of discharging groundwater seeping through the sediments of the marsh channels. The deepest sample collected at station ST32 (ST32-D5), where a focused, point-sourced groundwater discharge was detected from salinity and temperature measurements, may be considered the best representation of the GW_{seep} endmember. Notice that neither ^{226}Ra nor salinities of the GW_{seep} have to be used in our model, because variations in the mixing between the GW_{deep}, the GW_{mid} and SW results in GW_{seep} having different salinities and Ra content, thus preventing to establish a precise Ra- and salinity- endmembers for the GW_{seep} (Fig. 3.6).

A summary of the selected endmembers is presented in Table 3.1. As extremely distinct tracer signatures characterize all the endmembers, the results of the mixing model are insensitive to small variations in the endmember values.

b) Estimation of ^{222}Rn gas exchange rate

As ^{222}Rn activities measured in marsh waters are 3-4 orders of magnitude higher than ^{222}Rn activities in air (~300 dpm·100L^{-1}) in Equations 3.1-3.4, atmospheric outputs are considered to only depend on the ^{222}Rn gas exchange rate (K) and the ^{222}Rn concentration in water (applying a factor h to normalize for depth) (Eq. 3.1-3.4). We take K = 0.16 m·d^{-1}, as obtained by Cook et al. (Cook et al. 2008) via an injected tracer experiment using SF_6 for a shallow (<1 m) wetland. This experimental ^{222}Rn gas exchange rate was preferred to empirical equations (e.g. (MacIntyre et al. 1995)) because it was obtained from an environment with similar characteristics to our study area. Although the results of the model are highly sensitive to the ^{222}Rn gas exchange rate (K), its variations would only influence the contribution of groundwater from the local shallow systems ($GW_{shallow}$ and GW_{mid}). For instance, had we used K=0.24 m·d^{-1} (i.e., a 50% higher), the fractions of the $GW_{shallow}$ and the GW_{mid} would be reduced and increased, respectively, by a factor of 10-15%, whereas the contribution of the GW_{deep} and the SW would remain constant.

c) Estimation of apparent marsh water age

The variation of the ratios between Ra isotopes of different half-lives can be used to determine the apparent age of marsh waters. Moore and coauthors (Moore et al. 2006) developed an approach that allows considering continuous additions of Ra throughout

the system. Assuming that there are no losses of Ra aside mixing or radioactive decay, the apparent marsh water age can be estimated by using equation (3.5):

$$T_R = \frac{F(^{224}Ra/^{228}Ra) - I(^{224}Ra/^{228}Ra)}{I(^{224}Ra/^{228}Ra)\cdot\lambda_{224}} \quad (3.5)$$

where F(^{224}Ra /^{228}Ra) is the ^{224}Ra/^{228}Ra activity ratio (AR) of the groundwater inputs into the system, I(^{224}Ra /^{228}Ra) is the ^{224}Ra/^{228}Ra AR of a given marsh water sample, and λ_{224} is the decay constant of ^{224}Ra (0.189 d^{-1}). Although other Ra isotopes may be used, here we used ^{224}Ra /^{228}Ra AR because the Peníscola marsh timescale is appropriate to the ^{224}Ra half-life and both radionuclides belong to the same decay chain.

Given that the GW_{seep} discharge is largely the main input of Ra isotopes into the Peníscola marsh, we used the ^{224}Ra /^{228}Ra AR of sample ST32-D5 (1.8 ± 0.2) as the best representation of inflowing groundwaters (F(^{224}Ra/^{228}Ra)) into the system. The apparent marsh water age calculated here represents the time elapsed since the GW_{seep} enters into the wetland. Notice that, although the Ra activities of the GW_{seep} depend on the mixing of the GW_{deep} with SW and the GW_{mid} prior to discharge to the wetland, the activity ratios between Ra isotopes are constant in the GW_{seep} (Fig. 3.6). Considering the wetland outflowing waters as the best representation of the Peníscola marsh waters, we used the ^{224}Ra /^{228}Ra AR at station ST47 (1.46 ± 0.13) to obtain an average marsh water age of 1.2±0.6 days.

The outflow of Peníscola marsh waters was measured using a propeller flow meter in August 2nd and September 13th 2007, with an average of 37,000 ± 4,000 m^3·d^{-1}. Since the marsh water volume is 64,000 m^3, we can independently estimate a Peníscola marsh waters residence time of 1.7 ± 0.2 days. The Ra-derived apparent age refers only to the time elapsed since the GW_{seep} enters into the Peníscola marsh, whereas the residence time derived from the direct measurements accounts also for the $GW_{shallow}$ discharge, which mainly occurs at the northern part of the Peníscola marsh. Therefore, as flow meter-derived residence time estimations are expected to be longer than Ra-based apparent ages, we can consider that both estimates are in good agreement.

Eq. 3.5 may be also used to determine the time that it takes for the GW_{seep} to reach a given station since it entered the wetland. Calculated ages for the different stations

ranged from 0 to 12.9 days. The longer water ages correspond to samples collected from sinkholes where water exchange with surrounding waters is limited, and thus a higher residence time is reasonable.

3.4.2.2. Relative contributions from different groundwater sources

Considering the outflowing marsh waters (ST47) as representative of the Peníscola marsh waters and the apparent marsh water age of 1.2 d calculated above, the shallow flow of groundwater discharging from the local systems of Vinarós-Peníscola and Irta Range ($GW_{shallow}$) would account for 32% of the total water inputs, whereas the intermediate flow of groundwater seeping through marsh sediments from the same local systems (GW_{mid}) would represent a half (48%) of the total inputs. The deep flow of groundwater from the regional Jurassic aquifer of El Maestrat (GW_{deep}) would represent 15% of the total water inputs and seawater contribution (SW) would only account for the remaining 5%. Applying these estimates to the direct measurements of the outflowing marsh waters (37,000 $m^3 \cdot d^{-1}$), we can calculate a groundwater discharge from the regional Jurassic aquifer of El Maestrat (GW_{deep}) of 5,600 $m^3 \cdot d^{-1}$ and a groundwater discharge from the local Vinaròs-Peníscola and Irta Range systems ($GW_{shallow} + GW_{mid}$) of 29,400 $m^3 \cdot d^{-1}$.

The outputs of the mixing model for all the stations are represented in Fig. 3.7. The samples collected in the north part of the marsh are primarily (>80%) nourished by the shallow flow of fresh groundwater ($GW_{shallow}$). When channelized marsh waters, that flow southward, reach the central part of the wetland, their GW_{seep} component (including the GW_{deep}, the GW_{mid} and the SW) increases suddenly, revealing the discharge of seeping groundwater in this area. From this region southwards, the marsh waters retain a fairly constant component of GW_{deep} (~15%), suggesting the continuous inputs of seeping groundwater along this marsh area. A relatively small (<5%) contribution of seawater is observed in nearly all the samples of the marsh.

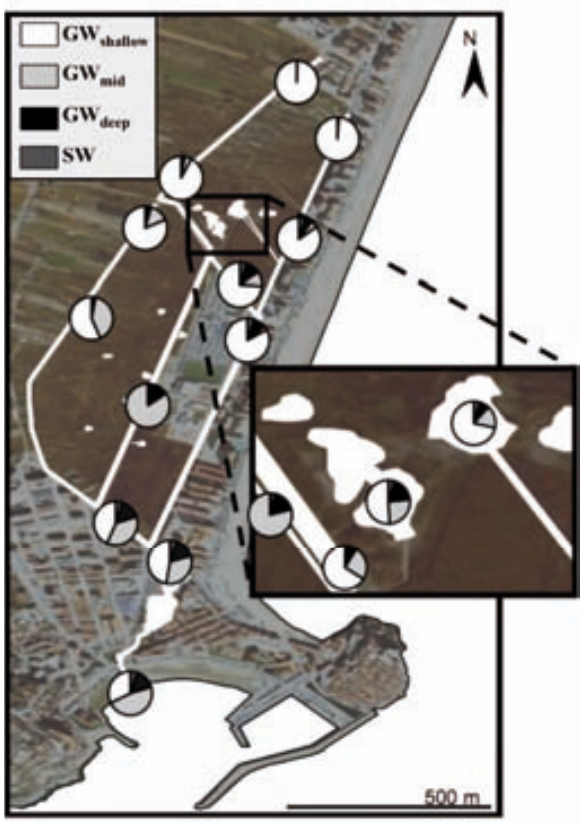

Figure 3.7. Relative contributions of the distinct groundwater flowpaths for each marsh station, corresponding to the August 2007 sampling: deep flow (GW_{deep} - black), shallow flow ($GW_{shallow}$ - white), intermediate flow (GW_{mid} – light grey) and seawater (SW – dark grey).

3.4.3. Comparison between ^{222}Rn-based groundwater contribution and direct measurements

Following the mixing model described above (section 3.4.2.1.), the relative contribution of each water source (i.e. $GW_{shallow}$, GW_{mid}, GW_{deep}, and SW) in the Peníscola marsh during the February 2011 sampling may be obtained from the ^{222}Rn, ^{226}Ra and salinity measurements of the outflowing waters (F-ST47) and the endmembers (Table 3.1). We used the results of ^{222}Rn, ^{226}Ra and salinity obtained at stations F-ST7 as the $GW_{shallow}$ and GW_{mid} endmember and the F-ST32-D5 as the GW_{seep} endmember. We used samples Pz1 and SW to characterize the GW_{deep} and the SW_{seep} endmembers, respectively (temporal variations in these endmembers are expected to be minimal). Notice that the ^{222}Rn activities for the GW_{seep} endmember do not present significant differences between the two sampling campaigns, although they were conducted in different seasons (summer 2007 and winter 2011). This reinforces the hypothesis that ^{222}Rn becomes enriched in GW_{seep} during its advection through marsh sediments. Unlike

^{222}Rn, as GW_{deep} is the main source of Ra isotopes to the wetland, a different mixing between GW_{deep}, SW and GW_{mid} before entering the wetland in February 2011 led to a diminution of the Ra content of GW_{seep} by a factor of about 2 relative to the August 2007 sampling. Considering the $^{224}Ra/^{228}Ra$ AR of the groundwater inputs into the system (1.5 ± 0.2) and the $^{224}Ra/^{228}Ra$ AR of the outflowing marsh waters (1.30 ± 0.13), we applied Eq. 3.5 to derive a marsh water apparent age of 0.9 ± 0.7 days for February 2011. This Ra-derived apparent age is also consistent with the residence time obtained from the direct measurements of outflowing marsh waters (1.3 days). The mixing model for February 2011 results in relative contributions of 35, 48, 9 and 8 % for $GW_{shallow}$, GW_{mid}, GW_{deep} and SW, respectively (65% for GW_{seep}, i.e., GW_{mid} + GW_{deep}+ SW).

These results can be compared with independent estimates from direct flow measurements carried out in four sections of the marsh channels (Fig 3.2). Three of the measurements (F1-F3) were conducted in the initial part of the three channels that are mainly nourished by the shallow groundwater flow, allowing us to estimate the inflowing $GW_{shallow}$. The section F4 was placed in the marsh outlet to the sea, in order to estimate the outflow of marsh waters. Assuming that there are no additional water inputs, the difference of inflowing $GW_{shallow}$ (5,000 , 7,200 and 5,400 $m^3 \cdot d^{-1}$ measured in sections F1, F2 and F3, respectively) and outflowing marsh waters (48,000 $m^3 \cdot d^{-1}$ in section F4) represents the flow of water that enters the marsh from submerged seeps (i.e. the GW_{seep}). We find that groundwater inputs from $GW_{shallow}$ would account for 37% of the outflowing marsh water, whereas GW_{seep} would represent the remaining 63%. These estimates are in good agreement with the Ra and ^{222}Rn derived groundwater fractions, evidencing the effectiveness of using these radionuclides, together with salinity measurements, to estimate the contribution of groundwater from different aquifers to a wetland.

3.4.4. Temporal variability of groundwater contributions

The monthly measurements of ^{226}Ra, ^{222}Rn and salinity in outflowing marsh waters (ST47), coupled with direct flow measurements, can be used to estimate the relative contributions of groundwater from each source over the annual cycle. These monthly contributions were obtained by applying the mixing model described in Eq. 3.1-3.4 to the monthly tracer measurements and the marsh water residence time derived from

the monthly flow measurements (i.e. water volume divided by flow) (Table 3.3). The application of this mixing model implicitly assumes that salinities, ^{226}Ra and ^{222}Rn concentrations in the endmembers are constant over the year.

Table 3.3. Monthly measurements of ^{222}Rn and ^{226}Rn activities, salinity and flow carried out at station ST47 from April 2007 to February 2008.

Sample	Salinity	^{226}Ra dpm·100L^{-1}	^{222}Rn ·10^{3} dpm·100L^{-1}	Flow m^{3}·d^{-1}
April 2007	4.8	2710 ± 110	1220 ± 30	59800
May 2007	5.0	3000 ± 400	1380 ± 80	73100
June 2007	6.0	3300 ± 140	1230 ± 50	66800
July 2007	6.0	3810 ± 150	1190 ± 40	47000
August 2007	5.6	4100 ± 200	1270 ± 60	39800
September 2007	5.7	3400 ± 200	1310 ± 30	34100
October2007	5.4	3290 ± 140	1260 ± 50	38800
November 2007	5.2	3100 ± 300	1220 ± 70	50900
December 2007	5.1	3000 ± 300	1130 ± 30	46300
January 2008	5.3	2600 ± 200	1190 ± 70	82900
February 2008	5.7	3000 ± 200	1330 ± 40	47100

Since temporal variations in groundwater discharge flows are largely controlled by seasonal changes in precipitation over the annual cycle, we conducted a qualitative comparison between the groundwater discharge derived from the mixing model and the precipitation pattern. The relative contributions of each groundwater source were converted to relative groundwater flows by multiplying them by the flow measured in the marsh outlet. The data on precipitation was obtained from the pluviometric stations of the Spanish Meteorological Agency (AEMET) at Alcalà de Xivert, located at 15 km from the study site. This comparison suggests that estimated groundwater flows from the local shallow systems of Vinaròs-Peníscola and Irta Range ($GW_{shallow}$ + GW_{mid}) respond to the accumulated precipitation during the 3 months previous to each sampling (Fig. 3.8). A similar lag between local recharge by rainfall and discharge, by 1 to 5 months, has been previously observed in other studies from coastal aquifers (e.g. (Smith et al. 2008; Garcia-Solsona et al. 2010b)). On the other side, groundwater fluxes from the regional deep Jurassic aquifer of El Maestrat (GW_{deep}) are relatively constant over the year (6,200 ± 1,400 m^{3}·d^{-1}), showing minor variations in response to the local precipitation (Fig. 3.8). Indeed, the temporal variations of deep groundwater discharge from the carbonate Jurassic aquifer of El Maestrat follows a hydrological functioning characteristic of most karstic aquifers (Padilla and Pulido-Bosch 1995): a permanent baseflow that softens the response to the rainfall (around 4,500 m^{3}·d^{-1}) and a

"quickflow" through the most transmissive part of the aquifer, resulting in fast responses to the recharging events.

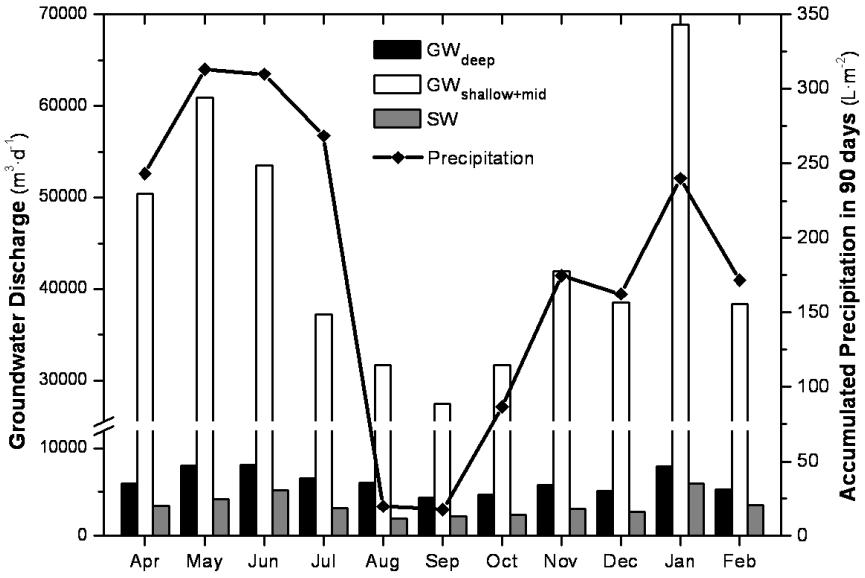

Figure 3.8. Monthly relative contributions of groundwater flows from the local shallow systems of Vinaròs-Peníscola and Irta Range ($GW_{shallow+mid}$ - white), the deep carbonate aquifer of El Maestrat (GW_{deep} - black) and seawater (SW - grey) to the Peníscola marsh from April 2007 to February 2008. The accumulated precipitation during the 90 days previous to the sampling day is also represented.

3.5. Conclusions

Ra isotopes and ^{222}Rn have been used, coupled with salinity measurements, to estimate the contribution of groundwater from different sources to the Peníscola marsh (Spain), a coastal wetland nourished by groundwater from the regional carbonate Jurassic aquifer of El Maestrat and the local systems of the Vinaròs-Peníscola and the Irta Range. The combined use of ^{222}Rn, Ra isotopes and salinity measurements proved to be a valuable tool to estimate the relative contribution of distinct groundwater flows into a wetland, confirmed by the comparison with a direct and independent method. Ra isotopes were also instrumental in providing with essential information of the wetland water age.

We also successfully monitored the evolution of groundwater discharges from two aquifers during a year by using ^{226}Ra, ^{222}Rn, salinity and direct measurements. Our results revealed that precipitation is an important driver of groundwater discharges from the local shallow systems, whereas inputs from the regional carbonate aquifer are dominated by a permanent baseflow.

CHAPTER 4

Submarine Groundwater Discharge into a coastal embayment: the influence of sediments on radium-derived estimates

This chapter is based on:

Rodellas, V., Garcia-Orellana, J., Masqué, P., Basterretxea, G. Submarine Groundwater Discharge into a coastal embayment: the influence of sediments on radium-derived estimates. In preparation.

4.1. Objective

The purpose of this study is to evaluate the influence of bottom sediments on the estimation of SGD into a coastal environment by using Ra isotopes. We selected the natural harbor of Maó (Minorca, Balearic Islands, NW Mediterranean) because there are evidences of fresh groundwater inflowing along the southern shore, but, more importantly, the Port of Maó is a shallow and semi-enclosed embayment covered by muddy sediments that is subject to frequent resuspension events provoked by maritime traffic of deep draft vessels (Garcia-Orellana et al. 2011), potentially representing a relevant mechanism to introduce Ra isotopes to the water column. This makes the Port of Maó an ideal setting to assess the potential contribution of bottom sediments on a Ra mass balance to estimate SGD. In this work, we constructed a comprehensive Ra mass balance for the waters of the Port of Maó, using both short- and long-lived Ra isotopes, ^{224}Ra and ^{228}Ra, respectively.

4.2. Methods

4.2.1. Field site

The Port of Maó (Fig. 4.1) is the second natural largest harbor in Europe. It is a semi-enclosed embayment with restricted exchange with the open sea, as a consequence of its elongated shape (5 km length and a maximum width of 0.8 km) and its shallow mouth (13 m). Indeed, the whole harbor is a shallow water body with depths lower than 10 m in the inner part and a maximum water column depth of 29 m in the central part of the harbor.

The Port of Maó is located in the middle of a fault that divides the island in two geomorphological settings: an impermeable northern sector of Mesozoic rocks and a broad permeable Miocene limestone platform that constitutes the main aquifer to the south (Fornós et al. 2004). This aquifer, named Migjorn, supplies most of the total extracted water from the island (~$11 \cdot 10^6$ m^3 yr^{-1}), mainly for tourism and agriculture purposes (Garcia-Solsona et al. 2010a). The aquifer permeability increases towards the coastline as a consequence of a major karstic development that results in direct or diffuse groundwater discharge to the sea (Garcia-Solsona et al. 2010a). Due to this

hydrogeological division, most of the groundwater inputs into the harbor are located on the southern shoreline. Indeed, several natural wells and springs exist along the southern area of the harbor and groundwater springs inflowing directly to the harbor can be visually identified. Aside from groundwater discharge, fresh water inputs are restricted to the discharge of a small stream in the inner harbor and runoff from eventual precipitation events. The average annual rainfall is about 600 mm, with dry summers and maxima in spring and autumn.

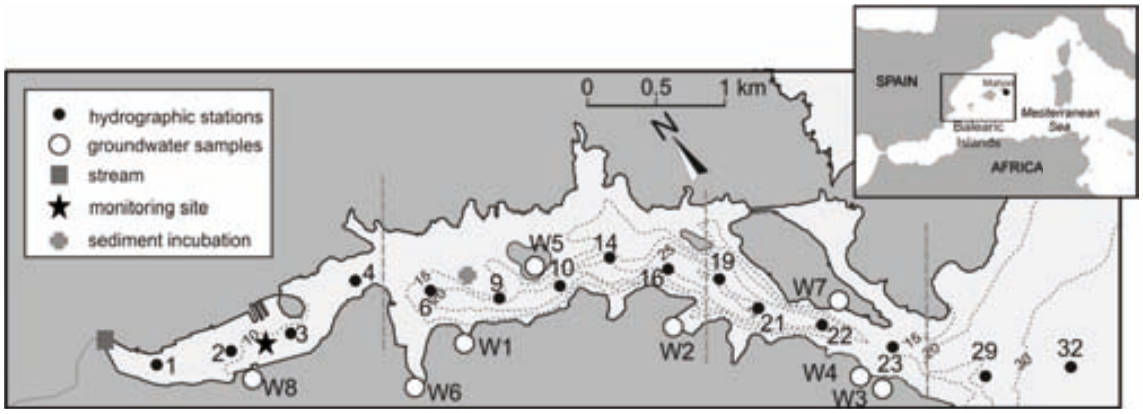

Figure 4.1. Map of the Port of Maó including the location of all the hydrographic stations and the site where the three-day monitoring was conducted. The location of the groundwater samples, the inflowing stream and the sediment core collected are also shown. Dashed-lines differentiate (from the left to the right) the inner, middle and outer areas of the harbor, and the boundary of the study site.

The Port of Maó has been subjected to continuous urban and industrial dumps from the city of Maó and the industries settled around the harbor. This has led, for instance, to a progressive contamination of bottom sediments with metals (Ag, Cd, Cu, Ni, Pb, among others; Garcia-Orellana et al. 2011). It is also an important touristic destination where cruises and large vessels frequently circulate along the harbor, especially during the summer season. Since most of these vessels have drafts between 6 to 9 m and given the shallowness of the harbor (transit channel of 10-14 m), propellers of large vessels frequently resuspend significant amounts of bottom sediments, particularly when maneuvering to dock. This favors the exchange and dispersion of contaminants from the sediments to the water column (Garcia-Orellana et al. 2011).

4.2.2. Sample collection

Four seasonal surveys (July 2010, October 2010, March 2011 and June 2011) were conducted at the Port of Maó. A detailed transect consisting of 15 stations distributed along the harbor was sampled during each survey (Fig. 4.1). Water samples (60 L) for Ra isotopes were collected from 1 m depth (surface) at each station. Depth profiles of temperature and salinity were measured at each station with a CTD (SBE-25, Seabird Electronics). A depth profile was also conducted at station #19 in October10, March11 and June11, collecting samples for Ra at the surface, 10 m and 20 m water depth. Samples for Ra analysis were stored in 60 L containers.

Groundwater was sampled from 8 coastal wells distributed along the southern shoreline and two small islands within the harbor (Fig. 4.1). Samples for Ra isotopes, salinity and temperature measurements were collected in each survey. The small stream, named Torrent des Gorg, inflowing to the inner harbor was also sampled for Ra isotopes, salinity and temperature. Whereas on July10 and October10 the stream was sampled in the freshwater area, on March11 and June11 the sample was collected from the estuarine zone. Finally, one shallow (15-20 cm), large (25 cm in diameter) sediment core was also collected at the inner harbor to determine the diffusive fluxes of Ra isotopes from bottom sediments to the harbor waters (Fig. 4.1).

In addition to the seasonal samplings, a 3-day intensive monitoring was conducted between 8 and 10 May 2012 to evaluate the relevance of sediment resuspension provoked by vessels maneuvering to dock as a source of Ra isotopes to the water column. Two resuspension events occurred during the studied period, driven by the same deep-draught vessel (draught = 6 m) that docked in the harbor the 1st and the 3rd day of the monitoring period. During this 3-day survey, a station located in the inner harbor (Fig. 4.1) was sampled 14 times, collecting filtered samples for Ra isotopes.
All the Ra samples collected were analyzed as described in Chapter 2 (Analytical Methods). Ra fluxes diffused from sediments were estimated from the incubation of the sediment core collected at the inner harbor, following the methodology described by (Rodellas et al. 2012: Chapter 3). Briefly, once at the laboratory, the overlying water of the sediment core was replaced with Ra-free seawater. The seawater added to the incubation core was continuously circulated through a Mn-fiber to extract the Ra isotopes and bring the Ra-free water back to the incubation chamber. After each of the

progressively longer incubation times (12, 24, 36, 48, 72 and 96 hours) the fiber was removed to determine its content on Ra isotopes and replaced by a new one. The Ra diffusive fluxes were determined by averaging the decay corrected Ra activity divided by the incubation time of each Mn-fiber and referenced to the core surface area.

4.3. Results

4.3.1. Seasonal sampling

Salinity distributions along the harbor showed marked differences among the 4 surveys conducted (Fig. 4.2), likely reflecting seasonal variations on freshwater inputs. During October10, a salinity gradient was observed along the Port of Maó, with lower salinities in the inner harbor and increasing salinities towards the harbor outlet. Contrarily, a strong vertical stratification was observed in March11, without a clear gradient along the harbor, likely suggesting the presence of freshwater inputs and a rapid horizontal mixing. During summer, minor freshwater inputs, characteristic of the dry season, were revealed by salinities measured at the inner harbor being similar (June11) or even higher (July10) than those measured in the open sea.

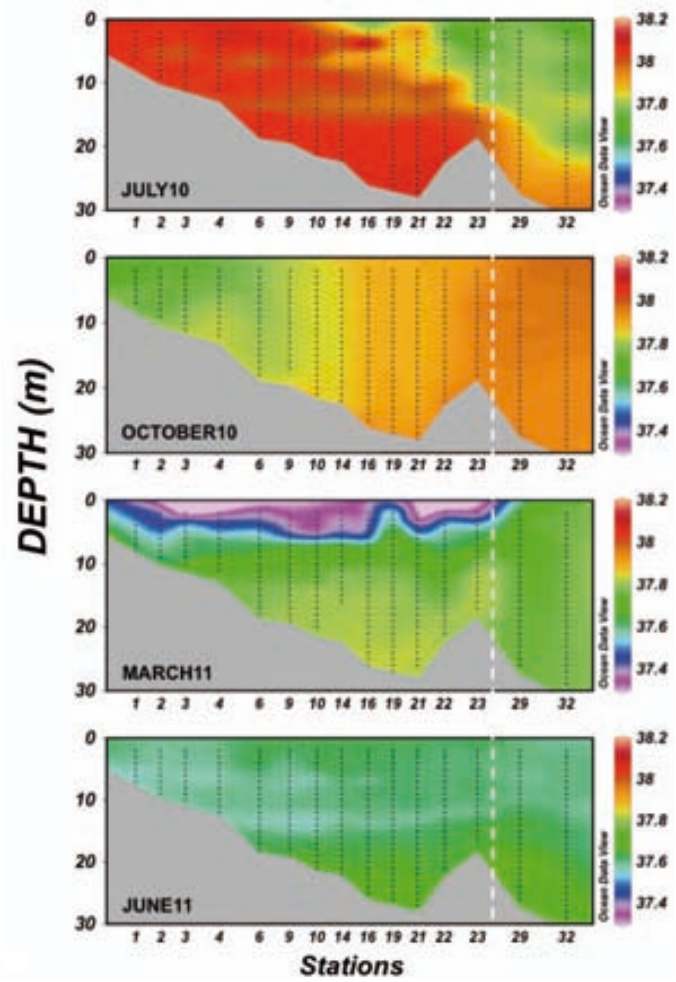

Figure 4.2. Salinity distribution on a cross section along the Port of Maó derived from CTD profiles conducted in each station. The dashed line highlights the boundary of the harbor.

The activities of Ra isotopes for the four samplings campaigns are presented in Fig. 4.3. An enrichment in activities of ^{223}Ra, ^{224}Ra and ^{228}Ra was observed in surface waters from the inner harbor relative to samples offshore, with concentrations decreasing towards the harbor outlet, suggesting that most of Ra inputs occur at the inner harbor and/or there is a major dilution with open sea water at external stations (Table 4.1). The stronger horizontal gradients along the harbor were observed for short-lived Ra isotopes, and, to a lesser extent, for ^{228}Ra (Table 4.1; Fig. 4.3). ^{226}Ra presented relatively homogeneous activities along the harbor in all the sampling surveys, comparable to those measured at the offshore station, revealing a lack of major ^{226}Ra inputs (Table 4.1; Fig. 4.3). Activity gradients for ^{223}Ra, ^{224}Ra and ^{228}Ra along the harbor were smoothed in the March11 sampling, likely as a consequence of a rapid horizontal homogenization of surface waters, as indicated by the surface salinity distribution (Fig. 4.2). Concentrations of long-lived Ra isotopes were relatively constant along the water column for all the seasons and regardless variations on salinity, as derived from the depth profile conducted at station #19 in October10, March11 and June11. However, concentrations of short-lived Ra isotopes showed a significant decrease with depth, likely related to radioactive decay, since mixing would also affect long-lived Ra isotopes. Activities of ^{224}Ra and ^{228}Ra are shown in Table 4.2 to highlight these differences among isotopes.

Table 4.1. Average Ra activities in surface waters of the inner harbor (stations #1 to #4) and at the offshore station (#32). Ratios between Ra activities in and out of the harbor are also shown.

		^{223}Ra	**^{224}Ra**	**^{226}Ra**	**^{228}Ra**
			dpm·100L^{-1}		
July10	Inner Harbor	1.31 ± 0.15	11.7 ± 1.3	13.7 ± 0.7	9.6 ± 1.1
	Offshore	0.08 ± 0.03	0.2 ± 0.2	13.7 ± 0.5	3.8 ± 0.7
	In/Out ratio	16	51	1.0	2.5
October10	Inner Harbor	1.24 ± 0.08	14 ± 2	12.2 ± 1.4	9.9 ± 1.0
	Offshore	0.18 ± 0.08	2.0 ± 0.3	9.1 ± 0.4	4.1 ± 0.6
	In/Out ratio	6.9	6.9	1.3	2.4
March11	Inner Harbor	0.77 ± 0.18	7.9 ± 1.4	11 ± 2	6.7 ± 0.3
	Seawater	0.20 ± 0.06	2.0 ± 0.3	12.8 ± 0.4	3.7 ± 0.5
	In/Out ratio	3.8	3.9	0.8	1.8
June11	Inner Harbor	0.96 ± 0.21	9.1 ± 1.3	12 ± 2	7.4 ± 0.8
	Seawater	0.10 ± 0.04	0.3 ± 0.2	12.6 ± 0.5	4.0 ± 0.8
	In/Out ratio	9.6	28	1.0	1.9

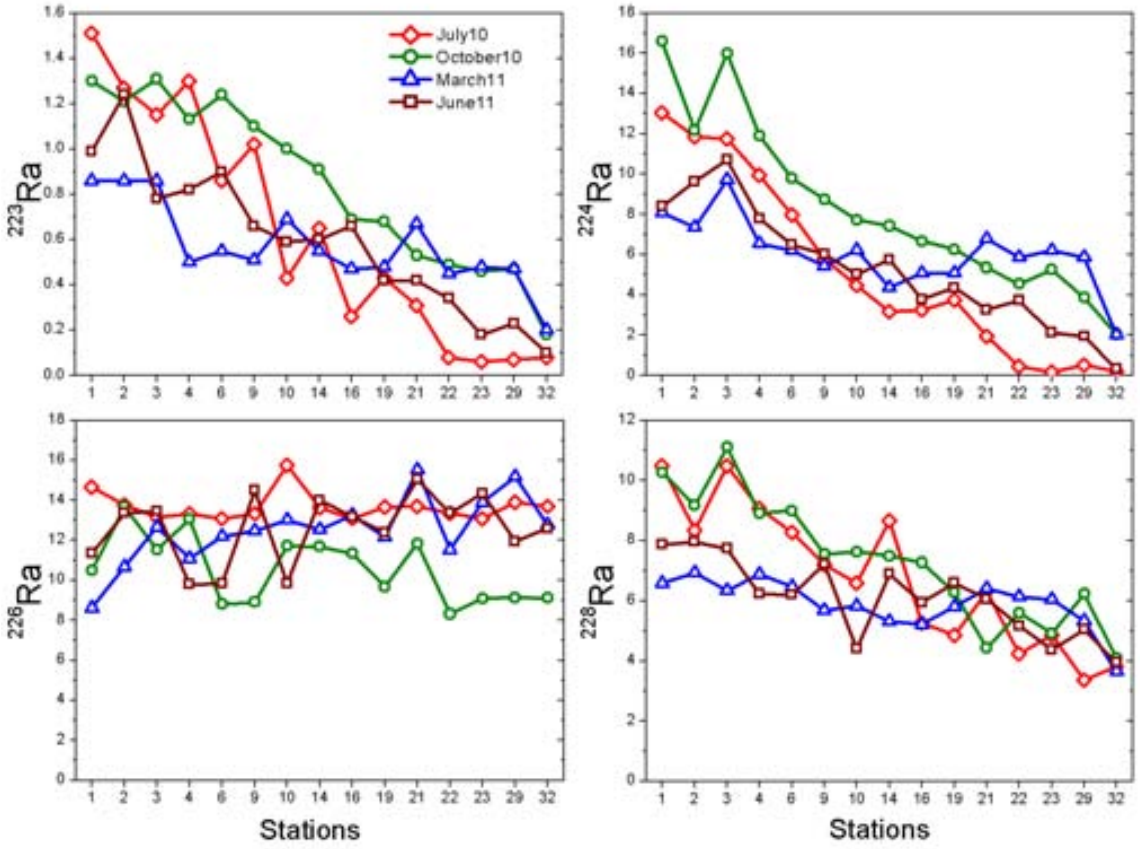

Figure 4.3. Ra activities in surface waters along the harbor for all the four surveys conducted. Average uncertainties associated to Ra activities are 0.1, 0.5, 0.7 and 0.8 dpm·100L^{-1} for ^{223}Ra, ^{224}Ra, ^{226}Ra and ^{228}Ra, respectively. Stations #29 and #32 are outside the harbor.

Table 4.2. ^{224}Ra and ^{228}Ra activities in the depth profile conducted at station #19 during the October10, March11 and June10 surveys.

	Depth	**Salinity**	**^{224}Ra**	**^{228}Ra**
	m		dpm·100L^{-1}	
October10	1	37.89	6.3 ± 0.6	6.3 ±0.7
	5	37.90	5.6 ± 0.6	5.3 ±0.9
	15	37.90	2.4 ± 0.5	6.0 ±1.2
	25	37.91	2.0 ± 0.4	n.a.
March11	1	37.588	5.1 ± 0.5	5.8 ±0.8
	10	37.73	3.8 ± 0.6	6.0 ±1.1
	20	37.80	2.8 ± 0.5	6.2 ±0.9
June11	1	37.623	4.4 ± 0.4	6.6 ±0.6
	10	37.61	3.4 ± 0.4	n.a.
	20	37.65	4.4 ± 0.5	n.a.

4.3.2. Characterization of groundwater and stream water

Most of the groundwater samples collected from wells and springs located close to the harbor shoreline (less than 50 m) presented salinities ranging from 0.7 to 1.6, suggesting minimal seawater intrusion. Only the wells located in small islands (W5 and W7) revealed some exchange with the sea (salinities of 8.9 and 12.6) (Table 4.3).

Ra isotopes concentrations measured in the coastal wells showed minimal seasonal variations (e.g. ^{228}Ra activities measured in W8 were 199 ± 11, 229 ± 10 and 228 ± 5 dpm·100L^{-1} for October10, March11 and June11 surveys, respectively). Given the minimal seasonal variation, activities of all the samples from the same well were averaged in order to provide with a single estimate for each site (Table 4.3).

Groundwater samples were enriched in all the Ra isotopes relative to seawater (Table 4.3). In general, ^{228}Ra activities in groundwater were higher than activities of ^{224}Ra and ^{226}Ra for most of the collected samples (median activity ratios (AR): ^{224}Ra/^{228}Ra = 0.65; ^{228}Ra/^{226}Ra = 2.0). These differences among Ra isotopes in groundwater are likely explained by two major factors: i) the ^{228}Ra/^{226}Ra AR in groundwater is reflecting the parental Th/U ratio in the carbonate host rocks (Moore 2003; Garcia-Solsona et al. 2010a); and ii) most of the sampled wells have large dimensions and nowadays are not frequently used, likely resulting in stagnant groundwater in the wells for long periods leading to the partial decay of short-lived Ra isotopes with respect to the long-lived ones.

Table 4.3. Average Ra concentrations in groundwater samples and in the freshwater (Stream-F) and estuarine regions (Stream-F) of the inflowing stream (uncertainties represent the standard deviation).

	Sal	^{223}Ra	^{224}Ra	^{226}Ra	^{228}Ra	^{228}Ra/^{224}Ra AR
			dpm·100L^{-1}			
W1	1.6	1.5±0.8	23±11	11.6±1.0*	21±2*	0.53±0.05*
W2	0.8	1.7±0.2	16±4	49±2*	46±2*	0.26±0.02*
W3	1.4	7.4±2.5	66±11	160±3*	115±5*	0.59±0.05*
W4	1.1	1.7±1.5	31±20	n.a.	n.a.	n.a.
W5	8.9	5.1±0.6	165±13	71±5*	230±20*	0.67±0.08*
W6	0.7	1.22±0.05	27±2	33±2*	231±4*	0.12±0.01*
W7	12.6	1.5±0.2	26±2	n.a.	n.a.	n.a.
W8	0.8	6.1±2.1	224±13	107±11	220±20	1.02±0.10
Stream-F	0.9	0.70±0.09*	11.4±0.8*	n.a.	n.a.	n.a.
Stream-E	11.2	0.50±0.11*	17.3±1.1*	9.0±0.8*	20±3*	0.85±0.12*

n.a. not determined

* Only measured in one survey: analytical uncertainties are reported

The activities of Ra isotopes measured in the stream inflowing to the inner part of the harbor are also presented in Table 4.3. Since the stream was sampled in the freshwater (Stream-F, in October10) and the estuarine (Stream-E, in March11) areas, results from both regions are included in Table 4.3. Ra activities measured in both the freshwater (salinity of 0.9) and the estuarine areas (salinity of 11.2) were comparable to those measured in the inner harbor.

4.3.3. Three-day intensive monitoring

The passing and maneuvering of vessels during the three-day sampling in may 2012 induced the resuspension of significant amounts of bottom sediments, which could be visually observed (Fig. 4.4), enhancing the concentration of suspended particles in the entire water column of the inner harbor. After the vessel-driven resuspension events, activities of short-lived Ra isotopes in the surface waters increased significantly, especially at the third day, after the 2nd docking of the vessel (1st docking: increases of 53 and 33 % with respect to the ^{223}Ra and ^{224}Ra activities before the resuspension event, respectively; 2nd docking: activity increases of 85 and 100 % for ^{223}Ra and ^{224}Ra, respectively) (Fig. 4.5). Unlike short-lived Ra isotopes, activities of ^{226}Ra and ^{228}Ra did not increase substantially (less than 20%) as a consequence of the sediment resuspension events (Fig. 4.5). This reduced increase on the activities of long-lived Ra isotopes is likely related to their long regeneration time, that results in minimum amounts of long-lived Ra isotopes available for desorption when sediment resuspension events occur.

Figure 4.4. Resuspension of sediments produced by the undocking maneuver of a vessel (draft ~6 m) departing from the Port of Maó.

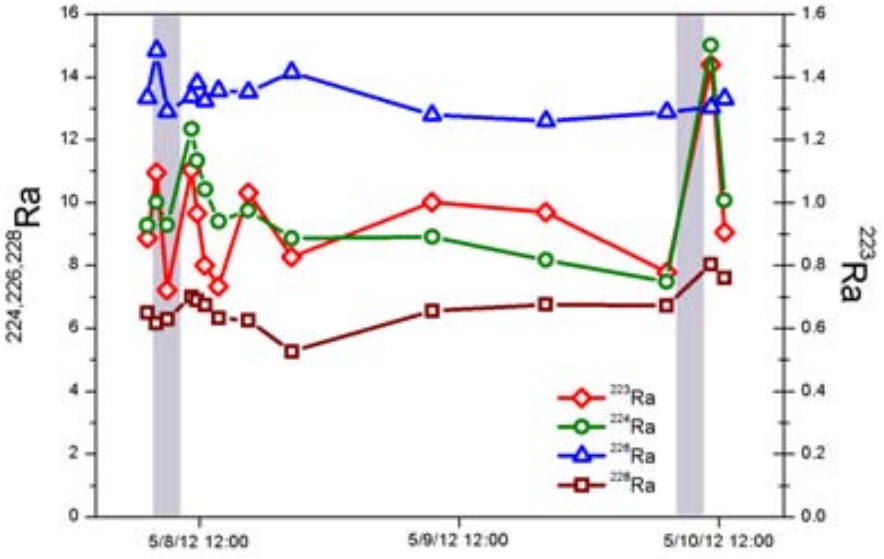

Figure 4.5. Variations of the Ra activities in surface waters of the inner part of the harbor recorded during the three-day intensive monitoring. Grey areas reflect the maneuvering of deep draft vessels to dock. Average uncertainties associated to Ra activities are 0.1, 0.7, 0.8 and 0.8 dpm·100L^{-1} for ^{223}Ra, ^{224}Ra, ^{226}Ra and ^{228}Ra, respectively.

4.3.4. Diffusive sediment fluxes

The diffusive fluxes of Ra isotopes from sediments obtained from the incubation experiment were 4.5 ± 1.1, 99 ± 17, 11.3 ± 2.4 and 11.7 ± 0.8 dpm·d^{-1}·m^{-2} for ^{223}Ra, ^{224}Ra, ^{226}Ra and ^{228}Ra, respectively. Differences among fluxes from different Ra isotopes are related to both the abundance in sediments and the regeneration time of each isotope, which is set by their respective decay constants. These fluxes are mainly reflecting molecular diffusion and represent an upper estimate, since the continuous replacement of overlying waters with Ra-free water maximizes the gradient between pore and overlying waters (Rodellas et al. 2012: Chapter 3). Fluxes are comparable to those obtained in previous studies in muddy sediments from coastal Mediterranean environments (Garcia-Solsona et al. 2008b) and throughout the world (Beck et al. 2007a; Moore et al. 2008; Garcia-Orellana et al. 2014).

4.4. Discussion

4.4.1. Ra mass balance

Several approaches have been used to estimate SGD into coastal areas by using Ra isotopes, including endmember mixing models (e.g. Charette et al. 2013), determining Ra fluxes offshore from eddy diffusive mixing (e.g. Dulaiova et al. 2006), or developing Ra mass balances (e.g. Beck et al. 2007). The use of a comprehensive Ra mass balance is likely the most appropriate method to assess the magnitude of SGD in coastal systems with several potential Ra sources, since the other approaches generally assume that SGD is the dominant Ra input. The Ra mass balance relies on the assumption that the Ra activities in the harbor are in steady state during a given period, and thus Ra isotopes must be continuously supplied to balance their outputs. By constraining all the potential Ra inputs and outputs, the Ra flux supplied by SGD can be evaluated by difference.

In the case of the Port of Maó, potential Ra inputs include diffusion from sediments (J_{diff}), desorption from resuspended bottom sediments (J_{des}), the stream water discharge (J_{str}) and SGD (J_{SGD}), whereas Ra is lost from the system by radioactive decay (J_{λ}) and net export to the coastal sea (J_{sea}). Biological uptake, in situ production from dissolved Th parents and atmospheric inputs are negligible relative to the other source or removal terms (Charette et al. 2008). Thus, the mass balance for Ra isotopes can be expressed as follows:

$$J_{\lambda}+J_{sea} = J_{diff} + J_{des} + J_{str} + J_{SGD} \quad (4.1)$$

where sinks and sources of Ra are on the left- and right- hand sides of the equation, respectively. For the purpose of this study, we focus the mass balance on a short-lived Ra isotope (^{224}Ra) and on a long-lived one (^{228}Ra). We have excluded ^{223}Ra, which would provide equivalent information to that obtained from ^{224}Ra but with larger uncertainties, and ^{226}Ra, because it is not significantly enriched in the harbor relative to open sea waters, revealing that there are no relevant sources in the harbor for this isotope.

a) Ra decay

The decay term of the Ra mass balance can be obtained by multiplying the total Ra inventory in harbor waters by the decay constants of ^{224}Ra (λ = 0.189 d^{-1}) and ^{228}Ra (λ = 0.330·10^{-3} d^{-1}). Total Ra inventories in the harbor are derived from the area-weighted average Ra inventories in each station and the area of the study site (3.0·10^{6} m^{2}). For each station, we assumed constant concentrations of ^{228}Ra over depth within the water column, as shown from the depth profiles of ^{228}Ra conducted at station #19 (Table 4.2). The same assumption was taken for ^{224}Ra in summer samplings (July10 and June11), as ^{224}Ra activities over depth also showed minimal variation. Contrarily, since ^{224}Ra activities decreased with depth in October10 and March11 (Table 4.2), we used deep samples collected at station #19 to characterize waters below 10 m depth. The limited set of deep samples does not allow being more accurate on determining the ^{224}Ra inventory for October10 and March11. The total Ra inventories ranged from (2.0 ± 0.1)·10^{9} to (2.8 ± 0.2)·10^{9} dpm for ^{224}Ra and from (2.5 ± 0.2)·10^{9} to (3.1 ± 0.2)·10^{9} dpm for ^{228}Ra, depending on the season.

Given the long life of ^{228}Ra, its radioactive decay (on the order of 10^{6} dpm·d^{-1}) can be neglected, but it is a relevant output term for the ^{224}Ra mass balance (~500·10^{6} dpm·d^{-1}) (Table 4.4).

b) Ra export offshore and water age

The Ra export offshore can be determined from the excess Ra inventories in harbor waters and the apparent water age (T_w). The excess ^{224,228}Ra inventories in the harbor are calculated by subtracting the contribution of Ra from the open sea (minimum Ra concentration at station #32 multiplied by the harbor water volume) from the total Ra inventory in the harbor.

The apparent age of harbor waters, defined as the time a water parcel has spent since it acquired the Ra signal, can be calculated by using the variation of the activity ratios (AR) of Ra isotopes of different half-lives (Moore et al. 2006). In an environment where Ra inputs occur throughout the system and there are no losses aside from mixing with offshore seawater and radioactive decay, the residence time can be calculated as follows:

$$T_w = \frac{AR_{in} - AR_H}{AR_H \lambda_{224}} \quad (5.2)$$

where AR_{in} is the $^{224}Ra/^{228}Ra_{ex}$ AR of the flux into the system, AR_H is the averaged $^{224}Ra/^{228}Ra_{ex}$ AR in the harbor and λ_{224} is the decay constant of ^{224}Ra. The subscript "ex" designates the excess concentration of ^{228}Ra obtained by subtracting the concentration in open sea to the concentration in the harbor waters. The AR_{in} term depends on Ra inputs from all the sources and its relative importance. The $^{224}Ra/^{228}Ra$ AR in all the potential Ra sources to the harbor span a wide range: 0.9 ± 0.12 in water inputs from the stream, 9.5 ± 1.4 in diffusion from sediments, 5.9 ± 5.2 in releases from resuspension events and 1.02 ± 0.10 in SGD. Since the contribution of the different sources is not properly known, here we used the highest $^{224}Ra/^{228}Ra_{ex}$ AR in harbor waters (3.3 ± 0.4), which was measured in the inner harbor (station #3). This value shall be similar to the $^{224}Ra/^{228}Ra_{ex}$ AR in the Ra source, because samples collected in the inner area of the harbor are likely close to the Ra source and, thus, a minimum decay is expected. Using the weighted average $^{224}Ra/^{228}Ra_{ex}$ AR of all the harbor samples (1.44 ± 0.14, 1.81 ± 0.11, 2.3 ± 0.2 and 2.1 ± 0.2 for July10, October10, March11 and June11, respectively), the estimated seasonal apparent water ages of surface waters are 6.7 ± 1.8 d for July10, 4.2 ± 1.3 d for October10, 2.3 ± 1.2 d for March11 and 3.1 ± 1.3 d for June11.

The flux of Ra exported offshore, obtained by dividing the excess Ra inventories by the water apparent age, ranged from $(290 \pm 80)\cdot10^6$ to $(1000 \pm 500)\cdot10^6$ dpm·d^{-1} for ^{224}Ra and from $(200 \pm 60)\cdot10^6$ to $(440 \pm 230)\cdot10^6$ dpm·d^{-1} for ^{228}Ra, depending on the season (Table 4.4).

c) Diffusion of Ra from bottom sediments

The total diffusive fluxes of radium from bottom sediments to the water column of the Port of Maó can be estimated from the Ra diffusive fluxes obtained from incubation experiments carried out in the lab and the bottom sediment area of the harbor ($3.0\cdot10^6$ m^2): $(340\pm50)\cdot10^6$ dpm·d^{-1} for ^{224}Ra and $(35\pm2)\cdot10^6$ dpm·d^{-1} for ^{228}Ra. No major seasonal differences on these fluxes are expected and thus Ra diffusion from bottom sediments is assumed to be constant along the year. Since the Ra diffusive fluxes estimated here are based in a single experimental value, using the uncertainty associated to this unique value seems unjustified (Garcia-Orellana et al. 2014). Thus, we assign an uncertainty of ± 50% to the resultant fluxes that shall integrate the actual variability of

diffusive fluxes from sediments, as observed in other studies (Moore et al. 2008; Garcia-Orellana et al. 2014).

d) Ra inputs from resuspended sediments

Sediment resuspension events recorded in the Port of Maó led to significant increases on short-lived Ra activities in the water column (Fig. 4.5). These Ra enhancements are likely a consequence of Ra desorption from resuspended particles, but could also result from resuspension-induced porewater exchange with overlying waters. Considering that the docking maneuver of deep-draft vessels provoke the resuspension events, the flux of Ra from resuspended sediments is determined from the increase of Ra inventories in the harbor after the docking of vessels and the frequency of resuspension events. Increased Ra inventories are calculated from the average vessel-driven enhancements of Ra concentrations at the inner harbor obtained from the 3-day intensive monitoring (5±3 dpm·100L^{-1} for ^{224}Ra and 0. 9±0.6 dpm·100L^{-1} for ^{228}Ra) multiplied by the water volume affected by resuspension events ($2 \cdot 10^6$ m^3; determined from aerial images and bathymetry). The frequency of deep draft vessels (draft > 5 m) that were docked in the harbor during the periods studied averaged 2.6, 2.0, 1.1, 1.9 vessels·d^{-1} in July10, October10, March11 and June11, respectively (data compiled from the website of Port Authority of Maó; www.portsdebalears.com). Inputs of Ra from resuspended sediments range from $120 \cdot 10^6$ to $270 \cdot 10^6$ dpm·d^{-1} for ^{224}Ra and from $15 \cdot 10^6$ to $46 \cdot 10^6$ dpm·d^{-1} for ^{228}Ra, depending on the season (Table 4.4). It is difficult to accurately assess the uncertainty associated the parameters involved in the determination of the Ra flux from resuspended sediments. Particularly, Ra enhancements derived from resuspension events can be largely variable, mainly depending on both the amount of sediments resuspended, which in turn is influenced by the vessel draft and the maneuvering procedure, and the time elapsed between resuspension events, which would determine the amount of Ra produced and available for desorption. To account for this variability and potential mischaracterization, we assign an uncertainty of ±100% to the final estimate of the Ra flux from resuspended sediments.

e) Inputs of Ra from stream waters

Both the activities of Ra dissolved and desorbed from suspended particles in stream waters need to be taken into account to estimate the inputs of Ra to the harbor waters

from the stream (Moore and Shaw 2008). The salinity (11.2, Table 4.3) of the sample collected on the estuarine section of the stream is high enough to assume that all Ra from suspended particles had been desorbed (Krest et al. 1999), and thus we can determine both the dissolved and desorbed Ra inputs. Since the water flow of the stream entering to the inner harbor could not be precisely measured, this flow can be constrained from the monthly precipitation in the area, the area draining to the stream ($2.8 \cdot 10^7$ m^2; IDEIB) and the percentage of impervious substrate (18%; IDEIB). Here it is implicitly assumed that all the precipitation inflowing the impervious drainage area discharge to the stream (i.e. no further infiltration, no evaporation, no biological consumption), leading to a large overestimation of the flow (flows obtained ranging from $1.9 \cdot 10^3$ to $29 \cdot 10^3$ $m^3 \cdot d^{-1}$). Even considering this overestimation of its flow, the stream only contributes to a minor fraction (<2%) of the total ^{224}Ra and ^{228}Ra inputs to the harbor (Table 4.4).

f) Inputs of Ra from SGD

For all the seasonal surveys, the previously evaluated Ra sources to the harbor are not sufficient to balance the total Ra outputs (Table 4.4). This difference on Ra fluxes can be reasonably ascribed to the remaining source, i.e. SGD. The estimated magnitude of the Ra fluxes derived from SGD, as well as its associated uncertainties, rely on the accuracy with which we characterize the most significant components of the Ra mass balance (Table 4.4; Fig. 4.6). For ^{224}Ra, these terms include: Ra gains by diffusion from bottom sediments (accounting for 23-51% of the total outputs, depending on the season) and resuspension events (8-41 %); losses by radioactive decay (30-56 %) and export offshore (44-70 %). For ^{228}Ra, diffusion and sediment resuspension are relevant but minor Ra sources (8-17 % and 3-22 %, respectively), whereas the only significant loss is the Ra exported offshore (>99 %).

Inputs of Ra from SGD range from $(50 \pm 330) \cdot 10^6$ $dpm \cdot d^{-1}$ for ^{224}Ra and $(120 \pm 70) \cdot 10^6$ $dpm \cdot d^{-1}$ for ^{228}Ra in July10 to $(980 \pm 540) \cdot 10^6$ $dpm \cdot d^{-1}$ for ^{224}Ra and (390 ± 230) $dpm \cdot d^{-1}$ for ^{228}Ra in March11. The propagation of the errors of all the components of the Ra mass balance leads to relative large uncertainties in the final estimates, ranging from 55 to 600% for ^{224}Ra and from 40 to 61% for ^{228}Ra, depending on the season (Table 4.4). These high uncertainties, particularly for ^{224}Ra, are mainly derived from the large uncertainties that were assigned to the Ra fluxes from sediments, including both

diffusion (uncertainty of 50%) and releases from resuspension events provoked by deep draft vessels (uncertainty of 100%).

Table 4.4. Inputs and outputs of ^{224}Ra and ^{228}Ra to the Port of Maó for all the four surveys. Difference between inputs and outputs is used to derive the flux of Ra from SGD and the final SGD estimate.

	July10		October10		March11		June11		
	^{224}Ra	^{228}Ra	^{224}Ra	^{228}Ra	^{224}Ra	^{228}Ra	^{224}Ra	^{228}Ra	Units
Export offshore	290±80	200±60	660±210	370±110	1000±500	440±230	720±300	350±150	$\cdot 10^6$ dpm·d^{-1}
Decay	370±11	0.95±0.04	528±13	1.01±0.03	438±13	0.84±0.03	418±11	0.86±0.04	$\cdot 10^6$ dpm·d^{-1}
TOTAL OUPUTS	660±80	204±57	1189±206	366±115	1441±501	443±225	1141±301	351±150	$\cdot 10^6$ dpm·d^{-1}
Sed. diffusion	340±170	35±18	340±170	35±18	340±170	35±18	340±170	35±18	$\cdot 10^6$ dpm·d^{-1}
Sed. resuspension	270±270	46±46	210±210	26±26	120±120	15±15	200±200	24±24	$\cdot 10^6$ dpm·d^{-1}
Stream	0.33±0.02	0.39±0.05	5.0±0.3	5.8±0.7	1.35±0.09	1.6±0.2	0.55±0.04	0.65±0.08	$\cdot 10^6$ dpm·d^{-1}
TOTAL INPUTS	610±320	82±49	550±270	67±32	460±210	52±23	530±260	60±30	$\cdot 10^6$ dpm·d^{-1}
SGD	50±330	120±80	630±340	300±120	980±540	390±230	610±400	290±150	$\cdot 10^6$ dpm·d^{-1}
SGD flow	20±150	56±35	280±150	140±60	440±240	180±100	270±180	130±70	$\cdot 10^3$ m^3·d^{-1}

4.4.2. SGD to the Port of Maó

The SGD flow to the Port of Maó can be estimated from the Ra flux supplied by SGD derived from the mass balance and the Ra concentration in coastal groundwater (the SGD endmember) (Table 5.4). Most of the groundwater samples were collected from wells not used for long periods (up to several decades) (W1, W3, W4, W5 and W7) or from large spring caves nourished by groundwater (W2 and W6). In both instances, the limited groundwater extraction, together with the large size of the reservoirs, would result in groundwater being poorly renewed, likely leading decreased Ra activities due to radioactive decay. This decay is indeed reflected by the low ^{224}Ra/^{228}Ra AR of all these samples (< 0.7; Table 5.3), since groundwater commonly have activities of ^{224}Ra and ^{228}Ra in equilibrium or even enriched in ^{224}Ra relative to ^{228}Ra, due to the faster regeneration of ^{224}Ra (Rama and Moore 1996; Charette et al. 2003; Swarzenski 2007). Therefore, these groundwater samples would not be appropriate for the characterization of Ra concentrations in SGD discharging to the Port of Maó. From all the sites sampled, W8 is the only one where groundwater is continuously flowing, since it is near-shore (10 m from the harbor waters) and frequently (almost daily) pumped for commercial purposes. Additionally, we purged the well (extracting hundreds of liters) before sampling, to ensure that groundwater was completely

renewed. Groundwater samples collected from this well are thus the best representation we have of the Ra activities in the SGD endmember. Average Ra activities collected from W8 are 224 ± 13 dpm·100L^{-1} for ^{224}Ra and 220 ± 20 dpm·100L^{-1} for ^{228}Ra, with an ^{224}Ra/^{228}Ra AR of ~1 (Table 5.3). ^{226}Ra activities in this well are considerably lower (2 times) than ^{228}Ra activities, justifying the low ^{226}Ra enrichment observed in harbor waters.

Results of the SGD fluxes derived from the ^{224,228}Ra mass balance and Ra activities measured in groundwater from W8 are shown in Table 5.4. For most of the seasonal samplings, SGD flows derived from ^{224}Ra are nominally higher (by a factor of ~2) than those obtained when using ^{228}Ra, although the values overlap within the uncertainties. The most likely reason for the differences on the nominal SGD flows is the mischaracterization of the sedimentary source, including the Ra supplied from both diffusion and resuspension events. A poor characterization of the Ra inputs from sediments would have a larger influence for ^{224}Ra than for ^{228}Ra, given its relative importance in the mass balance (Fig. 4.6). Indeed, this is reflected in the larger uncertainties associated with ^{224}Ra-derived SGD flows. SGD flows obtained from ^{228}Ra would thus be more reliable, as they are less conditioned on the appropriate characterization of the Ra fluxes from diffusion and resuspension events.

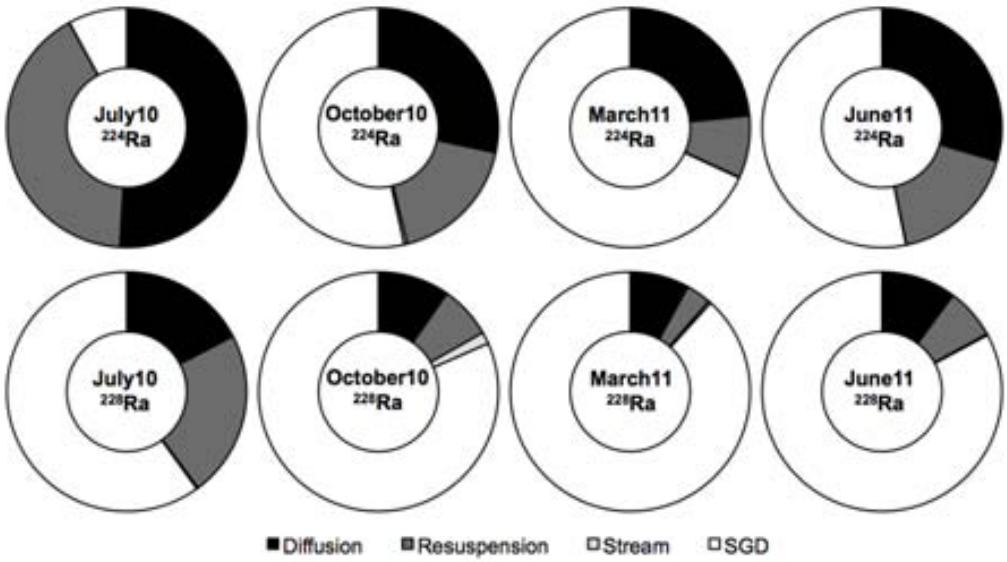

Figure 4.6. Contribution of different sources (diffusion from sediments, sediment resuspension events, stream discharge and SGD) to the ^{224}Ra and ^{228}Ra total inputs to the Port of Maó in all the seasonal surveys conducted.

Based on the ^{228}Ra-derived estimates, SGD flow presents a seasonal pattern likely dominated by changes in precipitation over the annual cycle, with maximum SGD rates in wet seasons ((180±100)·10^3 $m^3 \cdot d^{-1}$ in March11) and minimum flows in the dry period ((56±35)·10^3 $m^3 \cdot d^{-1}$ in July10). The seasonal discharge pattern is in phase with the recharge cycle of the aquifers with maximum annual precipitations in spring and fall, suggesting a rapid response of the limestone aquifer to precipitation events, as previously reported in other Mediterranean coastal areas (Garcia-Solsona et al. 2010b; Rodellas et al. 2012: Chapter 3). Variations on precipitation may lead to seasonal oscillation in the freshwater-seawater interface, driving the discharge of both fresh groundwater and seawater previously infiltrated to the coastal aquifer (Michael et al. 2005). However, the low salinities measured in most of the wells located close to the harbor suggest that SGD into the Port of Maó likely contains a minor fraction of saline groundwater. When normalizing the estimated SGD to the harbor shore length (~18 km), the annual SGD flow is ((1.1 – 3.6)·10^6 $m^3 \cdot yr^{-1} \cdot km^{-1}$), which is in good agreement with other estimates for Mediterranean islands (Moore 2006; Garcia-Solsona et al. 2010a; Rodellas et al. 2014: Chapter 5).

4.4.3. Sediment influence on Ra mass balances

The Ra mass balance conducted in the Port of Maó reveals that the Ra flux from bottom sediments, including both diffusion and releases from resuspension events, represents a significant source of Ra to the harbor waters (Table 4.4; Fig. 4.6). This sedimentary source accounts for a major fraction of the ^{224}Ra supplied to the system, particularly in summer, when SGD fluxes are minima and the resuspension events are more frequent. For instance, while the sediment source represents 32% of the total inputs of ^{224}Ra during the March11 survey, it is the dominant (92%) source in July10 (Fig. 4.6). The influence of sediments on the ^{228}Ra mass balance is lower but still significant, ranging from 11% of the total ^{228}Ra inputs in March11 to 40% in July10 (Fig. 4.6). These differences on the relative importance of sediments for ^{224}Ra and ^{228}Ra are related to differences on their production rates, which are set by their decay constants (Charette et al. 2008). Short-time and small scale processes, such as diffusion from bottom sediments or daily sediment resuspension events, do not allow a significant ingrowth of long-lived Ra isotopes, resulting in relatively low fluxes to the water column compared to short-lived Ra isotopes (King 2012; Santos et al. 2012).

Bottom sediments may be a continuous source of Ra isotopes to the water column through diffusion, erosion or resuspension, but also through short-scale (mm to cm) recirculation processes, such as topography-induced advection, wave pumping, ripple migration, shear or bioirrigation (Rama and Moore 1996; Breier et al. 2009; Santos et al. 2012; Garcia-Orellana et al. 2014). Although these latter mechanisms include recirculation of seawater, they are often excluded from the definition of SGD, which includes only those processes "with scale lengths of meters to kilometers" (Moore 2010b). Following this definition, here we grouped together all these processes as inputs from sediments. Most of the SGD studies involving Ra isotopes as tracers of SGD have shown that inputs of Ra from bottom sediments are often small in relation to the SGD source term (Rama and Moore 1996; Charette et al. 2003; Beck et al. 2007a; Garcia-Solsona et al. 2008b; Rodellas et al. 2012: Chapter 3). However, in shallow embayments with muddy sediments and/or affected by processes that favor Ra exchange across the sediment-water interface (e.g. bioirrigation, resuspension, hypoxia), the sedimentary source can supply a relevant flux of Ra isotopes, which may be comparable to SGD-derived Ra inputs, particularly for short-lived Ra isotopes (Breier et al. 2009, 2010; Gleeson et al. 2013; Garcia-Orellana et al. 2014). From a larger scale perspective, recent studies conducted in entire basins (Atlantic Ocean and the Mediterranean Sea) have also shown that Ra inputs from sediments are comparable to those gains from SGD (Moore et al. 2008). Therefore, attributing Ra inputs to the water column solely to SGD may not always be well justified, requiring a detailed evaluation of the sedimentary source. However, the contribution of Ra isotopes from sediments is often difficult to quantify, since it may be highly variable in space and time (Garcia-Orellana et al. 2014). For instance, (Moore et al. 2008) showed that Ra fluxes from muddy sediments are commonly 1-2 orders of magnitude higher than those from coarse-grained sediments. In a recent study conducted in Long Island Sound (New York), (Garcia-Orellana et al. 2014) suggested that seasonally variable bioirrigation and Mn cycling exerts important controls on the ^{224}Ra flux from bottom sediments, resulting on diffusive fluxes significantly higher in summer. Thus, estimates of Ra inputs from sediments based on few measurements and simplistic assumptions may not adequately represent spatial or temporal variations of the sedimentary source.

Accordingly, in those systems where sediments can represent a major contributor to the Ra mass balance (e.g. shallow water bodies, muddy systems or areas prone to bioturbation or resuspension events), Ra-derived SGD estimates can only be resolved

to the extent that sedimentary inputs are constrained. Using the example derived from the Port of Maó, the estimation of SGD flows relies on an appropriate characterization of Ra fluxes from sediment diffusion or resuspension events. Failing on estimating the long-lived Ra fluxes from sediments is smoothed out by their minor influence on the final SGD estimate. Thus, in systems highly influenced by bottom sediments, long-lived isotopes are likely the most appropriate Ra tracers of SGD. Yet, given that Ra isotopes reflect input mechanisms on time scales similar to their regeneration rates, the selection of the appropriate Ra tracer would also depend on the target processes of the study (King 2012; Santos et al. 2012). For instance, using long-lived Ra isotopes may not capture short (days) scale recirculation processes, such as tidally-driven SGD.

4.5. Conclusions

SGD to the Port of Maó has been estimated by using a comprehensive mass balance of ^{224}Ra and ^{228}Ra. The results show that the Ra flux from bottom sediments, through diffusion and due to releases associated to resuspension events, represents a significant source of Ra to the harbor waters. Difficulties on accurately estimating the Ra fluxes from sediments, which account for 32-91% of the ^{224}Ra supplied to the system and 11-39 % of the ^{228}Ra inputs, result on large uncertainties on the final SGD estimates. Uncertainties are particularly high for ^{224}Ra, given its larger relative importance in the Ra mass balance derived from their faster production rate in sediments. Based on ^{228}Ra, the SGD flows to the Port of Maó obtained range from $(57\pm40)\cdot10^3$ to $(180\pm100)\cdot10^3$ $m^3\cdot d^{-1}$, showing a seasonal cycle likely dominated by the recharge cycle. Findings derived from this work evidence that attributing Ra inputs to the water column solely to SGD in systems where sediments may play a relevant role (e.g. shallow water bodies, muddy systems or areas prone to bioturbation or resuspension events) might not be accurate, requiring a detailed evaluation of the sediment source. Since inputs from sediments are often difficult to quantify, using long-lived Ra isotopes to estimate the SGD flow may minimize the effect of a poor characterization of the sediment source.

Besides the influence of sediments as a source of Ra isotopes to the water column of the Port of Maó, harbor sediments could also represent a relevant source of other compounds, such as major nutrients (e.g. nitrogen or phosphorous) or heavy metals (e.g. Cu, Pb, Hg), to the harbor waters. Inputs of metals from bottom sediments may be

particularly relevant because the sediments of the Port of Maó contain significant amounts of metals as a consequence of industrial and urban activities (Garcia-Orellana et al. 2011). Considering its frequency and magnitude, the resuspension of bottom sediments triggered by vessel docking maneuvers could represent a major mechanism favoring the release of sediment-bound metals into the water column (Kalnejais et al. 2010; Superville et al. 2014). Inputs of metals from bottom sediments may have profound implications on the biogeochemical cycles of the water column, by limiting algal growth or acting as toxic agents (Morel and Price 2003; Lafabrie et al. 2013; Twining and Baines 2013). Thus, fluxes of trace metals from bottom sediments, as well as the effects of the sedimentary source on the phytoplankton composition or growth, should be further studied.

CHAPTER 5

Submarine Groundwater Discharge as a source of nutrients and trace metals in a Mediterranean Bay (Palma Beach, Balearic Islands)

This chapter is based on:

Rodellas, V., Garcia-Orellana, J., Tovar-Sanchez, A., Basterretxea, G., Masqué, P., Garcia-Solsona, E., Sánchez-Quiles, D., López, J.M., 2014. Submarine Groundwater Discharge as a source of nutrients and trace metals in a Mediterranean bay (Palma Beach, Balearic Islands). Mar.Chem., 160, 56-66

5.1. Objective

The present study is devoted to determine the magnitude of SGD-driven fluxes of nutrients and trace metals into a detrital Mediterranean bay (Palma Beach, Majorca, Balearic Islands) by using Ra isotopes. This study is also aimed to evaluate the contribution of SGD to the nearshore nutrient pools and the potential linkages between SGD and coastal productivity. Palma Beach is selected because preferential groundwater flow paths inflow to the sea along this region and agriculture and tourism are potential sources of groundwater contamination. This study represents a comprehensive study of SGD in a detrital Mediterranean site and it is the first work where the magnitude of trace metal inputs through SGD into the Mediterranean Sea is evaluated.

5.2. Methods

5.2.1. Study site: Palma Beach

Palma Beach is a carbonated sediment beach extending ~5km in the south-east of the Palma Bay, located in the southwestern part of the island of Majorca (Balearic Islands, NW Mediterranean; Fig. 5.1a). The Palma Bay is the primary touristic resort in the Balearic Islands and one of the main touristic destinations in the Mediterranean Sea. The population in the area is concentrated along the coastal zone (~450 x 10^3 permanent inhabitants), seasonally peaking in summer. The city of Palma, located in the NW area of the bay, accommodates most of this population and also supports the main commercial harbor in the island (Fig. 5.1b).

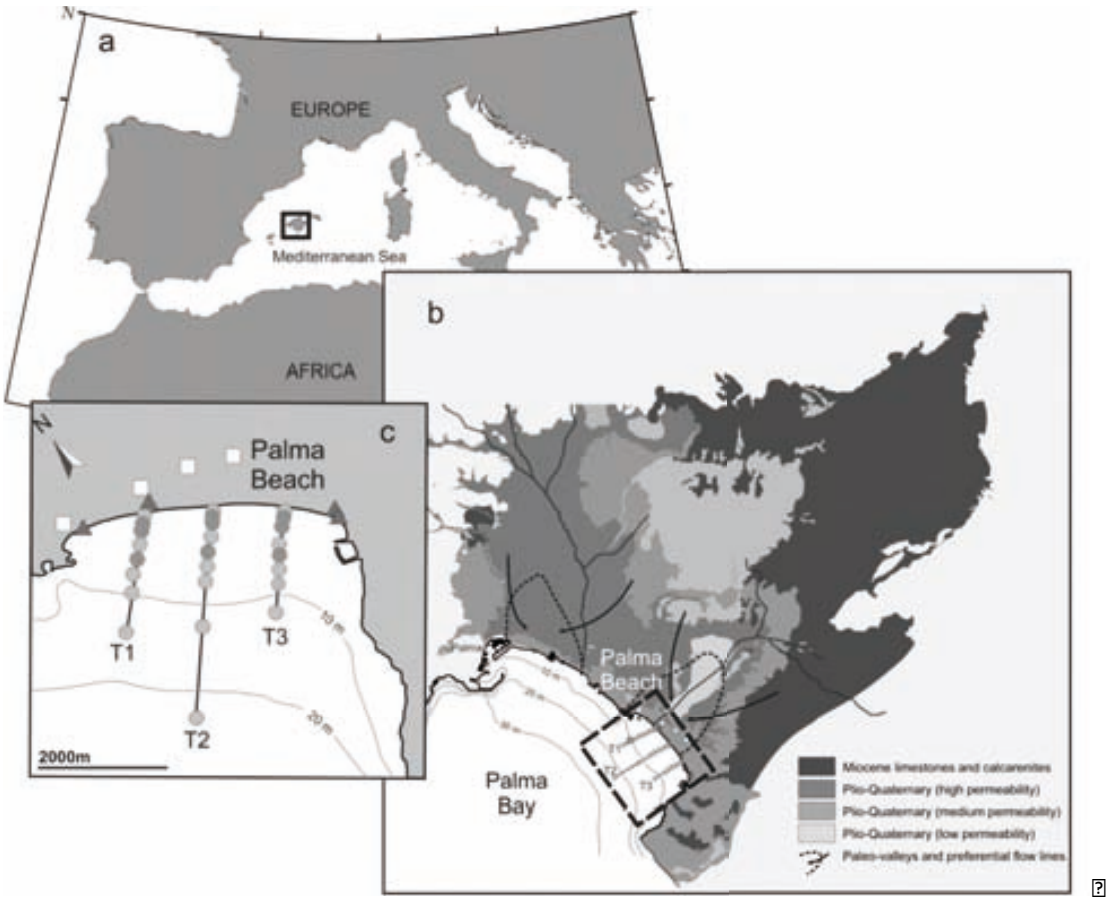

Figure 5.1. a) The study area is located at the southeastern part of Majorca Island (Balearic Islands), at the Western Mediterranean Sea. b) The hydrological formations of Palma Basin are represented based on Nielsen et al. (2004) and the preferential groundwater flow lines are also indicated. The location of the study site (Palma Beach), at the south-east of Palma Bay, is also highlighted. c) Sampling stations in Palma Beach on summer 2010. Stations include groundwater from wells (white squares), porewater from piezometers (dark grey triangles) and beach seawater (grey circles). Trace metal samples in beach seawater were collected in those stations highlighted with dark grey.

Climate conditions in the area are typically Mediterranean with mild winter temperatures (mean ~9.3 ºC) and dry and warm summers (24.6 ºC). Average annual rainfall in the area is 410 mm and surface fresh water flow to Palma Bay is restricted to sporadic events following heavy rains. The inland system (Palma Basin) corresponds to a sedimentary basin filled with marine and continental deposits, from the Miocene to the Quaternary, extending over an area of ~ 370 km^2 (Nielsen et al. 2004; Candela et al. 2008). There are two main aquifers in the basin: (i) a deep Miocene carbonate aquifer formed by limestones, extending along the north boundary of the basin and not present in the Palma Beach area, and (ii) a shallow unconfined detrital aquifer, from the PlioQuaternary, occupying most of the sedimentary basin (Fig. 5.1b). This shallow aquifer, which is impacted by human activities (i.e. agriculture, industry or urban

activities), mainly discharges through a dune-beach system (now urbanized) located in the Palma Beach, at the southeastern region of the Palma Basin. This sandy area hides a paleo-valley that represents a preferential groundwater flowpath to the sea (N. Courtois, F. Brissaud, D. Crespí, P. Lachassagne, P. Le Strat and P. Xu, unpubl). The shallow unconfined detrital aquifer could thus represent a major SGD source to the study site.

Coastal circulation is mainly regulated by wind forcing which can result in poor renewal during summer (Jordi et al. 2011). The tides have a minor influence on coastal waters, as the tidal range is less than 0.3 m. The bathymetry varies smoothly (~ 1% slope) reaching 15 m water depth at about 2000 m offshore, with the isobaths nearly parallel to the shoreline (Fig. 5.1b). Environmental monitoring surveys reveal that Palma Beach presents signs of eutrophication related to the availability of nutrients and microalgal accumulation in nearshore waters (PHIB 2008).

5.2.2. Sample collection

A detailed survey focused on nearshore waters of Palma Beach was carried out from 17th to 21st of May 2010 to determine the magnitude of SGD, its associated flux of nutrients and trace metals, and the potential connections between SGD and the enhanced coastal phytoplankton biomass. Three detailed transects running perpendicular to the shoreline (T1 to T3) were sampled (Fig. 5.1c). Each transect consisted of 8 stations at approximately 5, 125, 250, 500, 750, 1000, 1250 and 2000 m from the shoreline. An additional station located farther offshore (~4000 m from the shoreline) was sampled in transect T2 as a reference of open seawater conditions. Surface water samples for Ra, nutrients, trace metals (only in 9 stations) and Chl*a* were collected at each station. Salinity and temperature at different depths were measured in situ using a YSI 556 multiparameter probe.

Samples for Ra analysis were stored in 60L containers. Nutrients and trace metals were sampled at 1 m water depth using a peristaltic pump. Seawater was pumped through acid-cleaned Teflon tubing coupled to a C-flex tubing (for the Cole-Parmer peristaltic pump head), filtered through an acid-cleaned polypropylene cartridge filter (0.22 μm; MSI, Calyx®), and collected in a 13 mL PE tubes for nutrients and 0.5 L low-density

polyethylene plastic bottle for metals (Tovar-Sánchez 2012). Water samples of 240 mL for Chl*a* analysis were filtered through Whatman GF/F glass fiber filters. Nutrients and Chl*a* samples were kept frozen until their analysis.

Groundwater was sampled from four coastal wells and five piezometers distributed along the beach shoreline. Each piezometer station was sampled at different depths and slightly different locations. A submersible pump was used to collect samples from wells for Ra isotopes. For trace metals and nutrients a 5 L Niskin bottle was used. A Retract-A-Tip piezometer system (AMS, Inc.) connected to a peristaltic pump was used to sample Ra isotopes in porewater. Porewater samples for trace metal and nutrient analysis were collected at several depths using a multi-pore piezometer made of non-metal components (Beck et al., 2007a). Notice that the term "groundwater" is used in this paper for both fresh-water from wells and porewater from piezometers, as it is commonly considered in SGD research. Three sediment samples were collected throughout the Palma Bay to characterize the concentration of long-lived Ra isotopes (^{226}Ra and ^{228}Ra) in bay sediments.

In addition to the sampling focused on Palma Beach, in June 2009 a sampling survey covering a grid of 37 stations throughout Palma Bay was conducted to characterize the distribution of trace metals in the study site. Trace metals in this previous sampling were collected as described above.

All the samples collected to determine the activities of Ra isotopes in both waters and sediments, as well as the concentrations of nutrients, trace metals and Chl*a* in waters were analyzed as described in Chapter 2 (Analytical methods).

5.3. Results

5.3.1. Palma Beach nearshore water characterization

Seawater salinities were relatively homogeneous (37.5 ± 0.2) throughout the three transects but a very narrow band with lower salinity was observed in the first tens of meters from the shoreline. Salinities at this band were lower at T1 (34.4) and to a lesser extent, at T3 (36.3). Salinity variations in depth (greater than 0.1) were detected at five

stations near the shoreline, with fresher salinities at the surface layer than those measured in deeper waters (down to 3 - 4 m depth).

Nearshore waters showed significant enrichments of ^{223}Ra, ^{224}Ra and ^{226}Ra relative to samples offshore (Krustal-Wallis test was applied to compare nearshore (<250 m) and offshore (>2000 m) samples: p ~ 0.01) (Fig. 5.2). Ra concentrations decreased with distance offshore (Fig. 5.2), suggesting that most Ra inputs occurred at the shoreline. The three transects surveyed presented comparable patterns and Ra activities suggesting homogeneous Ra inputs along the shoreline and/or rapid homogenization driven by currents flowing parallel to the shore. Onshore-offshore gradients of ^{228}Ra were not evident (Kruskal-Wallis, p = 0.19), as nearshore activities ranged from 4.2 to 8.5 dpm·100L^{-1}, which is in the range of ^{228}Ra activities measured offshore (3.2 – 5.7 dpm·100L^{-1}). The fairly constant ^{228}Ra distribution suggests a lack of major inputs of this isotope at the shoreline, most likely due to the low concentrations in ^{228}Ra measured in inflowing SGD (see section 3.4.), thus preventing the use of this radionuclide as a SGD tracer at this setting. Although the tidal cycle could affect the Ra distribution observed (Knee et al. 2011), we considered that the low tidal range of Palma Bay (< 0.3 m) had a minor influence on the Ra activities measured in seawater.

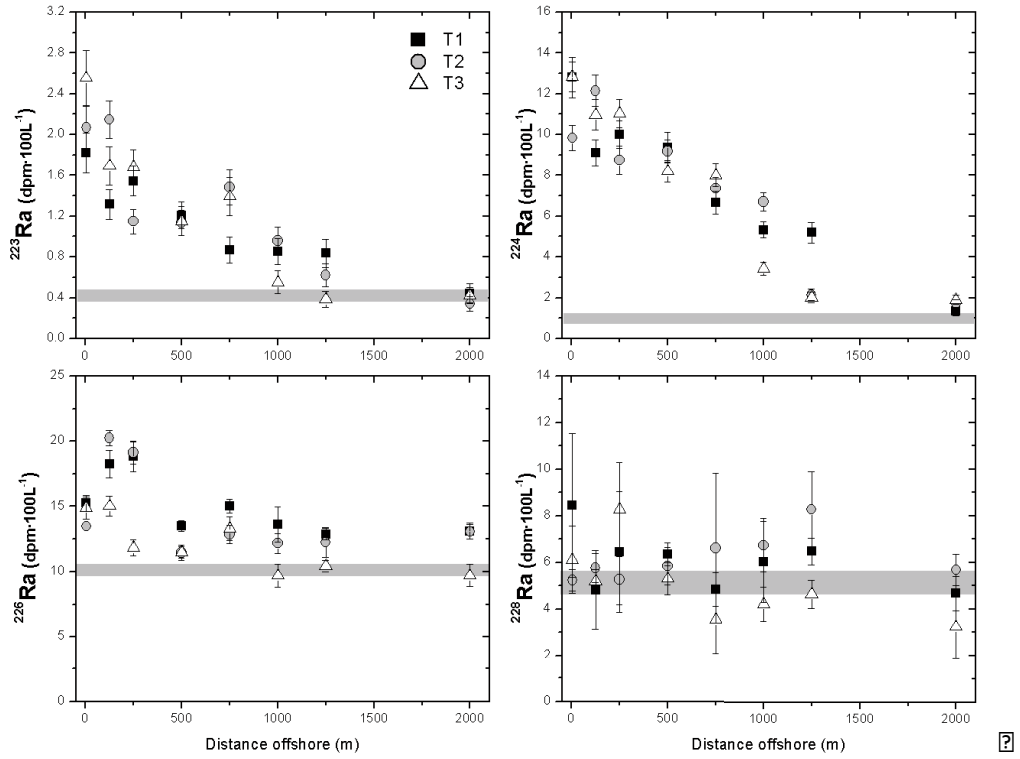

Figure 5.2. Ra activities in surface nearshore waters of Palma Beach plotted against distance offshore, for all the three transects. The grey area represents the Ra activity of the offshore sample with its associated uncertainty.

Significant differences in DIN concentrations were observed between nearshore and offshore waters (Krustal-Wallis test, $p < 0.01$), suggesting a terrestrial input of DIN (Fig. 5.3). Some of the shoreline concentrations were very high (> 64 μmol·L^{-1}) and corresponded to samples with low salinities and high Ra activities. DIP concentrations were higher than 0.05 μmol·L^{-1} in only a few samples, all of them located nearshore and mainly along T2 (Fig. 5.3).

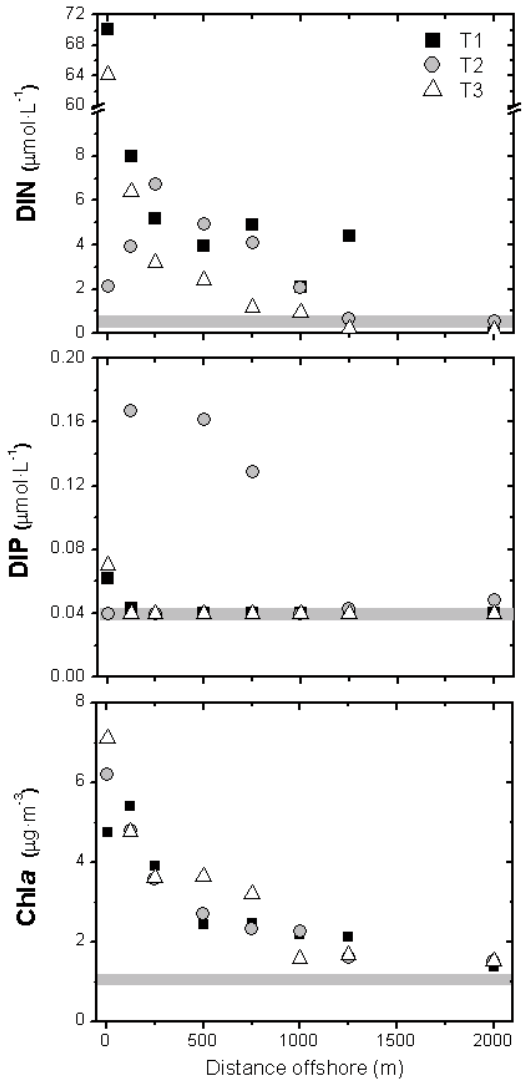

Figure 5.3. Nutrient (DIN and DIP) and Chl*a* concentrations in nearshore Palma Beach waters as a function of distance offshore, for all the three transects. The grey area represents the nutrient and Chl*a* concentrations measured at the offshore station.

Concentrations of Fe (3.0 – 6.0 nmol·L^{-1}), Ni (2.9– 5.6 nmol·L^{-1}), Cu (5.9 - 13 nmol·L^{-1}), Zn (3.3 – 10 nmol·L^{-1}), Mo (81 - 160 nmol·L^{-1}) and Pb (0.28 – 0.40 nmol·L^{-1}) were relatively constant in nearshore waters of Palma Beach. No particular spatial distribution of trace metals could be delineated with the limited set of samples we collected (n=9). However, the sampling conducted in 2009 allowed us to assess the general distribution of trace

metals in the entire Palma Bay (Fig 5.4). Concentrations of Mo and Ni were homogeneous and showed little contrast between nearshore and offshore waters. Concentrations of Cu, Pb and Zn were remarkably higher in the NW region of the bay, near the harbor and the city of Palma, whereas Fe was enriched at nearshore waters of Palma Beach, at the SE of the bay.

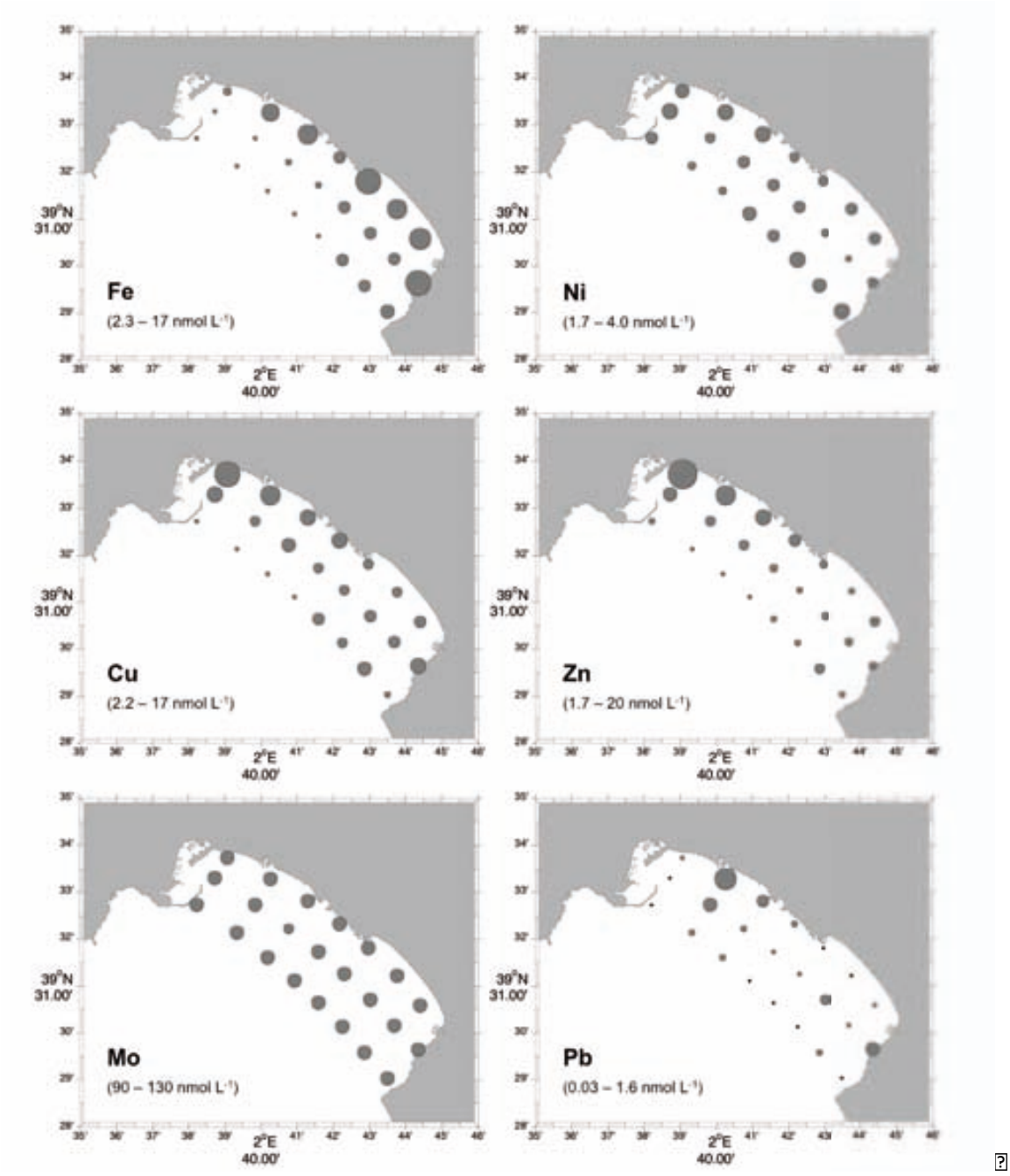

Figure 5.4. Concentrations of dissolved (<0.22 μm) Fe, Ni, Cu, Zn, Mo and Pb measured in surface waters from the entire Palma Bay in a previous survey conducted in summer 2009. The range of concentrations for each metal is indicated in parentheses.

The spatial distribution of phytoplankton biomass along the three transects revealed significant onshore enhancements of Chl*a* (4.7 – 7.1 $mg \cdot m^{-3}$) relative to offshore concentrations (1.1 - 1.5 $mg \cdot m^{-3}$ farther than 2000 m offshore) (Krustal-Wallis test, $p \sim 0.01$) (Fig. 3). These biomass concentrations are high when compared with summer coastal waters of the Majorca island (0.1-0.7 $mg \cdot m^{-3}$) and in the range of the beaches experiencing eutrophication in this region (Basterretxea et al. 2007, 2010).

5.3.2. Groundwater characterization

Groundwater sampled from wells revealed some exchange between the aquifer and the sea, with salinity values ranging from 2.1 to 3.8. Salinities of porewater samples obtained with coastal piezometers varied widely, showing a notable gradient between the NW (6.2-19.6) and the SE (24.1 – 31.0) boundaries of the beach. The lower salinities measured at the NW region are consistent with the existence of a Paleocene valley that funnels the outflow from the shallow aquifer in this area (Fig. 5.1b).

Activities of Ra isotopes measured in groundwater either from piezometers or wells ranged from 2.7 to 23 $dpm \cdot 100L^{-1}$ for ^{223}Ra, 23 to 110 $dpm \cdot 100L^{-1}$ for ^{224}Ra, 3.5 to 61 $dpm \cdot 100L^{-1}$ for ^{226}Ra, 4.5 to 100 $dpm \cdot 100L^{-1}$ for ^{228}Ra, most of them exceeding the activities measured in nearshore seawater (Fig. 5.5). Similar activities of Ra isotopes in SGD have been reported in other studies conducted in Western Mediterranean islands (e.g. Moore 2006; Garcia-Solsona et al. 2010). The high salinity porewaters collected from the SE area of the Palma Beach showed the highest activities of ^{223}Ra, ^{224}Ra and ^{228}Ra, whereas the highest activities of ^{226}Ra were measured in fresher porewaters from the NW region, where the shallow aquifer connects with the sea (Fig. 5.5). Porewater samples collected from all the shoreline piezometers showed a fairly constant $^{224}Ra/^{223}Ra$ activity ratio (5.5 ± 0.3; $r^2 = 0.833$; $p < 0.001$; Fig. 5.5a), suggesting that the transit time of porewaters through coastal sandy sediments was long enough to allow the water to be enriched with the Ra desorbed from the sediments. No linear correlation was found between ^{228}Ra and ^{226}Ra (Fig. 5.5b). Indeed, minimal influence of the sediment is expected for long-lived Ra, as the Ra signals acquired from a previous solid matrix (i.e. an aquifer) do not significantly decay and the concentration of long-lived Ra isotopes in the sediments may be low due to their low production rates from their parent isotopes (Hancock and Murray 1996).

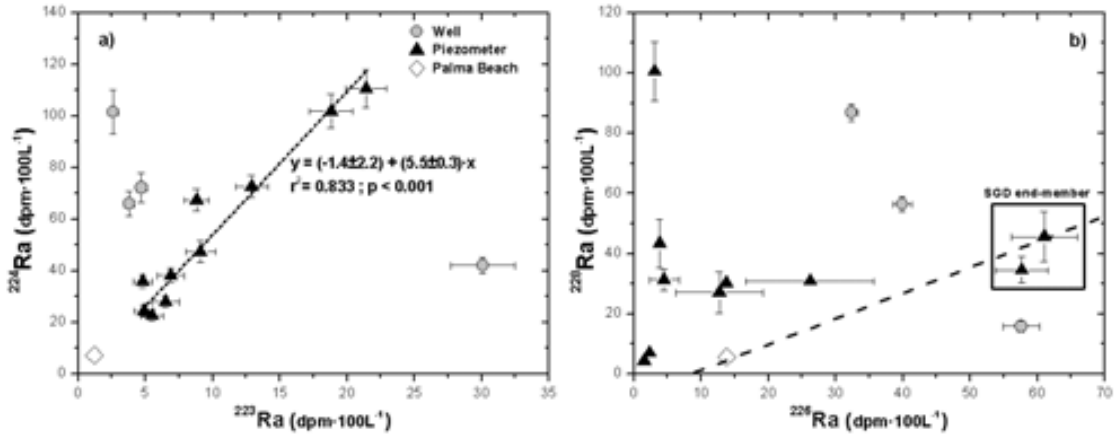

Figure 5.5. (a) ^{224}Ra vs ^{223}Ra and (b) ^{228}Ra vs ^{226}Ra activities in the potential SGD endmembers (groundwater from wells and piezometers). The average concentrations of Ra isotopes measured in Palma Beach waters are also shown. The dashed-line in (a) represents the best linear fit to the ^{224}Ra vs ^{223}Ra activities in porewaters. In (b), the dashed line represents the constraint in ^{228}Ra and ^{226}Ra concentrations in inflowing SGD obtained from Eq 5.3-5.5. This line is used to select those samples used as SGD endmember for Ra isotopes.

Nitrate concentrations in the aquifer were very high (200 - 1600 μmol·L^{-1} in wells and 0.05 - 2800 μmol·L^{-1} in beach piezometers), with higher concentrations generally measured in fresher waters (Fig. 5.6). Unlike nitrate, phosphate concentrations were very low in fresh groundwater (either from wells or fresh piezometers) and the highest phosphate concentrations (up to 5.2 μmol·L^{-1}) were measured in mid-salinity porewater samples from piezometers (Fig. 5.6).

Concentrations of Fe (20 – 8145 nmol·L^{-1}), Ni (5.7 – 15 nmol·L^{-1}), Cu (0.6 - 110 nmol·L^{-1}), Zn (7.0 – 1600 nmol·L^{-1}) and Pb (0.1 – 6.5 nmol·L^{-1}) in coastal porewaters and wells markedly exceeded those measured in seawater (Fig. 5.6). Porewaters were particularly enriched in Fe, with concentrations 1 to 3 orders of magnitude higher than in seawater, suggesting that SGD may be an important source of this metal to the coastal sea, as previously reported for other regions (e.g. Windom et al. 2006; Jeong et al. 2012). In contrast, concentrations of Mo (4.3 - 320 nmol·L^{-1}) in porewaters and wells were comparable to those measured in coastal seawater.

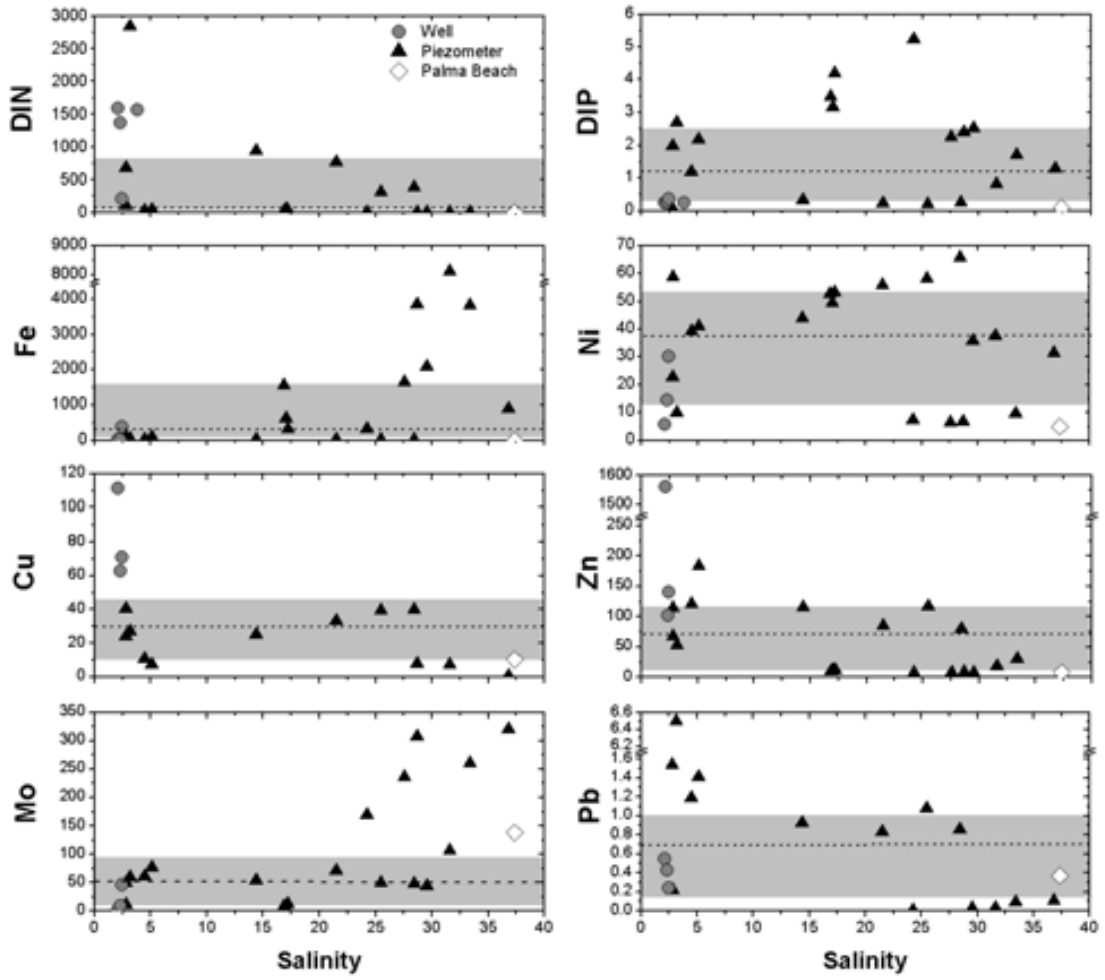

Figure 5.6. Salinity distribution of nutrients (DIN and DIP; μmol L^{-1}) and dissolved metals (Fe, Ni, Cu, Zn, Mo and Pb; nmol L^{-1}) in groundwater from wells (grey circles) and piezometers (black triangles). The dashed line and the shadowed area, respectively, represent the median and the range comprised between the 1st and the 3rd quartiles of the set of groundwater concentrations. The averaged concentration of Palma Beach waters is also included for comparison (white diamond).

5.3.3. SGD flux estimations

The trend with distance offshore (Fig. 5.2) displayed by Ra isotopes may be used to estimate the eddy diffusion coefficient (K_h) and the advection offshore (u), following an approach described by (Moore 2000b) and modified by Li and Cai (2011) (2011). The equations used in this approach are given below:

$$u = \frac{L_1^2\lambda_1 - L_2^2\lambda_2}{L_2 - L_1} \quad (5.1)$$

$$K_h = L_2^2\lambda_2 + L_2 u = L_1^2\lambda_1 + L_1 u \quad (5.2)$$

where L_1 and L_2 are the inverse (1/m) of the slopes from the log-linear fit for ^{223}Ra and ^{224}Ra versus distance offshore respectively, u is the offshore advective velocity (m s^{-1}), K_h is the horizontal eddy diffusivity coefficient (m^2 s^{-1}), and λ_1 and λ_2 are the radioactive decay coefficients of the two short-lived Ra isotopes (s^{-1}). Here, ^{223}Ra and ^{224}Ra are used because their half-lives are comparable to the expected residence time of nearshore waters. This approach assumes that there are no additional inputs of the tracer beyond the coastline. Assuming shore-based Ra sources to the Palma Beach, an exponential decrease offshore should be observed for the distribution of the $^{224}Ra/^{226}Ra$ activity ratio (AR), since ^{224}Ra decays faster than ^{226}Ra. However, this AR was constant from the coastline to ~500 m offshore (Fig. 5.7), suggesting either that Ra inputs are occurring all along the first 500 m (what would violate the initial assumption of the approach) or that there is a fast mixing in this nearshore area (what would imply a higher diffusion/advection in this specific region than in the rest of the bay). Thus, only the samples collected beyond 500 m of the coastline are considered to obtain the diffusion and advection coefficients for the entire bay. The log-linear fit of ^{223}Ra and ^{224}Ra concentrations versus distance offshore allows estimating a diffusive mixing coefficient (K_h) of 2.6±0.4 $m^2 \cdot s^{-1}$ and a very low advection velocity (0.0011±0.0006 $m \cdot s^{-1}$). This almost negligible estimated advection velocity is in good agreement with the bay circulation patterns modeled by Jordi et al. (2011) that resulted in a minor net offshore water current.

If the advection and diffusive mixing coefficients are known, the fluxes offshore of any conservative material can be calculated. As advection in our system has been shown to be negligible, the flux of ^{226}Ra offshore from the Palma bay can be estimated as the product of the offshore ^{226}Ra concentration gradient and the Ra-derived eddy diffusivity constant (K_h) (Moore 2000b). Since all the three transects conducted perpendicular to the coastline present similar ^{226}Ra patterns, they are integrated in order to obtain a value for the study site. Taking the linear ^{226}Ra gradient (-9.6 ± 1.8) 10^{-3} $dpm \cdot m^{-3} \cdot m^{-1}$ (r^2 = 0.817; $p < 0.001$) and assuming that the tracer was transported offshore in the 3.5 m fresher surface layer, the offshore ^{226}Ra flux is 0.088 ± 0.020 $dpm \cdot m^{-1} \cdot s^{-1}$. The ^{226}Ra flux offshore must be balanced by an input in the coastal zone, most likely SGD. Other potential sources of ^{226}Ra can be neglected: surface water inputs to the bay are insignificant during the dry season and ^{226}Ra release from sediments is minimal due to its low activity in bay sands (0.85 ± 0.21 $dpm \cdot g^{-1}$; n=3) and long regeneration time (Beck et al. 2007a).

This estimated ^{226}Ra flux may be converted into a SGD flow by characterizing the ^{226}Ra concentration in SGD. Considering that long-lived Ra isotopes are not significantly decaying on the time scale of nearshore processes, the ^{226}Ra and ^{228}Ra concentration in SGD must accomplish the following mixing equations:

$$f_{SGD} + f_{SW} = 1 \quad (5.3)$$

$$^{226}Ra_{SGD} f_{SGD} + {}^{226}Ra_{SW} f_{SW} = {}^{226}Ra_{BW} \quad (5.4)$$

$$^{228}Ra_{SGD} f_{SGD} + {}^{228}Ra_{SW} f_{SW} = {}^{228}Ra_{BW} \quad (5.5)$$

where f is the fraction of SGD (SGD) and open sea water (SW) endmembers in Palma Beach waters (BW), respectively, and Ra_{SGD}, Ra_{SW} and Ra_{BW} are the average concentration of ^{226}Ra and ^{228}Ra in SGD, open sea waters (^{226}Ra = 9.4 dpm·100L^{-1} and ^{228}Ra = 2.3 dpm·100L^{-1}; Moore 2006) and Palma Beach waters (^{226}Ra =13.8 dpm·100L^{-1} and ^{228}Ra = 5.7 dpm·100L^{-1}), respectively. Given that there are more unknowns (f_{SGD}, f_{SW}, AR_{SGD} and $^{226}Ra_{SGD}$) than equations, ^{226}Ra in SGD can be only constrained by evaluating a range of ^{228}Ra concentrations. As seen from Fig. 5.5b, only two samples collected present ^{228}Ra and ^{226}Ra concentrations in accordance to the requirements imposed by these equations, and thus they were considered as the representative SGD endmember for Ra isotopes. Indeed, these are two porewater samples collected in the NW part of the Palma Beach, where the shallow aquifer connects with the sea (preferential groundwater flow lines in Fig 5.1). Using the average ^{226}Ra concentration in these two porewater samples (59 ± 2 dpm·100L^{-1}), the calculated SGD seepage flow 12.8 ± 3.0 m^3·m^{-1}·d^{-1}. Assuming that diffusive groundwater discharge occurred all along the Palma Beach coastline (4,400 m), the total flow to the Bay is 56,000 ± 1,300 m^3·d^{-1}. This value is almost three times higher than the groundwater discharge derived from the regional hydrological balance (20,000 m^3 d^{-1}; PHIB 2008). This discrepancy likely reflects the fact that the hydrological budget takes into account only the fresh groundwater discharge, while the Ra approach also includes the recirculated seawater, which can also be an important source of terrestrial compounds to the coastal sea.

5.3.4. Residence time of conservative compounds

An estimation of the time that coastal conservative compounds remained in the study site (i.e. residence time) is needed to evaluate the implications of SGD-driven fluxes on the coastal ecosystem. The residence time of conservative compounds can be calculated using the variation of the activity ratios (AR) between Ra isotopes of different half-lives, based on an approach described by Moore (2000a). This approach assumes that (i) Ra is only added to coastal water in the source region, (ii) there are no losses of Ra aside from mixing and radioactive decay, (iii) Ra entering the system has a uniform AR and (iv) the open sea contains negligible concentrations of Ra. Given that Ra inputs in Palma Beach are likely occurring along the first 500 m from the shoreline (Fig 5.7), here we define residence time of conservative compounds as the time it takes for them to leave the study site (2,000 m offshore) since they were isolated from the source area (0 – 500 m). Following the approach described by Moore (2000a), residence time of conservative compounds (T_R) can be calculated as follows:

$$T_R = \frac{\ln (AR_{2000}) - \ln (AR_{SR})}{\lambda_{224} - \lambda_{226}} \quad (5.6)$$

where AR_{2000} is the $^{224}Ra/^{226}Ra$ AR at 2,000 m offshore (0.14 ± 0.05) and AR_{SR} is the average $^{224}Ra/^{226}Ra$ AR in the source region (0.70 ± 0.09), and λ_{224} (0.189 d^{-1}) and λ_{226} (negligible relative to λ_{224}) are the decay constants of ^{224}Ra and ^{226}Ra, respectively. Here, ^{224}Ra was selected because its half-life is appropriate for the expected residence time of the site and ^{226}Ra as a normalizing isotope because its decay is negligible and it has lower relative uncertainties than ^{223}Ra. Applying Eq. 5.6, a residence time for conservative compounds in the study site of 8.4 ± 1.9 days was obtained (Fig. 5.7).

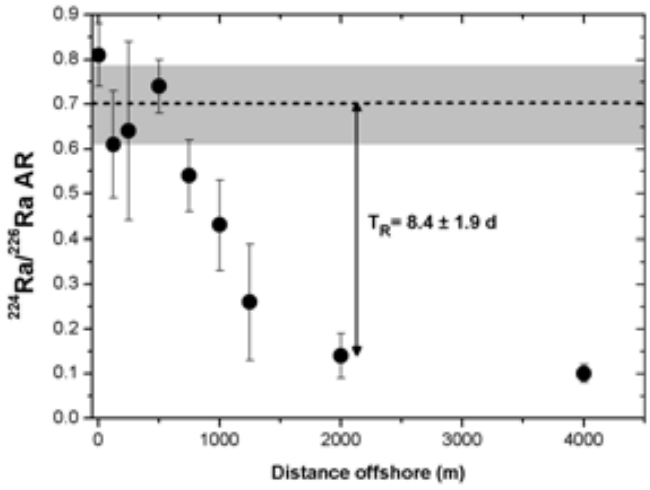

Figure 5.7. $^{224}Ra/^{226}Ra$ AR plotted against distance offshore. The three transects offshore were integrated in one as all of them present similar activities and distribution. The dashed line and the shadowed area, respectively, represent the average AR and the standard deviation (1s) of the samples collected within the first 500 m from the shoreline, values used to estimate the residence time of conservative compounds in the study site.

5.4. Discussion

5.4.1. Nutrient inputs through SGD

The analysis of nutrient concentrations in coastal piezometers and wells suggest that fresh groundwater is a dominant supplier of DIN to Palma Beach (Fig. 5.6). Porewater samples roughly fall along the mixing line between nutrient-rich fresh groundwater and nutrient-poor seawater endmembers, revealing that the mixing with recirculated seawater acts mainly as a dilution agent. However, several samples lie below this conservative mixing line, likely reflecting the complex geochemical behaviour of nutrients in the subterranean estuary. The high DIN pools measured in fresh groundwater samples, largely as nitrate (~ 99 %), agree with other results reported along the island (López-García and Mateos-Ruiz 2003). These high nitrate concentrations in groundwater are mainly a consequence of intensive irrigation practices based on wastewater reuse and fertilizers use (López-García and Mateos-Ruiz 2003; Candela et al. 2008). Unlike DIN, DIP concentrations are very low in fresh groundwater (Fig. 5.6), which is attributed to its rapid removal from groundwater (Slomp and Van Cappellen 2004) and a minor influence of anthropogenic inputs. The highest DIP concentrations were measured in mid-salinity porewater, most likely due

to the mobilization of phosphate in the subterranean estuary by recirculated seawater (Weinstein et al. 2011).

The nutrient fluxes from SGD to the Palma Bay can be calculated by multiplying the amount of SGD derived from Ra isotopes by the concentration of nutrients in inflowing SGD (Table 5.1). Given that nutrients do not behave conservatively along the groundwater path and concentration in the subterranean estuary are extremely variable, the estimation of the nutrient concentration in the actual SGD endmember becomes particularly difficult (see discussion on nutrient endmember selection in Santos et al. (2008) and Knee et al. (2010)). To provide a reasonable characterization of nutrient concentrations in SGD a large number of samples along the study site was used, focusing on groundwater sampled just before discharging and in the upper 2 m of the subterranean estuary, considered the most permeable layer where most biogeochemical reactions are occurring (Santos et al. 2008). The range comprised between the 1st and 3rd quartiles of the set of nutrient concentration in groundwater (wells and piezometers; n = 23) was used as a reasonable upper and lower estimate of nutrients in discharging SGD (Table 5.1). The dissolved nutrient concentrations in these endmembers spanned a wide range (e.g. up to two orders of magnitude for DIN; Table 5.1) and thus result in SGD-driven nutrient fluxes with large uncertainties (Table 5.1). The contribution of seawater was removed to calculate the nutrient flux derived from SGD (Santos et al. 2008). The resulting flux of nutrients into Palma Beach ranges from 100 to 10000 and from 3 to 31 mmol·m^{-1} d^{-1} for DIN and DIP, respectively, with a median flux of 1900 mmol·m^{-1}·d^{-1} of DIN and 16 mmol·m^{-1}·d^{-1} of DIP. DIN fluxes are in the upper range of values reported in different coastal areas (Slomp and Van Cappellen (2004) for a compilation), mainly as a consequence of the high DIN concentrations in groundwater (López-García and Mateos-Ruiz 2003; Candela et al. 2008). Conversely, DIP fluxes are low, as dissolved phosphate is rapidly removed from groundwater through sorption to Fe-oxides or co-precipitation with metal into mineral phases (Slomp and Van Cappellen 2004). This contrasting behavior translates into ratios of dissolved inorganic N:P in inflowing SGD of 160:1, much higher than the requirements by phytoplankton growth (Redfield N:P ratio of 16:1). Similar ratios in inflowing SGD have been reported in other Mediterranean settings (Garcia-Solsona et al. 2010a, 2010b). Thus, this SGD input may contribute to P limitation in the area, what is a common situation in the Mediterranean Sea (e.g. Diaz et al. 2001).

The significance of SGD as a source of nutrients into nearshore waters of Palma Beach can be assessed through the comparison of the SGD-derived nutrient inventory (i.e. nutrient flux from SGD multiplied by the residence time obtained from Ra isotopes) and the excess inventory of nutrients in the study site (i.e. average nutrient concentration in nearshore water minus nutrient concentration offshore, multiplied by the volume of the study site). Notice that the study site must be described by the same boundaries used when SGD is estimated (3.5 m depth and 2,000 m width) and that constant nutrient concentrations are assumed for the 3.5 m surface layer. This qualitative comparison reveals that the amount of DIN and DIP supplied by SGD would account for 120% and 40%, respectively, of the excess pools of these nutrients measured in nearshore waters (Fig. 5.8). Although this comparison does not take into account the complex cycling of nutrients in seawater (e.g. transformation, removal or release of nutrients due to biological processes or fluxes from/to bottom sediments), it still provides valuable information on the relevance of SGD as a source of nutrients to the study site. In doing so, we found that SGD is a major source of DIN and can also contribute substantial amounts of DIP to nearshore waters of this Mediterranean bay. Indeed, strong offshore gradients of DIN and, to a lesser extent, DIP concentration, were measured in seawater (Fig. 5.3), which provides independent evidence of the significant role of SGD as a source of these compounds to the sea.

Table 5.1. Average concentrations of nutrients (3 transects of 7 samples each one) and trace metal (n=9) in Palma Beach waters. The concentration of nutrients and trace metals in SGD is obtained from both the median and the range comprised between the 1st (Q1) and 3rd (Q3) quartiles of the set of concentrations in groundwater (wells and piezometers; n = 23). The SGD-driven flux of nutrients and trace metals normalized by shore length is estimated from both the median concentration of those compounds in SGD and the range Q1 – Q3. The SGD-driven flux of nutrients and trace metals into the entire bay and normalized by the area of the study site are also shown.

			DIN	DIP		Fe	Ni	Cu	Zn	Mo	Pb
Seawater concentration	Mean	$\mu mol \cdot L^{-1}$	2.0	0.05	$nmol \cdot L^{-1}$	4.9	4.9	10	7	140	0.37
	SD		0.4	0.02		1.0	0.9	3	2	30	0.04
SGD concentration	Median	$\mu mol \cdot L^{-1}$	152	1.3	$nmol \cdot L^{-1}$	320	38	30	73	49	0.69
	(Q1-Q3)		7-810	0.3-2.5		40-160	12-53	10-46	12-120	12-92	0.14-1.0
SGD-driven flux	Median	$mmol \cdot m^{-1} \cdot d^{-1}$	1900	17	$mmol \cdot m^{-1} \cdot d^{-1}$	4	0.48	0.38	0.9	0.6	0.009
	(Q1-Q3)		89-10000	3-31		0.5-21	0.16-0.68	0.13-0.59	0.1-1.5	0.2-1.2	0.002-0.013
	Median	$mol \cdot d^{-1}$	8600	73	$mol \cdot d^{-1}$	18	2.1	1.7	4.1	2.8	0.039
	Median	$\mu mol \cdot m^{-2} \cdot d^{-1}$	975	8.3	$nmol \cdot m^{-2} \cdot d^{-1}$	2000	240	190	470	320	4

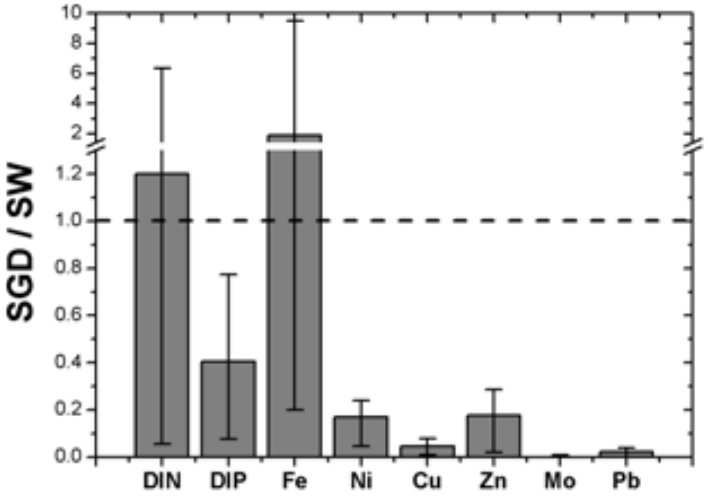

Figure 5.8. Ratio of SGD-driven inventories of dissolved major nutrients and trace metals (SGD) to the inventories actually measured in seawater (SW). SGD-driven inventories are obtained from the median of all the concentrations in groundwater with lower and upper limits being the 1st and the 3rd quartiles.

5.4.2. Trace metal inputs through SGD

Biogeochemical processes occurring at the subterranean estuary commonly result in non-conservative behavior for trace metals in groundwater (Beck et al. 2010). The distribution of trace metals in piezometers and wells relative to salinities (Fig. 5.6) could provide some insight about their relative sources and behavior in the subterranean estuary. Dissolved Cu and Zn show higher concentrations in fresh groundwater (concentrations in wells up to 1 and 2 orders of magnitude, respectively, higher than in seawater) and their removal from solution may be controlled by dilution, redox conditions and by the dissolution or precipitation of Mn oxides (Charette and Sholkovitz 2006; Beck et al. 2010). Unfortunately, neither Mn concentration nor oxido-reductive potential were monitored in this study. On the other side, distribution of dissolved Mo show higher concentration in high-salinity waters. Indeed, when normalizing Mo concentrations to salinity, only few samples have higher concentrations than those contributed by seawater, revealing that groundwater is not a source of this metal. The other dissolved metals analyzed in this study (Fe, Ni and Pb) are markedly enriched in porewaters compared to fresh groundwater from wells and seawater, most likely as a consequence of the geochemical processes occurring at the subterranean estuary. As an example, dissolved Fe shows low levels in both fresh groundwater and seawater, but it is highly enriched (1 to 3 orders of magnitude) in the high-salinity piezometers. Similar enrichments of dissolved Fe in the subterranean

estuary have been attributed to Fe-oxide reduction due to elevated dissolved organic carbon (DOC) concentrations at the freshwater-saltwater boundary (Snyder et al. 2004; Roy et al. 2010). Moreover, Fe-oxides may be reduced as pore water is likely anoxic, what prevents Fe-oxides precipitation and promotes their release to the pore waters (Roy et al. 2010).

The behavior of these trace metals within the subterranean estuary must be taken into account when determining the SGD-driven metal fluxes (Beck et al. 2007b). As detailed earlier, the range comprised between the 1st and 3rd quartiles of the set of metal concentration in groundwater (including wells and piezometers; n = 23) are considered the best characterization of the metal concentration in SGD (Table 5.1). These metal concentration ranges are then multiplied by the Ra-derived groundwater discharge and the metal contribution from seawater is subtracted, to obtain the SGD-driven trace metal fluxes to the Palma Beach (Table 5.1). Although subject to large uncertainties due to the measured variability and complex distribution patterns of trace metal in the subterranean estuary (Fig. 5.6; Table 5.1), these estimated fluxes provide valuable information, as this is the first study in the Mediterranean Sea where trace metal fluxes from SGD have been estimated. As expected from the concentration of trace metals in porewaters, the flux of dissolved Fe from SGD (median flux of 4.1 $mmol \cdot m^{-1} \cdot d^{-1}$) is 1 to 3 fold higher than fluxes of other elements (Table 5.1). All the SGD-driven fluxes of trace metals calculated here are considerably lower (~1 order of magnitude) than fluxes reported in coastal areas worldwide (e.g. Charette and Sholkovitz 2006; Beck et al. 2007b; Jeong et al. 2012), mainly because the magnitude of the SGD in all the other settings is 1-2 orders of magnitude higher than in Palma Bay.

In order to evaluate the significance of the SGD-driven metal fluxes to the coastal seawater pools, the contribution of metals from SGD can be compared with the excess metal inventory measured in the study site (estimated as explained for nutrients; Section 5.4.1.). The SGD-driven inventory of Fe into Palma Beach represents 0.2 – 9 times (median of 1.9) the inventory of dissolved Fe actually measured in the bay, indicating that SGD is a significant source of dissolved Fe into the study site (Fig. 5.8). It may also suggest a significant removal of dissolved Fe due to precipitation, scavenging by particles or biological uptake, as this comparison does not take into account other sources or sinks of trace metals. In contrast, the estimated SGD-driven inventories for all the other measured trace metals are 1-2 orders of magnitude lower

than the measured inventories of these metals in seawater (Fig. 5.8). Similar differences among trace metals were reported in a volcanic island (Jeju Island, Korea) by Jeong et al. (2012). These authors concluded that SGD is particularly important for the transport of major elements of the earth's crust, such as Fe and Al, to the coastal waters, where they exist at trace levels. Indeed, the distribution of trace metals in the entire Palma Bay (Fig. 5.4) shows a marked Fe enrichment in nearshore samples from Palma Beach, where the shallow aquifer is directly connected to the sea and where the main SGD inputs are expected. This provides significant independent evidence of the relevance of SGD as a Fe source. This pattern is not observed for all the other trace metals (Ni, Cu, Zn, Mo and Pb; Fig. 5.4), agreeing well with the comparison of SGD-driven and measured inventories derived in this study (Fig. 5.8). It is worth noticing that there is an important source of Cu, Zn and Pb to nearshore waters from the NW part of the Palma Bay, close to the city of Palma and the harbor. The high concentration of Cu and Zn measured there could be related to the maritime traffic, as boating traffic is considered an important source of Cu and Zn to the coastal environments (Matthiessen et al. 1999; Garcia-Orellana et al. 2011).

Atmospheric inputs are considered the major supplier of dissolved metals to Mediterranean surface waters on a basin-wide scale, mainly due to Saharan dust deposition events (Guerzoni et al. 1999; Bonnet and Guieu 2006). Focusing on coastal areas, a comparison between atmospheric inputs of dissolved Fe in the Western Mediterranean during summer time (0.3 μmol m^{-2} d^{-1}; Bonnet and Guieu 2006) and the Fe supply from SGD obtained in this work (2.0 μmol m^{-2} d^{-1}; Table 5.1) illustrates the potential significance of SGD as a relevant source of dissolved Fe to Mediterranean coastal areas. SGD could represent a major source of trace metals to the coastal sea and needs to be considered in future studies of trace metal cycling in the coastal Mediterranean Sea.

5.4.3. Conclusions and ecological implications of SGD

The results obtained in this study reveal that the fluxes of chemical constituents, especially nutrients and dissolved Fe, associated to SGD play a significant role on the coastal budgets of these elements in Palma Beach and may also have a critical impact on the primary productivity. In fact, an onshore-offshore gradients of phytoplankton biomass (Fig. 5.3) and strong linear relationships between Chl*a* concentrations and Ra

activities in coastal water samples ($r^2 > 0.7$; $p < 0.001$; Fig. 5.9) suggest a connection between phytoplankton biomass and SGD. The high phytoplankton biomass measured in the region thus seems reasonably sustained by the inputs of chemical constituents derived from SGD. A significant impact of SGD on the coastal productivity of Mallorca Island has been previously suggested by Basterretxea et al. (2010). Further studies (e.g. in situ groundwater addition experiments such as those conducted by Garcés et al (2011)) are needed in order to more thoroughly assess the role of SGD on phytoplankton growth. As the bioproductivity in the Mediterranean Sea is largely limited by phosphate availability (e.g. Diaz et al. 2001), inputs of DIP through SGD may be especially important. However, the high N:P ratio in SGD actually seems to promote P limitation. It is worth noting that SGD inputs of dissolved Fe are also relevant because other major Fe inputs in the study area are nonexistent and dissolved Fe is often a limiting bioactive element for many primary producers and marine organisms, such as *Posidonia oceanica* (Marbà et al. 2007; Tovar-Sánchez et al. 2010) and *Synechoccocus* (Garcés et al. 2011).

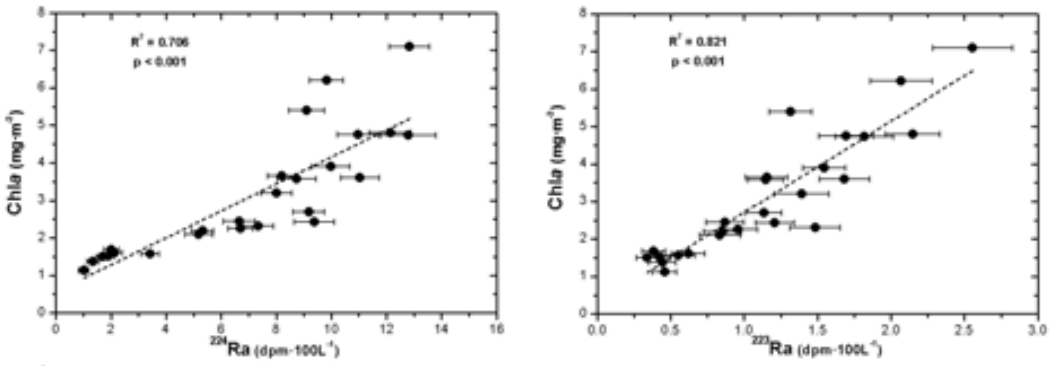

Figure 5.9. Relations between Chl*a* and (a) ^{224}Ra and (b) ^{223}Ra. The dashed line represents the best linear fit to the data.

Inputs of nutrients and other micronutrients via SGD may play an important role in the regulation of nearshore phytoplankton communities, especially in oligotrophic areas such as the Mediterranean Sea. The SGD-driven inputs of terrestrial compounds, together with physical factors (such as summer calm conditions and bay geomorphology), provide an ideal environment for bloom outbreaks and biomass accumulation in nearshore waters (Basterretxea et al. 2007). SGD could thus contribute explaining the high frequency of Mediterranean coastal blooms, an emerging problem with significant ecological and economical implications.

CHAPTER 6

Submarine Groundwater Discharge: a major source of nutrients to the Mediterranean Sea

This chapter is based on:
Rodellas, V., Garcia-Orellana, J., Masqué, P., Feldman, M., Weinstein, Y. Submarine Groundwater Discharge: a major source of nutrients to the Mediterranean Sea. Submitted.

6.1. Objective

The Mediterranean Sea is one of the most oligotrophic seas in the world (Bethoux et al. 1998), resulting from an anti-estuarine circulation by which Mediterranean intermediate waters export nutrients to the Atlantic Ocean. In such an oligotrophic system, external inputs of nutrients play a significant role in sustaining the marine productivity (Herut et al. 1999; Markaki et al. 2003; Bonnet and Guieu 2006; Ludwig et al. 2009; Pujo-Pay et al. 2011). Among these inputs, atmospheric deposition and riverine runoff have been traditionally considered the major sources of nutrients to the Mediterranean Sea (Guerzoni et al. 1999; Krom et al. 2004; Ludwig et al. 2009). Even though Submarine Groundwater Discharge (SGD) has been recognized as an important source of terrestrial compounds (e.g. nutrients, metals, carbon) to the ocean (Cai et al. 2003; Slomp and Van Cappellen 2004; Windom et al. 2006), its role as a conveyor of dissolved chemicals to the Mediterranean Sea has been largely overlooked.

This study is devoted to evaluate the magnitude of SGD and its associated inputs of nutrients to the entire Mediterranean Sea, by using a mass balance of ^{228}Ra. Previous studies have estimated the fresh groundwater discharge to the Mediterranean Sea using hydrological approaches (PNUE/PAM/Plan Blue 2004; Zektser et al. 2007), but none of them has evaluated the total SGD flow and the associated total contribution of terrestrial compounds to the Mediterranean Sea. Since recirculated SGD usually dominates the water flow (Burnett et al. 2003), its quantification could be key to fully understand the role of SGD in the biogeochemical cycles of nutrients and other chemical species in the Mediterranean Sea.

6.2. Methods

Water samples were collected throughout the Mediterranean Sea during several oceanographic cruises to determine the concentrations of ^{228}Ra: M84/3 (April 2011, onboard the R/V Meteor), GA04S-MedSeA (May 2013, B/O Ángeles Alvariño), 65PE370-MedBlack (June 2013, R/V Pelagia), FAMOSO I (March 2009, B/O Sarmiento de Gamboa) and EDASMAR (May 2008, B/O Garcia del Cid). Large volume seawater samples (100 -360 L) were filtered through columns loaded with MnO_2-impregnated acrylic fiber, which quantitatively adsorbs radium isotopes from seawater (Moore and

Reid 1973). The fibers containing ^{228}Ra were analyzed as described in Chapter 2. Additional data available from the literature (n=28) was also used to complement the dataset. The ^{228}Ra data include samples collected at surface (SW, n=80), intermediate (LIW, n=15) and deep waters (DW, n=13).

Given the limited vertical ^{228}Ra resolution obtained using the samples gathered together, these discrete ^{228}Ra samples were combined with salinity depth profiles to infer the vertical variability of ^{228}Ra along the entire water column for all the stations. Vertical salinity profiles collected at each of the stations were used to derive vertical mixing between water masses, since the main water masses (surface, intermediate and deep) of the Mediterranean Sea are characterized by significant differences in salinity. Vertical distributions of ^{228}Ra obtained following this approach allowed solving the expected continuous decrease of ^{228}Ra concentrations with depth (Fig. 6.1). A similar approach was followed to obtain vertical profiles of ^{228}Ra in the Atlantic Ocean (S(Moore et al. 1985, 2008)), using tritium instead of salinity.

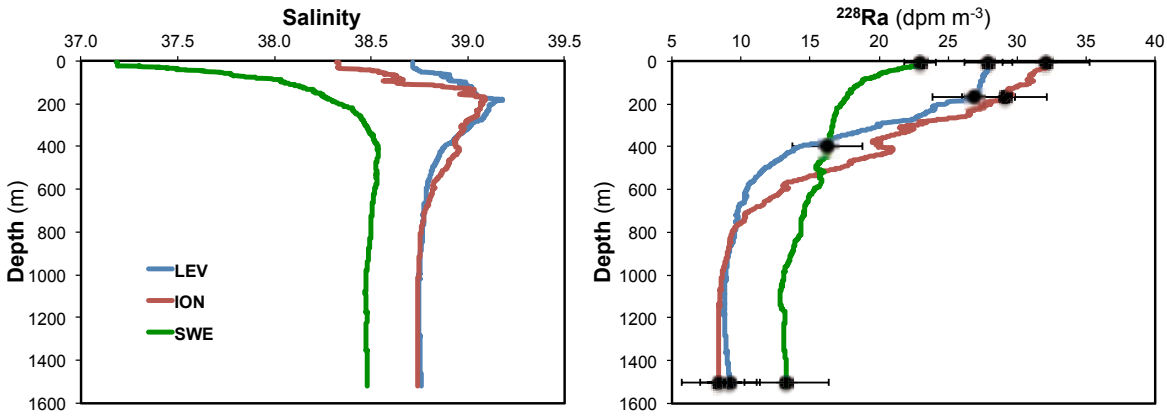

Figure 6.1. (Left panel) Example of three salinity profiles collected in the Levantine (LEV), Ionian (ION) and South-Western (SWE) sub-basins of the Mediterranean Sea. (Right panel) ^{228}Ra vertical distributions obtained from the salinity profiles and the ^{228}Ra discrete samples (black dots).

Several samples (n = 38) were also collected to determine the concentrations of ^{228}Ra in SGD fluids or coastal groundwater. All ^{228}Ra concentrations in the Mediterranean Sea used in this study are presented in the Appendix, including data obtained from the literature.

6.3. Results and discussion

The approach we followed to estimate the magnitude of SGD into the entire Mediterranean Sea is based on a mass balance of ^{228}Ra (Moore et al. 2008). Assuming steady state, ^{228}Ra outputs must be equal to its inputs, most of which originate from continental margins. By evaluating all the sink and source terms, the ^{228}Ra supplied by SGD can be determined as the difference between its inputs and outputs, and this flux can be converted to an SGD flow by characterizing the ^{228}Ra concentration in the SGD fluids. We used ^{228}Ra because its half-life ($T_{1/2}$= 5.75 yr) is considerably lower than the residence time of the Mediterranean Sea waters (~100 yr (Lacombe and Richez 1982)), hence its radioactive decay is the primary sink of ^{228}Ra in the Mediterranean Sea and allows to accurately constrain the ^{228}Ra removal terms (Moore et al. 2008).

Estimating all the terms of the ^{228}Ra mass balance requires the characterization of the distribution of ^{228}Ra in the water column of the Mediterranean Sea (Fig 6.2). The highest ^{228}Ra concentrations are observed in coastal areas, consistently with radium inputs from continental margins. ^{228}Ra concentrations measured along the Mediterranean Sea mainly reflect the anti-estuarine thermohaline circulation of the basin: surface ^{228}Ra concentrations generally increase from west to east (from 17 to 34 dpm·m^{-3}), implying that waters moving eastwards receive ^{228}Ra from the continental margins at a greater rate than radioactive decay or other forms of removal. Since Levantine Intermediate Waters (LIW), which are regularly formed in the Eastern Mediterranean, circulate westward to the Strait of Gibraltar and there are no other major sources of ^{228}Ra at intermediate depths, ^{228}Ra concentrations in LIW generally decrease from east to west (from 29 to 12 dpm·m^{-3}). ^{228}Ra concentrations in deep waters (DW: depth > 600 m) are considerably lower (5 - 13 dpm·m^{-3}; Fig 6.2), confirming that the main ^{228}Ra inputs occur at the uppermost layers.

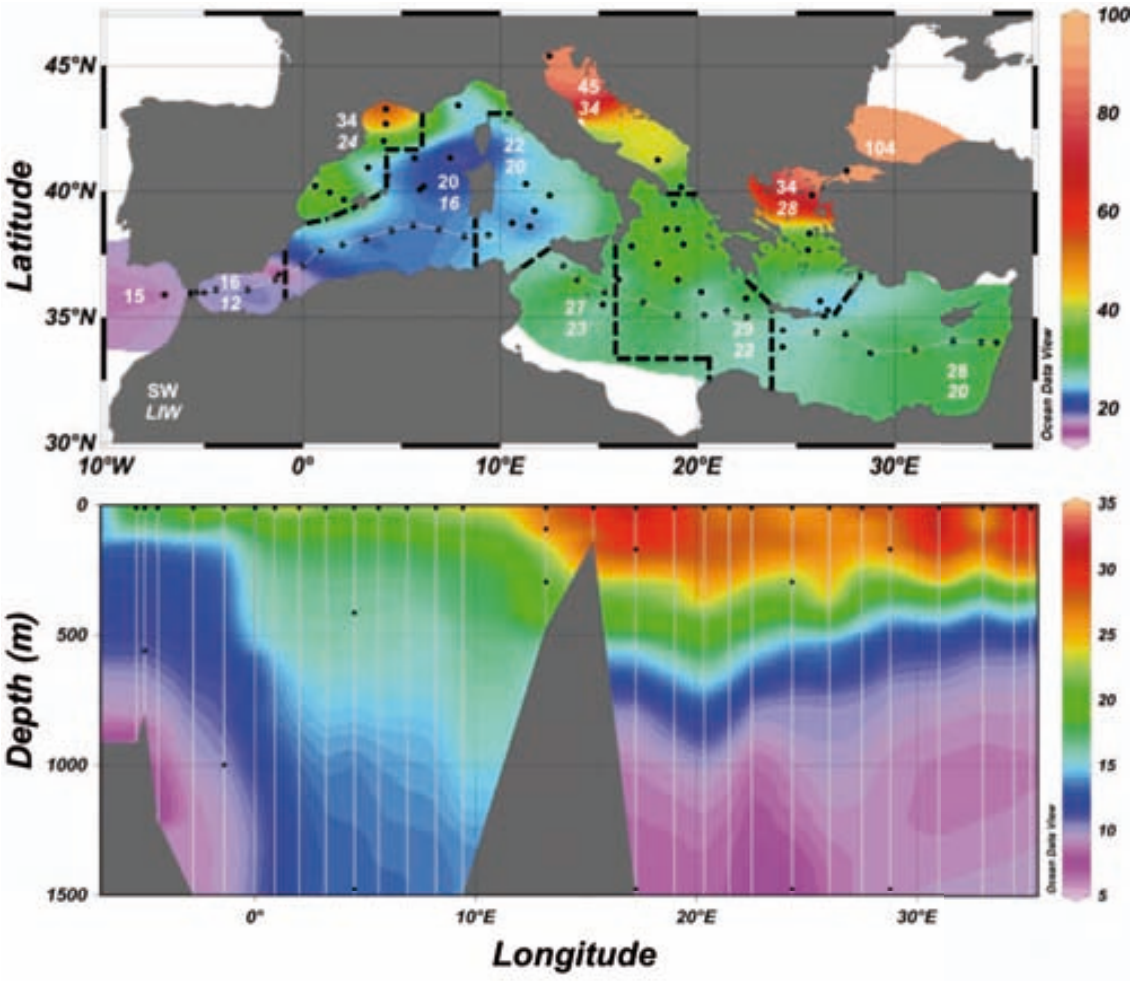

Figure 6.2. Distribution of ^{228}Ra in the Mediterranean Sea. a) Contour plot of the ^{228}Ra concentrations (dpm·m^{-3}) in surface waters of the Mediterranean Sea. Dots indicate sampled stations. The sub-basin division and the weighted average ^{228}Ra concentration in each sub-basin for surface (SW) and intermediate (LIW) are indicated. b) Contour plot of the ^{228}Ra concentrations (dpm·m^{-3}) in the water column in a W-E transect (light grey line in a) panel) along the Mediterranean Sea. Light gray lines represent ^{228}Ra vertical profiles used to infer the contour plot, which are derived from salinity profiles and ^{228}Ra discrete samples (black dots).

6.3.1. ^{228}Ra mass balance for the upper Mediterranean Sea

The loss of ^{228}Ra due to radioactive decay can be determined from the total ^{228}Ra inventory multiplied by its decay constant (λ = 0.120 yr^{-1}). To calculate the total ^{228}Ra inventory, the Mediterranean Sea was divided into nine sub-basins (Fig. 6.2), defined according to their physiography and general circulation patterns (Bethoux et al. 1998; Sanchez-Cabeza et al. 2002). Each sub-basin was split into three water layers (SW, LIW and DW). Weighted average ^{228}Ra concentrations for SW (0-220 m depth), LIW (220-600 m) and DW (> 600 m) for all the sub-basins were estimated from the ^{228}Ra depth

profiles. These averaged ^{228}Ra concentrations were multiplied by the box volume to estimate the inventories of ^{228}Ra in each box (see Appendix). The total ^{228}Ra inventory for the upper water column of the Mediterranean Sea (including SW and LIW, i.e. from 0 to 600 m depth) was obtained from the integration of the box inventories, resulting in $(33 \pm 5)\cdot10^{15}$ dpm. The loss of ^{228}Ra by radioactive decay is thus of $(4.0 \pm 0.5)\cdot10^{15}$ dpm·yr^{-1}.

The DW layer was excluded from the total inventory because the main ^{228}Ra inputs occur at uppermost layers (Moore et al. 2008). In doing so, ^{228}Ra released from deep-sediments can be neglected, but vertical exchange fluxes need to be considered. The migration of ^{228}Ra from upper waters to DW was estimated from the average ^{228}Ra box concentrations and using water transfer rates obtained in previous studies (Bethoux and Gentili 1996; Sanchez-Cabeza et al. 2002). This results in a total ^{228}Ra loss of $(2.0 \pm 0.1)\cdot10^{15}$ dpm·yr^{-1} due to downward water flow (see Appendix). Additionally, ^{228}Ra could also be transported downwards due to particle scavenging. Assuming a radium residence time with respect to scavenging of ~500 yr (Moore et al. 2008), the ^{228}Ra removal due to particle scavenging would only be of $(0.07 \pm 0.01)\cdot10^{15}$ dpm·yr^{-1}.

^{228}Ra is also lost from the Mediterranean Sea due to the water outflow to the Atlantic Ocean ($25\cdot10^{12}$ m^3·yr^{-1}) (Soto-Navarro et al. 2010) and the Black Sea ($1.0\cdot10^{12}$ m^3·yr^{-1}) (Tugrul et al. 2002), through the straits of Gibraltar and Dardanelles, respectively. From the characterization of the ^{228}Ra concentrations in outflowing waters, a total loss of ^{228}Ra of $(0.35 \pm 0.03)\cdot10^{15}$ dpm·yr^{-1} through the straits is obtained.

The total loss of ^{228}Ra from the upper Mediterranean Sea ($(6.4 \pm 0.5)\cdot10^{15}$ dpm·yr^{-1}) (Table 6.1), must be balanced by continuous new inputs of ^{228}Ra, that can consist on: i) riverine discharge; ii) atmospheric input; iii) release from sediments; iv) deep water vertical advection; v) water input through the straits; and vi) SGD.

The input of ^{228}Ra from river discharge includes Ra in the dissolved fraction and desorption of Ra from river-borne particles (Moore and Shaw 2008). A concentration of 130 ± 50 dpm·m^{-3} captures all the dissolved ^{228}Ra concentrations measured in rivers discharging into the Mediterranean Sea (see Appendix). A desorbed ^{228}Ra flux of 0.5 ± 0.4 dpm per gram of sediment includes most of the ^{228}Ra desorption estimates reported throughout the world (see Appendix). Considering the river flow ($0.31\cdot10^{12}$ m^3·yr^{-1})

(Ludwig et al. 2009) and the riverine particle flux into the Mediterranean Sea ($730 \cdot 10^{12}$ g·yr^{-1}) (UNEP/MAP/MED POL 2003), the total supply of ^{228}Ra from river discharge represents $(0.40 \pm 0.29) \cdot 10^{15}$ dpm·yr^{-1}.

Table 6.1. Summary of the ^{228}Ra mass balance for the upper Mediterranean Sea.

	^{228}Ra flux ($\cdot 10^{15}$) dpm·yr^{-1}	**^{228}Ra flux** % total flux
^{228}Ra outputs		
Decay	4.0 ± 0.5	53 - 73
Advection to DW	1.97 ± 0.08	28 - 34
Particle Scavenging	0.07 ± 0.01	~1
Outflow (Gibraltar)	0.30 ± 0.03	4 - 5
Outflow (Dardanelles)	0.06 ± 0.01	~1
TOTAL OUTPUTS	6.4 ± 0.5	88 - 112
^{228}Ra inputs		
Rivers	0.40 ± 0.29	2 - 11
Atmospheric dust	0.08 ± 0.03	1 - 2
Sediments	2.7 ± 0.9	27 - 57
Advection from DW	1.1 ± 0.2	14 - 20
Inflow (Gibraltar)	0.37 ± 0.03	5 - 7
Inflow (Dardanelles)	0.14 ± 0.01	~2
TOTAL INPUTS (w/o SGD)	4.7 ± 1.0	57 - 91
^{228}Ra from SGD	1.7 ± 1.1	8 - 44

The atmospheric dust input to the entire Mediterranean Sea is estimated in ($41 \cdot 10^{12}$ g·yr^{-1}) (Guerzoni et al. 1999). Assuming a desorption of ^{228}Ra from dust of 2 dpm·g^{-1}, which is close to the maximum reported in the literature (Moore and Shaw 2008; Moore et al. 2008), the atmospheric input of ^{228}Ra to the entire basin is of $(0.08 \pm 0.03) \cdot 10^{15}$ dpm·yr^{-1}.

The flux of ^{228}Ra released from shelf sediments due to diffusion and bioturbation might be highly variable and, in large-scale studies, can represent a major source of ^{228}Ra due to the large extension of the continental shelf (Moore et al. 2008). Moore et al. (Moore et al. 2008) conducted a detailed review of the literature in order to determine the appropriate ^{228}Ra fluxes from fine-grained shelf sediments ($11 \cdot 10^3 \pm 5 \cdot 10^3$ dpm·m^{-2}·yr^{-1}), coarse-grained shelf sediments (230 ± 110 dpm·m^{-2}·yr^{-1}) and slope sediments ($2.3 \cdot 10^3 \pm 1.1 \cdot 10^3$ dpm·m^{-2}·yr^{-1}). Using the areas of continental shelf and the slope of the Mediterranean Sea above 600 m ($490 \cdot 10^9$ and $310 \cdot 10^9$ m^2, respectively (IOC 1981)) and

considering that fine-grained sediments represent about 35% of the shelf area (Emelyanov et al. 1996), the total flux of ^{228}Ra from sediments would account for (2.7 ± 0.9)·10^{15} dpm·yr^{-1}.

Vertical advection of DW can also be a source of ^{228}Ra to the upper Mediterranean Sea. A flux of (1.1 ± 0.2)·10^{15} dpm·yr^{-1} of ^{228}Ra from DW is estimated from the ^{228}Ra concentration box average and the water transfer rates between layers (Bethoux and Gentili 1996; Sanchez-Cabeza et al. 2002) (see Appendix).

Water inflows through the straits of Gibraltar and Dardanelles are 26·10^{12} m^3·yr^{-1} (Soto-Navarro et al. 2010) and 1.3·10^{12} m^3·yr^{-1} (Tugrul et al. 2002), respectively. Using ^{228}Ra concentrations measured in the inflowing waters, the total ^{228}Ra input through both straits amounts to (0.5 ± 0.03)·10^{15} dpm·yr^{-1}.

Fluxes from the sources and sinks of ^{228}Ra are summarized in Table 6.1. Total outputs and inputs are largely dominated by the radioactive decay and the sediment flux from the continental shelf and slope, respectively. The results show a difference of (1.7 ± 1.1)·10^{15} dpm·yr^{-1} between the total loss of ^{228}Ra ((6.4 ± 0.5)·10^{15} dpm·yr^{-1}) and the inputs from evaluated sources ((4.7 ± 1.0)·10^{15} dpm·yr^{-1}), which must be balanced by a continual input of ^{228}Ra from the remaining source, i.e. SGD.

6.3.2. SGD flow to the Mediterranean Sea

The SGD-derived ^{228}Ra flux can be converted to an SGD flow by characterizing the ^{228}Ra concentration in the SGD fluids inflowing to the Mediterranean Sea. Several studies have reported ^{228}Ra data in SGD along the Mediterranean Sea (45 different locations, mainly located on the North-Western Mediterranean), with concentrations spanning a wide range (130 to 72·10^3 dpm·m^{-3}; Fig 6.3). The highest ^{228}Ra concentrations are found mainly in SGD dominated by recirculated seawater, since radium mobilization from the solid matrix strongly depends on water salinity. SGD at karstic areas usually shows lower activities than that at granular coastal aquifers. This is due to several reasons, including the relatively low ^{232}Th (^{228}Ra parent) in carbonates and the typical point-sourced discharge at karstic coastal terrains, which results in a low water-rock interaction in the coastal aquifer and allows the direct discharge of fresh groundwater with low ^{228}Ra content. A ^{228}Ra concentration of 640 - 2,300 dpm·m^{-3}

covers the range between the 1st and 3rd quartiles of the groundwater dataset, accounting for the variability of ^{228}Ra in SGD and excluding extreme values. Using this range, the resulting SGD flow to the Mediterranean Sea ranges from $0.2 \cdot 10^{12}$ to $4.3 \cdot 10^{12}$ $m^3 \cdot yr^{-1}$ (median of $1.2 \cdot 10^{12}$ $m^3 \cdot yr^{-1}$). The SGD flow estimated here appears to be equal or larger by a factor of 14 to the riverine discharge to the Mediterranean Sea ($0.3 \cdot 10^{12}$ $m^3 \cdot yr^{-1}$) (Ludwig et al. 2009).

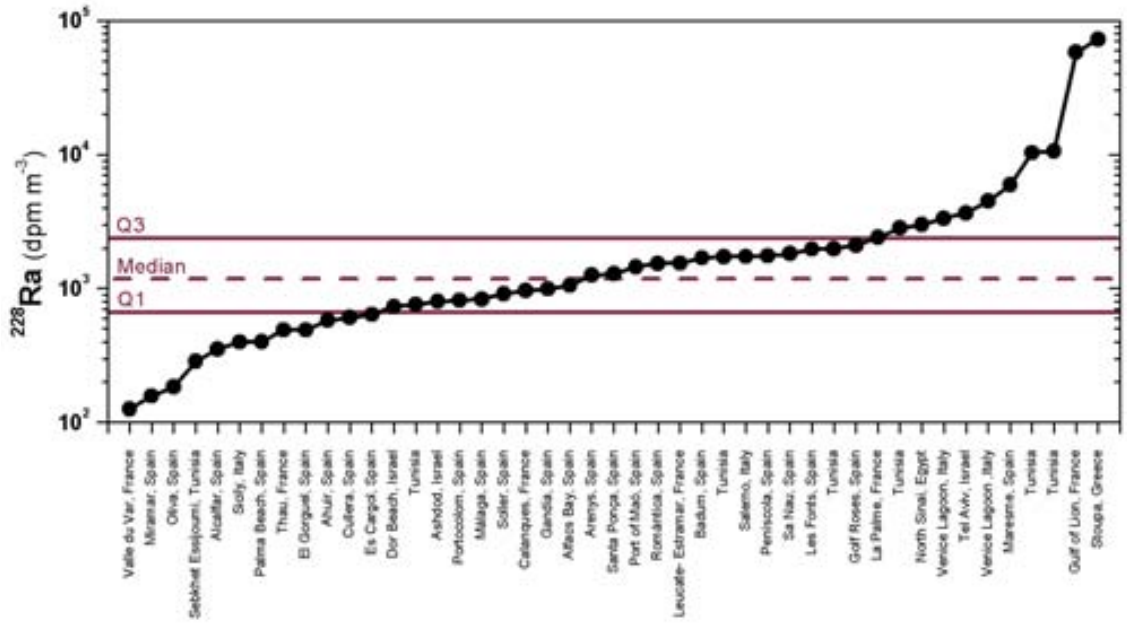

Figure 6.3. ^{228}Ra concentrations in SGD and coastal groundwater from throughout the Mediterranean Sea (Appendix for references). The median and the 1st and 3rd quartiles of the dataset are also shown. The range between the 1st and 3rd quartiles is used to estimate the ^{228}Ra concentration in SGD.

A recent study based on an integrated hydrologic-hydrogeological approach, estimated the fresh SGD flow to the Mediterranean Sea to be on the order of $0.07 \cdot 10^{12}$ $m^3 \cdot yr^{-1}$ (Zektser et al. 2007). Therefore, fresh groundwater inputs would represent 5 – 30 % of the total SGD inputs to the MS, revealing that seawater recirculating through coastal sediments constitute the main fraction of SGD inflowing to the Mediterranean Sea. As detailed above, ^{228}Ra may be low in fresh groundwater discharge and, therefore, using ^{228}Ra as a tracer could underestimate fresh (and consequently total) SGD inputs. However, given that substantial ^{228}Ra enrichments (higher than 1,000 dpm m^{-3}) have been reported in several fresh groundwater springs (e.g. Badum, Port of Maó, Leucate-Estramar, Gulf of Roses; see Appendix) and fresh groundwater is commonly mixed with saline waters before inflowing to the sea, the ^{228}Ra approach followed in this study is likely capturing most of the fresh groundwater inputs. In any case, since fresh

groundwater fraction represents a minor fraction of the total SGD, such underestimation would not compromise the range of total SGD calculated here.

Normalizing the total SGD to the Mediterranean shore length (64,000 km) (Stewart and Morhange 2009) results in a flow ranging from $4 \cdot 10^6$ to $93 \cdot 10^6$ $m^3 \cdot km^{-1} \cdot yr^{-1}$. This shore-normalized SGD estimate is in good agreement with local studies conducted along the Mediterranean Sea (Fig 6.4), reinforcing the consistency of our estimates. The only other SGD estimate for a basin-wide scale is that of Moore et al. (Moore et al. 2008) for the Atlantic Ocean ($(230\text{-}470) \cdot 10^6$ $m^3 \cdot km^{-1} \cdot yr^{-1}$). The shore-normalized SGD to the Mediterranean Sea is lower than the SGD flow to the Atlantic Ocean, likely as a consequence of the arid/semi-arid conditions on the eastern and southern Mediterranean coast (low groundwater recharge rates) and the lack of significant tidal ranges (low tidally pumped SGD). However, when normalizing to the total ocean-sea surface area, SGD to the Mediterranean Sea ($(80\text{-}1700) \cdot 10^3$ $m^3 \cdot km^{-2} \cdot yr^{-1}$) turns to be comparable or even higher than the flow to the Atlantic Ocean ($(200\text{-}410) \cdot 10^3$ $m^3 \cdot km^{-2} \cdot yr^{-1}$), highlighting the potential importance of SGD to the biogeochemical cycles of the Mediterranean Sea.

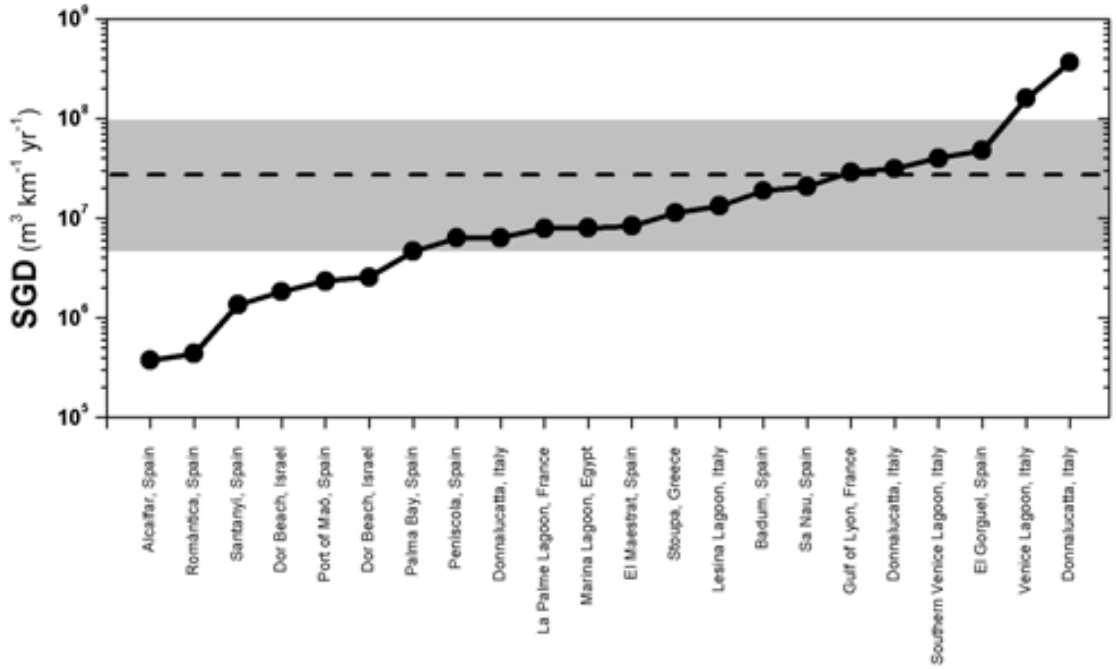

Figure 6.4: Estimates of SGD normalized to shore length in different studies along the Mediterranean Sea (see Appendix for references). The gray band represents the range of SGD estimated for the entire Mediterranean Sea (the median flow is represented by a dashed line).

6.3.3. SGD-derived nutrient inputs

Considering the estimated magnitude of SGD to the entire basin, SGD-driven inputs of terrestrial compounds (e.g. nutrients, metals, carbon) to the Mediterranean Sea could be of great importance and need to be evaluated. Given the oligotrophic nature of the Mediterranean Sea, external inputs of essential nutrients for marine productivity (e.g. nitrogen, phosphorous, silica, iron) are particularly important for this basin. The flux of bioavailable nutrients (dissolved inorganic nitrogen (DIN), phosphorous (DIP) and silica (DSi)) supplied by SGD can be estimated from the SGD flow and nutrient concentrations reported in SGD studies along the Mediterranean coastline (see Appendix). This results in SGD-driven fluxes of (20 - 1,300)·10^9 mol·yr^{-1} of DIN, (0.09 - 4.0)·10^9 mol·yr^{-1} of DIP and (13-570)·10^9 mol·yr^{-1} of DSi (Fig. 6.5). These figures could be overestimated due to the fact that some of the recirculated seawater may be nutrient-poor, while most of the data used was measured at coastal sites containing a fraction of fresh groundwater. Nevertheless, the enrichment in nutrients of recirculated seawater may be relevant for long-scale recirculation processes (Weinstein et al. 2011; Santos et al. 2012), which are the only recirculation processes captured using the ^{228}Ra approach (due to the long regeneration time of ^{228}Ra). A conservative estimate of nutrient inputs from SGD can be obtained from the fresh SGD estimated by Zektser and coauthors (Zektser et al. 2007) and the concentration of nutrients measured in fresh SGD (see Appendix). Nutrient inputs derived from this conservative approach (30·10^9, 0.02·10^9 and 13·10^9 mol·yr^{-1} for DIN, DIP and DSi, respectively) are at the low end of the estimates from total SGD (Fig. 6.5).

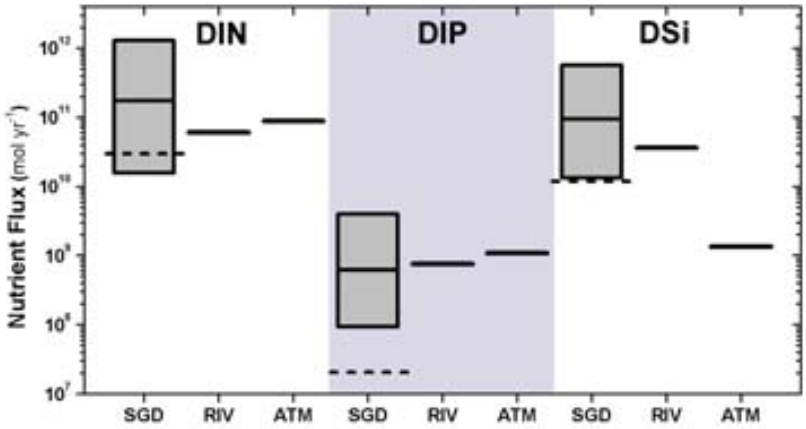

Figure 6.5. Comparison of nutrient inputs to the Mediterranen Sea derived from SGD to inputs from rivers (RIV) and atmospheric deposition (ATM). Dashed lines represent nutrient inputs derived exclusively from fresh SGD. Fluxes from rivers and atmosphere were obtained from the literature (Ludwig et al. 2009; Koçak et al. 2010; Markaki et al. 2010) (see Appendix).

The significance of these nutrient fluxes becomes apparent when compared to the nutrient supply from rivers (Ludwig et al. 2009) and atmospheric deposition (Koçak et al. 2010; Markaki et al. 2010) to the entire Mediterranean Sea (Fig 6.5), which reveals that SGD is likely a major external source of DIN, DIP and especially DSi to the Mediterranean Sea. Unlike atmospheric inputs (distributed throughout the basin) and riverine discharge (restricted to river mouth surroundings), SGD is essentially ubiquitous in coastal areas. Thus, the relative significance of SGD as a source of nutrients may be even higher for most of the Mediterranean coastal areas, where SGD can represent by far the dominant source of terrestrial compounds and the major sustainment for coastal ecosystems.

SGD-derived nutrient inputs to the Mediterranean Sea have high DIN:DIP ratios (80:1 – 430:1, according to the 1st and 3rd quartiles of the set of data collected (see Appendix)), mainly because DIP is rapidly removed from groundwater (Slomp and Van Cappellen 2004). DIN:DIP ratios from SGD are comparable to those from riverine (40:1 – 140:1 (Ludwig et al. 2009)) and atmospheric inputs (60:1 - 120:1 (Markaki et al. 2010)), all of them well above the average N:P ratio in Mediterranean waters (24:1 in the western basin and 38:1 in the eastern one (Pujo-Pay et al. 2011)). Thus, nutrient inputs from SGD could provide an additional source for the actual P limitation in the Mediterranea Sea (Krom et al. 2010). The influence of SGD on the nutrient cycling in both, coastal areas and in open waters should be further studied, because a fraction of the nutrient inputs driven by SGD might be removed by biological activity in areas proximal to the discharge sites.

This study demonstrates the importance of SGD to the coastal biogeochemical cycles of the Mediterranean Sea and emphasizes the need for a better characterization of the SGD-related inputs of terrestrial compounds and its inclusion in coastal and basin-wide material balances. Considering the calculated magnitude of the SGD flow, the SGD-driven supply of iron could also rival riverine and atmospheric iron inputs to the Mediterranean Sea, as previously suggested for a western Mediterranean bay (Rodellas et al. 2014: Chapter 5). SGD could also represent a relevant source of other compounds to the Mediterranean Sea, such as carbon (Cai et al. 2003), toxic metals (e.g. Hg(Bone et al. 2007)) or rare earth elements (Kim and Kim 2014).

CHAPTER 7

Conclusions and future perspectives

7.1. Conclusions

The overall goal of this PhD Thesis was to evaluate the importance of Submarine Groundwater Discharge (SGD) in the Mediterranean Sea by using Ra isotopes, paying attention to the role that SGD plays as a source of dissolved compounds to the sea..

Three contrasting coastal Mediterranean environments (Peníscola marsh, Port of Maó and Palma Beach) were selected to: i) evaluate the relevance of SGD from a local perspective; ii) test the applicability of Ra isotopes in different hydrogeological settings; and iii) assess the SGD-derived inputs of dissolved compounds (nutrients and trace metals). In addition to these local studies, an evaluation of the magnitude of SGD and its associated inputs of nutrients into the entire Mediterranean Sea was also conducted. The above-mentioned works constitute the 4 main chapters of this dissertation (Chapters 3-6). The conclusions of these studies can be summarized as follows:

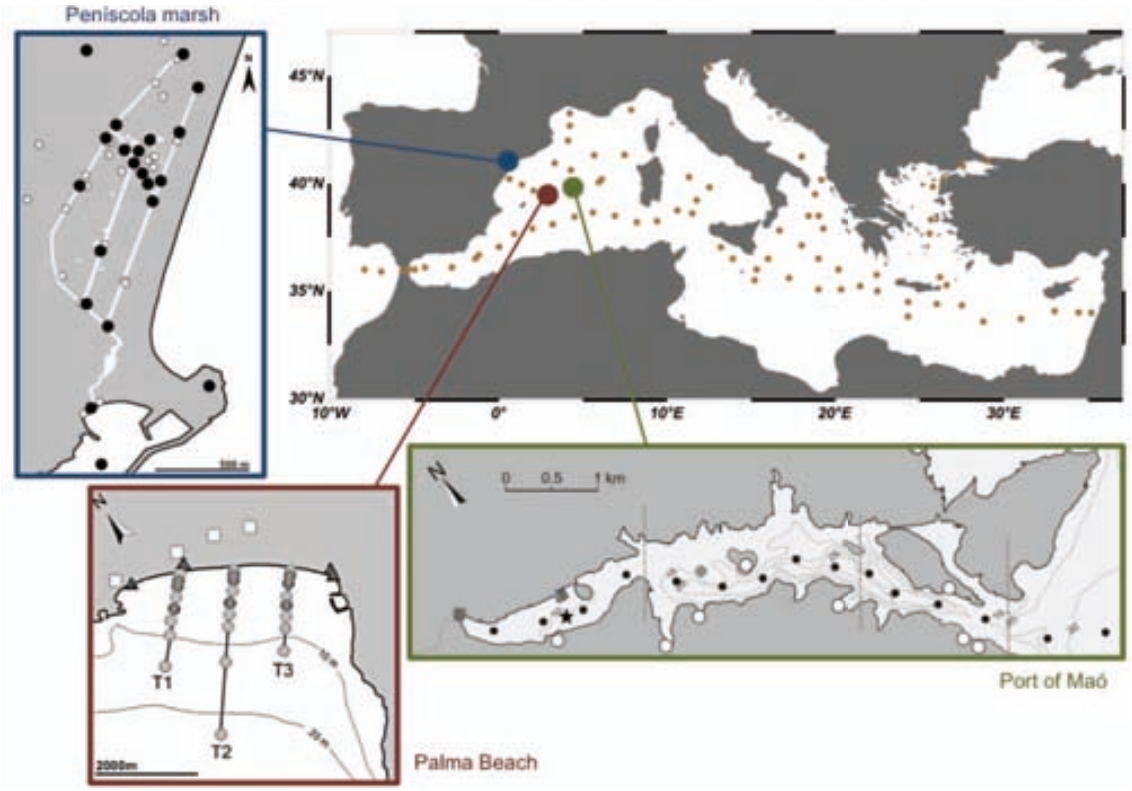

Figure 7.1. Study areas selected to evaluate the importance of SGD in the Mediterranean Sea. Sampling stations for Ra isotopes are also shown.

Chapter 3: Peníscola marsh (Castelló)

The main objective of this study was to evaluate the use of Ra isotopes and ^{222}Rn to identify the origin and contribution of distinct SGD sources into a Mediterranean coastal wetland (Peníscola marsh, Castelló, Spain). The Peníscola marsh is a small shallow wetland nourished by groundwater coming from four different flowpaths: (i) a deep flow from the regional carbonate aquifer of El Maestrat, (ii) and (iii) shallow and an intermediate flows, both from the Irta Range and the detritic Vinaròs-Peníscola aquifers, and (iv) seawater intrusion. Data on concentrations of ^{226}Ra, ^{222}Rn and salinity in water samples was used to build a 4 endmember mixing model to obtain the flow contributions from the mentioned pathways. The results revealed that the deep groundwater contribution was 15% of the total water inflow (5600 $m^3 \cdot d^{-1}$), whereas the shallow and intermediate flow paths represented 32% (11800 $m^3 \cdot d^{-1}$) and 48% (17500 $m^3 \cdot d^{-1}$), respectively. Seawater accounted only for the remaining 5% of the water inputs to the wetland. Ra isotopes also allowed estimating an age of the marsh water of 1.2 ± 0.6 days. Both the groundwater contributions derived from ^{226}Ra, ^{222}Rn and salinity measurements and the Ra-derived marsh water age agreed well with direct measurements obtained using propeller flow meters, evidencing the effectiveness of ^{226}Ra and ^{222}Rn as hydrological tracers. By using these tracers, we also successfully monitored the annual variability of SGD inputs into the wetland. An interannual comparison between the estimated groundwater inflow and the precipitation revealed that shallow and intermediate groundwater flow rapidly (~1-3 months), responding to regional precipitation, whereas the deep groundwater flow from the carbonate aquifer is dominated by a constant baseflow.

This work underlines the potential of radioactive tracers (Ra isotopes and ^{222}Rn) to accurately estimate the contribution of multiple SGD sources and to monitor the seasonal variability of groundwater inputs.

Chapter 3 is based on:

Rodellas, V., Garcia-Orellana, J., Garcia-Solsona, E., Masqué, P., Domínguez, J.A., Ballesteros, B.J., Mejías, M., Zarroca, M., 2012. Quantifying groundwater discharge from different sources into a Mediterranean wetland by using ^{222}Rn and Ra isotopes. J. Hydrol. 466-467, 11-22.

Chapter 4: Port of Maó (Minorca, Balearic Islands)

The study conducted in the Port of Maó (Balearic Islands, Spain) aimed to evaluate the influence of bottom sediments on the determination of SGD into coastal environments by using Ra isotopes. This natural harbor was selected because it is a natural embayment where SGD occurs all along the southern boundary of the harbor and where bottom muddy sediments are subjected to frequent sediment resuspension events due to vessel maneuvering. Comprehensive seasonal Ra mass balances were constructed for the waters using both short- (^{224}Ra) and long- (^{228}Ra) lived Ra isotopes. The results showed that the Ra flux from bottom sediments, through diffusion and due to releases associated to resuspension events, represented a significant source of Ra to the harbor waters. This sedimentary source accounted for a major fraction of the ^{224}Ra supplied to the system (27-90%, depending on the season), whereas the sediment influence on the ^{228}Ra mass balance was significantly lower (11-40 %) due to its slower production rate. These findings suggested that attributing Ra inputs to the water column solely to SGD in systems where fine sediments are present might not be accurate, requiring a detailed evaluation of the sedimentary source. Since inputs from the sediments are often difficult to quantify, using long-lived Ra isotopes to estimate the SGD flow may minimize the effect of a poor characterization of the sediment source. The SGD flows to the Port of Maó obtained by using a mass balance of ^{228}Ra revealed a seasonal pattern, likely dominated by the recharge cycle, with maximum SGD rates during the wet seasons ($(170\pm90)\cdot10^3$ $m^3\cdot d^{-1}$ in fall) and minimum flows during summer ($(43\pm19)\cdot10^3$ $m^3\cdot d^{-1}$).

This study highlights the importance of accurately characterize the sedimentary source in Ra-derived SGD estimates, particularly when investigating systems potentially affected by bottom sediments (e.g. shallow water bodies, muddy systems or areas prone to bioturbation and/or resuspension events). In these systems, long-lived Ra isotopes would be the most appropriate tracers of SGD.

Chapter 4 is based on:
Rodellas, V., Garcia-Orellana, J., Masqué, P., Basterretxea, G. Submarine Groundwater Discharge into a coastal embayment: the influence of sediments on radium-derived estimates. In preparation.

Chapter 5: Palma Beach (Majorca, Balearic Islands)

This work was devoted to the determination of the SGD-driven fluxes of nutrients and trace metals into a detrital Mediterranean bay (Palma Beach, Balearic Islands). This allowed to ascertain the contribution of SGD to the nearshore nutrient pools and the potential linkages between SGD and coastal productivity. Palma Beach was selected because preferential groundwater flow paths inflow to the sea along this region and agriculture and tourism are potential sources of groundwater contamination. Groundwater sampling from wells and coastal piezometers indicated high concentrations of dissolved inorganic nitrogen (DIN) and Fe (up to 2800 $\mu mol \cdot L^{-1}$ and 8100 $nmol \cdot L^{-1}$, respectively). Other nutrients, such as dissolved inorganic phosphorous (DIP), and trace elements were not particularly enhanced, which is attributed to the adsorptive characteristics of the carbonated composition of this detrital aquifer and/or the lack of major sources. The sampling conducted in Palma Beach bay waters revealed significant enhancements of DIN and Fe in nearshore areas, which were associated to regions of preferential diffusive SGD inputs from the nearby coastal aquifer. Cross-shore gradients of $^{223,224}Ra$ isotopes were used to derive an eddy mixing coefficient that allowed estimating an SGD flow of 56000 ± 13000 $m^3\ d^{-1}$ to the bay by using ^{226}Ra. Results from this study showed that SGD is a major pathway for delivering DIN (1900 $mmol \cdot m^{-1} \cdot d^{-1}$), dissolved Fe (4.1 $mmol \cdot m^{-1} \cdot d^{-1}$) and, to a lesser extent, DIP (16 $\mu mol \cdot m^{-1} \cdot d^{-1}$) into the nearshore waters. SGD-derived fluxes of other trace metals (Ni, Cu, Zn, Mo, Pb) were also determined, suggesting that SGD representes a minor source of these compounds to Palma Beach waters. The allochtonous inputs of land-derived compounds (DIN, DIP and Fe) associated to SGD may sustain the enhanced phytoplankton biomass measured in the bay, producing a remarkable onshore-offshore gradient (4.7–7.1 $mg \cdot m^{-3}$ in nearshore seawater; <1 $mg \cdot m^{-3}$ in offshore stations).

This work emphasizes the relevance of SGD as a source of nutrients and trace metals to coastal Mediterranean areas and its importance on the regulation of coastal biogeochemical cycles. It constitutes the first study where trace metal inputs from SGD have been evaluated in the Mediterranean Sea.

Chapter 5 is based on:

Rodellas, V., Garcia-Orellana, J., Tovar-Sanchez, A., Basterretxea, G., Masqué, P., Garcia-Solsona, E., Sánchez-Quiles, D., López, J.M., 2014. Submarine Groundwater Discharge as a source of nutrients and trace metals in a Mediterranean bay (Palma Beach, Balearic Islands). Mar.Chem., 160, 56-66.

Chapter 6: Mediterranean Sea

This study aimed to evaluate the magnitude of SGD and its associated inputs of nutrients to the entire Mediterranean Sea. A ^{228}Ra mass balance including all the potential ^{228}Ra sources to surface waters (sediments, riverine discharge, atmospheric inputs, water inflowing through the straits and deep waters) and sinks (radioactive decay, water outflow to deep waters and through the straits, and particle scavenging) was used to derive the total SGD flow to the Mediterranean Sea. Results showed that SGD to the entire basin is a volumetrically important process ((2-43)·10^{11} m^3 yr^{-1}), of a comparable or even larger magnitude than the riverine discharge (~3·10^{11} m^3 yr^{-1}). The SGD-driven fluxes of dissolved inorganic nitrogen ((0.2-16)·10^{11} mol yr^{-1}), phosphorus ((0.9-40)·10^8 mol yr^{-1}) and silica ((1.2-40)·10^{10} mol yr^{-1}) to the entire Mediterranean Sea were also estimated, revealing that SGD represents a major source of nutrients to the basin that rivals the established external sources (i.e. atmospheric deposition and river discharge). Considering the magnitude of the estimated flow, SGD could also represent a relevant source of other chemical compounds (e.g. iron, carbon) to the Mediterranean Sea.

This study is the first evaluation of the magnitude of total SGD and nutrient fluxes into the entire Mediterranean Sea. It demonstrates that SGD is a relevant mechanism delivering dissolved nutrients to the whole Mediterranean basin, having profound implications in the biological and chemical cycles of this oligotrophic basin.

Overall, the present PhD Thesis has contributed to the understanding of the significance of SGD to the Mediterranean Sea, from a local to a basin-wide perspective. The magnitude of SGD and its associated fluxes of dissolved compounds points to its relevance in the biogeochemical cycles of the Mediterranean Sea and the need for its consideration in coastal and basin-wide studies. This dissertation has also provided new insights into the use of Ra isotopes as a tool to quantify SGD.

Chapter 6 is based on:

Rodellas, V., Garcia-Orellana, J., Masqué, P., Feldman, M., Weinstein, Y. Submarine Groundwater Discharge: a major source of nutrients to the Mediterranean Sea. Submitted.

7.2. Future perspectives

Relevant improvements on the understanding of the occurrence of SGD and its influence in coastal biogeochemical cycles have been achieved during the last decades, but many questions still remain unanswered. Some of the current and future research areas in which I plan to work in the future are summarized in this section.

- *SGD at a global scale.* The magnitude of SGD and derived fluxes of nutrients, metals and other compounds at a global scale is still unknown. This knowledge is important not only to understand the potential effects of SGD on coastal ecosystems, but also to correctly interpret the biogeochemical cycles of several compounds in the open ocean. Efforts to determine SGD at a global scale should focus on both conducting large-scale SGD studies (entire islands, marginal seas or oceans) and estimating SGD fluxes in a wider range of locations with different boundary conditions. Indeed, while SGD have been studied in detail in several sites, some parts of the world (e.g. Africa, Pacific coast of Southern America, areas located at high latitudes, most regions of Asia) have received little attention. In the Mediterranean Sea, the African shoreline have been poorly studied, even though SGD may have a relevant impact on the coastal geochemical cycles of this arid region, given the oligotrophic nature of its waters and the limited surface runoff to the sea.

- *SGD associated fluxes.* Several studies conducted during the last decade have evaluated the relevance of SGD as a source of trace metals, carbon and, particularly, nutrients to the coastal sea. Less it is known about the SGD-driven fluxes of other compounds, such as rare earth elements, bacteria or chemicals derived from anthropogenic activities (caffeine, pharmaceuticals or personal care products), among others. SGD studies to be conducted should explore the relevance of SGD as a source of this variety of compounds.

- *SGD driving forces and cycling within the subterranean estuary.* The cycling of Ra (and other SGD tracers), nutrients or trace metals within the subterranean estuary has a fundamental influence on the chemical fluxes discharging via SGD. Thus, a more detailed and precise understanding of the biogeochemical cycles in the subterranean estuary is required to appropriately estimate both Ra-derived SGD flows and its associated fluxes of dissolved chemical compounds. Recent studies have focused on

how nutrients or trace metals are transformed along the flowpath within the coastal aquifer (e.g. Beck et al. 2010; Erler et al. 2014). However, most of this knowledge is derived from studies based on single time points or transects, and little is known about the time scale or the magnitude of temporal variability (Gonneea et al. 2013). Future works should attempt to understand the biogeochemical cycling in dynamic mixing zones, resulting from the interplay between marine (e.g. tides, ocean oscillations) and terrestrial forces (e.g. precipitation). The driving forces contributing to the spatial and temporal variability of SGD fluxes should also be further investigated. To this aim, and as already pointed out by some authors (Kazemi 2008; Moore 2010b; Santos et al. 2012), "SGD", "hydrogeological" and "porewater exchange" scientific communities should work together.

- *Global change.* Global change will likely impact both the quantity and the quality of SGD in the future (Moore 2010b; Knee and Paytan 2011). The magnitude of SGD-related fluxes will be likely affected by different local and global predicted changes, including sea level rise, changes in precipitation regimes and temperature, increases of groundwater mining or coastline modification, among others. The overall effect of these changes on SGD is still unknown. Hence, one of the current challenges of the SGD community is to understand the evolution of SGD fluxes in systems that are rapidly changing as a result of anthropogenic activities. Besides, the influence of SGD in the water column carbonate chemistry of coastal ecosystems should also be studied, since SGD-related carbon inputs could represent a positive feedback to the current ocean acidification (Cyronak et al. 2014).

- *Radium as SGD tracer.* More information regarding the cycling of Ra isotopes in the coastal ocean and advancements on the analytical techniques have been acquired during the last years. However, some further refinement on the use of Ra isotopes as tracers of SGD needs to be achieved. For instance, efforts should focus on an accurate characterization of the Ra endmembers (considering its both spatial and temporal variability), on an appropriate estimation of the most important components of the Ra budgets (e.g. Ra export offshore, riverine and sediment inputs) and on correctly assessing the uncertainties associated to the Ra-based estimates, since they can represent up to 200% of the final SGD estimate. Studies combining Ra isotopes with other SGD tracers (e.g. ^{222}Rn, Sr isotopes) or methods (e.g. seepage meters, electromagnetic techniques, modeling, water-balances approaches) should also be

conducted. Such a combination of techniques would allow obtaining more accurate SGD estimates, providing new information on the driving forces and the composition of SGD, and evaluating the effectiveness of the methods used.

References

Added A, Ben Mammou A, Fernex F, Rezzoug S, Bernat M. Distribution of uranium and radium isotopes in an aquifer of a semi-arid region (Manouba-Essijoumi, Northern Tunisia). J Environ Radioact. 2005 Jan;82(3):371–81.

Alley WM, Healy RW, LaBaugh JW, Reilly TE. Flow and storage in groundwater systems. Science. 2002 Jun 14;296(5575):1985–90.

Anschutz P, Smith T, Mouret A, Deborde J, Bujan S, Poirier D, et al. Tidal sands as biogeochemical reactors. Estuar Coast Shelf Sci. 2009 Aug;84(1):84–90.

Bakken TH, Ruden F, Mangset LE. Submarine Groundwater: A New Concept for the Supply of Drinking Water. Water Resour Manag. 2011 Mar 12;26(4):1015–26.

Ballesteros B, Marina M, Mejías M, Domínguez J. Caracterización hidroquímica del acuífero carbonatado profundo de El Maestrazgo (Castellón).[Hydrochemical characterisation of the deep, carbonated El. Coast aquifers challenges …. Instituto Geológico y Minero de España - Hidrogeología y aguas subterráneas, 23; 2007. p. 549–64.

Basterretxea G, Garcés E, Jordi A, Anglès S, Masó M. Modulation of nearshore harmful algal blooms by in situ growth rate and water renewal. Mar Ecol Prog Ser. 2007;352:53–65.

Basterretxea G, Tovar-Sanchez A, Beck AJ, Masqué P, Bokuniewicz HJ, Coffey R, et al. Submarine Groundwater Discharge to the Coastal Environment of a Mediterranean Island (Majorca, Spain): Ecosystem and Biogeochemical Significance. Ecosystems. 2010 Jun 5;13(5):629–43.

Bates R, Jackson J. Dictionary of geological terms. New York: American Geological Institute; 1984.

Beck AJ, Charette MA, Cochran JK, Gonneea ME, Peucker-Ehrenbrink B. Dissolved strontium in the subterranean estuary – Implications for the marine strontium isotope budget. Geochim Cosmochim Acta. 2013 Sep;117:33–52.

Beck AJ, Cochran JK, Sañudo-Wilhelmy SA. Temporal Trends of Dissolved Trace Metals in Jamaica Bay, NY: Importance of Wastewater Input and Submarine Groundwater Discharge in an Urban Estuary. Estuaries and Coasts. 2009 Feb 4;32(3):535–50.

Beck AJ, Cochran JK, Sañudo-Wilhelmy SA. The distribution and speciation of dissolved trace metals in a shallow subterranean estuary. Mar Chem. 2010 Aug;121(1-4):145–56.

Beck AJ, Cochran MA. Controls on solid-solution partitioning of radium in saturated marine sands. Mar Chem. 2013 Oct;156:38–48.

Beck AJ, Rapaglia JP, Cochran JK, Bokuniewicz HJ. Radium mass-balance in Jamaica Bay, NY: Evidence for a substantial flux of submarine groundwater. Mar Chem. 2007 a Aug;106(3-4):419–41.

Beck AJ, Tsukamoto Y, Tovar-Sanchez A, Huerta-Diaz M, Bokuniewicz HJ, Sañudo-Wilhelmy SA. Importance of geochemical transformations in determining submarine groundwater discharge-derived trace metal and nutrient fluxes. Appl Geochemistry. 2007 b Feb;22(2):477–90.

Van Beek P, Sternberg E, Reyss J-L, Souhaut M, Robin E, Jeandel C. 228Ra/226Ra and 226Ra/Ba ratios in the Western Mediterranean Sea: Barite formation and transport in the water column. Geochim Cosmochim Acta. 2009 Aug;73(16):4720–37.

Bethoux J, Morin P, Chaumery C, Connan O. Nutrients in the Mediterranean Sea, mass balance and statistical analysis of concentrations with respect to environmental change. Mar Chem. 1998;63(1-2):155–69.

Bethoux JP, Gentili B. The Mediterranean Sea, coastal and deep-sea signatures of climatic and environmental changes. J Mar Syst. 1996;7(2-4):383–94.

Black FJ, Paytan A, Knee KL, de Sieyes NR, Ganguli PM, Gray E, et al. Submarine Groundwater Discharge of Total Mercury and Monomethylmercury to Central California Coastal Waters. Environ Sci Technol. American Chemical Society; 2009 Aug;43(15):5652–9.

Boehm AB, Paytan A, Shellenbarger GG, Davis KA. Composition and flux of groundwater from a California beach aquifer: Implications for nutrient supply to the surf zone. Cont Shelf Res. 2006 Feb;26(2):269–82.

Boehm AB, Shellenbarger GG, Paytan A. Groundwater Discharge: Potential Association with Fecal Indicator Bacteria in the Surf Zone. Environ Sci Technol. 2004 Jul;38(13):3558–66.

Bokuniewicz H. Groundwater seepage into Great South Bay, New York. Estuar Coast Mar Sci. 1980 Apr;10(4):437–44.

Bokuniewicz H, Buddemeier R, Maxwell B, Smith C. The typological approach to submarine groundwater discharge (SGD). Biogeochemistry. 2003 Nov;66(1/2):145–58.

Bokuniewicz H, Pavlik B. Groundwater seepage along a Barrier Island. Biogeochemistry. 1999 Jun 1;10(3):257–76.

Bokuniewicz H, Pollock M, Blum J, Wilson R. Submarine Ground Water Discharge and Salt Penetration Across the Sea Floor. Ground Water. 2004 Dec;42(7):983–9.

Bone SE, Charette MA, Lamborg CH, Gonneea ME. Has Submarine Groundwater Discharge Been Overlooked as a Source of Mercury to Coastal Waters? Environ Sci Technol. 2007 May;41(9):3090–5.

Bone SE, Gonneea ME, Charette MA. Geochemical Cycling of Arsenic in a Coastal Aquifer. Environ Sci Technol. American Chemical Society; 2006 May;40(10):3273–8.

Bonnet S, Guieu C. Atmospheric forcing on the annual iron cycle in the western Mediterranean Sea: A 1-year survey. J Geophys Res Ocean. 2006;111:C09010.1–C09010.13.

Breier JA, Breier CF, Edmonds HN. Seasonal dynamics of dissolved Ra isotopes in the semi-arid bays of south Texas. Mar Chem. 2010 Oct;122(1-4):39–50.

Breier JA, Nidzieko N, Monismith S, Moore W, Paytan A. Tidally regulated chemical fluxes across the sediment-water interface in elkhorn slough, california: Evidence from a coupled geochemical and hydrodynamic approach. Limnol Oceanogr. 2009;54(6):1964–80.

Burnett WC, Aggarwal PK, Aureli A, Bokuniewicz H, Cable JE, Charette MA, et al. Quantifying submarine groundwater discharge in the coastal zone via multiple methods. Sci Total Environ. 2006 Aug 31;367(2-3):498–543.

Burnett WC, Bokuniewicz H, Huettel M, Moore WS, Taniguchi M. Groundwater and pore water inputs to the coastal zone. Biogeochemistry. 2003 Nov;66(1/2):3–33.

Burnett WC, Dulaiova H. Estimating the dynamics of groundwater input into the coastal zone via continuous radon-222 measurements. J Environ Radioact. 2003 Jan;69(1-2):21–35.

Burnett WC, Dulaiova H. Radon as a tracer of submarine groundwater discharge into a boat basin in Donnalucata, Sicily. Cont Shelf Res. 2006 May;26(7):862–73.

Burnett WC, Kim G, Lane-Smith D. A continuous monitor for assessment of 222Rn in the coastal ocean. J Radioanal Nucl Chem. 2001a. p. 167–72.

Burnett WC, Lambert M, Dulaiova H. Tracing groundwater discharge into the ocean via continuous radon-222 measurements. Ocean Conf Rec. 2001b. p. 251–5.

Burnett WC, Taniguchi M, Oberdorfer J. Measurement and significance of the direct discharge of groundwater into the coastal zone. J Sea Res. 2001 c Sep;46(2):109–16.

Burnett WC, Wattayakorn G, Taniguchi M, Dulaiova H, Sojisuporn P, Rungsupa S, et al. Groundwater-derived nutrient inputs to the Upper Gulf of Thailand. Cont Shelf Res. 2007 Jan;27(2):176–90.

Cable JE, Bugna GC, Burnett WC, Chanton JP. Application of 222Rn and CH4 for assessment of groundwater discharge to the coastal ocean. Limnol Oceanogr. American Society of Limnology and Oceanography; 1996;41(6):1347–53.

Cable JE, Burnett WC, Chanton JP. Magnitude and variations of groundwater seepage along a Florida marine shoreline. Biogeochemistry. 1997 a;38(2):189–205.

Cable JE, Burnett WC, Chanton JP, Corbett DR, Cable PH. Field Evaluation of Seepage Meters in the Coastal Marine Environment. Estuar Coast Shelf Sci. 1997 b Sep;45(3):367–75.

Cable JE, Martin JB. In situ evaluation of nearshore marine and fresh pore water transport into Flamengo Bay, Brazil. Estuar Coast Shelf Sci. 2008 Feb;76(3):473–83.

Cai W, Wiebe W, Wang Y, Sheldon J. Intertidal marsh as a source of dissolved inorganic carbon and a sink of nitrate in the Satilla River-estuarine complex in the southeastern US. Limnol Oceanogr. 2000;45:1743–52.

Cai W-J, Wang Y, Krest J, Moore WS. The geochemistry of dissolved inorganic carbon in a surficial groundwater aquifer in North Inlet, South Carolina, and the carbon fluxes to the coastal ocean. Geochim Cosmochim Acta. 2003 Feb;67(4):631–9.

Candela L, Wallis KJ, Mateos RM. Non-point pollution of groundwater from agricultural activities in Mediterranean Spain: the Balearic Islands case study. Environ Geol. 2008 Jun 20;54(3):587–95.

Capo RC, Stewart BW, Chadwick OA. Strontium isotopes as tracers of ecosystem processes: theory and methods. Geoderma. 1998 Feb;82(1-3):197–225.

Chanton JP, Burnett WC, Dulaiova H, Corbett DR, Taniguchi M. Seepage rate variability in Florida Bay driven by Atlantic tidal height. Biogeochemistry. 2003 Nov;66(1/2):187–202.

Charette MA. Hydrologic forcing of submarine groundwater discharge: Insight from a seasonal study of radium isotopes in a groundwater-dominated salt marsh estuary. Limnol Oceanogr. 2007;52(1):230–9.

Charette MA, Buesseler KO. Submarine groundwater discharge of nutrients and copper to an urban subestuary of Chesapeake Bay (Elizabeth River). Limnol Oceanogr. 2004;49(2):376–85.

Charette MA, Buesseler KO, Andrews JE. Utility of radium isotopes for evaluating the input and transport of groundwater-derived nitrogen to a Cape Cod estuary. Limnol Oceanogr. 2001;46(2):465–70.

Charette MA, Dulaiova H, Gonneea ME, Henderson PB, Moore WS, Scholten JC, et al. GEOTRACES radium isotopes interlaboratory comparison experiment. Limnol Oceanogr Methods. 2012;10(JUNE):451–63.

Charette MA, Henderson PB, Breier CF, Liu Q. Submarine groundwater discharge in a river-dominated Florida estuary. Mar Chem. 2013 Oct;156:3–17.

Charette MA, Moore WS, Burnett WC. Uranium- and Thorium-Series Nuclides as Tracers of Submarine Groundwater Discharge (in U-Th Series Nuclides in Aquatic Systems). Radioact Environ. Elsevier; 2008. p. 155–91.

Charette MA, Sholkovitz ER. Oxidative precipitation of groundwater-derived ferrous iron in the subterranean estuary of a coastal bay. Geophys Res Lett. 2002 May 15;29(10):85–1–85–4.

Charette MA, Sholkovitz ER. Trace element cycling in a subterranean estuary: Part 2. Geochemistry of the pore water. Geochim Cosmochim Acta. 2006 Feb;70(4):811–26.

Charette MA, Splivallo R, Herbold C, Bollinger MS, Moore WS. Salt marsh submarine groundwater discharge as traced by radium isotopes. Mar Chem. 2003;84(1-2):113–21.

Chen K, Jiao JJ. Hydrochemical Evolution of Ground Water in Shenzhen after Land Reclamation: Major Ion Chemistry of Coastal Ground Water. 2007 Gr Water Summit. Albequerque, NM, USA; 2007.

Church TM. An underground route for the water cycle. Nature. 1996 Apr 18;380:579–80.

Cook PG, Wood C, White T, Simmons CT, Fass T, Brunner P. Groundwater inflow to a shallow, poorly-mixed wetland estimated from a mass balance of radon. J Hydrol. 2008 Jun;354(1-4):213–26.

Corbett DR, Dillon K, Burnett W, Chanton J. Estimating the groundwater contribution into Florida Bay via natural tracers, 222Rn and CH4. Limnol Oceanogr. 2000;45(7):1546–57.

Corbett DR, Dillon K, Burnett WC, Schaefer G. The spatial variability of nitrogen and phosphorus concentration in a sand aquifer influenced by onsite sewage treatment and disposal systems: a case study on St. George Island, Florida. Environ Pollut. 2002 Apr;117(2):337–45.

Crotwell AM, Moore WS. Nutrient and Radium Fluxes from Submarine Groundwater Discharge to Port Royal Sound, South Carolina. Aquat Geochemistry. 2003 Sep;9(3):191–208.

Crusius J, Berg P, Koopmans DJ, Erban L. Eddy correlation measurements of submarine groundwater discharge. Mar Chem. 2008 Feb;109(1-2):77–85.

Cyronak T, Santos IR, Erler D V., Maher DT, Eyre BD. Drivers of p CO 2 variability in two contrasting coral reef lagoons: The influence of submarine groundwater discharge. Global Biogeochem Cycles. 2014 Apr 15;28(4):398–414.

Diaz F, Raimbault P, Boudiellal B, Garcia N, Moutin T. Early spring phosphorus limitation of primary productivity in a NW Mediterranean coastal zone (Gulf of Lions). Mar Ecol Prog Ser. 2001;211:51–62.

Dimova N, Dulaiova H, Kim G, Burnett WC. Uncertainties in the preparation of 224Ra Mn fiber standards. Mar Chem. 2008 Apr;109(3-4):220–5.

Downs TM, Schallenberg M, Burns CW. Responses of lake phytoplankton to micronutrient enrichment: a study in two New Zealand lakes and an analysis of published data. Aquat Sci. 2008 Jun 6;70(4):347–60.

Dulaiova H, Burnett WC. An efficient method for γ-spectrometric determination of radium-226,228 via manganese fibers. Limnol Oceanogr Methods. 2004;2(AUG.):256–61.

Dulaiova H, Burnett WC, Chanton JP, Moore WS, Bokuniewicz HJ, Charette MA, et al. Assessment of groundwater discharges into West Neck Bay, New York, via natural tracers. Cont Shelf Res. 2006 a Oct;26(16):1971–83.

Dulaiova H, Burnett WC, Wattayakorn G, Sojisuporn P. Are groundwater inputs into river-dominated areas important? The Chao Phraya River - Gulf of Thailand. Limnol Oceanogr. 2006 b;51(5):2232–47.

Dulaiova H, Peterson R, Burnett WC, Lane-Smith D. A multi-detector continuous monitor for assessment of <Superscript>222</Superscript>Rn in the coastal ocean. J Radioanal Nucl Chem. 2005 Jan;263(2):361–3.

Dymond J, Suess E, Lyle M. Barium in Deep-Sea Sediment: A Geochemical Proxy for Paleoproductivity. Paleoceanography. 1992 Apr 4;7(2):163–81.

El-Gamal AA, Peterson RN, Burnett WC. Detecting Freshwater Inputs via Groundwater Discharge to Marina Lagoon, Mediterranean Coast, Egypt. Estuaries and Coasts. 2012 Aug 2;35(6):1486–99.

Eleftheriou G, Tsabaris C, Androulakaki EG, Patiris DL, Kokkoris M, Kalfas CA, et al. Radioactivity measurements in the aquatic environment using in-situ and laboratory gamma-ray spectrometry. Appl Radiat Isot. 2013 Dec;82:268–78.

Elsinger RJ, Moore WS. 226Ra behavior in the Pee Dee River-Winyah Bay estuary. Earth Planet Sci Lett. 1980;48(2):239–49.

Emelyanov E, Shimkus K, Kuprin P. Unconsolidated Bottom Surface Sediments of the Mediterranean and Black Seas. Intergov Oceanogr Comm (UNESCO), IBCM Geol Geogr Ser. St Petesburg, Russia: Intergovernmental Oceanographic Commission (UNESCO); 1996;

Erler D V., Santos IR, Zhang Y, Tait DR, Befus KM, Hidden A, et al. Nitrogen transformations within a tropical subterranean estuary. Mar Chem. 2014 Aug;164:38–47.

Fetter C. Applied hydrogeology. New York: McMillan Publishing Co; 1988. p. 592 p.

Fisher AT. Marine hydrogeology: recent accomplishments and future opportunities. Hydrogeol J. 2005 Feb 25;13(1):69–97.

Fleury P, Bakalowicz M, de Marsily G. Submarine springs and coastal karst aquifers: A review. J Hydrol. 2007 Jun;339(1-2):79–92.

Fornós JJ, Obradors A, Rosell VM. Història Natural del Migjorn de Mallorca. Soc d'Història Nat les Balear. 2004 Jan;11:1–378.

Freeze R, Cherry J. Groundwater, 1979. Englewood Cliffs, NJ: Printice-Hall Inc.; 1979. p. 604p.

Fukuo Y, Kaihotsu I. A theoretical analysis of seepage flow of the confined groundwater into the lake bottom with a gentle slope. Water Resour Res. 1988 Nov 9;24(11):1949–53.

Ganju NK. A novel approach for direct estimation of fresh groundwater discharge to an estuary. Geophys Res Lett. 2011 Jun 4;38(11):n/a–n/a.

Garcés E, Basterretxea G, Tovar-Sánchez A. Changes in microbial communities in response to submarine groundwater input. Mar Ecol Prog Ser. 2011;438:47–58.

Garcia-Orellana J, Cañas L, Masqué P, Obrador B, Olid C, Pretus J. Chronological reconstruction of metal contamination in the Port of Maó (Minorca, Spain). Mar Pollut Bull. 2011 Aug;62(8):1632–40.

Garcia-Orellana J, Cochran JK, Bokuniewicz H, Daniel JWR, Rodellas V, Heilbrun C. Evaluation of 224Ra as a tracer for submarine groundwater discharge in Long Island Sound (NY). Geochim Cosmochim Acta. 2014 Sep;141:314–30.

Garcia-Orellana J, Cochran JK, Bokuniewicz H, Yang S, Beck AJ. Time-series sampling of 223Ra and 224Ra at the inlet to Great South Bay (New York): a strategy for characterizing the dominant terms in the Ra budget of the bay. J Environ Radioact. 2010 Jul;101(7):582–8.

Garcia-Orellana J, Rodellas V, Casacuberta N, Lopez-Castillo E, Vilarrasa M, Moreno V, et al. Submarine groundwater discharge: Natural radioactivity accumulation in a wetland ecosystem. Mar Chem. 2013 Oct;156:61–72.

Garcia-Orellana J, Sanchez-Cabeza JA, Masqué P, Àvila A, Costa E, Loÿe-Pilot MD, et al. Atmospheric fluxes of 210 Pb to the western Mediterranean Sea and the Saharan dust influence. J Geophys Res. 2006;111(D15):D15305.

Garcia-Solsona E. Submarine groundwater discharge in coastal Mediterranean areas by using radium isotope: Venice Lagoon, Minorca and Castelló. Universitat Autònoma de Barcelona; 2009. p. 242.

Garcia-Solsona E, Garcia-Orellana J, Masqué P, Dulaiova H. Uncertainties associated with 223Ra and 224Ra measurements in water via a Delayed Coincidence Counter (RaDeCC). Mar Chem. 2008 a Apr;109(3-4):198–219.

Garcia-Solsona E, Garcia-Orellana J, Masqué P, Garcés E, Radakovitch O, Mayer A, et al. An assessment of karstic submarine groundwater and associated nutrient discharge to a Mediterranean coastal area (Balearic Islands, Spain) using radium isotopes. Biogeochemistry. 2010 a Sep 11;97(2-3):211–29.

Garcia-Solsona E, Garcia-Orellana J, Masqué P, Mejías M, Ballesteros B, Marina M. Radium isotopes as tracers of submarine groundwater discharge from coastal springs in Les Fonts beach (Castelló, spain). Gordon Res Conf – Permeable Sediments. Waterville, Maine; 2006.

Garcia-Solsona E, Garcia-Orellana J, Masqué P, Rodellas V, Mejías M, Ballesteros B, et al. Groundwater and nutrient discharge through karstic coastal springs (*Castelló*, Spain). Biogeosciences. 2010 b Sep 7;7(9):2625–38.

Garcia-Solsona E, Jeandel C, Labatut M, Lacan F, Vance D, Chavagnac V, et al. Rare earth elements and Nd isotopes tracing water mass mixing and particle-seawater interactions in the SE Atlantic. Geochim Cosmochim Acta. 2014 Jan;125:351–72.

Garcia-Solsona E, Masqué P, Garcia-Orellana J, Rapaglia J, Beck AJ, Cochran JK, et al. Estimating submarine groundwater discharge around Isola La Cura, northern Venice Lagoon (Italy), by using the radium quartet. Mar Chem. 2008 b Apr;109(3-4):292–306.

Gattacceca JC, Mayer A, Cucco A, Claude C, Radakovitch O, Vallet-Coulomb C, et al. Submarine groundwater discharge in a subsiding coastal lowland: A 226Ra and 222Rn investigation in the Southern Venice lagoon. Appl Geochemistry. 2011 May;26(5):907–20.

Geibert W, Rodellas V, Annett A, van Beek P, Garcia-Orellana J, Hsieh Y-T, et al. 226Ra determination via the rate of 222Rn ingrowth with the Radium Delayed Coincidence Counter (RaDeCC). Limnol Oceanogr Methods. 2013;11(NOV):594–603.

Gibbes B, Robinson C, Li L, Lockington D, Li H. Tidally driven pore water exchange within offshore intertidal sandbanks: Part II numerical simulations. Estuar Coast Shelf Sci. 2008 Dec;80(4):472–82.

Giffin C, Kaufman A, Broecker W. Delayed coincidence counter for the assay of actinon and thoron. J Geophys Res. 1963 Mar 15;68(6):1749–57.

Gleeson J, Santos IR, Maher DT, Golsby-Smith L. Groundwater–surface water exchange in a mangrove tidal creek: Evidence from natural geochemical tracers and implications for nutrient budgets. Mar Chem. 2013 Oct;156:27–37.

Gobler C, Sañudo-Wilhelmy S. Temporal variability of groundwater seepage and brown tide blooms in a Long Island embayment. Mar Ecol Prog Ser. 2001;217:299–309.

Goñi MA, Gardner IR. Seasonal Dynamics in Dissolved Organic Carbon Concentrations in a Coastal Water-Table Aquifer at the Forest-Marsh Interface. Aquat Geochemistry. 2003 Sep;9(3):209–32.

Gonneea ME, Charette MA, Liu Q, Herrera-Silveira JA, Morales-Ojeda SM. Trace element geochemistry of groundwater in a karst subterranean estuary (Yucatan Peninsula, Mexico). Geochim Cosmochim Acta. 2014 May;132:31–49.

Gonneea ME, Morris PJ, Dulaiova H, Charette MA. New perspectives on radium behavior within a subterranean estuary. Mar Chem. 2008 Apr;109(3-4):250–67.

Gonneea ME, Mulligan AE, Charette MA. Seasonal cycles in radium and barium within a subterranean estuary: Implications for groundwater derived chemical fluxes to surface waters. Geochim Cosmochim Acta. 2013 Oct;119:164–77.

Grasshoff K, Ehrhardt M, Kremling K. Methods of seawater analyses. Wiley-VCH. Verlah Chemie. Weinheim, Germany; 1983.

Guerzoni S, Chester R, Dulac F, Herut B, Loÿe-Pilot M-D, Measures C, et al. The role of atmospheric deposition in the biogeochemistry of the Mediterranean Sea. Prog Oceanogr. 1999 Aug;44(1-3):147–90.

Hancock GJ, Martin P. Determination of Ra in environmental samples by α-particle spectrometry. Int J Radiat Appl Instrumentation Part A Appl Radiat Isot. 1991 Jan;42(1):63–9.

Hancock GJ, Murray AS. Source and distribution of dissolved radium in the Bega River estuary, Southeastern Australia. Earth Planet Sci Lett. 1996 Feb;138(1-4):145–55.

Hancock GJ, Webster IT, Stieglitz TC. Horizontal mixing of Great Barrier Reef waters: Offshore diffusivity determined from radium isotope distribution. J Geophys Res. 2006 Dec 23;111(C12):C12019.

Heiss JW, Michael HA. Saltwater-freshwater mixing dynamics in a sandy beach aquifer over tidal, spring-neap, and seasonal cycles. Water Resour Res. 2014 Aug 21;50(8):6747–66.

Herut B, Krom MD, Pan G, Mortimer R. Atmospheric input of nitrogen and phosphorus to the Southeast Mediterranean: Sources, fluxes, and possible impact. Limnol Oceanogr. 1999;44(7):1683–92.

Hoefel FG, Evans RL. Impact of Low Salinity Porewater on Seafloor Electromagnetic Data: A Means of Detecting Submarine Groundwater Discharge? Estuar Coast Shelf Sci. 2001 Feb;52(2):179–89.

Holliday D, Stieglitz T, Ridd P, Read W. Geological controls and tidal forcing of submarine groundwater discharge from a confined aquifer in a coastal sand dune system. J Geophys Res …. 2007;

Horn DP. Measurements and modelling of beach groundwater flow in the swash-zone: a review. Cont Shelf Res. 2006 Apr;26(5):622–52.

Hsieh Y-T, Henderson GM. Precise measurement of 228Ra/226Ra ratios and Ra concentrations in seawater samples by multi-collector ICP mass spectrometry. J Anal At Spectrom. The Royal Society of Chemistry; 2011 Jul 1;26(7):1338.

Hu C, Muller-Karger FE, Swarzenski PW. Hurricanes, submarine groundwater discharge, and Florida's red tides. Geophys Res Lett. 2006;33(11):L11601.

Hwang D-W, Kim G, Lee Y-W, Yang H-S. Estimating submarine inputs of groundwater and nutrients to a coastal bay using radium isotopes. Mar Chem. 2005 a Aug;96(1-2):61–71.

Hwang DW, Lee YW, Kim G. Large submarine groundwater discharge and benthic eutrophication in Bangdu Bay on volcanic Jeju Island, Korea. Limnol Oceanogr. 2005 b;50(5):1393–403.

IDEIB. IDEIB Infraestructura de dades espacials de les Illes Balears. Govern de les llles Balears. [Internet]. [cited 2014 Mar 20]. Available from: www.ideib.caib.es/visualitzador

IOC. International bathymetric chart of the Mediterranean. Head Dep Navig Oceanogr Minist Defense, USSR, under Auth IOC. International Oceanographic Commission; 1981;

Jackson J, Mehl J, Neuendorf K. Glossary of geology. Alexandria, VA: American Geological Institute; 2005. p. 420p.

Jeong J, Kim G, Han S. Influence of trace element fluxes from submarine groundwater discharge (SGD) on their inventories in coastal waters off volcanic island, Jeju, Korea. Appl Geochemistry. 2012 Jan;27(1):37–43.

Johannes R. Ecological significance of the submarine discharge of groundwater. Mar Ecol Prog Ser. 1980;(3):365–73.

Johannesson KH, Burdige DJ. Balancing the global oceanic neodymium budget: Evaluating the role of groundwater. Earth Planet Sci Lett. 2007 Jan;253(1-2):129–42.

Johannesson KH, Chevis DA, Burdige DJ, Cable JE, Martin JB, Roy M. Submarine groundwater discharge is an important net source of light and middle REEs to coastal waters of the Indian River Lagoon, Florida, USA. Geochim Cosmochim Acta. 2011 Feb;75(3):825–43.

Johnson AG, Glenn CR, Burnett WC, Peterson RN, Lucey PG. Aerial infrared imaging reveals large nutrient-rich groundwater inputs to the ocean. Geophys Res Lett. 2008 Aug 13;35(15):L15606.

Jordi A, Basterretxea G, Tovar-Sánchez A, Alastuey A, Querol X. Copper aerosols inhibit phytoplankton growth in the Mediterranean Sea. Proc Natl Acad Sci U S A. 2012 Dec 26;109(52):21246–9.

Jordi A, Basterretxea G, Wang D-P. Local versus remote wind effects on the coastal circulation of a microtidal bay in the Mediterranean Sea. J Mar Syst. 2011 Nov;88(2):312–22.

Kalnejais LH, Martin WR, Bothner MH. The release of dissolved nutrients and metals from coastal sediments due to resuspension. Mar Chem. 2010 Aug;121(1-4):224–35.

Kazemi GA. Editor's Message: Submarine groundwater discharge studies and the absence of hydrogeologists. Hydrogeol J. 2008 Jan 4;16(2):201–4.

Kearey P. The new Penguin dictionary of geology. New York: Penguin Publishers; 1996. p. 366p.

Kelly J, Glenn C, Lucey P. High-resolution aerial infrared mapping of groundwater discharge to the coastal ocean. Limnol Oceanogr Methods. 2013;11:262–7.

Kim G, Hwang DW. Tidal pumping of groundwater into the coastal ocean revealed from submarine 222Rn and CH4 monitoring. Geophys Res Lett. 2002;29(14):23–1 .

Kim G, Kim S-J, Harada K, Schultz MK, Burnett WC. Enrichment of Excess 210 Po in Anoxic Ponds. Environ Sci Technol. 2005 Jul;39(13):4894–9.

Kim G, Lee KK, Park KS, Hwang DW, Yang HS. Large submarine groundwater discharge (SGD) from volcanic island. Geophys Res Lett. 2003;30(21).

Kim I, Kim G. Large fluxes of rare earth elements through submarine groundwater discharge (SGD) from a volcanic island, Jeju, Korea. Mar Chem. 2011 Dec;127(1-4):12–9.

Kim I, Kim G. Submarine groundwater discharge as a main source of rare earth elements in coastal waters. Mar Chem. 2014 Mar;160:11–7.

King JN. Synthesis of benthic flux components in the Patos Lagoon coastal zone, Rio Grande do Sul, Brazil. Water Resour Res. 2012 Dec 22;48(12):n/a–n/a.

Knee K, Street JH, Grossman EG, Paytan A. Nutrient inputs to the coastal ocean from submarine groundwater discharge in a groundwater-dominated system: Relation to land use (Kona coast, Hawaii, U.S.A.). Limnol Oceanogr. 2010;55(3):1105–22.

Knee KL, Paytan A. Submarine Groundwater Discharge: A Source of Nutrients, Metals, and Pollutants to the Coastal Ocean. In: Wolanski E, McLusky D, editors. Treatise Estuar Coast Sci. Elsevier; 2011. p. 205–33.

Knee KL, Solsona EG-, Orellana JG-, Boehm AB, Paytan A. Using radium isotopes to characterize water ages and coastal mixing rates: A sensitivity analysis. Limnol Oceanogr Methods. 2011;9(SEP):380–95.

Koçak M, Kubilay N, Tugrul S, Mihalopoulos N. Atmospheric nutrient inputs to the northern levantine basin from a long-term observation: sources and comparison with riverine inputs. Biogeosciences. 2010;7:4037–50.

Kohout FA. Submarine springs: a neglected phenomenon of coastal hydrology. Hydrology. 1966;26:391–413.

Krest JM, Moore WS, Gardner LR, Morris JT. Marsh nutrient export supplied by groundwater discharge: Evidence from radium measurements. Global Biogeochem Cycles. 2000;14(1):167–76.

Krest JM, Moore WS, Rama. and in the mixing zones of the Mississippi and Atchafalaya Rivers: indicators of groundwater input. Mar Chem. 1999 Mar;64(3):129–52.

Krom MD, Emeis K-C, Van Cappellen P. Why is the Eastern Mediterranean phosphorus limited? Prog Oceanogr. 2010 Jun;85(3-4):236–44.

Krom MD, Herut B, Mantoura RFC. Nutrient budget for the Eastern Mediterranean: Implications for phosphorus limitation. Limnol Oceanogr. 2004;49(5):1582–92.

Labidi S, Mahjoubi H, Essafi F, Ben Salah R. Natural radioactivity levels in mineral, therapeutic and spring waters in Tunisia. Radiat Phys Chem. 2010 Dec;79(12):1196–202.

Lacan F, Jeandel C. Neodymium isotopes as a new tool for quantifying exchange fluxes at the continent–ocean interface. Earth Planet Sci Lett. 2005 Apr;232(3-4):245–57.

Lacombe H, Richez C. The regime of the Strait of Gibraltar. In: Nihoul JCJ, editor. Hydrodinamics semi-enclosed seas. Amsterdam: Elsevier; 1982. p. 13–74.

Lafabrie C, Garrido M, Leboulanger C, Cecchi P, Grégori G, Pasqualini V, et al. Impact of contaminated-sediment resuspension on phytoplankton in the Biguglia lagoon (Corsica, Mediterranean Sea). Estuar Coast Shelf Sci. 2013 Sep;130:70–80.

Langevin CD. Simulation of Submarine Ground Water Discharge to a Marine Estuary: Biscayne Bay, Florida. Ground Water. 2003 Nov;41(6):758–71.

Lapointe B. Nutrient thresholds for bottom-up control of macroalgal blooms and coral reefs. 1997;42:1119–31.

Laroche J, Nuzzi R, Watters R, Wyman K, Falkowski P, Wallace D. Brown Tide blooms in Long Island's coastal waters linked to interannual variability in groundwater flow. Glob Chang Biol. 1997 Oct;3(5):397–410.

Laurier FJG, Cossa D, Beucher C, Brévière E. The impact of groundwater discharges on mercury partitioning, speciation and bioavailability to mussels in a coastal zone. Mar Chem. 2007 Mar;104(3-4):143–55.

Lee D. A device for measuring seepage flux in lakes and esturies. Limnol Oceanogr. 1977;22:140–7.

Lee E, Hyun Y, Lee K-K. Sea level periodic change and its impact on submarine groundwater discharge rate in coastal aquifer. Estuar Coast Shelf Sci. 2013 Apr;121-122:51–60.

Lee Y, Kim G, Lim W, Hwang D. A relationship between submarine-groundwater borne nutrients traced by Ra isotopes and the intensity of dinoflagellate red-tides occurring in the southern sea. Limnol …. 2010;

Lee Y, Rahman MM, Kim G, Han S. Mass balance of total mercury and monomethylmercury in coastal embayments of a volcanic island: significance of submarine groundwater discharge. Environ Sci Technol. American Chemical Society; 2011 Dec 1;45(23):9891–900.

Lee Y-W, Kim G. Linking groundwater-borne nutrients and dinoflagellate red-tide outbreaks in the southern sea of Korea using a Ra tracer. Estuar Coast Shelf Sci. 2007 Jan;71(1-2):309–17.

Li C, Cai W-J. On the calculation of eddy diffusivity in the shelf water from radium isotopes: High sensitivity to advection. J Mar Syst. 2011 May;86(1-2):28–33.

Li L, Barry D. Wave-induced beach groundwater flow. Adv Water Resour. 2000 Jan;23(4):325–37.

Li Y-H, Mathieu G, Biscaye P, Simpson HJ. The flux of 226Ra from estuarine and continental shelf sediments. Earth Planet Sci Lett. 1977 Dec;37(2):237–41.

Liu Q, Dai M, Chen W, Huh C-A, Wang G, Li Q, et al. How significant is submarine groundwater discharge and its associated dissolved inorganic carbon in a river-dominated shelf system? Biogeosciences. 2012 May 22;9(5):1777–95.

López-García J, Mateos-Ruiz R. La intrusión marina en los acuíferos de la isla de Mallorca. Tecnol la Intrusión Agua Mar en Acuíferos Costeros Países Mediterráneos. Publicaciones del Instituto Geológico y Mineros de España. Serie: Hidrogeología y Aguas Subterráneas nº8. Tomo I.; 2003.

Ludwig W, Dumont E, Meybeck M, Heussner S. River discharges of water and nutrients to the Mediterranean and Black Sea: Major drivers for ecosystem changes during past and future decades? Prog Oceanogr. 2009 Mar;80(3-4):199–217.

MacIntyre S, Wanninkhof R, Chanton JP. Trace gas exchange across the air-water interface in freshwater and coastal marine environments. In: Matson PA, Harris RC, editors. Biog trace gases Meas Emiss from soil water. Cambridge, MA: Blackwell Science Ltd; 1995. p. 52–97.

Manheim FT, Krantz DE, Bratton JF. Studying Ground Water Under Delmarva Coastal Bays Using Electrical Resistivity. Ground Water. 2004 Dec;42(7):1052–68.

Marbà N, Calleja ML, Duarte CM, Álvarez E, Díaz-Almela E, Holmer M. Iron Additions Reduce Sulfide Intrusion and Reverse Seagrass (Posidonia oceanica) Decline in Carbonate Sediments. Ecosystems. 2007 Jun 20;10(5):745–56.

Markaki Z, Loÿe-Pilot MD, Violaki K, Benyahya L, Mihalopoulos N. Variability of atmospheric deposition of dissolved nitrogen and phosphorus in the Mediterranean and possible link to the anomalous seawater N/P ratio. Mar Chem. 2010 Jun;120(1-4):187–94.

Markaki Z, Oikonomou K, Kocak M, Kouvarakis G, Chaniotaki A, Kubilay N, et al. Atmospheric deposition of inorganic phosphorus in the Levantine Basin, eastern Mediterranean: Spatial and temporal variability and its role in seawater productivity. Limnol Oceanogr. 2003;48(4):1557–68.

Martin AJ, Pedersen TF. Seasonal and Interannual Mobility of Arsenic in a Lake Impacted by Metal Mining. Environ Sci Technol. American Chemical Society; 2002 Apr;36(7):1516–23.

Matthiessen P, Reed J, Johnson M. Sources and Potential Effects of Copper and Zinc Concentrations in the Estuarine Waters of Essex and Suffolk, United Kingdom. Mar Pollut Bull. 1999 Oct;38(10):908–20.

Mejías M, Ballesteros BJ, Antón-Pacheco C, Domínguez JA, Garcia-Orellana J, Garcia-Solsona E, et al. Methodological study of submarine groundwater discharge from a karstic aquifer in the Western Mediterranean Sea. J Hydrol. 2012 Sep;464-465:27–40.

Mejías M, Garcia-Orellana J, Plata JL, Marina M, Garcia-Solsona E, Ballesteros B, et al. Methodology of hydrogeological characterization of deep carbonate aquifers as potential reservoirs of groundwater. Case of study: the Jurassic aquifer of El Maestrazgo (Castellón, Spain). Environ Geol. 2007 Jun 20;54(3):521–36.

Michael HA. Characterizing submarine groundwater discharge: A seepage meter study in Waquoit Bay, Massachusetts. Geophys Res Lett. 2003;30(6):1297.

Michael HA, Charette MA, Harvey CF. Patterns and variability of groundwater flow and radium activity at the coast: A case study from Waquoit Bay, Massachusetts. Mar Chem. 2011 Dec;127(1-4):100–14.

Michael HA, Mulligan AE, Harvey CF. Seasonal oscillations in water exchange between aquifers and the coastal ocean. Nature. 2005 Aug 25;436(7054):1145–8.

Mijatović B. The groundwater discharge in the Mediterranean karst coastal zones and freshwater tapping: set problems and adopted solutions. Case studies. Environ Geol. 2006 Aug 10;51(5):737–42.

Miller DC, Ullman WJ. Ecological Consequences of Ground Water Discharge to Delaware Bay, United States. Ground Water. 2004 Dec;42(7):959–70.

Monsen NE, Cloern JE, Lucas L V., Monismith SG. A comment on the use of flushing time, residence time, and age as transport time scales. Limnol Oceanogr. American Society of Limnology and Oceanography; 2002;47(5):1545–53.

Moore WS. Sampling 228Ra in the deep ocean. Deep Sea Res Oceanogr Abstr. 1976 Jul;23(7):647–51.

Moore WS. Radium isotope measurements using germanium detectors. Nucl Instruments Methods Phys Res. 1984;223(2-3):407–11.

Moore WS. Large groundwater inputs to coastal waters revealed by 226Ra enrichments. Nature. 1996 a Apr 18;380(6575):612–4.

Moore WS. Using the radium quartet for evaluating groundwater input and water exchange in salt marshes. Geochim Cosmochim Acta. 1996 b Dec;60(23):4645–52.

Moore WS. High fluxes of radium and barium from the mouth of the Ganges-Brahmaputra River during low river discharge suggest a large groundwater source. Earth Planet Sci Lett. 1997;150(1-2):141–50.

Moore WS. The subterranean estuary: a reaction zone of ground water and sea water. Mar Chem. 1999 May;65(1-2):111–25.

Moore WS. Ages of continental shelf waters determined from 223Ra and 224Ra. J Geophys Res C Ocean. 2000 a;105(C9):22117–22.

Moore WS. Determining coastal mixing rates using radium isotopes. Cont Shelf Res. 2000 b Nov;20(15):1993–2007.

Moore WS. Sources and fluxes of submarine groundwater discharge delineated by radium isotopes. Biogeochemistry. 2003 Nov;66(1/2):75–93.

Moore WS. Radium isotopes as tracers of submarine groundwater discharge in Sicily. Cont Shelf Res. 2006 May;26(7):852–61.

Moore WS. Fifteen years experience in measuring 224Ra and 223Ra by delayed-coincidence counting. Mar Chem. 2008 Apr;109(3-4):188–97.

Moore WS. A reevaluation of submarine groundwater discharge along the southeastern coast of North America. Global Biogeochem Cycles. 2010 a Dec 14;24(4):GB4005.

Moore WS. The Effect of Submarine Groundwater Discharge on the Ocean. Ann Rev Mar Sci. 2010 b Jan;2(1):59–88.

Moore WS, Arnold R. Measurement of223Ra and224Ra in coastal waters using a delayed coincidence counter. J Geophys Res C Ocean. 1996;101(C1):1321–9.

Moore WS, Astwood H, Lindstrom C. Radium isotopes in coastal waters on the Amazon shelf. Geochim Cosmochim Acta. 1995;59(20):4285–98.

Moore WS, Blanton JO, Joye SB. Estimates of flushing times, submarine groundwater discharge, and nutrient fluxes to Okatee Estuary, South Carolina. J Geophys Res. 2006;111(C9):C09006.

Moore WS, Cai P. Calibration of RaDeCC systems for 223Ra measurements. Mar Chem. 2013 Oct;156:130–7.

Moore WS, Key RM, Sarmiento JL. Techniques for precise mapping of 226Ra and 228Ra in the ocean. J. Geophys. Res. 1985 p. 6983–94.

Moore WS, Krest J. Distribution of 223Ra and 224Ra in the plumes of the Mississippi and Atchafalaya Rivers and the Gulf of Mexico. Mar Chem. 2004 May;86(3-4):105–19.

Moore WS, Reid DF. Extraction of radium from natural waters using manganese-impregnated acrylic fibers. J Geophys Res. 1973 Dec 20;78(36):8880–6.

Moore WS, Sarmiento JL, Key RM. Submarine groundwater discharge revealed by 228Ra distribution in the upper Atlantic Ocean. Nat Geosci. Nature Publishing Group; 2008 Apr 20;1(5):309–11.

Moore WS, Shaw TJ. Fluxes and behavior of radium isotopes, barium, and uranium in seven Southeastern US rivers and estuaries. Mar Chem. 2008 Jan;108(3-4):236–54.

Moore WS, Wilson AM. Advective flow through the upper continental shelf driven by storms, buoyancy, and submarine groundwater discharge. Earth Planet Sci Lett. 2005 Jul;235(3-4):564–76.

Morel FMM, Price NM. The biogeochemical cycles of trace metals in the oceans. Science. 2003 May 9;300(5621):944–7.

Nakada S, Yasumoto J, Taniguchi M, Ishitobi T. Submarine groundwater discharge and seawater circulation in a subterranean estuary beneath a tidal flat. Hydrol Process. 2011 Aug 15;25(17):2755–63.

Nelson A, Nelson K. Dictionary of applied geology. London: Philosophical Library N.Y.; 1967. p. 421p.

Nielsen KA, Clemmensen LB, Fornós JJ. Middle Pleistocene magnetostratigraphy and susceptibility stratigraphy: data from a carbonate aeolian system, Mallorca, Western Mediterranean. Quat Sci Rev. 2004 Sep;23(16-17):1733–56.

Nielsen P. Tidal dynamics of the water table in beaches. Water Resour Res. 1990 Sep 9;26(9):2127–34.

Oliveira J, Costa P, Braga ES. Seasonal variations of 222Rn and SGD fluxes to Ubatuba embayments, São Paulo. J Radioanal Nucl Chem. 2006 Sep;269(3):689–95.

Ollivier P, Claude C, Radakovitch O, Hamelin B. TIMS measurements of 226Ra and 228Ra in the Gulf of Lion, an attempt to quantify submarine groundwater discharge. Mar Chem. 2008 Apr;109(3-4):337–54.

Padilla A, Pulido-Bosch A. Study of hydrographs of karstic aquifers by means of correlation and cross-spectral analysis. J Hydrol. 1995 Jun;168(1-4):73–89.

Paerl H. Coastal eutrophication and harmful algal blooms: Importance of atmospheric deposition and groundwater as“ new” nitrogen and other nutrient sources. Limnol Oceanogr. 1997;42:1154–65.

Parsons T, Maita Y, Lalli C. A manual of chemical and biological methods for seawater analysis. Pergamon P. Oxford, UK; 1984.

Paulsen RJ, Smith CF, O’Rourke D, Wong T-F. Development and Evaluation of an Ultrasonic Ground Water Seepage Meter. Ground Water. 2001 Nov;39(6):904–11.

Pavlidou A, Papadopoulos VP, Hatzianestis I, Simboura N, Patiris D, Tsabaris C. Chemical inputs from a karstic submarine groundwater discharge (SGD) into an oligotrophic Mediterranean coastal area. Sci Total Environ. 2014 May 7;488-489C:1–13.

Paytan A, Boehm AB, Shellenbarger GG. Bacterial Contamination and Submarine Groundwater Discharge—A Possible Link. Environ Chem. CSIRO PUBLISHING; 2004 Jul 1;1(1):29.

Paytan A, Mackey KRM, Chen Y, Lima ID, Doney SC, Mahowald N, et al. Toxicity of atmospheric aerosols on marine phytoplankton. Proc Natl Acad Sci U S A. 2009 Mar 24;106(12):4601–5.

Paytan A, Shellenbarger GG, Street JH, Gonneea ME, Davis K, Young MB, et al. Submarine groundwater discharge: An important source of new inorganic nitrogen to coral reef ecosystems. Limnol Oceanogr. 2006;51(1 I):343–8.

Pearce F, Crivelli AJ. Characteristics of Mediterranean wetlands — Medwet. Arles: Conservation of Mediterranean wetlands no1; 1994.

Peterson RN, Burnett WC, Glenn CR, Johnson AG. Quantification of point-source groundwater discharges to the ocean from the shoreline of the Big Island, Hawaii. Limnol Oceanogr. 2009;54(3):890–904.

Pfannkuch H. Elsevier's dictionary of hydrogeology. Amsterdam: Elsevier Publishing Company; 1969. p. 168p.

PHIB. Propuesta del Plan Hidrológico de la Demarcación de Baleares. 2008.

Pinardi N, Arneri E, Crise A, Ravaioli M, Zavatarelli M. The physical, sedimentary and ecological structure and variability of shelf areas in the Mediterranean sea (27). In: Robinson AR, Brink KH, editors. Sea, Vol 14B Glob Coast Ocean. Harvard University Press; 2006.

PNUE/PAM/Plan Blue. L'Eau des méditerranéens: Situation et perspectives. Athens: Des, No. 158 de la Série rapports techiques du PAM, PNUE/PAM; 2004.

Polemio M, Casarano D, Limoni PP. Karstic aquifer vulnerability assessment methods and results at a test site (Apulia, southern Italy). Nat Hazards Earth Syst Sci. Copernicus GmbH; 2009 Aug 19;9(4):1461–70.

Porcelli D, Swarzenski P. The behavior of U-and Th-series nuclides in groundwater. Rev Mineral Geochemistry. 2003;52(1):317–61.

Porubsky WP, Weston NB, Moore WS, Ruppel C, Joye SB. Dynamics of submarine groundwater discharge and associated fluxes of dissolved nutrients, carbon, and trace gases to the coastal zone (Okatee River estuary, South Carolina). Geochim Cosmochim Acta. 2014 Apr;131:81–97.

Potot C. Etude hydrochimique du système aquifère de la basse vallée du Var. Apport des éléments traces et des isotopes (Sr, Pb, δ18O, 226, 228Ra). Universite de Nice-Sophia Antipolis-UFR; 2011.

Pujo-Pay M, Conan P, Oriol L, Cornet-Barthaux V, Falco C, Ghiglione J-F, et al. Integrated survey of elemental stoichiometry (C, N, P) from the western to eastern Mediterranean Sea. Biogeosciences. Copernicus GmbH; 2011 Apr 8;8(4):883–99.

Rahaman W, Singh SK. Sr and 87Sr/86Sr in estuaries of western India: Impact of submarine groundwater discharge. Geochim Cosmochim Acta. 2012 May;85:275–88.

Rahman MM, Lee Y, Kim G, Lee K, Han S. Significance of submarine groundwater discharge in the coastal fluxes of mercury in Hampyeong Bay, Yellow Sea. Chemosphere. 2013 Apr;91(3):320–7.

Rama PS, Moore WS. Using the radium quartet for evaluating groundwater input and water exchange in salt marshes. Geochim Cosmochim Acta. 1996 Dec;60(23):4645–52.

Ramadan KA, Seddeek MK, Nijim A, Sharshar T, Badran HM. Radioactivity of sand, groundwater and wild plants in northeast Sinai, Egypt. Isotopes Environ Health Stud. 2011 Dec;47(4):456–69.

Rapaglia J. Submarine groundwater discharge into Venice Lagoon, Italy. Estuaries. 2005;28(5):705–13.

Rapaglia J, Ferrarin C, Zaggia L, Moore WS, Umgiesser G, Garcia-Solsona E, et al. Investigation of residence time and groundwater flux in Venice Lagoon: comparing radium isotope and hydrodynamic models. J Environ Radioact. 2010 a Jul;101(7):571–81.

Rapaglia J, Koukoulas S, Zaggia L, Lichter M, Manfé G, Vafeidis AT. Quantification of submarine groundwater discharge and optimal radium sampling distribution in the Lesina Lagoon, Italy. J Mar Syst. 2012 Mar;91(1):11–9.

Rapaglia J, Di Sipio E, Bokuniewicz H, Maria Zuppi G, Zaggia L, Galgaro A, et al. Groundwater connections under a barrier beach: A case study in the Venice Lagoon. Cont Shelf Res. 2010 b Feb;30(2):119–26.

Rapaglia JP, Bokuniewicz HJ. The effect of groundwater advection on salinity in pore waters of permeable sediments. Limnol Oceanogr. 2009;54(2):630–43.

Reich C, Shinn E, Hickey T, Tihansky A. Tidal and Meteorological Influences on Shallow Marine Groundwater Flow in the Upper Florida Keys. In: Porter J, Porter K, editors. Everglades, Florida Bay, coral reefs Florida Keys. Boca Raton, FL: CRC Press; 2002. p. 659 – 76.

Riedl RJ, Huang N, Machan R. The subtidal pump: a mechanism of interstitial water exchange by wave action. Mar Biol. 1972 Apr;13(3):210–21.

Robinson C, Li L, Prommer H. Tide-induced recirculation across the aquifer-ocean interface. Water Resour Res. 2007 Jul 18;43(7):n/a–n/a.

Rocha C. Density-driven convection during flooding of warm, permeable intertidal sediments: the ecological importance of the convective turnover pump. J Sea Res. 2000 Feb;43(1):1–14.

Rodellas V, Garcia-Orellana J, Garcia-Solsona E, Masqué P, Domínguez JA, Ballesteros BJ, et al. Quantifying groundwater discharge from different sources into a Mediterranean wetland by using 222Rn and Ra isotopes. J Hydrol. 2012;466-467:11–22.

Rodellas V, Garcia-Orellana J, Tovar-Sánchez A, Basterretxea G, López-Garcia JM, Sánchez-Quiles D, et al. Submarine groundwater discharge as a source of nutrients and trace metals in a Mediterranean Bay (Palma Beach, Balearic Islands). Mar Chem. 2014 Jan;160:56–66.

Röper T, Greskowiak J, Massmann G. Detecting Small Groundwater Discharge Springs Using Handheld Thermal Infrared Imagery. Ground Water. 2013 Dec 17;

Roy M, Martin JB, Cherrier J, Cable JE, Smith CG. Influence of sea level rise on iron diagenesis in an east Florida subterranean estuary. Geochim Cosmochim Acta. 2010 Oct;74(19):5560–73.

Sanchez F, Rodriguez-Alvarez MJ. Effect of pH, temperature, conductivity and sediment size on thorium and radium activities along Jucar River (Spain). J Radioanal Nucl Chem. 1999 Dec;242(3):671–81.

Sánchez Navarro JÁ, Coloma López P, Perez-Garcia A. Evaluation of geothermal flow at the springs in Aragón (Spain), and its relation to geologic structure. Hydrogeol J. 2004 Jul 29;12(5):601–9.

Sanchez-Cabeza JA, Ortega M, Merino J, Masqué P. Long-term box modelling of 137Cs in the Mediterranean Sea. J Mar Syst. 2002 Jun;33-34:457–72.

Santos IR, Burnett WC, Chanton J, Mwashote B, Suryaputra IGNA, Dittmar T. Nutrient biogeochemistry in a Gulf of Mexico subterranean estuary and groundwater-derived fluxes to the coastal ocean. Limnol Oceanogr. 2008;53(2):705–18.

Santos IR, Burnett WC, Dittmar T, Suryaputra IGNA, Chanton J. Tidal pumping drives nutrient and dissolved organic matter dynamics in a Gulf of Mexico subterranean estuary. Geochim Cosmochim Acta. 2009 Mar;73(5):1325–39.

Santos IR, Burnett WC, Misra S, Suryaputra IGNA, Chanton JP, Dittmar T, et al. Uranium and barium cycling in a salt wedge subterranean estuary: The influence of tidal pumping. Chem Geol. 2011 Aug;287(1-2):114–23.

Santos IR, Erler D, Tait D, Eyre BD. Breathing of a coral cay: Tracing tidally driven seawater recirculation in permeable coral reef sediments. J Geophys Res. 2010 Dec 3;115(C12):C12010.

Santos IR, Eyre BD, Huettel M. The driving forces of porewater and groundwater flow in permeable coastal sediments: A review. Estuar Coast Shelf Sci. 2012 Feb;98:1–15.

Schmidt A, Gibson JJ, Santos IR, Schubert M, Tattrie K, Weiss H. The contribution of groundwater discharge to the overall water budget of two typical Boreal lakes in Alberta/Canada estimated from a radon mass balance. Hydrol Earth Syst Sci. 2010;14(1):79–89.

Schmidt S, Reyss J-L. Radium as internal tracer of Mediterranean Outflow Water. J Geophys Res. 1996;101(C2):3589.

Scholten JC, Osvath I, Pham MK. 226Ra measurements through gamma spectrometric counting of radon progenies: How significant is the loss of radon? Mar Chem. 2013 Oct;156:146–52.

Scholten JC, Pham MK, Blinova O, Charette MA, Dulaiova H, Eriksson M. Preparation of Mn-fiber standards for the efficiency calibration of the delayed coincidence counting system (RaDeCC). Mar Chem. 2010 Aug;121(1-4):206–14.

Sekulic B. Balance of Average Annual Fresh Water Inflow into the Adriatic Sea. Int J Water Resour Dev. Routledge; 1996 Mar;12(1):89–98.

Shaw TJ, Moore WS, Kloepfer J, Sochaski MA. The flux of barium to the coastal waters of the southeastern USA: the importance of submarine groundwater discharge. Geochim Cosmochim Acta. 1998 Sep;62(18):3047–54.

Shellenbarger GG, Monismith SG, Genin A, Paytan A. The importance of submarine groundwater discharge to the nearshore nutrient supply in the Gulf of Aqaba (Israel). Limnol Oceanogr. 2006;51(4):1876–86.

Sholkovitz E, Herbold C, Charette M. An automated dye-dilution based seepage meter for the time-series measurement of submarine groundwater discharge. Limnol Oceanogr Methods. 2003;1:16 – 28.

Sieyes N de, Yamahara K, Layton B. Submarine discharge of nutrient-enriched fresh groundwater at Stinson Beach, California is enhanced during neap tides. Limnol Oceanogr. 2008;53:1434–45.

Slomp CP, Van Cappellen P. Nutrient inputs to the coastal ocean through submarine groundwater discharge: controls and potential impact. J Hydrol. 2004 Aug;295(1-4):64–86.

Smith AJ. Mixed convection and density-dependent seawater circulation in coastal aquifers. Water Resour Res. 2004 Aug 28;40(8):n/a–n/a.

Smith CG, Cable JE, Martin JB, Roy M. Evaluating the source and seasonality of submarine groundwater discharge using a radon-222 pore water transport model. Earth Planet Sci Lett. 2008 Sep;273(3-4):312–22.

Snyder M, Taillefert M, Ruppel C. Redox zonation at the saline-influenced boundaries of a permeable surficial aquifer: effects of physical forcing on the biogeochemical cycling of iron and manganese. J Hydrol. 2004 Aug;296(1-4):164–78.

Soto-Navarro J, Criado-Aldeanueva F, García-Lafuente J, Sánchez-Román A. Estimation of the Atlantic inflow through the Strait of Gibraltar from climatological and in situ data. J Geophys Res. 2010 Oct 12;115(C10):C10023.

Stewart I, Morhange C. Coastal geomorphology and sea-level change. In: Woodward J, editor. Phys Geogr Mediterr. New York: Oxford University Press Inc.; 2009. p. 385–413.

Stieglitz T, Rapaglia J, Bokuniewicz H. Estimation of submarine groundwater discharge from bulk ground electrical conductivity measurements. J Geophys Res. 2008 a Aug 6;113(C8):C08007.

Stieglitz T, Taniguchi M, Neylon S. Spatial variability of submarine groundwater discharge, Ubatuba, Brazil. Estuar Coast Shelf Sci. 2008 b Feb;76(3):493–500.

Stieglitz TC, van Beek P, Souhaut M, Cook PG. Karstic groundwater discharge and seawater recirculation through sediments in shallow coastal Mediterranean lagoons, determined from water, salt and radon budgets. Mar Chem. 2013 Oct;156:73–84.

Stieglitz TC, Rapaglia J, Krupa SC. An effect of pier pilings on nearshore submarine groundwater discharge from a (partially) confined aquifer. Estuaries and Coasts. 2007;30(3):542–50.

Street JH, Knee KL, Grossman EE, Paytan A. Submarine groundwater discharge and nutrient addition to the coastal zone and coral reefs of leeward Hawai'i. Mar Chem. 2008 Apr;109(3-4):355–76.

Su N, Burnett WC, MacIntyre HL, Liefer JD, Peterson RN, Viso R. Natural Radon and Radium Isotopes for Assessing Groundwater Discharge into Little Lagoon, AL: Implications for Harmful Algal Blooms. Estuaries and Coasts. 2013 Nov 8;1–18.

Sun Y, Torgersen T. The effects of water content and Mn-fiber surface conditions on measurement by emanation. Mar Chem. 1998 Nov;62(3-4):299–306.

Superville P-J, Prygiel E, Magnier A, Lesven L, Gao Y, Baeyens W, et al. Daily variations of Zn and Pb concentrations in the Deûle River in relation to the resuspension of heavily polluted sediments. Sci Total Environ. 2014 Feb 1;470-471:600–7.

Swarzenski P., Reich C., Spechler R., Kindinger J., Moore W. Using multiple geochemical tracers to characterize the hydrogeology of the submarine spring off Crescent Beach, Florida. Chem Geol. 2001 Sep;179(1-4):187–202.

Swarzenski PW. U/Th series radionuclides as coastal groundwater tracers. Chem Rev. American Chemical Society; 2007 Feb;107(2):663–74.

Swarzenski PW, Burnett WC, Greenwood WJ, Herut B, Peterson R, Dimova N, et al. Combined time-series resistivity and geochemical tracer techniques to examine submarine groundwater discharge at Dor Beach, Israel. Geophys Res Lett. 2006 Dec 23;33(24):L24405.

Talbot JM, Kroeger KD, Rago A, Allen MC, Charette MA. Nitrogen flux and speciation through the subterranean estuary of Waquoit Bay, Massachusetts. Biol Bull. 2003;205(2):244–5.

Taniguchi M, Burnett WC, Cable JE, Turner J V. Investigation of submarine groundwater discharge. Hydrol Process. 2002 Aug 15;16(11):2115–29.

Taniguchi M, Burnett WC, Dulaiova H, Kontar EA, Povinec PP, Moore WS. Submarine groundwater discharge measured by seepage meters in sicilian coastal waters. Cont Shelf Res. 2006 May;26(7):835–42.

Taniguchi M, Burnett WC, Smith CF, Paulsen RJ, O'Rourke D, Krupa SL, et al. Spatial and temporal distributions of submarine groundwater discharge rates obtained from various types of seepage meters at a site in the Northeastern Gulf of Mexico. Biogeochemistry. 2003 Nov;66(1/2):35–53.

Taniguchi M, Fukuo Y. Continuous Measurements of Ground-Water Seepage Using an Automatic Seepage Meter. Ground Water. 1993 Jul;31(4):675–9.

Tolman C. Ground Water. New York: McGraw Hill Book Co.; 1937. p. 593p.

Top Z, Brand L, Corbett R, Burnett W, Chanton J. Helium and radon as tracers of groundwater input into Florida Bay. J Coast Res. 2001;17:859–68.

Torres MA, Barros MP, Campos SCG, Pinto E, Rajamani S, Sayre RT, et al. Biochemical biomarkers in algae and marine pollution: a review. Ecotoxicol Environ Saf. 2008 Oct;71(1):1–15.

Tovar-Sánchez A. Comprehensive Sampling and Sample Preparation. Compr. Sampl. Sample Prep. Elsevier; 2012. p. 317–34.

Tovar-Sanchez A, Basterretxea G, Rodellas V, Sánchez-Quiles D, Garcia-Orellana J, Masqué P, et al. Contribution of groundwater discharge to the coastal dissolved nutrients and trace metal concentrations in Majorca Island: karstic vs detrital systems. Environ Sci Technol. American Chemical Society; 2014 Sep 12;

Tovar-Sánchez A, Serón J, Marbà N, Arrieta JM, Duarte CM. Long-term records of trace metal content of western Mediterranean seagrass (Posidonia oceanica) meadows: Natural and anthropogenic contributions. J Geophys Res. 2010 Apr 24;115(G2):G02006.

Tribovillard N, Algeo TJ, Lyons T, Riboulleau A. Trace metals as paleoredox and paleoproductivity proxies: An update. Chem Geol. 2006 Aug;232(1-2):12–32.

Tse KC, Jiao JJ. Estimation of submarine groundwater discharge in Plover Cove, Tolo Harbour, Hong Kong by 222Rn. Mar Chem. 2008 Sep;111(3-4):160–70.

Tugrul S, Besiktepe T, Salihoglu I. Nutrient exchange fluxes between the Aegean and Black Seas through the Marmara Sea. Mediterr Mar Sci. 2002 Jun 1;3(1):33–42.

Twining BS, Baines SB. The trace metal composition of marine phytoplankton. Ann Rev Mar Sci. 2013 Jan;5:191–215.

UNEP/MAP. State of the Mediterranean Marine and Coastal Environment. Athens; 2012.

UNEP/MAP/MED POL. Riverine transport of water, sediments and pollutants to the Mediterranean Sea. MAP Techni. MAP Tech. Rep. Ser. No 141. Athens: UNEP/MAP; 2003.

UNESCO. Submarine Groundwater Discharge: Management Implications, Measurements and Effects. Paris: UNESCO; 2004. p. 35.

UNSCEAR. Sources and effects of ionizing radiation. Vol I: sources. United Nations. Scientific Committee on the Effects of Atomic Radiation. United Nations Publications; 2000.

Valiela I, Costa J, Foreman K, Teal JM, Howes B, Aubrey D. Transport of groundwater-borne nutrients from watersheds and their effects on coastal waters. Biogeochemistry. 1990 Jun 1;10(3):177–97.

Valiela I, Foreman K, LaMontagne M, Hersh D, Costa J, Peckol P, et al. Couplings of Watersheds and Coastal Waters: Sources and Consequences of Nutrient Enrichment in Waquoit Bay, Massachusetts. Estuaries. 1992 Dec;15(4):443.

Waska H, Kim S, Kim G, Peterson RN, Burnett WC. An efficient and simple method for measuring (226)Ra using the scintillation cell in a delayed coincidence counting system (RaDeCC). J Environ Radioact. 2008 Dec;99(12):1859–62.

Webster IT, Hancock GJ, Murray AS. Modelling the effect of salinity on radium desorption from sediments. Geochim Cosmochim Acta. 1995;59(12):2469–76.

Webster IT, Norquay SJ, Ross FC, Wooding RA. Solute Exchange by Convection Within Estuarine Sediments. Estuar Coast Shelf Sci. 1996 Feb;42(2):171–83.

Weinstein Y, Burnett WC, Swarzenski PW, Shalem Y, Yechieli Y, Herut B. Role of aquifer heterogeneity in fresh groundwater discharge and seawater recycling: An example from the Carmel coast, Israel. J Geophys Res. 2007 Dec 25;112(C12):C12016.

Weinstein Y, Less G, Kafri U, Herut B. Submarine groundwater discharge in the southeastern Mediterranean (Israel). Radioact Environ. Elsevier; 2006;8(C):360–72.

Weinstein Y, Yechieli Y, Shalem Y, Burnett WC, Swarzenski PW, Herut B. What is the role of fresh groundwater and recirculated seawater in conveying nutrients to the coastal ocean? Environ Sci Technol. 2011 Jun 15;45(12):5195–200.

Werner AD, Alcoe DW, Ordens CM, Hutson JL, Ward JD, Simmons CT. Current Practice and Future Challenges in Coastal Aquifer Management: Flux-Based and Trigger-Level Approaches with Application to an Australian Case Study. Water Resour Manag. Springer Netherlands; 2011 May 1;25(7):1831–53.

De Weys J, Santos IR, Eyre BD. Linking groundwater discharge to severe estuarine acidification during a flood in a modified wetland. Environ Sci Technol. 2011 Apr 15;45(8):3310–6.

Wilson AM. Fresh and saline groundwater discharge to the ocean: A regional perspective. Water Resour Res. 2005 Feb 16;41(2):n/a–n/a.

Wilson AM, Moore WS, Joye SB, Anderson JL, Schutte CA. Storm-driven groundwater flow in a salt marsh. Water Resour Res. 2011 Feb 19;47(2):n/a–n/a.

Wilson AM, Morris JT. The influence of tidal forcing on groundwater flow and nutrient exchange in a salt marsh-dominated estuary. Biogeochemistry. 2011 Jan 15;108(1-3):27–38.

Wilson J, Rocha C. Regional scale assessment of Submarine Groundwater Discharge in Ireland combining medium resolution satellite imagery and geochemical tracing techniques. Remote Sens Environ. 2012 Apr;119:21–34.

Windom HL, Moore WS, Niencheski LFH, Jahnke RA. Submarine groundwater discharge: A large, previously unrecognized source of dissolved iron to the South Atlantic Ocean. Mar Chem. 2006 Dec;102(3-4):252–66.

Yang H-S, Hwang D-W, Kim G. Factors controlling excess radium in the Nakdong River estuary, Korea: submarine groundwater discharge versus desorption from riverine particles. Mar Chem. 2002 Apr;78(1):1–8.

Yau VM, Schiff KC, Arnold BF, Griffith JF, Gruber JS, Wright CC, et al. Effect of submarine groundwater discharge on bacterial indicators and swimmer health at Avalon Beach, CA, USA. Water Res. 2014 Aug 1;59:23–36.

Young MB, Gonneea ME, Fong DA, Moore WS, Herrera-Silveira J, Paytan A. Characterizing sources of groundwater to a tropical coastal lagoon in a karstic area using radium isotopes and water chemistry. Mar Chem. 2008 Apr;109(3-4):377–94.

Zarroca M, Linares R, Rodellas V, Garcia-Orellana J, Roqué C, Bach J, et al. Delineating coastal groundwater discharge processes in a wetland area by means of electrical resistivity imaging, 224 Ra and 222 Rn. Hydrol Process. 2014 Feb 15;28(4):2382–95.

Zektser IS, Everett LG, Dzhamalov RG. Submarine Groundwater. Boca Raton, FL: CRC Press; 2007.

Appendix

A.1. ^{228}Ra concentration in samples from the Mediterranean Sea

Table A1. ^{228}Ra concentrations in the Mediterranean Sea

Sample code	Date	Lat.	Lon.	Depth	^{228}Ra	Cruise/Ref
	d/m/y			m	dpm·m^3	
MET00	05/04/11	25.795	39.847	5	56.1 ± 1.7	M84/3
MET01	06/04/11	25.686	38.329	5	34.6 ± 1.6	M84/3
MET287	06/04/11	25.600	37.667	5	31.1 ± 1.8	M84/3
MET288	07/04/11	26.218	35.649	5	24.3 ± 0.7	M84/3
MET289	07/04/11	26.604	35.274	5	23.4 ± 1.6	M84/3
MET290	07/04/11	27.500	34.335	5	30.4 ± 3.6	M84/3
MET291	08/04/11	33.001	34.067	5	25.0 ± 1.8	M84/3
MET292	09/04/11	35.173	33.990	5	33.6 ± 1.4	M84/3
MET293	09/04/11	34.421	34.000	5	29.6 ± 1.8	M84/3
MET294	10/04/11	31.002	33.700	5	32.6 ± 1.7	M84/3
MET295	10/04/11	28.772	33.580	5	27.9 ± 1.7	M84/3
MET295	11/04/11	28.772	33.580	170	26.9 ± 3.0	M84/3
MET295	11/04/11	28.770	33.580	1500	9.2 ± 2.2	M84/3
MET297	11/04/11	26.019	34.399	5	25.9 ± 1.5	M84/3
MET298	12/04/11	24.332	34.500	5	24.3 ± 1.5	M84/3
MET299	12/04/11	22.500	35.000	5	29.3 ± 1.8	M84/3
MET300	12/04/11	22.466	35.750	5	33.8 ± 3.3	M84/3
MET301	13/04/11	21.484	35.233	5	24.9 ± 1.8	M84/3
MET302	13/04/11	20.350	35.067	5	25.7 ± 1.7	M84/3
MET303	13/04/11	19.001	35.067	5	31.0 ± 1.3	M84/3
MET304	14/04/11	17.250	35.601	5	32.1 ± 3.2	M84/3
MET304	14/04/11	17.250	35.601	170	29.1 ± 3.1	M84/3
MET304	14/04/11	17.250	35.600	1500	8.4 ± 2.7	M84/3
MET306	15/04/11	19.000	36.500	5	33.9 ± 2.0	M84/3
MET307	15/04/11	19.300	37.900	5	30.4 ± 1.5	M84/3
MET308	15/04/11	18.999	38.500	5	28.9 ± 1.8	M84/3
MET309	16/04/11	18.801	39.500	5	30.1 ± 1.9	M84/3
MET310	16/04/11	19.166	40.167	5	27.2 ± 1.4	M84/3
MET312	16/04/11	18.000	41.250	5	44.2 ± 2.0	M84/3
MET312	16/04/11	18.000	41.250	350	32.3 ± 3.0	M84/3
MET312	16/04/11	18.000	41.250	900	33.2 ± 3.8	M84/3
MET314	17/04/11	18.417	38.500	5	35.4 ± 1.9	M84/3
MET315	17/04/11	18.000	37.130	5	33.8 ± 1.9	M84/3
MET316	19/04/11	11.499	38.601	5	22.2 ± 1.4	M84/3
MET317	19/04/11	11.751	39.220	5	23.9 ± 1.7	M84/3
MET318	19/04/11	11.302	40.300	5	24.8 ± 1.5	M84/3
MET318	20/04/11	11.302	40.300	400	20.6 ± 2.5	M84/3
MET318	19/04/11	11.300	40.300	1500	14.7 ± 3.1	M84/3
MET320	20/04/11	10.610	38.750	5	23.0 ± 1.6	M84/3
MET321	20/04/11	9.400	38.250	5	26.7 ± 2.9	M84/3
MET322	21/04/11	8.198	38.201	5	22.4 ± 1.9	M84/3
MET323	21/04/11	6.899	38.500	5	22.9 ± 1.5	M84/3
MET324	21/04/11	5.599	38.650	5	22.8 ± 1.3	M84/3
MET325	22/04/11	4.500	38.450	5	22.9 ± 1.2	M84/3
MET325	22/04/11	4.500	38.450	400	16.3 ± 2.6	M84/3
MET325	22/04/11	4.500	38.450	1500	13.0 ± 3.0	M84/3
MET327	22/04/11	3.200	38.099	5	20.3 ± 1.7	M84/3
MET328	22/04/11	2.001	37.900	5	25.7 ± 1.4	M84/3
MET330	23/04/11	0.900	37.650	5	24.4 ± 1.8	M84/3
MET331	23/04/11	0.000	37.050	5	21.1 ± 1.4	M84/3
MET332	24/04/11	-1.400	36.500	5	25.2 ± 1.7	M84/3
MET333	24/04/11	-2.800	36.100	5	20.0 ± 1.4	M84/3

MET334	24/04/11	-4.400	36.101	5	17.7 ± 1.5	M84/3
MET335	24/04/11	-5.000	36.000	5	16.8 ± 1.6	M84/3
MET335	24/04/11	-5.000	36.000	600	11.8 ± 1.4	M84/3
MET337	25/04/11	-5.366	36.001	5	21.1 ± 1.7	M84/3
MET339	25/04/11	-7.000	35.900	5	14.6 ± 1.1	M84/3
MS_Ra_1	11/05/13	13.184	37.037	5	27.4 ± 1.7	GA04S
MS_Ra_1	11/05/13	13.184	37.037	100	28.5 ± 2.9	GA04S
MS_Ra_1	11/05/13	13.184	37.037	300	21.7 ± 2.3	GA04S
MS_Ra_4	11/05/13	15.317	36.006	5	31.5 ± 1.8	GA04S
MS_Ra_5	14/05/13	24.323	33.811	5	26.5 ± 1.6	GA04S
MS_Ra_5	14/05/13	24.323	33.811	200	28.0 ± 2.8	GA04S
MS_Ra_5	14/05/13	24.323	33.811	1500	6.2 ± 2.5	GA04S
MS_Ra_8	26/05/13	16.668	37.818	5	30.4 ± 1.1	GA04S
MS_Ra_9	27/05/13	12.514	39.829	5	27.4 ± 4.8	GA04S
MS_Ra_10	29/05/13	7.472	41.335	5	17.0 ± 3.4	GA04S
MS_Ra_11	30/05/13	5.666	41.317	5	19.5 ± 1.4	GA04S
MS_Ra_11	30/05/13	5.666	41.317	225	15.2 ± 2.0	GA04S
MS_Ra_11	30/05/13	5.666	41.317	1500	7.7 ± 1.7	GA04S
MS_Ra_14	30/05/13	5.946	40.070	5	25.4 ± 1.6	GA04S
MS_Ra_15	31/05/13	4.277	40.624	5	21.5 ± 1.6	GA04S
MS_Ra_16	31/05/13	3.319	40.951	5	23.8 ± 1.3	GA04S
Geost2	05/05/08	0.614	40.215	5	42.7 ± 6.7	EDASMAR
Geost5	05/05/08	1.354	39.952	5	35.7 ± 3.9	EDASMAR
Geost8	06/05/08	2.077	39.663	5	30.9 ± 3.8	EDASMAR
Pac32	22/03/09	4.110	41.999	5	28.4 ± 3.3	FAMOSO1
Pac32	22/03/09	4.110	41.999	245	14.9 ± 3.6	FAMOSO1
Pac32	22/03/09	4.110	41.999	1000	14.4 ± 4.2	FAMOSO1
Dardanelles	04/06/13	26.375	40.116	5	108 ± 8.3	65PE370
Marmara	04/06/13	27.565	40.833	5	101 ± 7.1	65PE370
BARMED1	15/02/03	7.870	43.420	30	21.0 ± 3.0	van Beek et al. 2009
BARMED1	15/02/03	7.870	43.420	100	15.0 ± 1.0	van Beek et al. 2009
BARMED1	15/02/03	7.870	43.420	250	12.0 ± 1.4	van Beek et al. 2009
BARMED1	15/02/03	7.870	43.420	400	7.0 ± 2.1	van Beek et al. 2009
BARMED2	23/03/03	7.870	43.420	15	23.0 ± 2.0	van Beek et al. 2009
BARMED2	23/03/03	7.870	43.420	100	12.0 ± 1.0	van Beek et al. 2009
BARMED2	23/03/03	7.870	43.420	185	12.0 ± 1.5	van Beek et al. 2009
BARMED2	23/03/03	7.870	43.420	400	6.0 ± 1.2	van Beek et al. 2009
BARMED2	23/03/03	7.870	43.420	600	7.0 ± 1.6	van Beek et al. 2009
BARMED2	23/03/03	7.870	43.420	1000	4.0 ± 0.8	van Beek et al. 2009
BARMED3	24/06/03	7.870	43.420	5	15.0 ± 2.0	van Beek et al. 2009
BARMED3	24/06/03	7.870	43.420	45	16.0 ± 2.0	van Beek et al. 2009
BARMED3	24/06/03	7.870	43.420	100	11.0 ± 2.0	van Beek et al. 2009
BARMED3	24/06/03	7.870	43.420	200	10.0 ± 1.0	van Beek et al. 2009
BARMED4	15/05/03	7.870	43.420	10	20.0 ± 1.0	van Beek et al. 2009
BARMED4	15/05/03	7.870	43.420	50	14.0 ± 1.5	van Beek et al. 2009
BARMED4	15/05/03	7.870	43.420	1000	4.0 ± 1.1	van Beek et al. 2009
BARMED4	15/05/03	7.870	43.420	1700	6.0 ± 1.4	van Beek et al. 2009
MT17	01/11/02	4.206	43.267	5	61.2	Ollivier et al. 2008
MT19	29/10/02	4.223	42.676	5	52.4	Ollivier et al. 2008
ADR-4miles	May 2004	12.497	45.382	5	88.0 ± 7.0	Garcia-Solsona et al. 2008b
E-sup	Aug 1989	6.130	40.200	10	17.9 ± 1.9	Schmidt and Reyss 1996
E-deep	Aug 1989	6.130	40.200	1000	6.1 ± 0.7	Schmidt and Reyss 1996
F-deep	Jan 1989	-1.200	36.680	1000	4.9 ± 0.4	Schmidt and Reyss 1996
SIC1	Apr 1967	36.500	13.900	5	38.9	Moore 2006
SIC2	Apr 1988	35.500	15.200	5	23.9	Moore 2006
SIC3	Jan 1990	36.500	16.000	5	23.2	Moore 2006
SIC56	Apr 1988	36.000	20.200	5	23.6	Moore 2006

A.2. Sub-basins: volumes, ^{228}Ra concentrations and inventories

The Mediterranean Sea was divided into nine sub-basins defined according to its physiography and general circulation patterns, based on the distribution suggested by Bethoux and Gentili (Bethoux and Gentili 1996) and Sánchez-Cabeza et al. (2002)). Each region was split in three layers according to the water masses (Sanchez-Cabeza et al. 2002): surface water (SW, from 0 to 220m), intermediate water (LIW, from 220 to 60 m), and deep water (DW, deeper than 600 m). Notice that the division depths for the Ionian and the Levantine sub-basins are slightly different (LIW range from 150 to 600 m there). The salinity-derived ^{228}Ra depth profiles for all the stations were used to obtain weighted average ^{228}Ra concentrations for each of the resulting 27 boxes, which are presented in Table A.2 and Fig. 6.1. The average ^{228}Ra concentrations were multiplied by the box volume to obtain a box inventory. All the SW and LIW boxes were added up to calculate the total ^{228}Ra inventory for the upper Mediterranean Sea. Inventories in DW are not included in Table S-2 because they are not used to derive the total inventory for the upper Mediterranean Sea.

The standard deviation was used as the uncertainty associated to the box average concentrations, while the uncertainty of the box volume was assumed to be 10%. Uncertainties associated to the ^{228}Ra box inventories and the total ^{228}Ra inventory for the Mediterranean Sea were obtained by uncertainty propagation for uncorrelated variables. Given that the Central basin could not be properly sampled due to political issues that limited our access to the area, the uncertainty associated to the ^{228}Ra inventory in this basin was considered to be 100%.

Table A2. Box volumes and average ^{228}Ra concentrations and total inventories.

Basin name	Depth	Volume	$^{228}Ra_{conc}$	$^{228}Ra_{inventory}$
	m	10^{12} m^3	dpm·m^3	10^{15} dpm
SURFACE (SW)				
Alboran (ALB)	0 - 220	128 ± 13	16.1 ± 0.5	0.27 ± 0.03
South-Western (SWE)	0 - 220	102 ± 10	20 ± 4	2.1 ± 0.5
North-Western (NWE)	0 - 220	28 ± 3	34 ± 16	0.9 ± 0.4
Tyrrhenian (TYR)	0 - 220	39 ± 4	22.2 ± 0.8	0.9 ± 0.1
Central (CEN)	0 - 220	88 ± 9	27.4 ± 1.1	2.4 ± 2.4
Adriatic (ADR)	0 - 220	25 ± 2	45 ± 17	1.1 ± 0.4
Ionian (ION)	0 - 150	71 ± 7	29 ± 2	2.1 ± 0.3
Aegean (AEG)	0 - 220	37 ± 4	34 ± 11	1.3 ± 0.4
Levantine (LEV)	0 - 150	68 ± 7	28 ± 2	1.9 ± 0.2
INTERMEDIATE (LIW)				
ALB	220 - 600	1.6 ± 0.2	12.1 ± 1.0	0.022 ± 0.003
SWE	220 - 600	150 ± 15	16 ± 3	2.8 ± 0.7
NWE	220 - 600	34 ± 3	25 ± 9	1.0 ± 0.4
TYR	220 - 600	58 ± 6	20.4 ± 0.1	1.36 ± 0.14
CEN	220 - 600	130 ± 13	23 ± 2	3.4 ± 3.4
ADR	220 - 600	33 ± 3	33.8 ± 0.6	1.28 ± 0.13
ION	150 - 600	170 ± 17	22 ± 3	4.9 ± 0.8
AEG	220 - 600	55 ± 6	28 ± 3	1.8 ± 0.3
LEV	150 - 600	160 ± 16	19 ± 2	4.0 ± 0.6
DEEP (DW)				
ALB	> 600		4.9 ± 0.4	
SWE	> 600		13 ± 3	
NWE	> 600		14 ± 4	
TYR	> 600		15 ± 3	
CEN	> 600		8 ± 8	
ADR	> 600		33 ± 4	
ION	> 600		8 ± 3	
AEG	> 600		34 ± 13	
LEV	> 600		9 ± 2	
TOTAL UPPER MS				334 ± 45

A.3. ^{228}Ra mass balance

All the parameters used in the ^{228}Ra mass balance to obtain the global estimate of SGD to the Mediterranean Sea are shown in Table S-3 (Outputs) and S-4 (Inputs). Details on the calculations are described in the following sections. Uncertainties associated to the calculations were obtained by uncertainty propagation for uncorrelated variables.

Table A3. ^{228}Ra mass balance - Outputs

^{228}Ra outputs		Units	Ref.
λ_{228}	0.12	yr^{-1}	
^{228}Ra inventory	33 ± 5	$(\cdot 10^{15})$ dpm	This study
Decay	**4.0** ± 0.5	**$(\cdot 10^{15})$ dpm·yr^{-1}**	
Advection to DW	**1.97** ± 0.08	**$(\cdot 10^{15})$ dpm·yr^{-1}**	
Scavenging rate (aprox)	0.002	yr^{-1}	Moore et al. 2008
Particle scavenging	**0.067** ± 0.009	**$(\cdot 10^{15})$ dpm·yr^{-1}**	
Outflow to the Atlantic	25 ± 2	$(\cdot 10^{12})$ m^3·yr^{-1}	Soto-Navarro et al. 2010
Outflow ^{228}Ra conc	12.1 ± 0.4	dpm·m^{-3}	a
Outflow (Gibraltar)	**0.30** ± 0.03	**$(\cdot 10^{15})$ dpm·yr^{-1}**	
Outflow to Black Sea	1.01	$(\cdot 10^{12})$ m^3·yr^{-1}	Tugrul et al. 2002
Outflow ^{228}Ra conc	56 ± 2	dpm·m^{-3}	b
Outflow (Dardanelles)	**0.057** ± 0.002	**$(\cdot 10^{15})$ dpm·yr^{-1}**	
TOTAL OUTPUTS	**6.4** ± 0.5	**$(\cdot 10^{15})$ dpm·yr^{-1}**	

a ^{228}Ra concentration measured in LIW from the Alboran Sea (MET335)
b ^{228}Ra concentration measured in SW from the northern Aegean Sea (MET00)

Table A4. ^{228}Ra mass balance - Inputs

^{228}Ra inputs			Units	Ref.
Riverine water discharge	0.31		$(\cdot 10^{12})$ $m^3 \cdot yr^{-1}$	Ludwig et al. 2009
Inputs of suspended particles	730		$(\cdot 10^{12})$ $g \cdot yr^{-1}$	UNEP/MAP/MED POL 2003
River ^{228}Ra conc	130	± 50	$dpm \cdot m^{-3}$	
Ra desorption from particles	0.5	± 0.4	$dpm \cdot g^{-1}$	
Riverine ^{228}Ra water inputs	0.04	± 0.02	$(\cdot 10^{15})$ dpm	
Riverine ^{228}Ra particle inputs	0.4	± 0.3	$(\cdot 10^{15})$ dpm	
Rivers	**0.4**	± 0.3	**$(\cdot 10^{15})$ $dpm \cdot yr^{-1}$**	
Atmospheric dust inputs	41	± 20	$(\cdot 10^{12})$ $g \cdot yr^{-1}$	Guerzoni et al. 1999
Ra desorption from particles	2		$dpm \cdot g^{-1}$	
Atmospheric dust	**0.08**	± 0.03	**$(\cdot 10^{15})$ $dpm \cdot yr^{-1}$**	
Continental shelf area	0.49		$(\cdot 10^{12})$ m^2	IOC 1981
Slope area	0.31		$(\cdot 10^{12})$ m^2	IOC 1981
Fraction fine-grained sediments	0.35			Emelyanov et al. 1996
Fraction coarse-grained sediments	0.65			Emelyanov et al. 1996
Flux from fine-grained shelf sediments	11	± 5	$(\cdot 10^{3})$ $dpm \cdot m^{-2} \cdot yr^{-1}$	Moore et al. 2008
Flux from coarse-grained shelf sediments	230	± 110	$dpm \cdot m^{-2} \cdot yr^{-1}$	Moore et al. 2008
Flux from slope	2.3	± 1.1	$(\cdot 10^{3})$ $dpm \cdot m^{-2} \cdot yr^{-1}$	Moore et al. 2008
Fine-grained shelf sediments	1.9	± 0.9	$dpm \cdot yr^{-1}$	
Coarse-grained shelf sediments	0.07	± 0.04	$dpm \cdot yr^{-1}$	
Slope sediments	0.7	± 0.3	$dpm \cdot yr^{-1}$	
Sediments	**2.7**	± 0.9	**$(\cdot 10^{15})$ $dpm \cdot yr^{-1}$**	
Advection from DW	**1.1**	± 0.2	**$(\cdot 10^{15})$ $dpm \cdot yr^{-1}$**	
Inflow from the Atlantic	26	± 2	$(\cdot 10^{12})$ $m^3 \cdot yr^{-1}$	Soto-Navarro et al. 2010
Inflow ^{228}Ra conc	14.6	± 1.1	$dpm \cdot m^{-3}$	c
^{228}Ra inflow (Gibraltar)	**0.4**	± 0.0	**$(\cdot 10^{15})$ $dpm \cdot yr^{-1}$**	
Input from Black Sea	1.3		$(\cdot 10^{12})$ $m^3 \cdot yr^{-1}$	Tugrul et al. 2002
Inflow ^{228}Ra conc	105	± 5	$dpm \cdot m^{-3}$	d
^{228}Ra inflow (Dardanelles)	**0.137**	± 0.006	**$(\cdot 10^{15})$ $dpm \cdot yr^{-1}$**	
TOTAL INPUTS (w/o SGD)	**4.7**	± 1.0	**$(\cdot 10^{15})$ $dpm \cdot yr^{-1}$**	

a. ^{228}Ra concentration measured in the Atlantic Ocean (MET339)
b. Average ^{228}Ra concentration measured in Dardanelles strait and Marmara Sea

A.4. Advection of ^{228}Ra from/to deep waters

Water flows between DW and upper layers (SW and LIW) detailed in Bethoux and Gentili (1996) and Sánchez-Cabeza et al. (2002) were used to derive the transfer rates of ^{228}Ra from/to DW. To do so, ^{228}Ra concentration in the initial box was multiplied by the water flow (Table A5).

Table A5. ^{228}Ra fluxes from/to deep waters obtained from water transfer rates and ^{228}Ra concentrations.

From	To	Water flux	$^{228}Ra_{con}$	$^{228}Ra_{flux}$
		10^{12} m^3·yr^{-1}	dpm·m^{-3}	10^{14} dpm·yr^{-1}
Outputs to DW				
SWE-LIW	SWE-DW	7.4	16 ± 3	1.2 ± 0.3
NWE-LIW	NWE-DW	3.7	25 ± 9	0.9 ± 0.3
CEN-LIW	CEN-DW	9.5	23 ± 2	2.1 ± 0.2
CEN-LIW	ION-DW	32	23 ± 2	7.1 ± 0.6
ADR-LIW	ADR-DW	9.8	33.8 ± 0.6	3.33 ± 0.06
ADR-LIW	ION-DW	0.1	33.8 ± 0.6	0.043 ± 0.010
ION-LIW	ION-DW	14	22 ± 3	3.0 ± 0.4
AEG-LIW	AEG-DW	3.0	28 ± 3	0.84 ± 0.10
AEG-LIW	LEV-DW	1.8	28 ± 3	0.51 ± 0.06
LEV-LIW	LEV-DW	3.0	19 ± 2	0.58 ± 0.07
TOTAL OUTPUTS				**19.7 ± 0.8**
Inputs from DW				
SWE-DW	SWE-LIW	6.3	13 ± 3	0.8 ± 0.2
TYR-DW	TYR-LIW	4.1	15 ± 3	0.60 ± 0.13
CEN-DW	CEN-LIW	9.5	8 ± 8	0.8 ± 0.8
ION-DW	CEN-LIW	50	8 ± 3	4.2 ± 1.4
ADR-DW	ADR-LIW	5.0	33 ± 4	1.7 ± 0.2
AEG-DW	AEG-LIW	3.0	34 ± 13	1.0 ± 0.4
LEV-DW	AEG-LIW	12	9 ± 2	1.1 ± 0.3
LEV-DW	LEV-LIW	5.0	9 ± 2	0.46 ± 0.11
ALB-DW	ALB-LIW	0.7	4.9 ± 0.4	0.036 ± 0.010
TOTAL INPUTS				**11 ± 2**

A.5. ^{228}Ra from river discharge

Few studies have reported the concentration of dissolved ^{228}Ra in rivers discharging to the Mediterranean Sea (Table A6). However, concentrations of dissolved ^{228}Ra in different rivers varied in a narrow range (from 80 to 180 dpm·m^{-3}), similar to concentrations measured elsewhere (e.g. Krest et al. 1999). A concentration of 130 ± 50 dpm·m^{-3} captures all the reported values.

Table A6. Dissolved ^{228}Ra concentration in rivers from the Mediterranean Sea

Study site	**^{228}Ra** dpm·m^3	**Ref.**
Rhone River, France	140 ± 3	Ollivier et al. 2008
Var River, France	78 ± 7	Potot 2011
Silone River, Italy	117 ± 20	Garcia-Solsona et al. 2008b
Venice rivers, Italy	180 ± 2	Rapaglia et al. 2010a
Ebre River, Spain	165 ± 14	This study

Several works have estimated the amount of ^{228}Ra desorbed from suspended riverine particles when they enter the coastal sea (Table S-7). A desorbed flux of 0.5 ± 0.4 dpm per gram of suspended particles includes most of these estimates, excluding only the upper range of the estimates for the Amazon River shelf area (Moore et al. 1995). The range selected includes the ^{228}Ra desorption flux estimated for suspended particles of the Rhone River (Ollivier et al. 2008), the only estimate for Mediterranean rivers.

Table A7. Estimated ^{228}Ra desorption fluxes from riverine suspended particles or suspended sediments

Study site	**Method**	**^{228}Ra** dpm·g^{-1}	**Ref.**
Mississipi River, USA	Experiment, river suspended particles	0.74	Krest et al. 1999
Atchafalaya River, USA	Experiment, river suspended particles	0.79	Krest et al. 1999
Gulf of Mexico, USA	Experiment, river suspended particles	0.25	Krest et al. 1999
Red River, USA	Experiment, bottom sediments	0.26	Krest et al. 1999
Amazon River, USA	Experiment, river suspended particles	0.80	Krest et al. 1999
Amazon River, USA	Experiment, river suspended particles	0.8 - 1.8	Moore et al. 1995
Amazon River, USA	Ra/Th activity ratio in sediments	0.80	Moore et al. 1995
Rhone River, France	Estimated combining literature and ^{228}Ra measurements	0.84	Ollivier et al. 2008
Peníscola Marsh, Spain	Experiment, bottom wetland sediments	0.31	Rodellas et al. 2012: Chapter 3

A.6. ^{228}Ra from bottom sediments (depth > 550 m)

The flux of ^{228}Ra released from sediments might be highly variable, as it is a function of several parameters such as ^{232}Th content in sediments, sediment porosity and physical or biological stirring of the sediment. Moore et al. (2008) conducted a detailed revision of the literature to obtain estimates for ^{228}Ra fluxes from continental shelf sediments, differentiating between fine-grained ($11 \cdot 10^3 \pm 6 \cdot 10^3$ dpm·m^{-2}·yr^{-1}) and coarse-grained sediments (230 ± 110 dpm·yr^{-1}), and slope sediments ($2.3 \cdot 10^3 \pm 1.1 \cdot 10^3$ dpm·yr^{-1}). The total continental shelf area of the Mediterranean Sea ($5.0 \cdot 10^{11}$ m^2) was determined by digitalizing the area above 200 m (S(Pinardi et al. 2006)) using the International Bathymetric Chart of the Mediterranean (S(IOC 1981)). The slope area in the upper Mediterranean Sea (depth <600 m) was obtained from the area between the isobaths of 200 and 600 m (IOC 1981) using the same method. To determine the proportion of fine-grained versus coarse-grained in shelf sediments, we digitalized the chart of bottom surface sediments of the Mediterranean Sea (Emelyanov et al. 1996). Continental shelf areas containing more than 50% of sand and silts (categories 1, 2, 3, 4, 5, 8 in the classification of sediments according to gran-size) were considered to be coarse-grained sediments. Areas where clays are the dominant type of sediment (categories 6, 7, 9, 10) were considered fine-grained sediments. We obtained that 35% of the sediments above 200 m are fine-grained sediments, whereas coarse-grained sediments occupy the remaining 65% of the area. The total flux of ^{228}Ra from sediments was estimated from the shelf area covered by fine- and coarse-grained sediments, the slope area in the upper Mediterranean Sea and the ^{228}Ra fluxes reported in Moore et al. (Moore et al. 2008). ^{228}Ra inputs from sediments to the upper Mediterranean Sea are mainly (72%) originated from fine-grained shelf sediments.

A.7. ^{228}Ra concentration in SGD

Since the mass balance is built in terms of ^{228}Ra fluxes, the estimated concentration of ^{228}Ra in coastal groundwater is needed to obtain a water flow. The selection of the appropriate ^{228}Ra concentration in SGD is one of the most critical issues. In order to obtain an appropriate characterization of the ^{228}Ra concentration in SGD inflowing to the Mediterranean Sea, all the ^{228}Ra data in SGD available along the Mediterranean Sea was considered. This includes data reported in the literature, unpublished data from other labs working along the Mediterranean Sea and kindly made available to us and data we collected for this study. Most of the studies collected several ^{228}Ra samples in SGD belonging to the same study site, that were averaged to obtain a single value from each location. Alternatively, in studies where the authors selected a specific sample to characterize the ^{228}Ra concentration in SGD, the selected concentration was used rather than the average of all the samples reported. More than 200 samples were gathered to yield 45 estimates belonging to different locations (Table A8). Given the variability of ^{228}Ra concentrations, the range comprised between the 1st and 3rd quartiles of the dataset is considered the best approach to characterize ^{228}Ra concentration in SGD inflowing to the Mediterranean Sea, as it includes most of the data and excludes extreme concentrations. Selecting this wide range adds large uncertainties to the final SGD estimation, but allows accounting for the likely actual variability of ^{228}Ra in SGD. The resulting SGD flow to the Mediterranean Sea ranges from $2 \cdot 10^{11}$ to $43 \cdot 10^{11}$ $m^3 \cdot yr^{-1}$, with a median SGD of $12 \cdot 10^{11}$ $m^3 \cdot yr^{-1}$. Had we used the mean concentration with lower and upper 1 standard error values (1400 ± 200 $dpm \cdot m^{-3}$), as proposed by Moore et al. (Moore et al. 2008), we would have obtained an SGD estimate with narrower bounds ($3 \cdot 10^{11}$ to $21 \cdot 10^{11}$ $m^3 \cdot yr^{-1}$, with a mean flow of $11 \cdot 10^{11}$ $m^3 \cdot yr^{-1}$).

Table A8. ^{228}Ra concentrations in SGD along the Mediterranean Sea

Study site	SGD $dpm \cdot m^{-3}$	Ref.
Ahuir, Spain	580	This study
Alcalfar, Spain	350	Garcia-Solsona et al. 2010a
Alfacs Bay, Spain	1100	Rodellas et al., in prep
Arenys, Spain	1300	This study
Ashdod, Israel	800	This study
Badum, Spain	1700	Garcia-Solsona et al. 2010b
Calanques, France	960	van Beek et al., pers. comm

Cullera, Spain	610	This study
Dor Beach, Israel	730	This study
El Gorguel, Spain	325	Trezzi et al., in prep
Es Cargol, Spain	640	Basterretxea et al. 2010
Gandia, Spain	1000	This study
Gulf of Roses, Spain	2100	Garcia-Solsona, pers.comm
Gulf of Lion, France	58000	Ollivier et al. 2008
La Palme, France	2400	van Beek et al., pers.comm
Les Fonts, Spain	2000	Garcia-Solsona et al. 2006
Leucate- Estramar, France	1500	van Beek et al., pers.comm
Málaga, Spain	830	Garcia-Solsona, pers.comm
Maresme, Spain	4600	Cerdà et al., in prep
Miramar, Spain	160	This study
North Sinai, Egypt	3000	Ramadan et al. 2011
Oliva, Spain	180	This study
Palma Beach, Spain	400	Rodellas et al. 2014: Chap 5
Peníscola, Spain	1800	Rodellas et al. 2012: Chap 3
Port of Maó, Spain	2300	Chapter 4
Portocolom, Spain	820	Basterretxea et al. 2010
Romàntica, Spain	1500	Tovar-Sanchez et al. 2014
Sa Nau, Spain	1800	Tovar-Sanchez et al. 2014
Salerno, Italy	1700	This study
Santa Ponça, Spain	1300	Basterretxea et al. 2010
Sebkhet Essijoumi, Tunisia	290	Added et al. 2005
Sicily, Italy	400	Moore 2006
Soller, Spain	910	Basterretxea et al. 2010
Stoupa, Greece	72000	Eleftheriou et al. 2013
Tel Aviv, Israel	3700	This study
Thau, France	490	van Beek et al., pers. comm.
Tunisia	2800	Labidi et al. 2010
Tunisia	1700	Labidi et al. 2010
Tunisia	2000	Labidi et al. 2010
Tunisia	10000	Labidi et al. 2010
Tunisia	11000	Labidi et al. 2010
Tunisia	760	Labidi et al. 2010
Valle du Var, France	130	Potot 2011
Venice Lagoon ,Italy	4500	Garcia-Solsona et al. 2008b
Venice Lagoon, Italy	3300	Rapaglia et al. 2010a
Mean (w/o outliers)	1400	
SD (w/o outliers)	1100	
SE (w/o outliers)	200	
Median	1300	
1st Quartile	640	
3rd Quartile	2300	
n	45	

A.8. SGD estimates in local studies

We compiled all the SGD studies conducted in the Mediterranean Sea of which we are aware that estimated a SGD flow for a specific area. For the purpose of comparison, we used flows normalized to the shoreline length. When reported SGD flows were not shore-normalized, we divided these flows by the shore length or bay mouth width. Shore-normalized SGD flows are shown in Table S-9, together with the approximate shore length of the study area. Some of the studies included here are minimum estimates, either because the authors only estimated the fresh fraction of SGD (e.g. Weinstein et al. (2007), Mejías et al. (2012)) or because they adopted conservative approaches (e.g. Moore (2006), Ollivier et al. (2008)).

Table A9. Shore-normalized SGD estimates for different sites of the Mediterranean Sea, together with the approximate coastline length of each study area

Study site	**Shore length** km	**SGD** $(\cdot 10^6)$ $m^3 \cdot km^{-1} \cdot yr^{-1}$	**Ref.**
Alcalfar, Spain	0.4	0.4	Garcia-Solsona et al. 2010a
Badum, Spain	2.5	19	Garcia-Solsona et al. 2010b
Donnalucatta, Italy	0.2	370	Moore 2006
Donnalucatta, Italy	0.04	39	Burnett and Dulaiova 2006
Donnalucatta, Italy	0.04	6	Taniguchi et al. 2006
Dor Beach, Israel	0.1	2.6	Swarzenski et al. 2006
Dor Beach, Israel	0.1	1.8	Weinstein et al. 2007
El Gorguel, Spain	0.73	48	Trezzi et al, in prep
El Maestrat, Spain	45	8.3	Mejías et al. 2012
Gulf of Lyon, France	300	29	Ollivier et al. 2008
La Palme Lagoon, France	6	7.9	Stieglitz et al. 2013
Lesina Lagoon, Italy	25	13	Rapaglia et al. 2012
Marina Lagoon, Egypt	11	8.0	El-Gamal et al. 2012
Palma Beach, Spain	4.4	4.6	Rodellas et al. 2014: Chap. 5
Peníscola, Spain	3	6.3	Rodellas et al. 2012: Chap. 3
Port of Maó, Spain	18	2.3	Chapter 4
Romàntica, Spain	0.15	0.4	Tovar-Sanchez et al. 2014
Sa Nau, Spain	0.08	21	Tovar-Sanchez et al. 2014
Santanyí, Spain	0.07	1.4	Tovar-Sanchez et al. 2014
South Venice Lag., Italy	15	40	Pavlidou et al. 2014
Stoupa, Greece	2	11	Pavlidou et al. 2014
Venice Lagoon, Italy	80	160	Rapaglia et al. 2010a

A.9. SGD-derived flux of nutrients

The flux of nutrients associated to SGD can be obtained as the product of the concentration of nutrients in coastal groundwater and the estimated SGD flow. Few studies have reported concentrations of nutrients in SGD to the Mediterranean Sea. Most of them reported dissolved inorganic major nutrients (mainly nitrogen (DIN), phosphate (DIP) and silica (DSi)), as it is the more relevant chemical form for biogeochemical cycles. We compiled all the data, averaging the samples belonging to the same study site to yield a single value from each location. We used the range comprised between the 1st and 3rd quartiles of all the nutrient data in SGD from Mediterranean Sea sites (Table S-10) to obtain a representative concentration range of dissolved inorganic nutrients in SGD. A SGD-derived flux range of DIN, DIP and DSi was estimated from the nutrient concentration range and the SGD flow range. The maximum nutrient concentrations in the interquartile range (Q3) were multiplied by the maximum estimated SGD flow to obtain maximum fluxes of nutrients from SGD. Minimum concentrations (Q1) and SGD flow were used to estimate the minimum nutrient flux, and a median nutrient flux was also obtained from the median nutrient concentration and the median SGD flow.

The flux of nutrients supplied exclusively by fresh groundwater can be obtained from the fresh groundwater discharge estimated by Zektser and coauthors (S(Zektser et al. 2007)) and the median nutrient concentration in fresh SGD from different Mediterranean coastal sites (Table S-11). In this case, only those samples with salinities lower than 5 were averaged to derive the nutrient concentration from each location.

Table A10. Average concentrations of dissolved inorganic nutrients (DIN, DIP and DSi) and DIN:DIP molar ratios in SGD from different sites of the Mediterranean Sea

Study site	DIN μmol L^{-1}	DIP μmol L^{-1}	DSi μmol L^{-1}	DIN:DIP	Ref.
Alcalfar cove, Spain	1000	0.25	66	4200	Garcia-Solsona et al. 2010a
Badum, Spain	61	0.41	56	150	Garcia-Solsona et al. 2010b
Dor Beach, Israel	80	0.50	100	160	Weinstein et al. 2011
Haifa, Israel	420	0.60	140	690	Weinstein et al. 2006
Marina Lagoon, Egypt	9	0.50	26	17	El-Gamal et al. 2012
Palma Bay, Spain	150	1.3	77	120	Rodellas et al. 2014; Chapter 5
Romántica, Spain	180		190		Tovar-Sanchez et al. 2014
Sa Nau, Spain	120		230		Tovar-Sanchez et al. 2014
Santanyí, Spain	74		77		Tovar-Sanchez et al. 2014
Venice Lagoon, Italy	350	9.0			Rapaglia et al. 2010a
Mean	250	1.8	110	770	
Median	130	0.50	77	150	
1st Quartile	76	0.45	66	79	
3rd Quartile	310	0.95	140	430	

Table S-11. Average concentrations of dissolved inorganic nutrients (DIN, DIP and DSi) in fresh (salinity < 5) groundwater from different sites of the Mediterranean Sea

Study site	**DIN**	**DIP**	**DSi**	**Ref.**
	μmol L^{-1}	μmol L^{-1}	μmol L^{-1}	
Alcalfar cove, Spain	1000	0.25	66	Garcia-Solsona et al. 2010a
Dor Beach, Israel	300	0.25	250	Weinstein et al. 2011
Haifa, Israel	420	0.60	140	Weinstein et al. 2006
Marina Lagoon, Egypt	9	0.50	26	El-Gamal et al. 2012
Palma Bay, Spain	1200	0.28	250	Rodellas et al. 2014: Chapter 5
Sa Nau, Spain	330		650	Tovar-Sanchez et al. 2014
Mean	540	0.38	230	
Median	370	0.28	190	
1st Quartile	310	0.25	83	
3rd Quartile	880	0.50	250	

Riverine inputs and atmospheric deposition have been commonly considered the major external sources of nutrients to the Mediterranean Sea, and some studies have evaluated them in a wide-basin scale. The flux of dissolved inorganic nutrients from rivers was taken from Ludwig et al. (2009), by considering the total nutrient inputs in 1998 and the fraction that the dissolved inorganic form represents. DIN and DIP fluxes from atmospheric deposition were obtained from the estimates of Markaki et al. (2010). DSi inputs for the entire Mediterranean Sea were obtained from the fluxes reported by Koçak et al. (2010) for the northern Levantine basin multiplied by the Mediterranean Sea surface area.